GAZİ ÜNİVERSİTESİ

1926

IMPACT OF USING RENEWABLE ENERGY ON IMPROVING THE STABILITY OF THE ELECTRIC POWER SYSTEM

Aasem Hussein Mustafa KOROT

IN PARTIAL FULFILLMENT OF THE REQUIREMENTS
FOR THE DEGREE OF MASTER OF SCIENCE
IN ELECTRICAL ELECTRONIC ENGINEERING DEPARTMENT

GAZİ UNIVERSITY
GRADUATE SCHOOL OF NATURAL AND APPLIED SCIENCES

JANUARY 2025

ETHICAL STATEMENT

I at this moment declare that in this thesis study, I prepared the thesis writing rules of Gazi University Graduate School of Natural and Applied Sciences;

- All data, information, and documents presented in this thesis have been obtained within the scope of academic rules and ethical conduct,
- All information, documents, assessments, and results have been presented by scientific ethical conduct and moral rules,
- All material used in this thesis that is not original to this work has been exhaustively cited and referenced,
- No change has been made in the data used,
- The work presented in this thesis is original,

or else, I admit all loss of rights to be incurred against me.

Aasem Hussein Mustafa KOROT
23/01/2025

IMPACT OF USING RENEWABLE ENERGY ON IMPROVING THE STABILITY OF THE ELECTRIC POWER SYSTEM

(M. Sc. Thesis)

Aasem Hussein Mustafa KOROT

GAZİ UNIVERSITY
GRADUATE SCHOOL OF NATURAL AND APPLIED SCIENCES

January 2025

ABSTRACT

Renewable energy sources (RES) must be integrated into modern power networks to reduce carbon emissions and address global energy issues. This study investigates the effects of renewable energy integration on the stability of the electric power system, with a particular emphasis on voltage stability and overall grid reliability. This study addresses the critical issue of maintaining stability in electric power networks as renewable energy sources (RES) which are increasingly integrated to meet rising energy consumption and climate goals. The unpredictable and intermittent nature of renewable energy sources, such as solar and wind, poses a severe threat to grid stability since it can result in dependability issues, frequency fluctuations, and voltage swings. The modified IEEE 13-bus test system's voltage stability is examined in this work as a case study due to DG penetrations as the load increases. This study conducted simulations using MATLAB/SIMULATION to analyze the impacts of using photovoltaic energy sources in distribution systems. According to the case study and simulation results, RES increases system resilience and stability in the face of dynamic shifts in supply and demand. Testing was carried out for both increased loads and network problems. The load was increased by the following percentages in buses 671 and 675 separately: 25%, 50%, 75%, and 100%. Then, the previous percentages increased the load in the two buses (671 + 675) together.

Science Code : 90542
Key Words: : PV system, active power, voltage stability, power system
Page Number : 187
Supervisor1 : Assoc. Prof. Dr. Korhan KAYIŞLI
Supervisor2 : Assist. Prof. Dr. Omar Sharaf AL-Deen Yehya AL-YOZBAKY

ELEKTRİK GÜÇ SİSTEMİ KARARLILIĞININ İYİLEŞTİRİLMESİNDE YENİLENEBİLİR ENERJİ KULLANIMIN ETKİSİ

(Yüksek Lisans Tezi)

Aasem HUSSEIN MUSTAFA KOROT

GAZİ ÜNİVERSİTESİ
FEN BİLİMLERİ ENSTİTÜSÜ

Ocak 2025

ÖZET

Yenilenebilir enerji kaynakları (YEK), karbon emisyonlarını azaltmak ve küresel enerji sorunlarını ele almak için modern güç şebekelerine entegre edilmelidir. Bu çalışma, yenilenebilir enerji entegrasyonunun elektrik güç sisteminin kararlılığı üzerindeki etkilerini, özellikle voltaj kararlılığı ve genel şebeke güvenilirliğine vurgu yaparak araştırmaktadır. Bu çalışma, yenilenebilir enerji kaynaklarının (YEK) artan enerji tüketimi ve iklim hedeflerini karşılamak için giderek daha fazla entegre edilmesiyle elektrik güç şebekelerinde kararlılığın sürdürülmesi gibi kritik bir sorunu ele almaktadır. Güneş ve rüzgar gibi yenilenebilir enerji kaynaklarının öngörülemez ve kesintili yapısı, güvenilirlik sorunlarına, frekans dalgalanmalarına ve voltaj dalgalanmalarına yol açabileceğinden şebeke kararlılığı için ciddi bir tehdit oluşturmaktadır. Yük arttıkça DG penetrasyonları nedeniyle değiştirilmiş IEEE 13-bus test sisteminin voltaj kararlılığı, bu çalışmada bir vaka çalışması olarak incelenmiştir. Bu çalışma, dağıtım sistemlerinde fotovoltaik enerji kaynaklarının kullanılmasının etkilerini analiz etmek için MATLAB/Simulink kullanarak simülasyonlar gerçekleştirmiştir. Vaka çalışması ve simülasyon sonuçlarına göre, YEK, arz ve talepteki dinamik değişimler karşısında sistem dayanıklılığını ve kararlılığını artırmaktadır. Hem artan yükler hem de ağ sorunları için testler yapıldı. Yük, 671 ve 675 numaralı bus ayrı ayrı şu yüzdelerde artırıldı: %25, %50, %75 ve %100. Daha sonra, önceki yüzdeler iki bus (671 + 675) yükü birlikte artırdı.

Bilim Kodu	:	90542
Anahtar Kelimeler	:	PV sistemi, aktif güç, voltaj kararlılığı, güç sistemi
Sayfa Adedi	:	187
Danışman1	:	Assoc. Prof. Dr. Korhan KAYIŞLI
Danışman2	:	Assist. Prof. Dr. Omar Sharaf AL-Deen Yehya AL-YOZBAKY

ACKNOWLEDGEMENTS

Öncesi ve sonrası Allah'a şükür.

Rabbim babamın kabrini cennet bahçesi eylesin. Anne, Allah seni dünyada ve ahirette mutlu etsin. Kardeşlerim, Allah sizleri korusun ve mutlu etsin.

Değerli arkadaşlarım ve meslektaşlarım, hepinize şükranlarımı ve takdirlerimi sunuyorum.

Özellikle değerli hocalarıma teşekkürlerimi ve saygılarımı sunuyorum. Doç. Dr. Korhan KAYIŞLI ve Doç. Dr. Omar Sharaf AL-Deen Yehya AL-YOZBAKY, Allah derecenizi yükseltsin, ilminizi artırsın. Bu süreçte bana moral, motivasyon ve destek veren hocalarıma ve adını sayamadığım tüm sevdiklerime canı gönülden teşekkür ediyorum.

CONTENTS

Page

Page

Page

LIST OF TABLES

Table **Page**

Table **Page**

Table **Page**

Table **Page**

LIST OF FIGURES

Figure **Page**

Figure **Page**

Figure **Page**

SYMBOLS AND ABBREVIATIONS

The symbols and abbreviations used in this study are presented below, along with their explanations.

Symbols	**Explanations**
GW	Gigawatt
Hz	Hertz
kV	Kilo Volt
kW	Kilowatt
MW	Megawatt
TW	Terawatt
TWh	Terawatt hour

Abbreviations	**Explanations**
AC	Alternating Current
ANN	Artificial Neural Network
AR	Auto Recloses
CCM	Continuous Conduction Mode
CO2	Carbon dioxide
C-SPVG	Centralized Solar Photovoltaic Generator
DC	Direct Current
DE	Distributed Energy
DER	Distributed Energy Resource.
DG	Distributed Generation
DLGF	Double-Line-To-Ground Fault
DOE	Department of Energy
DR	Distributed Resources
DSPVG	Distributed Solar Photovoltaic Generator
EPSs	Electric Power Systems
FACTS	Flexible Alternating Current Transmission Systems
GA	Genetic Algorithm

Abbreviations	Explanations
GHG	Greenhouse Gas.
HVDC	High-Voltage Direct Current
IC	Incremental Conductance
IEA	International Energy Agency
IEEE	Institute of Electrical and Electronics Engineers
IRENA	International Renewable Energy Agency.
ISS	Input-To-State Stability
LLF	Line-To-Line Fault
LLLF	Three-Phases Faults
LLLGF	Three-Phases-To-Ground Fault
LV	Low Voltage.
MPP	Maximum Power Point
MPPT	Maximum Power Point Tracking
NVSI	New Voltage Stability Index
O&M	Operating And Maintenance
P&O	Perturb & Observe
PSAT	Power System Analysis Toolbox
PV	Photovoltaic
PVG	Photovoltaic Generator
RE .	Renewable Energy
RES	Renewable Energy Systems
RNN	Recurrent Neural Networks
SLGF	Single-Line-To-Ground Fault
SPVG	Solar Photovoltaic Generator.
STC	Standard Test Conditions
SVC	Static Var Compensators
T&D	Transmission And Distribution
UG	Utility Grid
VRE	Variable Renewable Energy
VSC	Voltage Source Converter
WP	Wind Power

1. INTRODUCTION

Energy is a basic necessity for all countries in the globe and is very important from a social and economic standpoint. When we hear the word energy, we typically think of electrical energy, which is regarded as the foundation of life. Human civilizations and economic systems have long placed a high premium on energy. To impact global environmental sustainability and accomplish development goals, energy is essential (Hussain et al., 2021).

Because a variety of resources are employed in its creation, energy may be used in many different ways in many facets of our lives. The expanding global population and the ongoing advancement of technology are contributing to the growth in energy consumption that we utilize in many aspects of our lives, including lighting, heating, industry, communications, and transportation. Our lives are full of energy resources, which may be divided into two groups: exhaustible and inexhaustible energy resources. In light of this differentiation, one type of energy source is renewable energy resources; it doesn't run out as it's consumed and doesn't alter over time. and second type Depleted resources, or non-renewable energy resources, are those that are used up in a single usage and are not reversible. Non-renewable resources include those derived from fossils and nuclei. As core-based non-renewable resources, uranium and thorium may be included with natural gas, coal, and oil, which we utilize on a regular basis (Kaya and Koç, 2015).

Most of the time, centralized generation, which uses traditional generators, is the foundation for providing consumers with electricity. Substations receive the produced electricity and scale down the voltage before distributing it for use in energy consumption. This process is done via a transmission line.

The greenhouse effect, which is the process by which part of the sun's energy is trapped by the atmosphere, transmission and distribution losses, and the high cost of fossil fuels are some of the issues that centralized generation faces (Zubo et al., 2017).

Long-distance transmission lines, massive fossil fuel-fired power plants, and hierarchical control centers are the foundations of traditional power networks, but they are evolving (El-Zonkoly, 2011).

Recent studies and research indicate that distributed generation is widely regarded as an efficient and cost-effective way to meet the steadily rising demands on the power grid. The Distributed Energy Office (DE) and the US Department of Energy (DOE) have determined that by 2020, 22% of newly installed power generation shall come from distributed generation (DG) capacity. This is because distributed generation (DG) is regarded as a key solution to alleviate the majority of the current network issues, including power outages, demand for power, voltage quality, line congestion, and security. And dependability. DG also makes it easier to accomplish the goal of using renewable and green energy sources if carbon dioxide emissions worldwide are decreased (Mohammadi et al., 2014).

The use of distributed generators, or DGs, has increased. DG is referred to by several names, including embedded generation, local generation, on-site generation, decentralized generation, district generation, and scattered generation. Different definitions of DG from the standpoint of location and/or capacity may be found in the literature currently in publication to aid in understanding the notion of DG.

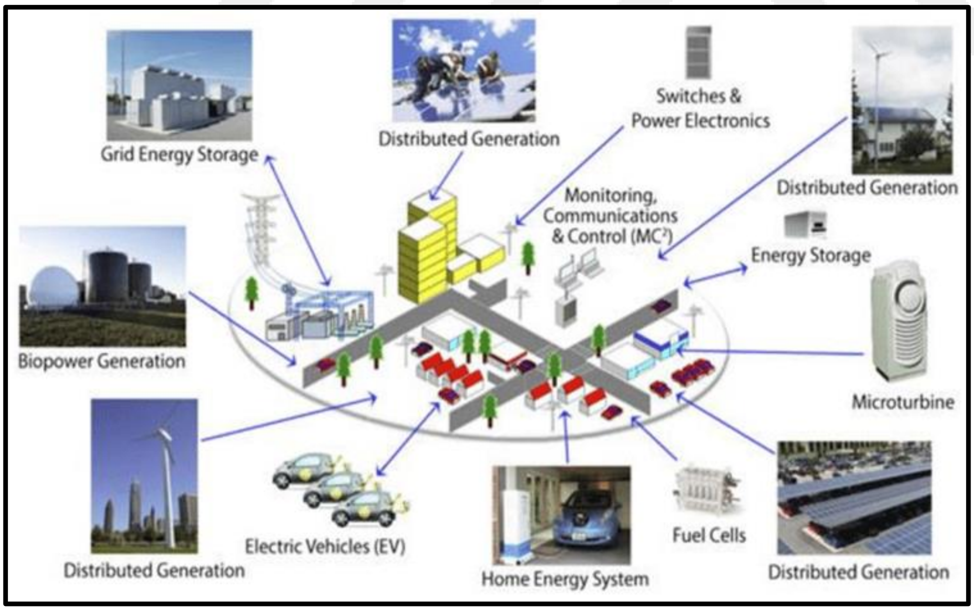

Figure 1.1. Types of distributed generations (Dashtdar and Dashtdar, 2019)

DG refers to a source of electric power generation that is either directly linked to the distribution network or located on the client side, meaning it is very near to the point of demand. It also refers to tiny generators positioned strategically near load centers inside the electrical grid. When looking at capacity, distributed generation (DG) is the act of dispersing a large number of small-scale power-producing units (500 kW and 1 MW) around the distribution network.

Similarly, the phrase is also used to describe small generating units, 30 MW or less, situated at or close to consumption centers. Generally speaking, distributed generation (DG) is any electric power source that is directly linked to the distribution network or located on the network's client site. Size-wise, distributed generation (DG) has been categorized into four groups: micro-distributed generation (generating up to 5 kW), small distributed generation (5–5 MW), medium distributed generation (5–50 MW), and big distributed generation (100–300 MW) (Zubo et al., 2017).

In addition to seeming to be a necessary component of energy security, renewable energy is also vital to the rapid economic growth and decrease in greenhouse gas emissions of many nations. Renewable energy is seen by several international organizations as an essential project for lowering environmental pollution. The International Energy Agency states that the existing patterns in the world's energy supply are unsustainable in terms of the economy, society, and environment. If immediate action is not taken, the predicts that CO2 emissions from energy-related sources will quadruple by 2050 (Hussain et al., 2021).

The structure of global energy consumption is changing fundamentally to fulfill the increasing demand for power and fight climate change. In this transition process, there is a lot of hope for renewable energy (RE), whose power output is expected to account for 25% to 41% of all energy by 2040. Variable renewable energy (VRE) sources, particularly solar photovoltaic (PV) and wind energy, have the potential to significantly improve the environment and change the global power sector. In the sustainable development scenario, their installed capacity could reach 7059 GW, or 49.21% of the total, by 2040 (Deng and Lv, 2020).

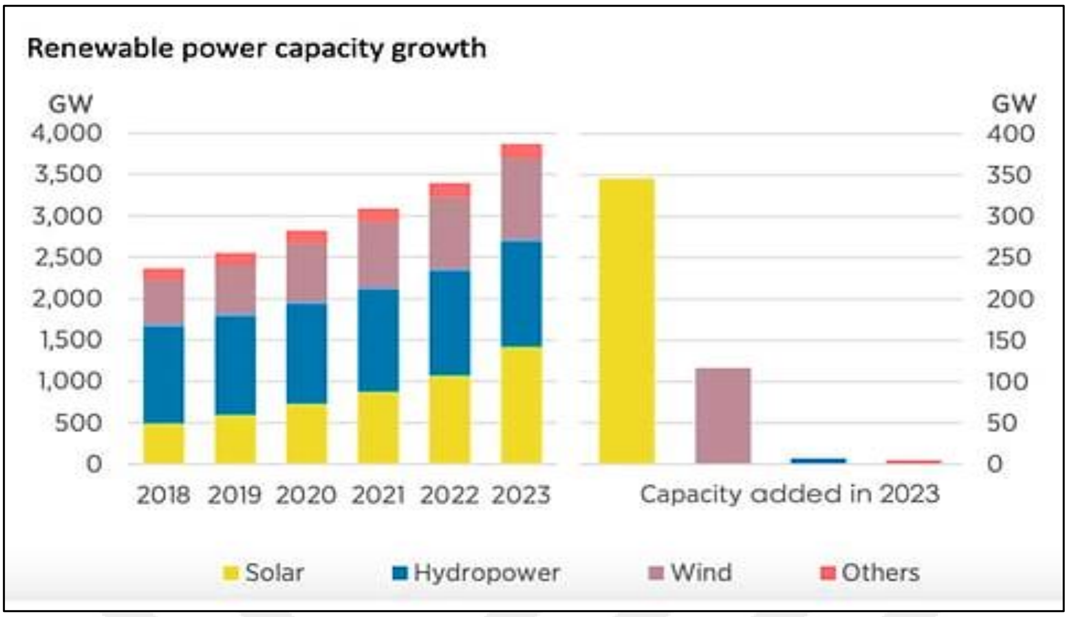

Figure 1.2. Renewable energy capacity in the world (International Renewable Energy Agency, 2023)

Based on data from the International Renewable Energy Agency (IRENA) (2023) as presented in Figure 1.2. The total capacity of renewable energy sources worldwide by the end of 2022 was 3372 GW. With a 1256 GW capacity, renewable hydropower made up the greatest portion of the total worldwide. With total capabilities of 1,053 GW and 899 GW, respectively, solar and wind energy made up the majority of the remaining energy. In addition, there were 524 MW of marine energy, 15 GW of geothermal energy, and 149 GW of biofuel.

In 2022, the capacity of renewable energy expanded by 295 GW (+9.6%). With a significant growth of 192 GW (+22%), solar energy continues to lead capacity expansion. Wind energy came in second with 75 GW (+9%). The capacity of renewable hydropower rose by 21 GW (+2%) and bioenergy by 8 GW (+5%). There was a very slight 181 MW increase in geothermal energy.

Together, solar and wind energy accounted for 90% of all net renewable additions in 2022, continuing to lead the way in the increase of renewable capacity. The capacity of renewable energy sources increased more annually as a result of the rise in wind and solar power, which also produced the second-highest percentage growth ever recorded.

With 174.9 GW more renewable capacity added to reach 1.63 TW (48% of the global total) in 2022, Asia accounted for around 60% of new capacity once more. China was the source of +141 GW of this rise. North America's capacity increased by 29.1 GW (+6.3%), while Europe's capacity increased by 57.3 GW (+8.8%). Africa grew by 2.7 GW (+4.8%), somewhat more than the previous year, as it continued its steady expansion. South America's capacity increase of 18.2 GW (+7.4%) continued its upward trend, while Oceania maintained its double-digit growth with an expansion of 5.2 GW (+10.6%), mostly due to expansion in Australia. With 3.2 GW of additional capacity put into service in 2022 (+12.8%), the Middle East likewise had its greatest increase on record (International Renewable Energy Agency, 2023).

According to recent data released by the IRENA, the world's total capacity for renewable energy increased by a record 473 GW (+14%) in 2023, reaching 3870 GW. The expansion was primarily driven by the development of solar energy capacity. In 2023, solar energy added +346 GW (+32%) to the global capacity of 1419 GW, surpassing renewable hydropower as the greatest renewable energy source. Additionally, the IRENA statistics demonstrated that the energy transition is quite uneven geographically, even with record additions. According to IRENA, "many countries are cut off from the benefits of energy transitions." China alone accounted for 63% of the 473 GW of additional renewable capacity in 2023, or 300 GW. Significantly, annual capacity additions from 2024 to 2030 must climb by more than 1000 GW annually in order to meet the global goal established at COP28 of tripling renewable power required to keep the increase in global temperature to 1.5°C of pre-industrial levels. The annual additions observed in the record year of 2023 are nearly doubled.

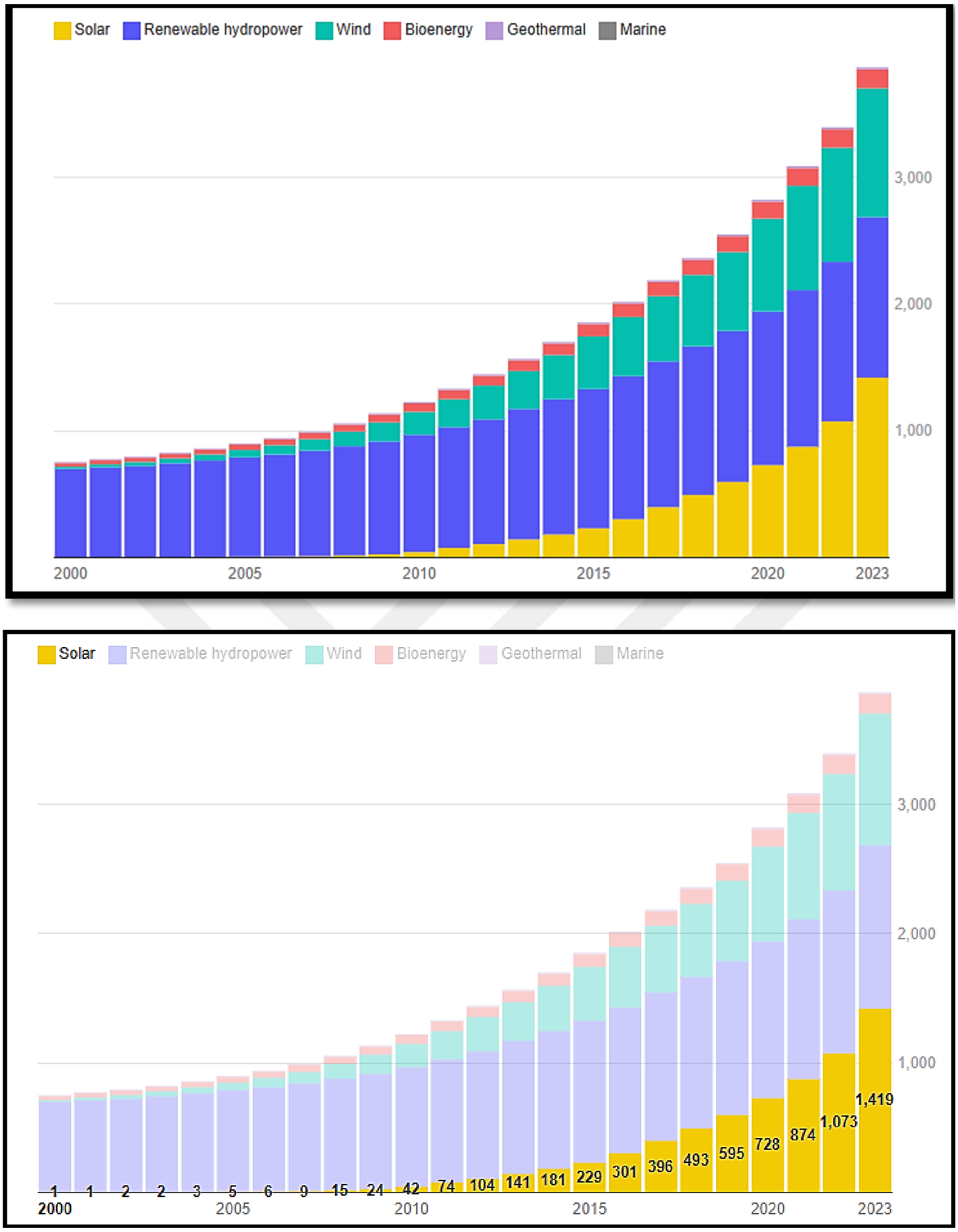

Figure 1.3. Renewable energy capacity grew at record rate in 2023

<u>Electric power grid</u>

Power networks in both rural and urban regions are supported by transmission and distribution lines. The phenomenon that affects electrical power networks worldwide is catastrophic breakdowns. The threat of power system breakdowns originates from several reasons, including meteorological conditions, human activity, and technological issues. Accidents involving vehicles, fallen trees, wind, storms, and defective equipment can all result in short-circuit problems in transmission and distribution lines. The development of widespread system failures is indicated by dynamically moving changes, most frequently caused by meteorological conditions. These changes result in cascade outages of power system fragments to frequency and voltage value infractions, which are caused by system protection settings (Furse et al., 2021; Zlotecka and Sroka, 2018).

Distributed energy resource (DER)

Distributed energy resource (DER) types

In order to lessen power interruptions, distributed generation (DG) technologies offer a substitute for traditional power systems. These devices are modular. Their features, advantages, and restrictions vary. Based on the kind of fuels they require to run, DG technologies are divided into renewable and non-renewable types. DG technologies are categorized in Figure 1.4.

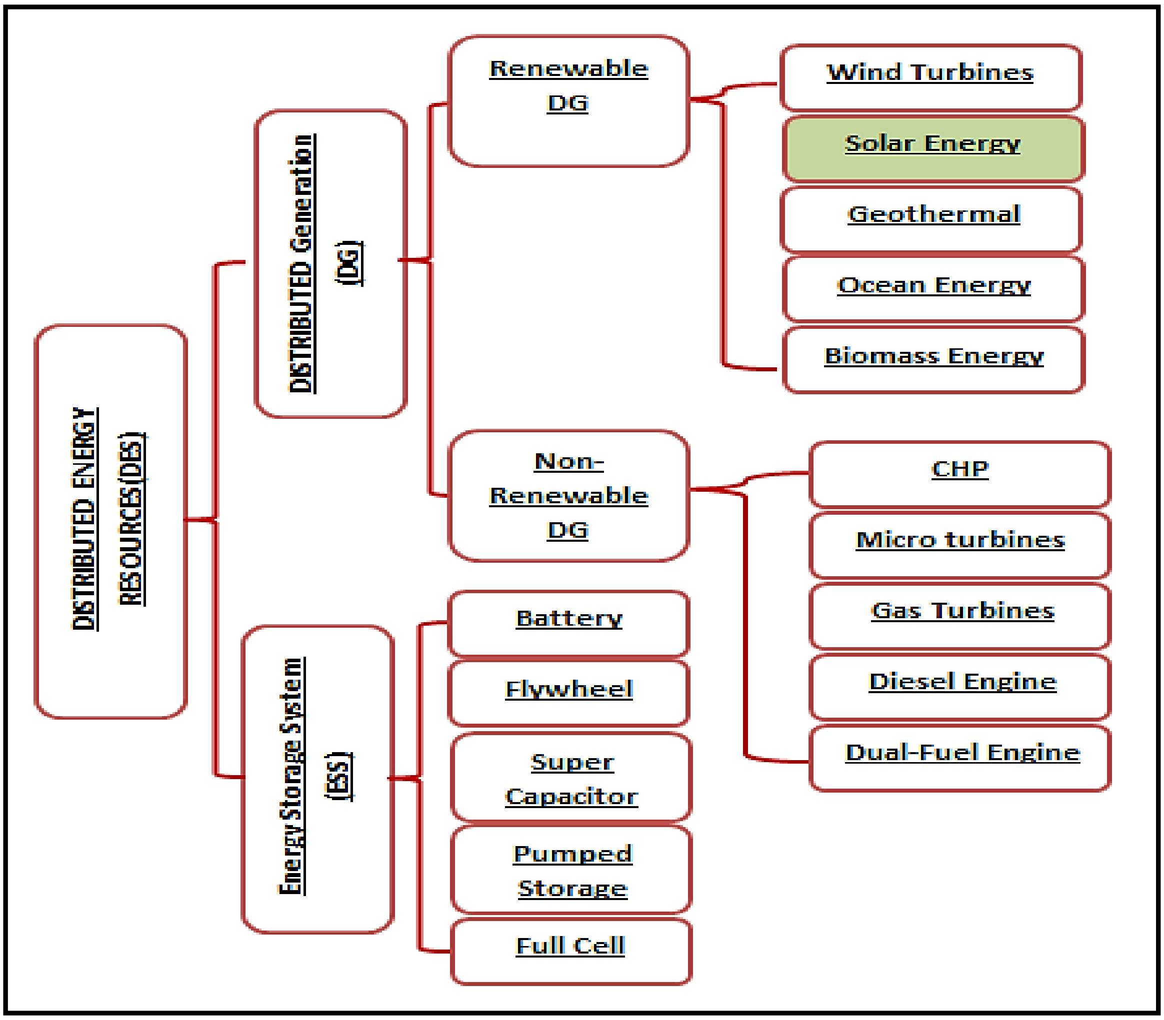

Figure 1.4. Types of distributed energy sources

Advantages of distributed generation (DG)

Because of how quickly power is being consumed worldwide, DG units are becoming more and more ingrained in the distribution grid. DG has made a significant contribution to the world's power generation at a low cost and high efficiency thanks to the current trend of technical improvement. Due to DG technologies' increased efficiency and dependability, their use in a contemporary power system enables customers to satisfy their load requirements with acceptable quality and continuity (El-Khattam and Salama, 2004; Banerjee and Islam, 2011).

Technological improvements in the design and manufacturing of distributed generation (DG) components, shifts in consumer power consumption patterns, and uncertainty surrounding the global petroleum market have increased opportunities for power utilities to use all available renewable energy resources to generate enough electricity to meet consumer load demand. Nowadays, everyone agrees that decentralized power systems will eventually take the place of centralized power systems due to the most recent electricity deregulation. To satisfy their customers' load demands, this will cause the utilities to pay much more attention to using DG units. Planning, coordination, and the integration of DG units into the power networks require the involvement of additional organizations to meet these goals (Adefarati and Bansal, 2016).

Technological advantages of distributed generation (DG) penetration

The electric power production resources known as renewable distributed generation (DG) are those that are directly linked to the load of customers on distribution networks operating at medium voltage, or LV. This group of DG technologies includes wind turbines, PV, biomass, geothermal, solar, and small/mini/micro-hydro power. At the request of the utility grid operators, the output power of the renewable distributed generation (DG) technologies can be sent to the grid or used as a stand-alone system to service a specific demand or region. According to recent research by the World Energy Council, by 2030, the world's power production from renewable energy sources is expected to rise from 23% in 2010 to around 34% (Adefarati and Bansal, 2016).

➢ *Reliability improvement:*
- Increased reliability of the power system.
- A decrease in capacity release.
- Increased diversity in generations.
- Reduced peak power.

➢ *Voltage profile and quality enhancement:*
- Enhancement of voltage quality.
- Enhancement of the voltage profile.
- Decreased flicker of voltage.
- Improved regulation and support for voltage.

➢ *Line loss/ energy reduction:*
- Decreased line losses.
- Improved reactive power control.

➢ *Security enhancement:*

- The crucial loads' security.
- Decreased risks to grid security.
- Enhanced security for electricity utilities.
- Impacts of cyberattacks are lessened.
- Decreased vulnerability to acts of terrorism.

➢ *Operational advantages:*

- Supplying auxiliary services.
- A rise in productivity.
- Installing it is simple and quick.
- O&M is simple.
- Lower reserved requirements.
- Enhancement of infrastructure resilience.
- Increased overall effectiveness.

➢ *The financial advantages of DG penetration:*

- Decreased O&M expenses.
- Infrastructure investment delays.
- Reduced expenses related to losses.
- With renewable DG, there are no fuel expenses.
- Lower acquisition expenses for right-of-ways.
- A decrease in the price of installation.
- Maintaining of constant running cost for longer time period.
- Cost reduction for auxiliary.

➢ *DG penetration's benefits for the environment:*

- Diminished impacts of land usage.
- Health care expenses are decreased with renewable energy.
- Eco-friendly with DG that is renewable.
- Lower greenhouse gas emissions and pollution from renewable DG.

<u>Non-renewable distributed generation technologies</u>

Non-renewable technologies provide energy for various processes using fossil fuels, including coal, petroleum, and natural gas. Nevertheless, the primary cause of the current global warming, greenhouse gas (GHG) emissions, acid rain, and petrochemical pollution is the combustion of fossil fuels. Natural processes cannot replenish non-renewable resources, making them non-sustainable. Because of these factors, the high rate of energy demand from non-renewable energy resources is far quicker than the pace at which they are being restored inside the Earth, which means that they will ultimately run out of use. By the use of co-generation arrangements, non-renewable distributed generation (DG) technologies may produce thermal energy for usage in both home and industrial settings in addition to power. Steam turbines, gas turbines, microturbines, and reciprocating engines are a few examples of non-renewable technology (Adefarati and Bansal, 2016).

Literature review

The study conducted by Behnam Tamimi and colleagues, an evaluation of the penetration level of solar photovoltaic generators (SPVGs) on the stability of the Ontario electrical system, was done in 2013. This research used Ontario's system data to better understand how the SPVG interacts with an actual system. Three cases were examined, each with corresponding grid-side dynamic models for the SPVG. These open-source models may be used for scattered rooftop installations and centralized farms with or without voltage management. Using small-signal stability, voltage stability, and time-domain contingency studies, the dynamic behavior of the system with SPVG installations was investigated at varying penetration levels. The system's overall small-signal stability is not significantly impacted by SPVGs, according to eigenvalue analysis. In contrast, investigations on voltage stability and transient stability showed that the distributed solar photovoltaic generators (D-SPVG) may significantly increase system stability in comparison to the centralized solar photovoltaic generator (C-SPVG) (Tamimi et al., 2013).

In 2014, researchers (Zetty Adibah Kamaruzzaman and Azah Mohamed) used the P-V curve and IVSI index to examine the effect of PV generators on static voltage stability in a variety of research scenarios. The power system's loading margin and voltage magnitude are both improved by adding a PV generator, according to simulation data. Upon integrating the PV generator at the weakest node inside the MV region, the system achieves voltage stability. Nevertheless, even with the far-reaching voltage collapse point, the increasing penetration level of PV generators impacts voltage stability. For this reason, it can be said that adding a PV generator to a power system enhances voltage stability; nevertheless, to guarantee a high-quality and dependable power supply, a thorough design, analysis, and integration of the PV system are required (Kamaruzzaman and Mohamed, 2014).

The effect of DG on a distribution network was investigated in 2015 by researchers (Lambros Ekonomou, Tareafa Alimardan, and Vasiliki Vita). Analysis has been done on the effects on voltage profiles and power losses of varying penetration levels of one nonrenewable and two renewable forms of distributed generation (DG). The extended Newton-Raphson approach has been applied to NEPLAN software analysis. The acquired data have demonstrated that various DG types have varying effects on the distribution network and that decreasing power losses and enhancing voltage stability depends heavily on the exact placement and size of these devices (Vita et al., 2016).

A new index was presented by researchers (Bahram Poornazaryan, Peyman Karimyan, G.B. Gharehpetian, and Mehrdad Abedi) in 2015 to help identify the ideal size and placement of distributed generation (DG) units to reduce active power losses and improve voltage stability margin while taking load changes into account. To address the optimization problem, a modified version of the Imperialistic Competitive Algorithm (ICA) approach is applied. The load fluctuations are taken into consideration to offer a comprehensive viewpoint for network scheduling. In 1% stages, the load linearly changes from 50% to 150% of the base load. The best position and size for the DG unit are established at each stage, and the curve-fitting approach is then used to derive generic expressions for DG sizes as a function of load level. Network planning may make good use of these general terms. The methodology is validated by applying the suggested approach to test systems consisting of 34 and 69 buses and comparing the outcomes with those derived using the cuckoo search algorithm (Poornazaryan et al., 2016).

(Warut Suampuna) suggested a CPFLOW-based method in 2016 to analyze grid-connected PV power plants' voltage stability. This algorithm's primary benefits are its quick calculation time and its capacity to go around the numerical challenge close to the voltage collapse point. A numerical investigation is carried out to examine the voltage stability of the IEEE 14-bus and 39-bus systems under various circumstances using the suggested technique. Numerical studies demonstrate how a higher level of PV penetration may significantly increase the overall voltage stability of the system. An assessment of the best places for PV installations reveals that there are variations in the degree of compatibility for each grid position in terms of the influence on stability. The voltage stability of the system may be seriously compromised by integrating PV generation in inconvenient places (Suampun, 2016).

In 2016, a technique of allocating DG units was proposed by the researchers (Mostafa H. Mostafa, Mostafa A. Elshahed, and Magdy M. Elmarsfawy). By using the DG units, this technique seeks to increase the voltage stability margin. The voltage stability, voltage profile, power flow, and P-V curve of a system with integrated PV or wind turbines in the distribution system are analyzed. Based on the findings of the simulation, the voltage stability margin can benefit from the placement and size of the DG. To meet the goal of increasing the voltage, an optimization approach may be utilized to design the placements and sizes of the DG units. To improve the voltage stability margin, it is therefore possible to design the locations and sizes of the DG units using an optimization approach. According to the modeling findings, it is advised to install wind turbine units at their maximum penetration level in the voltage buses that are most susceptible to voltage fluctuations in order to increase the voltage stability margin. The findings of the simulation suggest that in order to increase the voltage stability margin, the PV system should be installed at the optimal penetration level in the most vulnerable voltage buses (H. et al., 2016).

In 2016, the researcher (Ramazan Bayindir) and others carried out investigations in which study cases were established in the case of the quantity of integrated renewable energy sources (RES) and energy demand on the built grid model, concerning the consequences of RES on the system voltage profile. To lessen reliance on imported energy, solar, geothermal, and wind power plant installations should proceed more quickly, and the share of renewable energy generation in overall energy generation should rise. It is important to look at how integrating RES would affect the electricity system and to implement the appropriate safety measures (A. Nassar and Weber, 2016).

Researchers (Tenarasi Subramaniam et al.) investigated voltage stability analysis on a power grid that included an integrated PV system in 2017. Additionally, various PV penetration rates might result from PV installation, which has an indirect impact on voltage stability. The weak bus for the injection of a three-phase fault for fault analysis was located in this research project using the New Voltage Stability Index (NVSI). The solar system was used to lessen the impact of the malfunctioning bus. They concluded that the goal of the study project was accomplished by being able to use renewable energy sources, such as solar, to reduce the voltage sag difficulties. It is demonstrated in this study that utilizing renewable energy, such as solar, is feasible to even compensate for the fault concerns when generating power instead of using the standard technique. Based on the data obtained, PVs are without a doubt one of the greatest solutions for accommodating fault compensation (Subramaniam et al., 2017).

The researcher (Burak YILDIRIM) presented and studied the impact of PV integration on voltage stability in 2017. The IEEE 30-bus test system is the target of the investigation. To determine the system's voltage stability critical value, a thorough modal analysis was conducted. The Power System Analysis Toolbox (PSAT) has been used to conduct the research that is reported in the study. The analysis's conclusions demonstrated that, by raising the voltage instability limit value for the critical bus of power systems that contain PV power plants, PV integration improves the voltage stability of the power system. According to the analysis's findings, in the IEEE-30 bus test system, dispersed PV penetration is more likely than collective PV penetration to increase the crucial bus's distance from the voltage instability (Yıldırım, 2017).

Researchers (Yan Li, Xinshou Tian, Chao Liu, Yuanyuan Su, and others) investigated the distribution network's voltage control issue in 2017 while large-scale renewable energy integration was in place. Under the uncertainty of the renewable energy output, the voltage characteristic analysis of the distribution network serves as the foundation for a well-established model for the voltage sensitivity analysis of the renewable energy connect network. On the basis of this, develop a large-scale renewable energy voltage control plan to verify the precision and effectiveness of the recommended strategy and plan. According to the findings, the distribution network will greatly benefit from allowing renewable energy power plants to fully utilize their reactive power control capability under the specified voltage regulation objective (Li et al., 2017).

The study conducted in 2017 by A. Elrheem E.A. Mostafa, Naglaa K. Bahgaat, Mohamed Ebrahim El Sayed, and El-Said A. Othman used a genetic algorithm technique for a photovoltaic generating (PVG) system connected to a three-phase electrical distribution grid. The results showed that when the PI controller-based genetic algorithm was used, the settling times and overshoot voltage values were smaller than when using conventional PI controllers. The GA technique produced the best results, with the settling time and overshoot voltage values being smaller than when using the conventional PI controller (Mostafa et al., 2017).

(Rudresha S. J. and Dr. Shekhappa G. Ankaliki, the researchers,) presented an algorithm in 2017 to determine the best size to match the ideal location for minimizing overall power losses and enhancing the voltage profile in the primary distribution network. The analysis and simulation in this paper are conducted using the Power World simulator software on the IEEE-13 and IEEE-33 bus systems. The findings indicate that the placement of the distributed generation (DG) has a major impact on power losses and that voltage stability can be enhanced by choosing the appropriate DG size at an ideal location within the distribution system (Rudresha and Ankaliki, 2017).

In 2018, the researcher, E. A. Feilat, together with others, presented Using DIgSILENT software, computer simulations are used to study how combining big PV and WP plants affects the operation of Jordan's national grid. Modeling results have shown that, in order to avoid line congestion, the penetration level of renewable energy sources should not increase by more than 10% of Jordan's annual peak demand, given the constraints of line flow capacity. The impact of connecting wind and PVs on the grid's dynamic and static voltage stability has also been evaluated. P-V curves generated by increasing the penetration levels of PVPs and WPPs show that adding functionality for managing voltage and reactive power can double the maximum generation of RE. Increasing the penetration levels of PVPs with zero inertia and/or WPPs with low inertia has been seen to cause a rapid and further reduction in the power frequency signal. Furthermore, it was found that the Jordanian system's frequency stability could be preserved while supporting PVP and WPP penetration levels of up to 40% of peak demand (Feilat et al., 2018).

(Enkhtsetseg Munkhchuluun and Lasantha Meegahapola) (2018) used a systematic strategy to integrate solar PV into the test network to examine the effect of solar PV generation on the long-term voltage stability of the power system. When replacing the current synchronous generation with solar-PV generation, the steady-state system characteristics are kept unchanged. According to the long-term voltage stability analysis results, partly solar PV systems have replaced OEL-activated synchronous generators that operate as over-excitation limiters, improving long-term voltage stability. To increase power system stability, the work's findings emphasize the need to efficiently use installed 978-1-5386-4950-3/17/$31.00 ©2017 IEEE solar-PV generation. It should be emphasized, nevertheless, that the dispersed solar-PV systems would not behave in the same way as the aggregated solar-PV model employed in this investigation (Munkhchuluun and Meegahapola, 2017).

Researchers (Kabulo Loji, Innocent E. Davidson, and Rémy Tiako) presented their findings and challenges in 2019 about PV-based electric power generation installations on distribution systems. Results of the application are shown, and the studies are conducted on a conventional IEEE 9 bus system. To learn about the voltage profile and power losses in the system, the system's load is first progressively raised, and the weak bus is found. Additionally, to enhance the voltage profile, the SVS, a well-known FACTS, is fitted. However, there is no appreciable increase in the system's active power; as a result, PV-based power sources are substituted for SVC in comparison, and all of the case studies conducted for this research project show a notable increase. Even while both SVS and PV system usage show comparable improvements in the voltage profile, case scenario three also shows a reduction in power losses from 63.55 MW to 50.24 MW, which may be seen as the strength and beauty of the current methodology (Loji et al., 2019).

In 2020, the researcher, Ammar Arpadžić, together with other presenters, showed how varying degrees of PV penetration in the IEEE 14-bus test system impact energy losses and transformer current loading. The findings support the notion that, with proper planning, allocation, and RES operation, renewable energy sources—in particular, PV can positively impact power system parapets. In summary, when the RES is sized and distributed properly, it may significantly enhance the power system characteristics (Arpadzic et al., 2020).

The researchers (Bilal Ahmad Bhatti, Robert Broadwater, and Murat Dilek) investigated, using Graph Trace Analysis (GTA)-based power flow, the voltage stability of integrated Transmission and Distribution (T&D) networks in the context of distributed PV generation in 2020. At different degrees of PV penetration, the load-carrying capacity of buses and the voltage stability of lines are examined. It is demonstrated that a rise in the system's steady-state voltage stability is seen when PV generation levels rise. Furthermore, it is demonstrated that variations in the loading of transmission lines have a linear relationship with variations in the voltage stability margins within specific ranges of stability margin changes. Two case studies are given; one case study has 784,000 nodes and eight voltage levels in the model. A voltage-stability heat map is utilized in one case study to show how weak lines and buses may be identified (Bhatti et al., 2020).

Presented a study in 2021 by researchers (Santiago Grijalva, Ahmad Usman Khan, Jordan Sihno Mbeleg, and Cristian Gomez-Peces) that outlined an effective technique for using voltage magnitude data streams to pinpoint the position of solar PV installations in distribution circuits. This approach makes use of the way fluctuations in solar injection affect circuit voltages. Utilizing voltage magnitude data and the distribution system model, the estimated model allows for the recovery of the PV system's most likely location. Three-phase and one-phase PV system scenarios are examined for the approach. A suggested metric is presented to evaluate the quality of the estimate techniques. PV sites may be consistently estimated using this approach, as shown by simulations conducted on the IEEE 13-bus radial distribution feeder (Grijalva et al., 2021).

The researchers, Renuga Verayiah and Mohamed Abdul Rasheed, proposed a concept in 2021 that would reduce system losses and enhance the voltage profile through the best possible PV-DG layout. The findings were confirmed by the striking similarities between the GA and analytical technique results. The active losses were found to have dropped by 53.4% and 48.8%, respectively, for the IEEE 14-bus system and IEEE 33-bus system. In summary, they have effectively demonstrated that optimum PV-DG may be used in distribution and transmission networks with acceptable outcomes. Furthermore, PV-DG penetration may greatly lower system power losses while enhancing the voltage profile of the system by choosing the right PV-DG placement, size, and power factor (Rasheed and Verayiah, 2021).

In 2021 To analyze the voltage stability of a power system integrated with PV systems and stochastic loads, the researcher (S. Rahman) and colleagues studied a unique framework. Regarding PV penetration level and solar irradiance changes, the suggested methodology assesses the predicted values of the voltage stability key performance indicators over seven hours of solar irradiance (7 a.m.–6 p.m.). This approach is new because it uses Monte Carlo simulation to determine voltage stability while taking into account the uncertainties and intermittencies related to PV energy sources and system loads. The location of the PV system significantly affects grid voltage stability, according to the case study's critical eigenvalue analysis. However, after the PV system is installed, variations in PV penetration have no appreciable impact on the critical eigenvalue. In particular, increasing PV penetration relative to the average load consumption of the PV-connected bus lowers the system's total line losses and improves the load bus's reactive power margin during the peak solar irradiation hours (10 a.m.–3 p.m.). Furthermore, the voltage control mode of a PV inverter is found to perform better than the power factor mode in terms of improving the voltage stability of a PV-connected grid (Rahman et al., 2021a).

Researchers (Yavuz Ateş, Tayfur Gökçek, and Ahmet Yiğit Arabul) in 2021 investigated how hybrid DG resources affected power losses, voltage improvement, and electricity bills in the distribution network under investigation in the ETAP environment. DGs cannot change the voltage profile of the buses close to the grid under the same increment rate, even if they increase the voltage magnitude of the integration or near buses under significant load increments at these buses. They also noted that the study's dispersed hybrid generation system contributed more to voltage improvement than single-location integration did. Similarly, to achieve the best results for the power losses, the location, DG capacity, and loading factor of an integration study should be taken into account. But when the demand load close to the DG integration point is less than the power produced by DG, the use of surplus power from other loads might cause an unanticipated rise in power losses (ATEŞ et al., 2021).

In 2022, Shuanbao Niu and others provided a quantitative approach to assess how the pace of penetration of renewable energy affects transient voltage stability. A quantitative framework for assessing transient stability in power systems with high renewable energy penetration is established, and the security/stability index is computed under varying power flow transferring scales and rates of renewable energy penetration, based on input-to-state stability (ISS) theory. The findings of the analysis indicate that as the rate at which renewable energy is incorporated into power systems increases, so do the security and stability margins of power systems when it comes to external disruptions in power flow transfer (Niu et al., 2022).

The researchers (T. Praveen Kumar, S. Ganapathy, and M. Manikandan) investigated how to effectively control voltage stability and reduce harmonics in 2022 by combining a recurrent neural network with a PV-fed static synchronous compensator. In this study, a Landsman converter has been used in conjunction with an adaptive neuro-fuzzy inference system maximum power point tracking system to track the maximum power from the solar system in addition to DC-link voltage management. When compared to other converters, the selected converter offers a higher voltage-gain ratio and efficiency. To properly attenuate the harmonics that arise in the system, recurrent neural networks help provide reference signals. It has been noted that the overall harmonic distortion is kept to a minimum of 5% by IEEE standards (T. P. Kumar et al., 2022).

The study conducted in 2024 by Praveen Kumar Thota, Ganapathy Somaskandan, and Manikandan Mani focused on the examination of a grid-connected PV power system with voltage stability on the IEEE 14 bus & 30 bus systems. They use two methodologies in this analysis. To test ANN- and RNN-based PV controllers, IEEE 14 and 30 bus systems are employed. Normally, a load-demand bus connects the PV module, and voltage stability is maintained even when the load demand is on the distribution side. Weak buses aren't getting stability because of the sun's erratic radiation. The proposed RNN & ANN controller assesses the voltage stability performance only upon solar irradiation throughout an analysis period spanning from 9 am to 6 pm. The comparison results in the average load demand of the array being connected to a weak bus, which enhances PV performance and reduces line losses (Kumarar, 2024).

2. THEORY AND BACKGROUND

2.1. Introduction

The demand for renewable energy sources and distributed generation (DG) has grown in light of the depletion of fossil fuels and the rise in energy use that alters energy balances. Distribution networks can become active distribution networks with the incorporation of DG. Even if DG has many benefits, certain drawbacks become conditional and operational difficulties. Among the benefits, a better voltage profile, a reduction in power losses, and lower electricity bills all contribute to more effective energy use. Before DG integration, losses and voltage profiles must be carefully considered while planning the system. Changes in the size and placement of DG allow for adjustments to the voltage profile and system losses. Depending on the features of the system and the DG, DGs can provide various advantages such as reduced losses, high power quality, system dependability, and voltage support. Additionally, selling back the excess energy produced helps lower consumers' expenses. However, DGs cause bidirectional power flow, harmonic distortion, transient difficulties, instability in voltage, and problems with safety and protection (Ateş et al., 2021).

PV has drawn the most attention out of all the RE-generating technologies now on the market since it is so widely available and has low installation and maintenance costs, especially in many regions where solar power is scarce. To improve the voltage profile and minimize losses, distribution grid planning (DG) considers the various forms of PV energy and how they integrate with it. Since the load profile affects the design and modeling of the generation unit, it is essential to study the load profile of a given location to make sure the PV operates as a dependable and efficient system there. Furthermore, the reliability of the system regarding generation size and allocation planning is impacted by customer behavior and peak times in the load profile. To achieve the best possible PV integration, it is imperative that both time-varying loads be taken into account during DREG design. The main goal is to evaluate the effects of PV while taking non-constant load models into account in order to minimize power losses and distribution system voltage variations. The assessment of voltage magnitudes and power losses under various load increments at each bus—which has varying distances from the main grid and DG locations—is the work's primary contribution (Jamahori et al., 2023).

The typical architecture of current distribution networks is a straightforward radial scheme that feeds passive downstream feeders and LV from the upstream Utility Grid (UG) sides. Because UG and the downstream feeder have the same directed current flowing in a unidirectional manner in radial networks, it is simple to determine the fault current level that the UG connection fully provides. While adding DGs to such networks enhances the voltage profile, it modifies the network impedance and the fundamental properties of the system. The system characteristics are significantly impacted by this inclusion, especially in terms of the responsiveness of the protective devices and the state of the system malfunction.

The fault current levels and sources of contribution are affected by the system transition that DGs make. In addition to its many benefits, distributed generation (DG) also entails certain complications, particularly for networks designed using antiquated or conventional topologies. To prevent losing network security and dependability, several angles of DG integration impacts should be looked at. The purpose of this study is to look into how DG integration affects radial distribution networks. First, a quick summary of PV distribution generation sources is provided. Next, an IEEE 13-bus radial distribution network built using Matlab/Simulink is presented. Finally, studies are conducted on how different DG penetrations in the network affect the steady state and fault voltage profile, fault current level, and UG contribution to faults (Mohammadi et al., 2014). In addition to voltage drop problems, variable electrical loads, and defects in such systems, this chapter discusses PV cells as a component of renewable energies and their implications on electrical energy systems.

2.2. Power system grid

Modern society's essential infrastructure is made up of electric power systems. In industrialized nations, electric power grids and distribution networks are widespread and can be found in almost every house, office, industry, and institution. However, their penetration into developing or emerging economies is still somewhat limited.

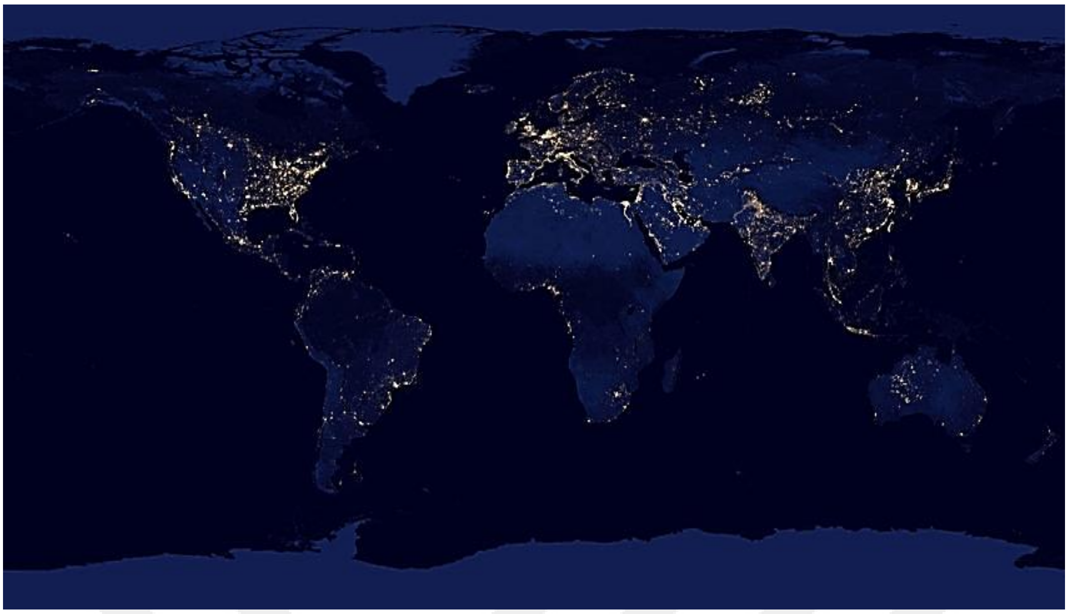

Figure 2.1. The nighttime satellite view of earth. The shadowy areas ındicate limited energy availability and the possibility of severe energy poverty (Hassani et al., 2019).

The whole system of lines and equipment that links the energy producers, or power plants, with the end users and their various requirements, is known as the electric power grid. Energy stored in coal, sunshine, wind pressure, or the chemical energy held in uranium atoms may all be converted into electricity by power plants. However, electricity is only a transient, adaptable, and portable kind of energy. Electricity with an alternating current (AC) frequency of 50 or 60 Hz is normally produced by the power plant. The three main components of the common electric grid—generation, transmission, and distribution—are depicted in Figure 2.2 as having a traditional radial architecture. The unidirectional power flow—that is, electricity flowing from the generator to the distribution—is one unique feature of the radial architecture (Hasanuzzaman et al., 2017).

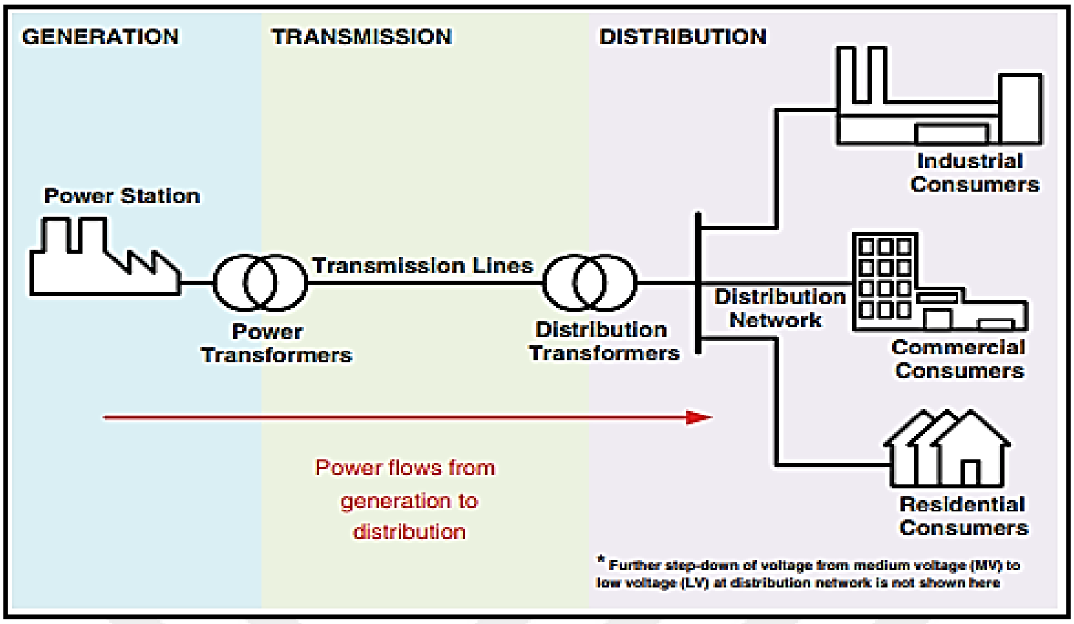

Figure 2.2. Radial topology of electricity supply (Hasanuzzaman et al., 2017).

Heat, information processing, light, torque for motors, and other useful forms of energy or activity are produced from electricity at the end of the grid, in homes and factories. The National Academy of Engineering has praised this grid, which forms the basis of our economy and culture, as the engineering achievement of the 20th century that has had the most positive impact on civilization. Over this period, the function of electric power has progressively expanded in both scope and importance. Electricity is now widely acknowledged as being essential to global social advancement, promoting economic stability and prosperity as well as raising living standards. Over the past few years, several nations have significantly privatized their electrical power sectors. Strong growth in electricity generation is anticipated. Furthermore, the electrical grid is confronted with at least three impending challenges: its structure, its technological capability to fulfill power demands for 25 and 50 years, and its ability to boost efficiency without compromising security and dependability (Amin and Stringer, 2008).

Most people refer to the electrical transmission system, which transports energy from power plants to substations near densely populated areas when they talk about the "grid." However, the distribution networks that transfer power from substations to individual consumers are also part of the grid.

The grid is a multilayer, multiscale hybrid system made up of three fundamental layers and the generating layer, which are vertically connected hierarchical networks (Amin and Stringer, 2008):

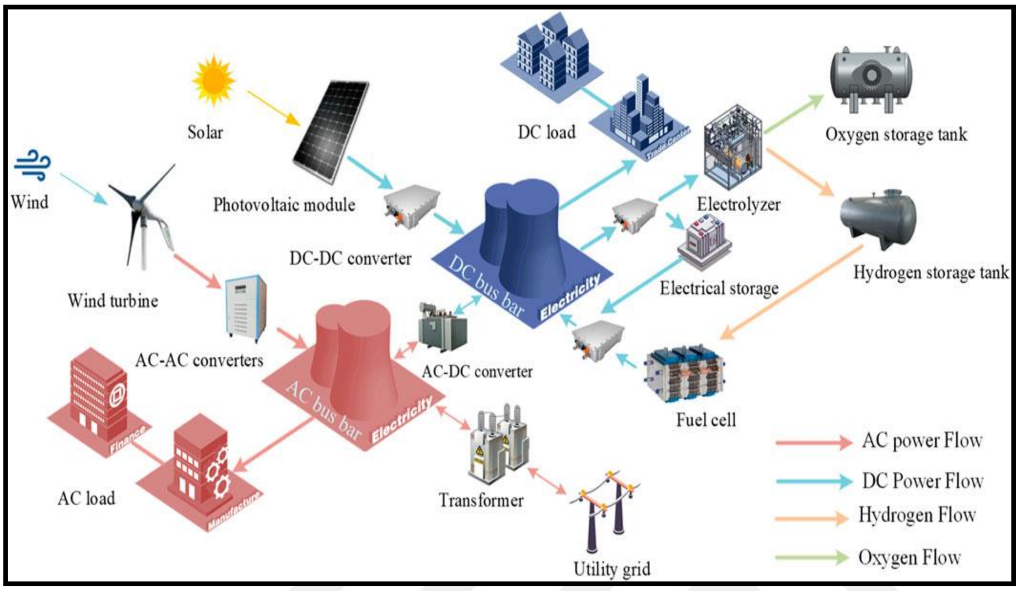

Figure 2.3. Power system grid

- Transmission Level: Linked to big generating units, adjacent transmission networks, sub-transmission levels, and large generation units via tie lines, this transmission level is made up of mesh networks that combine high voltage (100–300 kV) and extra high voltage (above 300 kV). Figure 2.4 shows transmission lines.

Figure 2.4. Transmission Lines (above 300 kV).

- Sub-transmission level: a radial or loosely linked network that is connected to medium-sized generators and big consumers, with some high voltage (between 100 and 300 kV) but mostly medium voltage (5 to 15 kV).
- Distribution level: this is usually a tree network with medium voltage (1-100 kV) and low voltage (110-115 V or 220-240 V) connected to medium-sized consumers, small generators, and local low-voltage networks for small customers.

Figure 2.5. Transmission lines (33 kV)

From local and regional grids, the transmission system expanded into a vast network of interconnected systems under the control of standardized operating and planning protocols. Technology advanced under an operational and regulatory framework that was mostly well-defined, while peak demand and energy consumption increased at predictable rates. In the last century, the bulk power grid has seen significant technological advancements. New technologies have been added to the power system regularly, such as (Henderson et al., 2017):

- More ecologically friendly and efficient producing sources.
- Equipment with a greater voltage.
- High-voltage direct current (HVDC) and flexible alternating current transmission systems (FACTS) power electronics.

- Developments in computerized protection, control, monitoring, and grid management strategies for scheduling, on-the-spot operations, and maintenance.
- Techniques for energy-efficient load control and demand response.

2.3. Problems in power system grid

Similar developments affect the electric power system, or the "grid," as they do the rest of civilization. A social development must affect either the grid itself, electricity generation, or electricity consumption for it to affect the grid. Several significant alterations that have this kind of effect include (Rönnberg and Bollen, 2016):

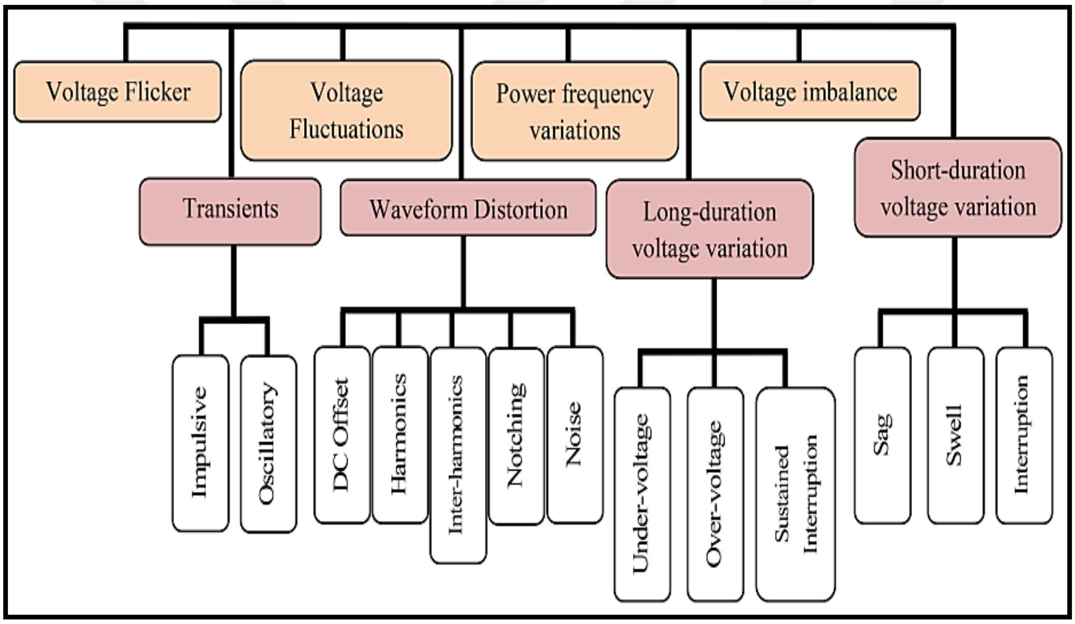

Figure 2.6. Power quality issues classification (Ahmadi et al., 2019).

Systems that impact society's way of life include critical infrastructures like communications and electric power networks. Because of their steadily increasing scale, complexity, degree of uncertainty, unexpected behavior, and interactions, designing, monitoring, and managing such systems is getting harder and harder. The electric power grid is fundamental to society's ability to operate. The increasing use of fluctuating renewable energy sources has made it more difficult for current power systems to operate securely and dependably.

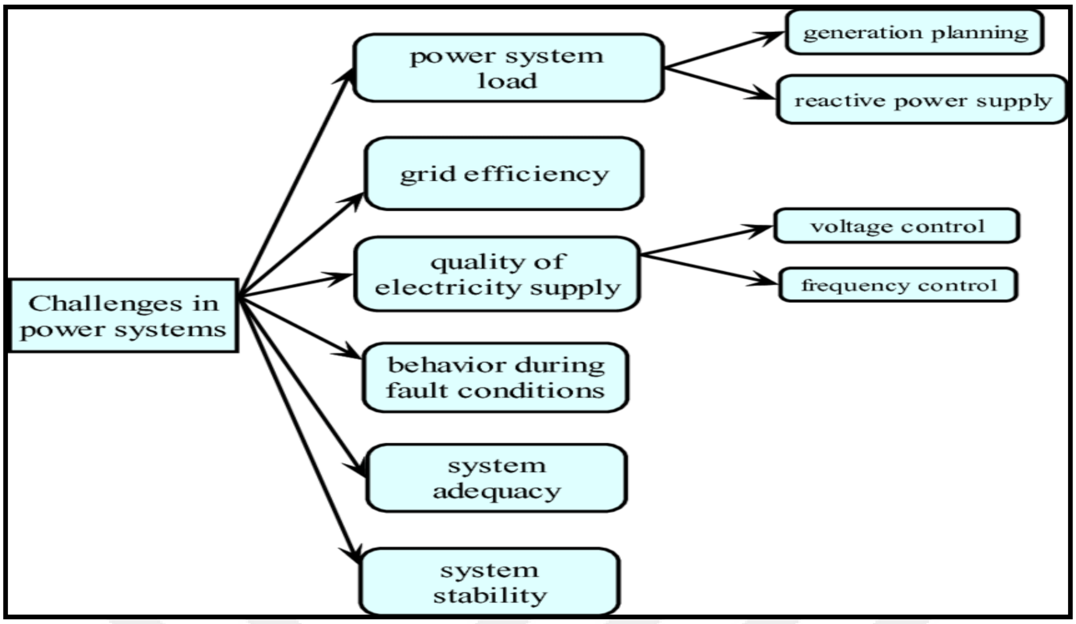

Figure 2.7. Challenges in power systems (Arghira et al., 2011)

As seen in Figure 2.7. the many relevant characteristics are connected to the new standards for electric networks.

To maintain the grid's power balance, or the ability to satisfy consumer demands through active power generation, the primary factor to be taken into account is the power system load. Forecasting and generation planning are necessary in order to keep the power system's load balance. Planning for a generation often entails having centralized, reasonably sized generating facilities under dispatching center supervision.

Network users (energy producers or consumers) as well as network operators are affected by issues with the quality of the electricity supply. Nevertheless, the system operator who is in charge of putting up the infrastructure that will allow the management of energy quality will address this matter. From the consumer's perspective, power quality primarily boils down to voltage characteristics and power supply continuity. The load balance and power supply continuity are connected. However, the features of a voltage, such as its frequency, amplitude, waveform, and symmetry, determine its voltage quality.

In terms of economic and environmental load balancing, grid efficiency is used. When load demand is low, power consumption should be increased; otherwise, it should be reduced during peak load demand.

To increase system stability, the behavior under fault situations should be observed and data should be kept in a historian server.

System adequacy is the capacity of the power system to adapt to changes in the power flux. There are two ways to look at system adequacy: the ability of the power system's producing units to meet demand (load). As well as the transmission system's capacity to move electricity flows from generation units to consumers.

Control over both voltage and frequency affects system stability (Arghira et al., 2011).

2.4. Types of faults in power system

Power is transferred from producing stations to consumers with the use of an electrical power system network made up of several sources and loads. All of the electricity system's sectors are becoming more complicated. A significant impediment that erodes the power system's economics, transmission, distribution quality, and performance is a fault (Datta et al., 2020).

Since transmission lines serve as the primary conduit between the generation and consumption of energy, they are an essential component of the power system network. Because they are immediately exposed to the environment, it has the greatest fault occurrence rate. Approximately 50% of power system breakdowns in reality happen on overhead lines (Singh and Vishwakarma, 2015). The intricate network of transmission lines that makes up the contemporary power system calls for a smart, precise, and dependable protection plan. Over the past few decades, there has been a significant rise in both the number of operational lines and their overall length due to the fast expansion of electric power networks. Lightning strikes, short circuits, malfunctioning machinery, improper operation, human error, overloading, and age can all cause problems with these lines (Recioui et al., 2015).

In comparison to other significant power system components, the likelihood of an electrical transmission line malfunctioning since the system's founding is often higher. For this reason, problem diagnosis and detection rank first among power protection engineers' main goals. Transmission line defects have a significant impact on the stability and economy of the power system. Therefore, it is imperative to quickly and accurately identify and address these flaws (Masood et al., 2017).

The primary objective of power systems is to supply a constant and dependable energy source. Power system faults typically cause significant variations in the following quantities: frequency, power factor, impedance, under- or over-power, over-current, current or power direction, and so on. Any power interruption in the electrical system these days results in significant financial losses for residential, commercial, and industrial customers. Power outages are mostly caused by random and irregular breakdowns in transmission networks (Alnaib et al., 2020).

An unacceptable departure from predetermined characteristics or variables that prevents the stated operation from being performed is referred to as a fault. Open circuit problems in the power system are typically caused by the melting of a fuse or wire, the failure of a circuit breaker, or the breakdown of one or more phase lines in the transmission system. Situations involving single- and double-phase open circuits can lead to imbalances in the power system's voltage and current, which can seriously harm the equipment. Increased voltage levels signify the existence of an open conductor defect, which stops the usual flow of current. Compared to short-distance power system component failures, overhead long transmission line failures are much more common and can have serious repercussions (*Power System Fault Detection Based On Discrete*, 2022).

To address more complex networks and a wider range of problem types, researchers' efforts are concentrated on creating effective techniques for fault detection, classification, and localization (Recioui et al., 2015). There have been several approaches for classifying and locating faults; they fall into four categories: software-based, traveling wave, artificial intelligence-based, and analytical techniques (Jena et al., 2023).

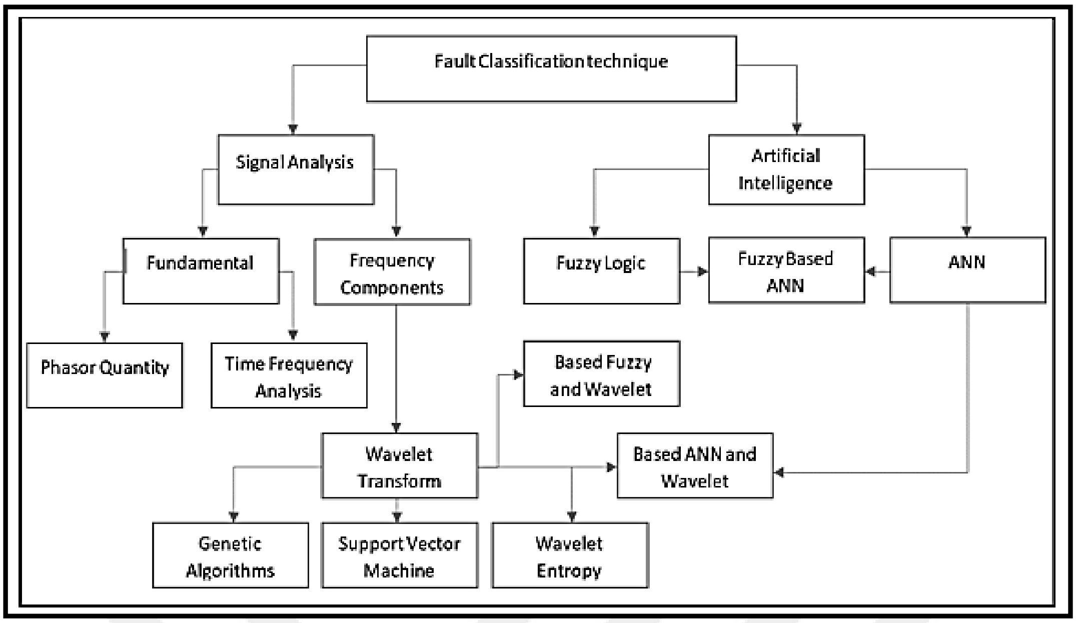

Figure 2.8. Types of techniques for fault classification (Power System Fault Detectıon Based On Dıscrete, 2022)

Various approaches have been suggested, and novel ways to fault classification in power systems have been developed significantly in recent years, and increasing numbers of technical papers have been published on high-voltage transmission and distribution systems to use the most effective method. The most commonly used methods for identifying faults in power systems are shown in Figure 2.8.

2.5. Classifications of Fault

A distribution system malfunction that causes the system to vary from its regular operating procedure can be classified as a temporary or permanent fault. Figure 2.9 shows the types of faults.

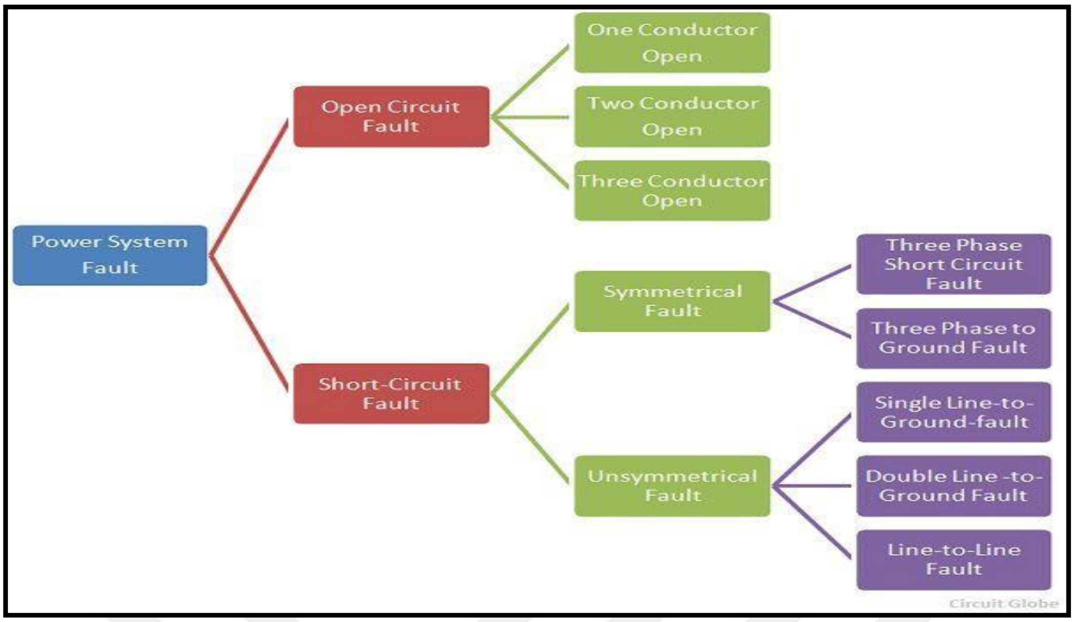

Figure 2.9. Types of faults

2.5.1. Temporary fault

Since a transitory defect in an electrical system seldom blows a fuse and there is no proof of the issue's source or location, it can be challenging to diagnose. Auto recloses, often called ARs, are commonly employed in distribution systems to allow for temporary fault removal. While momentary faults automatically resolve, repeated AR operation might interfere with the generator system and lower the amount of energy supplied to the network. Furthermore, because it impacts delicate customer loads like motor drives with changeable speeds, which may lower the quality of power delivered, temporary self-clearing has grown to be a cause for worry. Usually, transitory events in the distribution system are the cause of a momentary problem (Asman et al., 2021).

2.5.2. Permanent fault

Protective relay equipment enables the connected circuit breaker to de-energize the malfunctioning area in the event of a permanent problem. The reclose-fast action would interrupt the fault first, then inrush. Subsequently, the reclose performs two slow operations and one quick operation to interrupt the fault once more. Ultimately, the issue is cleared by the final sluggish procedure. If the malfunctioning lines are not maintained, the linked load will not be provided. As a result, the line may trip, which would result in lengthy blackouts for major power systems. A permanent defect can result from several things, including an object landing on the overhead line, insulation cable failure, and the line collapsing to the ground (Asman et al., 2021).

A temporary or permanent problem might result from one of two fault types connected to overhead line distribution systems. Both balanced and unbalanced faults are the two sorts.

2.5.3. Unbalanced faults

Unbalanced faults are the most common types of errors that happen since their occurrence causes unbalance in the system. These are also called non-symmetrical faults. There are two types of unbalanced faults: shunt faults and series faults.

2.5.4. Series fault

An anomaly known as a series fault occurs when one or two phases are interrupted, resulting in an imbalance in the impedances of the three phases. An open-circuit fault is represented by the series fault. Unlike short circuits, changes in the current in an open circuit are quite small. A drop in current during the faulty phase and an increase in voltage and frequency are characteristics of series faults. Although the system won't often shut down as a result of an open-circuit error, its operation will be compromised (Gururajapathy et al., 2017; Moosavi et al., 2019; Ben Youssef et al., 2017).

2.5.5. Shunt fault

Current flows across a shunt fault between phase and ground or between two, or more phases. Increased current accompanied by drops in frequency and voltage are the hallmarks of shunt failures. Line-to-line (LLF), double-line-to-ground (DLGF), three-phases-to-ground (LLLGF), and single-line-to-ground (SLGF) are the different categories of shunt faults. Lightning, wind, or falling trees are the typical causes of the two most frequent faults in overhead lines: SLGF and DLGF. Approximately 70% of faults are categorized as short-circuit faults (SLGFs), 20% are classed as differential logic faults (DLGFs), and 10% as (LLF) (Gururajapathy et al., 2017).

2.5.6. The L-G single-phase to ground fault

Another name for it is a single-phase ground fault, as shown in Figure 2.10. The primary cause of it is a breakdown in the insulation between one phase and the ground. In the electricity system, single-line faults occur most commonly.

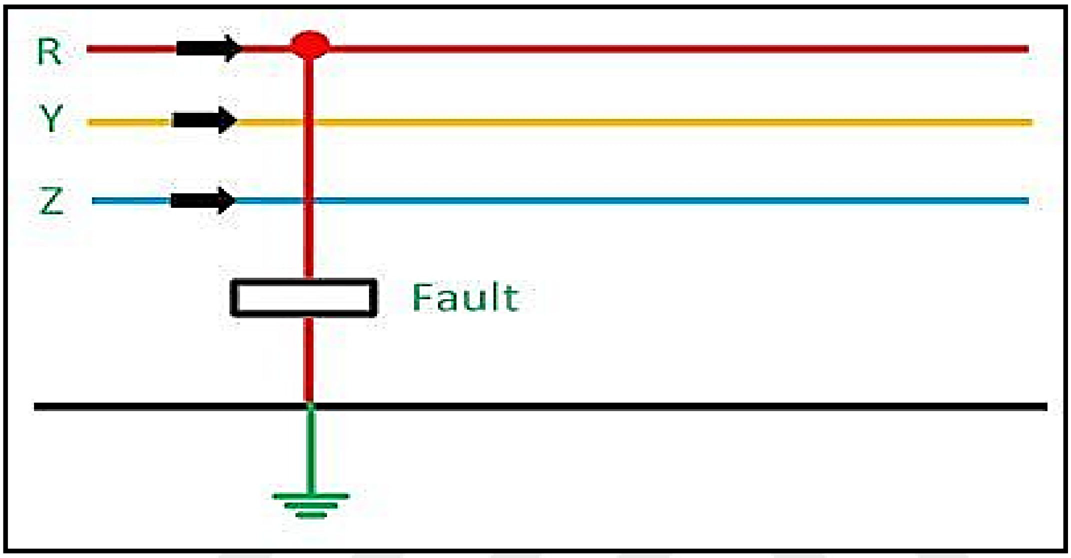

Figure 2.10. Representation of (L-G) fault

They have a 70%–80% likelihood of showing up in the power grid.

2.5.7. Double-phase line (L – L) fault

A phase-to-phase fault is another name for it, as shown in Figure 2.11. A short circuit between two conductors causes it to happen. The strong winds are the main factor causing this kind of malfunction. A severe wind might force the line conductors to swing, perhaps touching one another and causing a short circuit.

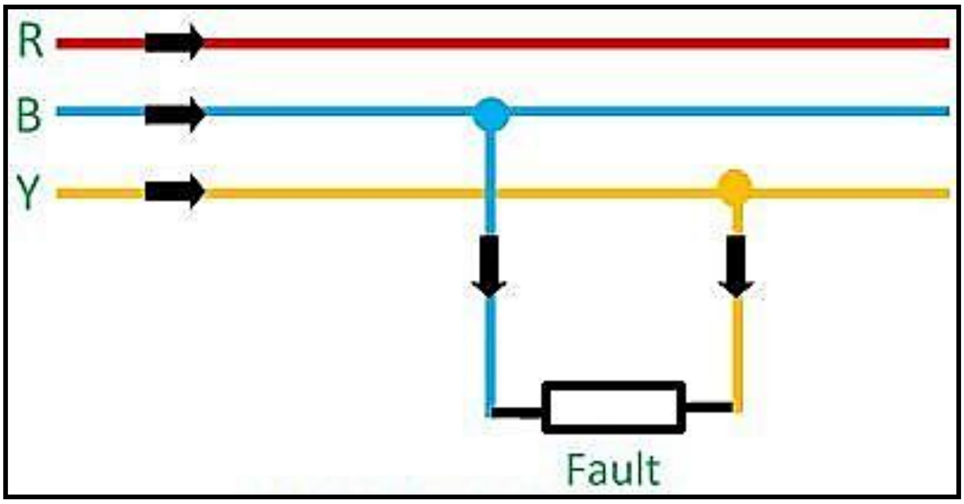

Figure 2.11. Representation of (L-L) fault

In the power system, their occurrence probability is between 10% and 15%.

2.5.8. Double-phase to ground (L – L – G) fault

The insulation between the two phases and the ground breaks down in this kind of fault.

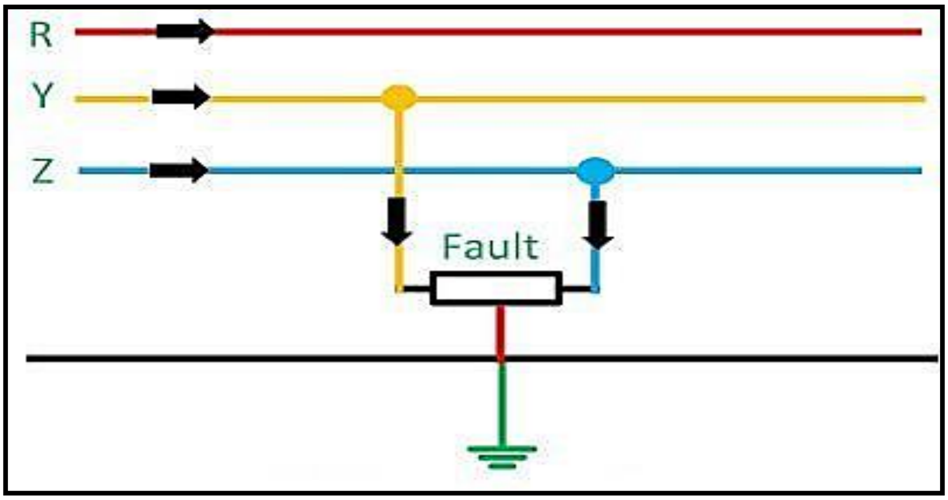

Figure 2.12. Representation of (L-L-G) fault

There are other names for it, such as two-phase to ground or line-to-line to ground fault. Even though it is a serious malfunction, the power system hardly ever experiences it. Such problems have about a 20% chance. Figure 2.12. shows the (L-L-G) fault.

2.5.9. Balance faults

In comparison to the other faults, three-phase-to-ground (LLLGF) and three-phase faults (LLLF) are classified as balanced faults since they occur relatively infrequently. But this fault—which is the most dangerous—usually results from a tower collapsing at the location where the line is attached to the tower construction. These are also known as symmetrical faults. Only 2% to 5% of system issues are caused by symmetrical faults. The system remains balanced in the event of these faults, but the equipment of the electrical power system is seriously damaged. It is easy to assess these issues, and it is frequently done in steps (Recioui et al., 2015).

2.5.10. Three-phase line (L – L – L) fault

The primary cause of this kind of issue is an insulation breakdown that affects all three phases. Such a problem occurs just 2% to 5% of the time. However, it is the most serious kind of failure that includes the highest short circuit current, and it is crucial to short circuit calculations when choosing circuit breakers and protection devices.

2.5.11. Three-phase to ground (L – L – L – G) fault

It is the most serious kind of failure and seldom ever happens in the power system. It happens because of a breakdown in the insulation that exists between the earth and each phase.

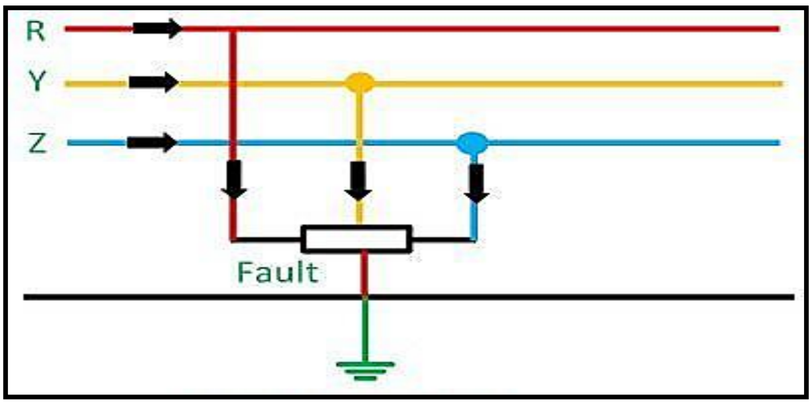

Figure 2.13. Representation of balanced fault

In the power system, it is between 2% and 5%. Figure 2.13 shows a balanced fault.

2.6. Photovoltaic System (PV)

The world's use of renewable energy systems (RES) has increased steadily during the past several years. Particularly when it comes to energy produced by wind and solar photovoltaics (PV), this tendency is probably here to stay. Because of the RES's well-known eco-friendly and sustainable properties, many traditional generating technologies, such as thermal power plants, are being replaced and put out of service.

Owing to their advantages, the spread of renewable energy sources (RES) has drawn the attention of international energy policymakers, who support and promote RES growth. RES and the energy transition are seen to be best promoted by the electrical energy output from PV solar plants in particular (Arpadzic et al., 2020).

The PV technology is regarded as one of the primary unrestricted supply sources of distributed renewable energy. Out of all the potential sources of renewable energy, PV technology is expected to contribute the most to the production of electricity by 2040. The global solar energy map in Figure 2.14. makes evident how solar energy may become a significant source of renewable energy (Alshahrani et al., 2019b). The generation of solar PV saw a notable uptick in 2022, rising at a stunning pace of 270 TWh, or 26%. With this spike, solar PV output reached a total of around 1,300 TWh (IEA, 2022).

The economic attractiveness of PV technology is expected to continue growing, supported by notable improvements in the supply chain and increased regulatory support, especially in China, the US, the EU, and India (Elgallai, 2024). Solar energy has drawn worldwide interest due to its enormous potential and endless nature, as it poses no danger to the environment. Real-time solar PV system testing is severely limited by variables including (i) high production costs, (ii) vast area requirements, and (iii) irregular solar radiation. In addition, the requirement for thorough testing of various power electronic setups was prompted by the need for conditioned, harmonic-free output and maximum power extraction. In general, real-time solar PV research spontaneity is impacted by the parameters listed above (Ram et al., 2018). The installation of solar PV systems in distribution networks and on client properties is still happening quickly. Installs that are typical include medium-sized central solar systems that are either owned by utilities or by medium- and small-sized commercial and industrial clients, as well as dispersed small home systems in a neighborhood or subdivision (Grijalva et al., 2021).

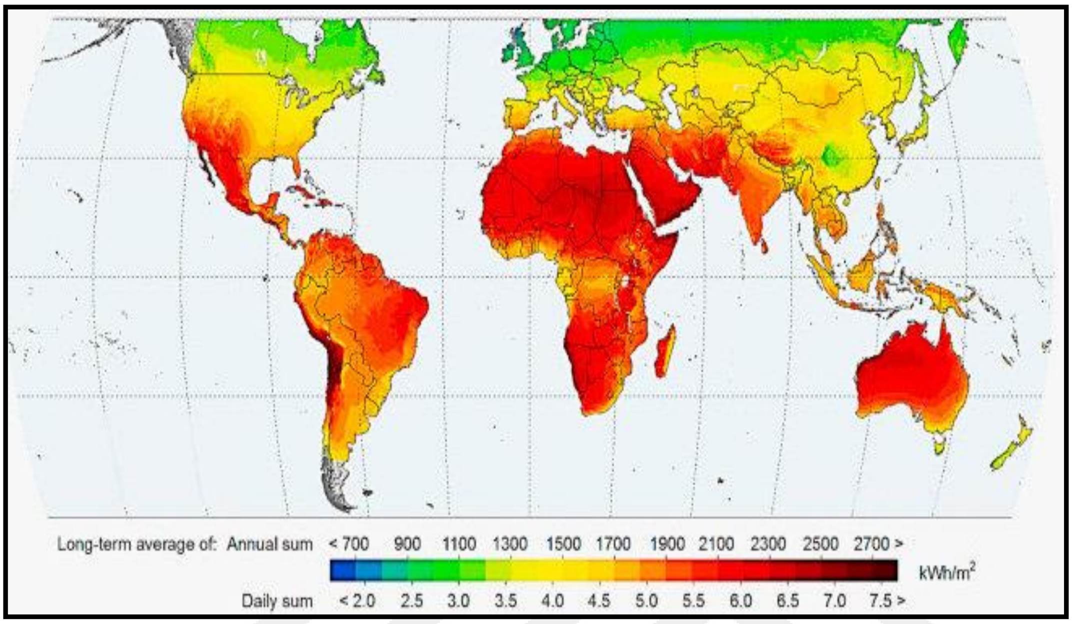

Figure 2.14. World solar energy map (Alshahrani et al., 2019a)

In 1839, the French physicist Edmund Bequerel found that some materials would produce trace amounts of electric current when exposed to light, which led to the discovery of the photoelectric effect. Albert Einstein's 1905 description of the photoelectric effect and the nature of light serves as the foundation for photoelectric technology. It led to his eventual receipt of the Physics Nobel Prize (Ram et al., 2018). Bell Labs in the United States developed PV for use in space operations in the 1950s. One may argue that this marks the inception of the PV industry.

2.6.1. Operatıon of A PV cell

A semiconductor diode with a p-n junction that is exposed to light is called a PV cell. Different approaches are employed to produce PV cells utilizing different types of semiconductors. At the moment, only two varieties of silicon cells are commercially available: monocrystalline and polycrystalline. Silicon PV cells are created by joining a thin film or thin layer of bulk silicon with an electric terminal. Doping one of the Si layer's sides creates the p–n junction. A thin metallic grid covers the surface of the semiconductor that faces the sun. Figure 2.15. depicts a solar cell's general layout.

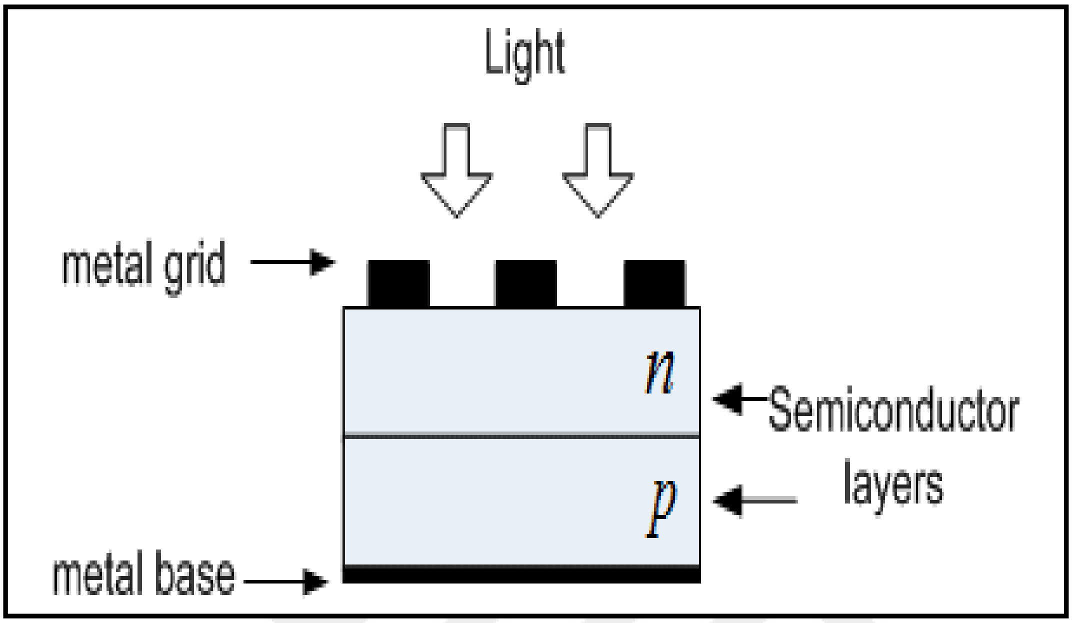

Figure 2.15. Physical structure of a PV cell (N.Sandeep, 2014).

When light strikes a cell, charge carriers are produced that, if the cell is shorted, start an electric current. The semiconductor material and the incident light's wavelength determine whether charges are produced when the incident photon's energy is high enough to separate the semiconductor's covalent electrons. The process of absorbing solar radiation, producing and transferring free carriers at the p–n junction, and gathering these electric charges at the PV device's terminals may all be characterized as the PV phenomenon (Villalva et al., 2009).

A PV system is a collection of cells connected to an electronics interface, controller, and other related auxiliaries. Its purpose is to directly convert solar radiation into electrical energy. A PV cell's output power is determined by the temperature, location of the PV module, and solar insolation. Depending on the needs of the load, PV systems may be configured to generate either direct current or alternating current with the right conversion devices.

PV systems can run independently to meet a particular load or in conjunction with the utility grid to function as a peak-shaving unit. Here are some reasons why adding PV systems to a power grid is beneficial: PV systems have several benefits, including extended service lives, low operating and maintenance (O&M) expenses, fuel independence, environmental compatibility, ease of installation, modular design, and minimal fuel expenditures. Global PV installations are predicted to reach 872 GW by 2030, according to research by the International Energy Agency (IEA) (Adefarati and Bansal, 2016). The PV systems employ semiconductors and the photovoltaic effect to convert solar energy into a continuous electrical current, which is then used to create electricity. It takes solar panels made up of several semiconductor-containing sun cells to produce energy using the photovoltaic effect.

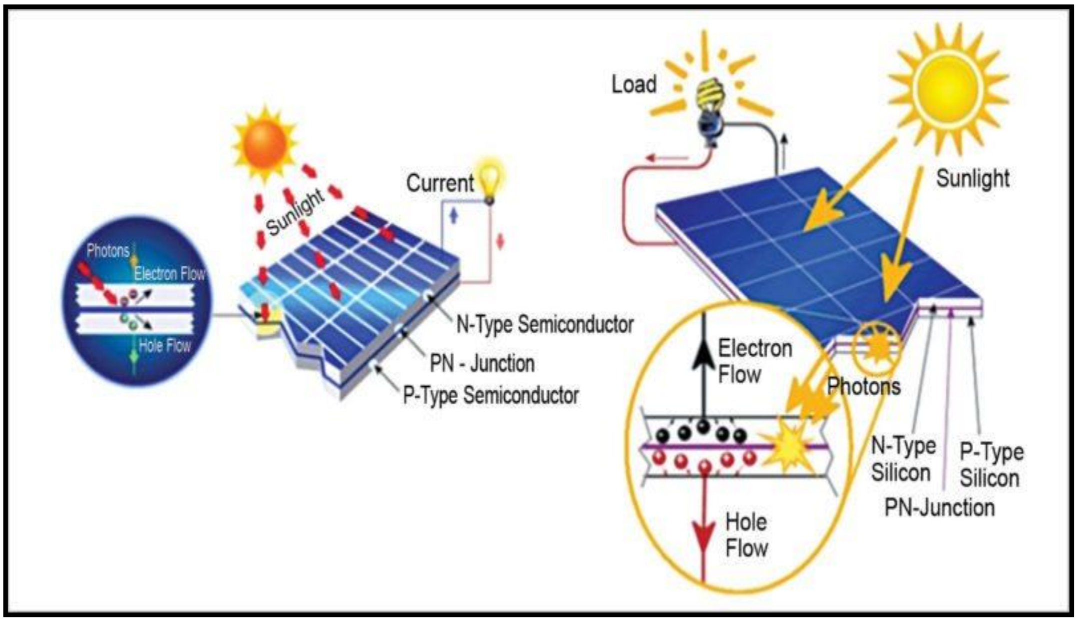

Figure 2.16. Working principle of Solar Cells (Kurniawan et al., 2022)

To use the photovoltaic effect to absorb photons and produce free electron transport, all solar cells need a light-absorbing substance inside the cell structure. Photovoltaic, or solar cells, work on the principle of the PV effect to convert light into electrical energy.

When pure energy from the sun strikes a PV cell, certain electrons—atomic particles with a negative charge—are given enough energy to elevate their energy level and become free. These electrons are subject to an internal potential barrier in the cell, which modifies them to create a voltage that powers a circuit's current flow. The working principle of the solar cell is shown in Figure 2.16.

2.6.2. The PV system's structure

A PV system typically consists of PV arrays, a DC-AC power electronic inverter, and related controls. A PV energy system's general structure is shown in Figure 2.17. Large-scale PV energy systems often need a step-up transformer to connect to the grid. DC-AC inverter control and MPPT control are two of the related control algorithms that power PV systems.

Maximizing solar power harvesting is made easier using the MPPT control method. Conversely, the DC-AC converter transforms the collected DC solar energy into useful AC electricity. The PV system's operating mode determines how the DC-AC inverter is controlled. When a PV system is functioning in a grid-connected setting, the DC-AC inverter is regulated to send as much solar energy as feasible to the grid. Conversely, while the PV system is functioning in its isolated mode, the DC-AC inverter is managed in harmony with other energy providers and energy-storing apparatuses to preserve the voltage and frequency of the isolated system (Rahman et al., 2021a).

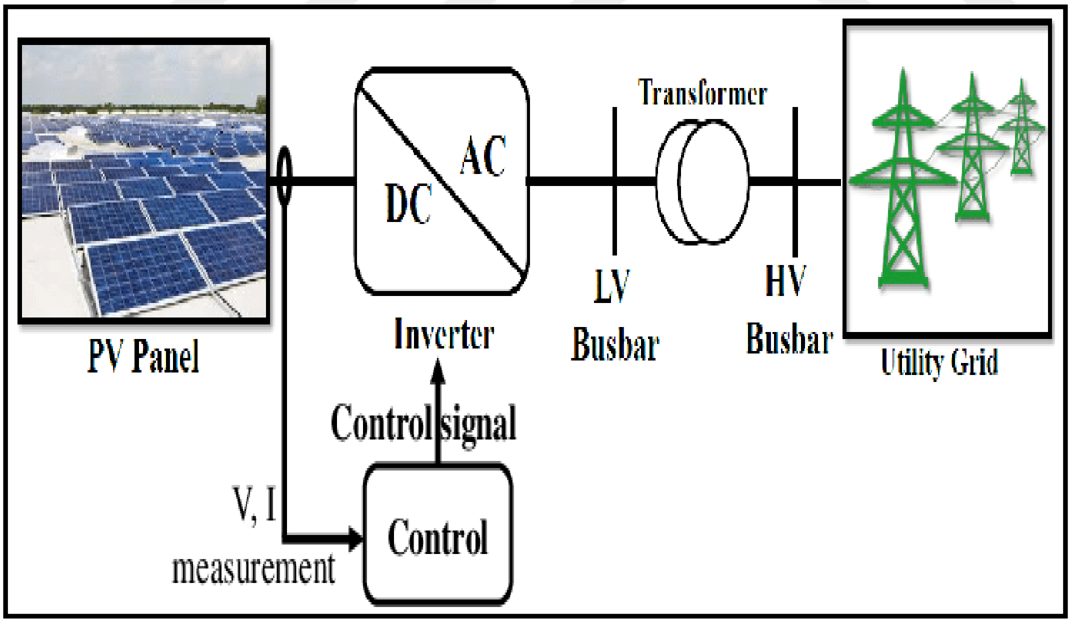

Figure 2.17. A schematic of a solar PV system that is connected to the grid (Rahman et al., 2021b).

2.6.3. Modeling PV cell

A PV cell's electrical circuit is represented as a mixture of a current source (I_{ph}), a parallel resistance (R_p), and a series resistance (R_s) to get around the drawbacks of modeling a single PV diode at high and low voltages. Two diodes (D_1, D_2) will be used to symbolize the photocell. Figure 2.18. shows the equivalent circuit.

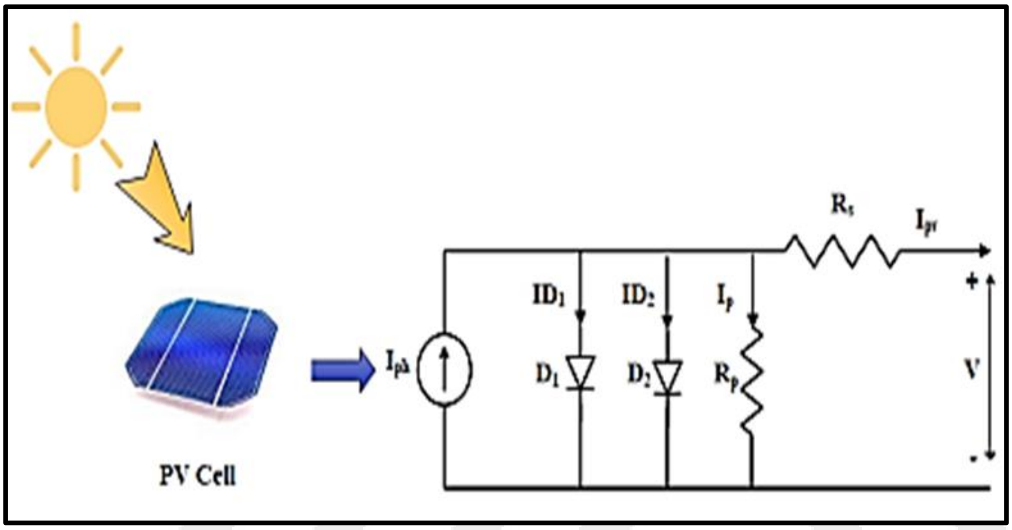

Figure 2.18. The equivalent circuit of a PV cell

- D_1: indicates the diffusion process .
- D_2: gives an idea of the vacuum charge region of the junction .
- R_s: represents the primary losses due to current flow.
- R_p: *represents the reverse saturation current losses.*

The voltage-current characteristics of a solar cell are represented by the following equations (Sudhakar Babu et al., 2016):

$$I_{pv} = I_{ph} - I_{d1} - I_{d2} - I_p \quad (2.1)$$

I_{pv}: PV current .

I_{ph}: PV current, which is a function of the radiation level and junction temperature.

$$I_{pv} = I_{ph} - I_{01}\left[e^{\left(\frac{(V+I.R_S)}{a_1.V_{T1}}\right)} - 1\right] - I_{02}\left[e^{\left(\frac{(V+I.R_S)}{a_2.V_{T2}}\right)} - 1\right] - \frac{V+I.R_S}{R_p} \quad (2.2)$$

I_{01} & I_{02}: the leakage currents for diodes D_1, D_2 .

- V: Photocell output voltage.
- V_{T1} , V_{T2} : The thermal voltage of the PV module is given by $\left(\frac{N_S.K.T}{q}\right)$
- N_s : The number of PV cells connected in series.
- T : (p − n) junction temperature (kelvin).
- K : Boltzmann constant $= 1.38 * 10^{-23}\ J/K$.
- q : Electron charge ($1.602 * 10^{-19}$ C).
- a_1& a_2 : ideality factors of diodes D_1, D_2.

The current generated by a PV cell (I_{pv})depends on temperature and radiation. Then the photocurrent is calculated as:

$$I_{pv} = (I_{scn} + K_i\Delta T)\frac{G}{G_n} \qquad ,\Delta T = T - T_n \quad (2.3)$$

- I_{scn} : Short circuit current at standard test conditions (STC).
- K_i : Thermal coefficient of current.
- G : The radiation to which solar panels are exposed.
- G_n: The radiation to which the solar panels atstandard test conditions STC ($1000\ Wm^2$).
- T: surface temperature of the solar panel.
- T_n: temperature at standard test conditions STC(25 ° c).

2.6.4. PV array

In PV arrays, a single cell produces very little voltage and current. A silicon PV cell can generate around 0.6 volts of electricity. Under normal test circumstances, or STCs (Standard Test Conditions), the efficiency of crystalline solar cells is typically 15%. This relies on the temperature outside and the amount of solar radiation being received. Module PVs are made up of a series and parallel arrangement of solar cells. These can be joined in parallel to produce an array PV or in series to form a string PV. It generates the quantity of power required by the load and is utilized to attain regularly used voltage levels, as in Figure 2.19.

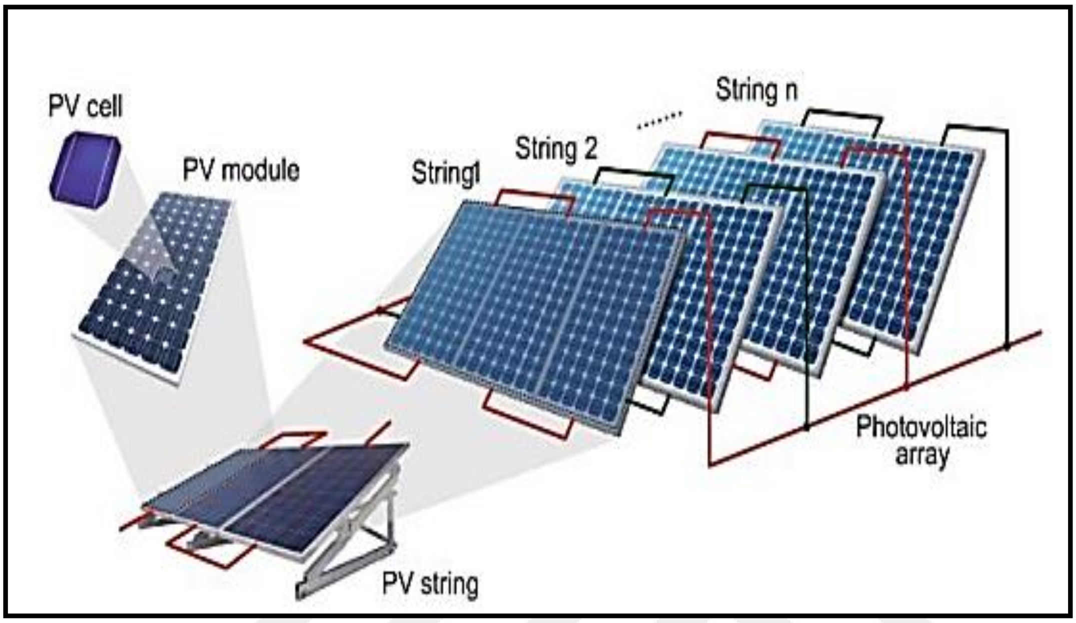

Figure 2.19. The basic building blocks of a solar PV energy system (Molina and Mercado, 2019)

The temperature and solar radiation are the array PV's inputs that determine its output, and when the array PV achieves its standard input of (STC), At a temperature of 25°C, solar radiation is 1000 W/m².

2.6.5. PV's effect on the distribution system

The primary effects of PV integration include voltage imbalance and fluctuations, current and voltage harmonics, grid islanding protection, flicker, and distribution transformer stress, among other power quality problems. Both steady-state and dynamic effects may be summed up as follows (Karimi et al., 2016):

- Voltage fluctuation in the feeder, which includes imbalanced and rising or falling voltage.
- The improper functioning of devices that regulate voltage, such as line voltage regulators, capacitor banks, and on-load tap changers.
- A distribution feeder overflow might occur.

- Variations in reactive power flow brought on by capacitor bank devices not operating properly.
- The malfunctioning of overvoltage and overcurrent protection mechanisms.
- In the event of a grid outage, islanding detection and operation.
- Security and dependability of the distribution network.

The degree of PV penetration, the distribution system's architecture, and the placement of PV inside the distribution system all affect how serious these problems are. In these situations, a significant PV penetration rate may introduce electricity into the transmission network, influencing the distribution system's voltage level and protection configuration. Under these circumstances, the distribution system functions as an active network.

2.6.6. Effects of ıntegrating PV ınto the electrical grid

Distributed, diurnal, converter-based, and intermittent are the four primary categories of PV characteristics that present integration issues for the power system (Gandhi et al., 2020).

Distributed

PV may be deployed directly at the load in modest quantities because of its adaptability. The PV system is non-dispatchable and may not be visible to grid operators when it is situated behind the meter. Reverse power flow happens when PV generation is greater than the load. Given that the grid was intended to handle unidirectional power transfers from high-voltage networks to low-voltage networks, this might be an issue. Voltage imbalance in the LV network can also result from dispersed PV installations that are not balanced among the phases.

Diurnal

The only time PV production is accessible is during the day. Although this is advantageous for daytime peak load systems, with higher PV penetration, and particularly in nighttime peak load systems, PV requires a high ramp rate and reserve to go from the low daytime net load to the peak evening load.

Converter-based

PV doesn't have a turbine or rotor as conventional generators do; hence it doesn't have any kinetic energy or inertia either. In order to keep the frequency and rotor angle stable during disruptions, inertia is necessary. Consequently, a high proportion of PV that lacks inertia in the power system may lead to instability. Harmonics and decreased power quality in the system can also be caused by non-linear switching and inverter operations.

Intermittent

Because of cloud movement, photovoltaic power can vary significantly in a short period of time. This quick shift in power might result in voltage flickers and harmonic distortions at high penetration.

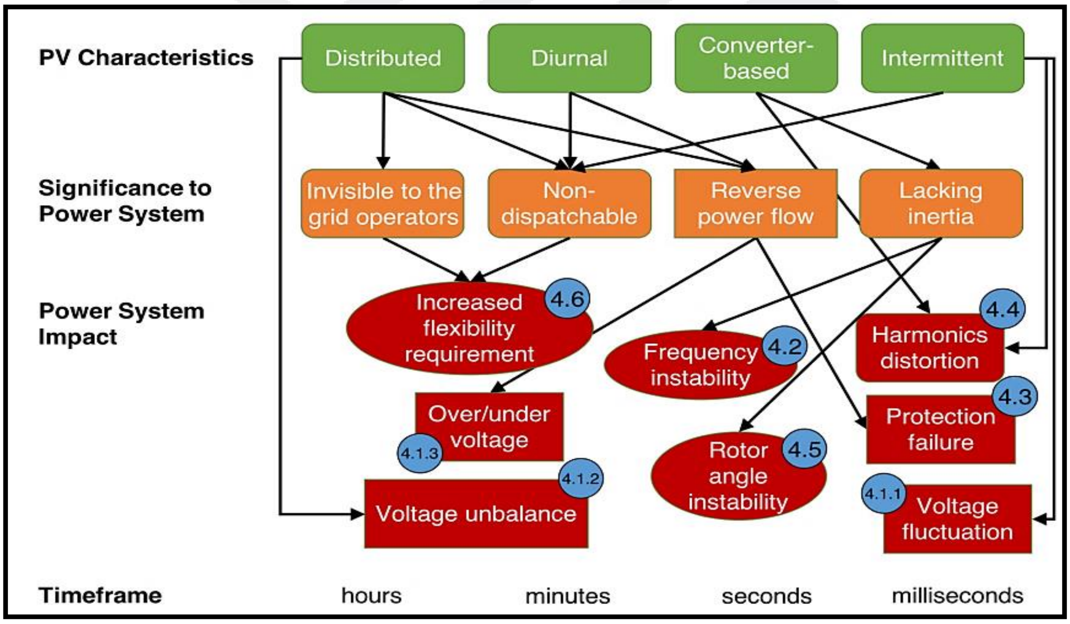

Figure 2.20. Overview of power system issues caused by the integration of PV.

The PV features, their importance, and their effects on the power system are shown in Figure 2.20.

2.6.7. Environmental effects on solar photovoltaic system performance

Solar energy systems, particularly photovoltaic systems, have emerged as a major supplier of electricity in recent years. Yet, PV systems' performance is influenced by a multitude of parameters, including temperature, wind, humidity, pollution, dust, rain, and sun intensity; geographical considerations also have a role, as does the kind of PV being utilized. PV manufacturers assess their products' output based on Standard Test Conditions (STC), which include a temperature of 25° C, a solar irradiance (intensity) of 1000 W/m2, and a solar spectrum filtered by 1.5 layers of atmosphere. In a factory, these settings can be easily replicated, but outside conditions are not the same (Zeki.A.darwish et al., 2013).

Solar radiation & temperature

The performance of the PV array is affected by the climate; however, this influence varies from place to place based on topographical and geographical factors.

As demonstrated by equations (2-4) and (2-5), the open circuit voltage and short circuit current are dependent on variables such as temperature and sun irradiation.

$$V_{os} = \frac{KT}{q} \ln \frac{I_{sc}}{I_0} \tag{2.4}$$

$$I_{sc} = bH \tag{2.5}$$

where is a constant that is dependent on the semiconductor junction's properties and includes the electronic charge, the Boltzmann constant, the saturation current, the absolute temperature, the intensity of the incident light, and so on (Ike, 2013). The intensity of the irradiance determines how much energy photovoltaic systems create. The features of the IV and PV curves are altered by the sun irradiation. The output produced power grows as the I_{sc} and V_{os} rise in turn.

On the other hand, the module temperature has a reversely proportional operational dependence. When the operational temperature rises, a PV module's power output and electrical efficiency both fall linearly. The temperature has a major impact on output voltage. Researchers discover that while the output power rises with increasing irradiance intensity, the current grows somewhat, then declines, and the MPP decreases as cell temperature rises. The degree of exposure of the array to incident solar radiation determines the amount of energy generated. On the other hand, the energy generated is directly proportional to the irradiance intensity, and its decrease is quickly impacted by the ambient temperature.

According to studies, temperatures exceeding 40.4 degrees Celsius cause the PV system to work less well. They illustrated the impact of temperature and radiation intensity. It was determined that photovoltaic energy efficiency rises with radiation intensity and falls with operational temperature. Based on the data, it was shown that the output power is directly proportional to the radiation intensity and that the conversion efficiency steadily declines with cell temperature (Al-Bashir et al., 2020).

Dust

Air pollution is the state of the atmosphere when certain pollutants are present in amounts greater than their typical ambient values. The effects of air pollution are detrimental to people, animals, plants, and materials (Zeki.A.darwish et al., 2013). These materials may be man-made or naturally occurring, like dust. The term "dust" or "soiling effect" describes the grainy particle contamination of PV modules' optical surfaces. Apart from the buildup of dust, soiling also involves the pollution of surfaces by plant materials, salt, bird feces, soot/smoke, and the development of biological breeds (Babatunde et al., 2018).

Dust is a significant environmental element that momentarily but substantially reduces the output energy produced by PV modules. Research has demonstrated the substantial impact dust has on PV system performance. The reduction in glass cover transmissivity and spectral sensitivity caused by an increase in dust collection rate lowers PV performance. For 12.5 g/m^2, 25 g/m^2, and 37.5 g/m^2 of dust density, respectively, there is a 10%, 16%, and 20% decline in PV module conversion efficiency. Dust might be less of an impact on PV modules with regular cleaning (Babatunde et al., 2018).

Aging

Aging is the reduction in a PV module's efficiency brought on by a loss in its capacity to convert sunlight into electrical power over time. It may be stated using the idea of the rate of degradation, which is the gradual reduction in the amount of electrical energy produced (Kazem et al., 2020).

PV systems are exposed to harsh weather conditions outside, including snow, rain, dust, high humidity, extreme highs and lows, bird droppings, partial shade, hotspots, and corrosion. All of these factors have an impact on the PV panels' operational life, which leads to an uneven distribution of the PV modules' aging (Zaraket et al., 2019).

After seven years of continuous operation, the impact of aging on the 1.4 kW GCPV system was assessed in Sohar, Oman. Aging has an impact on every aspect that has been researched. For instance, losses from system losses (Ls) and array capture loss (Lc) grew to 6.95% and 6.13%, respectively, as a result of aging after seven years of continuous operation. Moreover, throughout this time, the average capacity factor dropped to 4.91%. The output rate fell by 5.38% as well. Seven years of continuous operation resulted in a 6.3% loss in system efficiency and a 5.88% decrease in PV module efficiency. This implies that the efficiency of both systems declined at a pace that was less than 1% for every year of operation. The summer months create a higher rate of degeneration because of the high temperatures brought on by strong solar radiation and very hot ambient air (Kazem et al., 2020).

Tilt angle

The angle at which the solar energy is tilted on its surface with respect to the horizontal plane and the azimuth angle (γ) of the PV modules are the primary determinants of the solar energy converted into solar PV panels. The azimuth angle shows the position of the earth with respect to the north-south axis. In order to determine the ideal tilt angles for the PV panel to achieve maximum output, it is necessary to comprehend the other angles linked to solar radiation. The solar PV panel's peak power production, economic value, overall energy production, rate structures, electricity market pricing, and other factors are all impacted by the azimuth and tilt angle. The angle formed between a vertical line on Earth's surface and the sun is called the zenith angle (θ). Equation (2-9) is used to compute the angle θ.

$$\cos\theta = sin\varphi\ sin\delta + cos\varphi\ cos\varphi\ cos\omega \tag{2.6}$$

where δ is the solar declination angle, or the angle between the line connecting the earth's center to the sun and the corresponding projection on the equatorial plane, and ω is the hour angle in local solar time. The location latitude, or φ, is the angle formed by the projection of a line on the equatorial plane and the radial line from the place to the earth's middle. Some of the countries and cities that are often studied are Izmir, Turkey (0°–61°), Malaysia (−17.16° to 29.74°), Singapore (0.11°–25°), Austria and Germany (10°–35°), India (30°–32°), Egypt (20°–30°), Saudi Arabia (8°–55°), several US locales (23°–40°), China (5°–10°), etc. These are some of the optimal tilt angles on a monthly basis. The frequent tilt angles found are as follows, based on extensive research on the best tilt angles using various techniques. When studied using mathematical, computational, experimental, and a combination of three approaches in different locations around the world, the optimal tilt angles recorded on a monthly basis range from −17.16° to 64°, −22.5° to 55°, 13° to 61°, and −6.5° to 100°(Yunus Khan et al., 2020).

2.6.8. Some optimization and control techniques used with MPPT technology to improve PV energy efficiency.

Perturb-and-observe (P&O) algorithm

The Perturb & Observe method has been widely utilized since it is simple to develop, as shown by the flowchart in Figure 2.21. Until the operating point converges at the Power Point Tracking (MPP), this observation and perturbation procedure is ongoing.

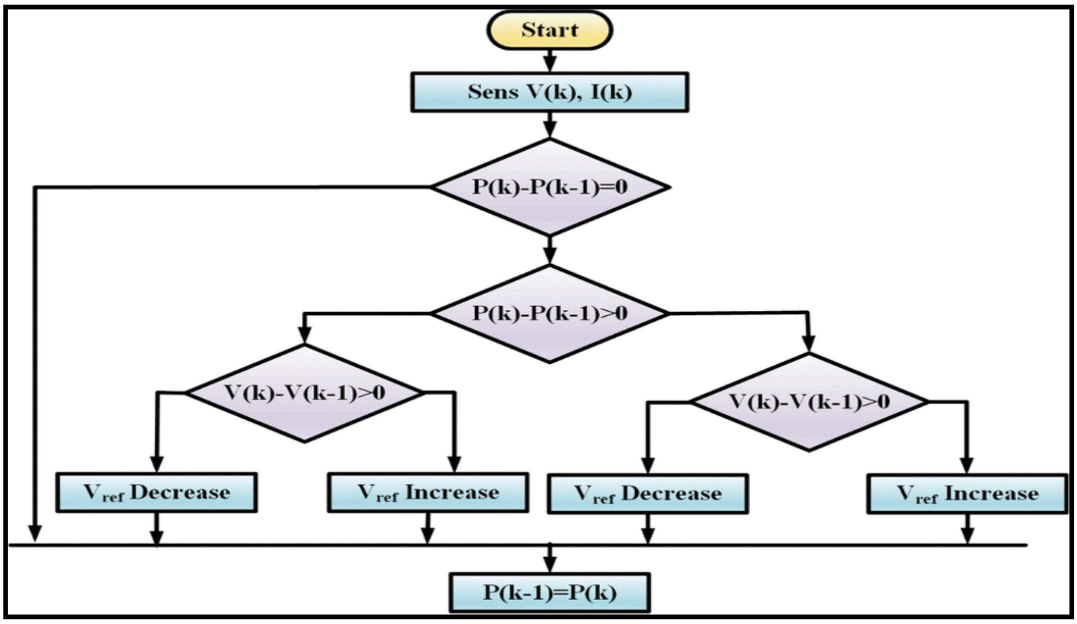

Figure 2.21. Flowchart of the P&O algorithm (Subrata et al., 2019)

The power and voltages of time (K) and the sample at a time (K-1) are compared in order to estimate the time to reach MPP. A slight variation in voltage alters the power of the solar panel; if the power fluctuates in a positive direction, the voltage fluctuation continues in the same direction. A negative delta power, on the other hand, indicates that the MPP is far away and that more perturbation is needed to get close to it. In this manner, the whole PV curve is examined through minor adjustments to identify the MPP that accelerates the algorithm's reaction time. On the other hand, steady-state oscillations around the MPP are produced if the perturbation magnitude is increased. To address the reaction time issue and steady-state oscillations, several academics have suggested changes to the P&O algorithm (Kamran et al., 2020).

Incremental conductance (IC) algorithm

The technique of IC finds widespread use because of its exceptional flexibility and precision, especially in the face of fluctuating meteorological circumstances. It is directly based on fluctuations in power (Sivakumar et al., 2015). The MPP is located by looking for the P-V curve's peak, and the slope of the curve is found via the IC procedure. Instantaneous conductance I/V and IC dI/dV are used by this approach for MPPT. In other words, (2.7) shows that the PV module functions at the MPP, whereas (2-8) and (2-9) show that it operates at the P-V curve's left and right sides, respectively. This relationship between the two values, as expressed in (2-7)–(2-9), can be used to determine the location of the PV module's operating point in the P–V curve.

$$\frac{d_i}{d_v} = -\frac{I}{V} \tag{2.7}$$

$$\frac{d_i}{d_v} > -\frac{I}{V} \tag{2.8}$$

$$\frac{d_i}{d_v} < -\frac{I}{V} \tag{2.9}$$

The following formulas stem from the idea that the P-V curve's slope at MPP equals zero:

$$\frac{d_p}{d_v} = 0 \tag{2.10}$$

Rewriting (2-9) yields the following equation:

$$I + V\frac{d_i}{d_v} = 0 \quad (2.11)$$

The MPPT controller measures the voltage and current of the PV module, and (2.11). is utilized in the IC method to identify the MPP.

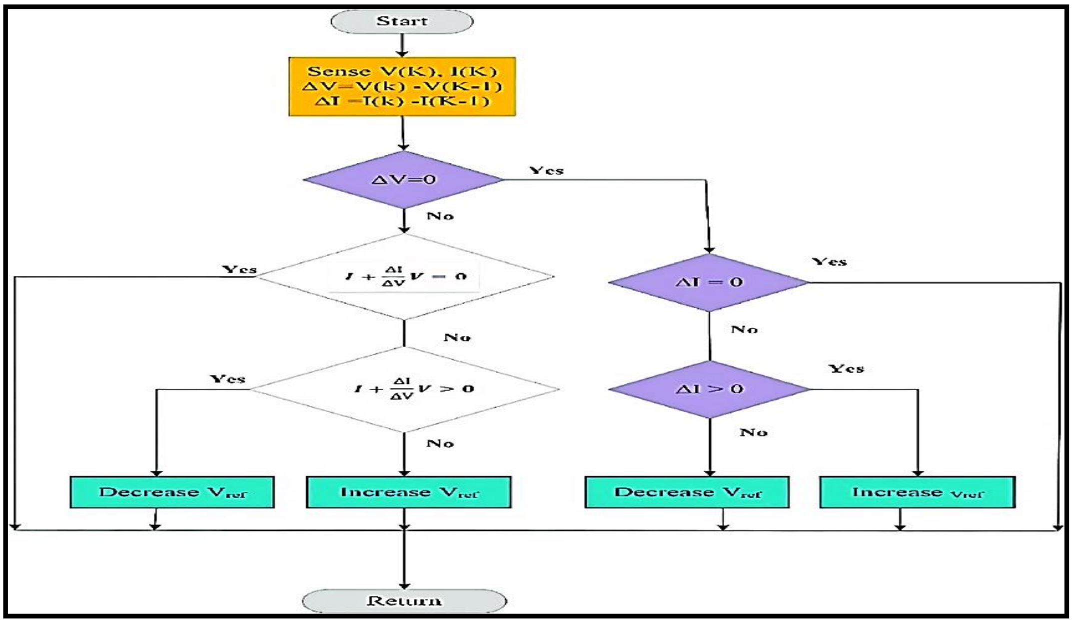

Figure 2.22. Flowchart of the incremental conductance algorithm (Abdullah et al., 2023)

The duty cycle of the converter must be lowered if (2-7) is satisfied and vice versa if (2-8) is met; however, if (2-10) is satisfied, the duty cycle remains unchanged (Shang et al., 2020).

3. POWER SYSTEM COMPUTATIONAL REPRESENTATION (MODELLING AND SIMULATION)

3.1. Introduction

This chapter deals with the modeling and simulation of the power system (photovoltaic grid) shown in Figure 3.1. which consists of a modified IEEE 13 bus standard electrical power system connected to a PV system. It first deals with the modeling and simulation of the PV system and explains the characteristics of the PV array used in this system, in addition to explaining the effect of solar radiation and temperature on it. To take advantage of the maximum power generated by the PV array, it is necessary to discuss the solar system's MPPT control algorithm. Following that, it will discuss the modeling and simulation of the power system (modified IEEE 13 bus system), the system's effects in the event of a fault or increased electrical loads, and, lastly, the integration of the two systems (photovoltaic system and modified IEEE 13 bus system) to describe and track the photovoltaic system's contribution to voltage stability.

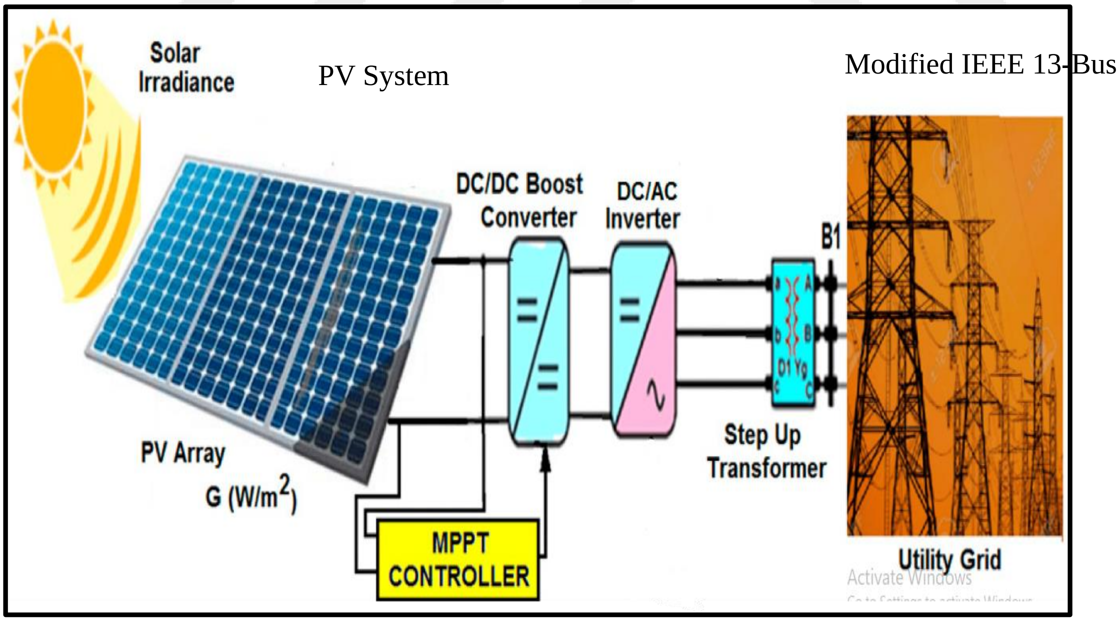

Figure 3.1. Schematic diagram of the proposed system circuit

3.2. IEEE standard grids

With governments pushing for their use and premium feed-in tariffs created internationally, the number of applications for wind, solar, and other renewable energy sources will rise quickly. Distributing systems that incorporate solar PV systems are among the renewable energy sources with the quickest pace of growth. Some technological considerations for the integration of renewable energy must be made as dispersed generating resources become more prevalent in the grid. The intermittent nature of renewable energy sources means that their widespread integration into power grids might have a significant impact on how distribution networks function. It is thus necessary to design suitable safeguards and preventative measures in order to guarantee the dependability and safety of the power supply (Wu et al., 2017).

PV integration standards and recommendations should include operational safety, grounding, protection against islanding, warning signals, access control, insulation, and other factors. In order to guarantee system safety and dependability, several nations and worldwide organizations have created a variety of standards or rules. While some standards exclusively address the integration of PV sources, others include the integration of all dispersed generators, including PV sources (Spooner and Harbidge, 2001), (Dang et al., 2011), (Moreno-Munoz et al., 2009).

The evolution of distributed power production may be influenced by a number of rules or regulations that control how distributed generators connect to power grids. Among these international standards, IEEE 1547 and IEC 61727 are the most commonly accepted and utilized.

Compatibility between solar systems and public networks is the focus of IEC 61727, which addresses utility-interconnected photovoltaic power systems with a rated capacity of less than 10 kVA that are connected to a low-voltage utility network. The IEEE 1547 standard includes tests and technical requirements for connecting dispersed resources (DR) with a maximum value of 10 MVA.

Regarding the interconnection of PV systems, there are several national standards and guidelines in addition to the previously listed international standards. Another international standard for photovoltaic systems is IEEE 929, which covers utility system operation, equipment protection, personnel safety, and power quality. It offers useful guidelines for the operation of compatible small photovoltaic systems under 10 kW when connected to a power system.

Specific criteria are outlined in some standards for PV, DR, or distributed generator (DG) integration alone. Certain nations or areas are not covered by these requirements. International laws include IEEE Std 929, IEEE 1547, and IEC 61727. Numerous nations, such as the United States, have integrated or adjusted these global norms into their domestic policies. IEEE 1547 is now the most extensively used standard for connecting various sorts of DR.

Nonetheless, several nations have published additional criteria for PV integration. For instance, the German VDE-AR-N 4105 is a crucial guideline for PV integration because Germany is a leading PV market. VDE-AR-N 4105 is used for PV integration in several European nations and electricity-generating firms, occasionally with changes. These published standards or recommendations offer broad specifications for PV integration; local power production businesses in a given nation can adjust them to suit their localities (Wu et al., 2017).

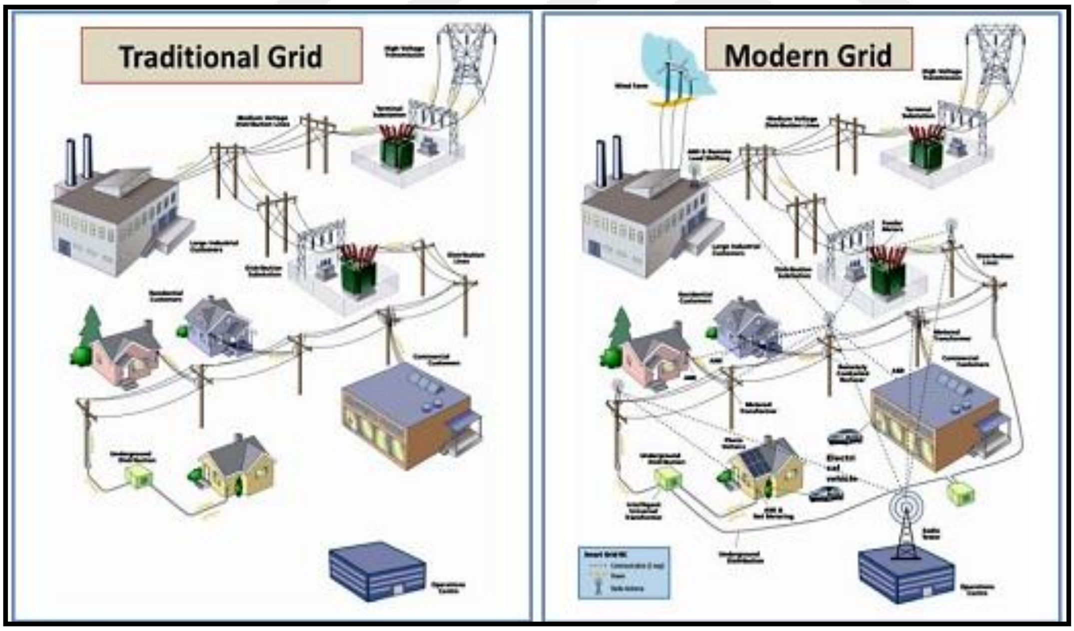

Figure 3.2. The transition from a conventional to a modern electrical grid with a two-way power flow (Henderson et al., 2017)

A new standard was unveiled by IEEE to assist utilities in utilizing excess power from nonconventional sources: Electric power systems and distribution resources are connected through the IEEE 1547 2003 Standard. For electric power systems (EPSs or electric grids), the standard outlines technical requirements for integrating with distributed generators, including fuel cells, PVs, microturbines, reciprocating engines, wind generators, large turbines, and other local generators.

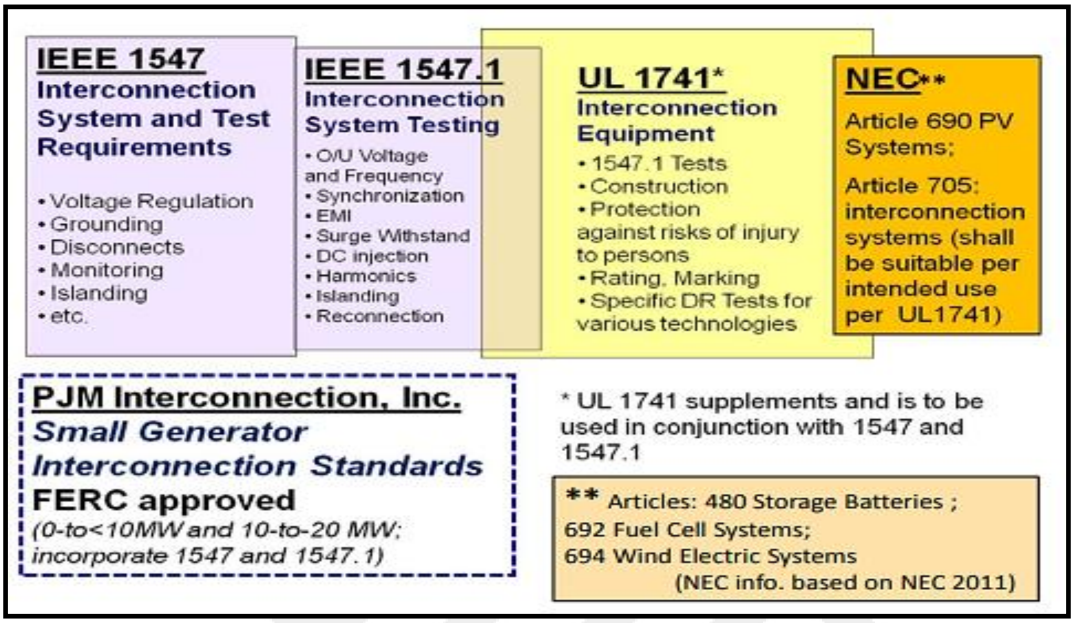

Figure 3.3. IEEE 1547 standards use in the United States (T. Basso, 2014)

Adherence to IEEE 1547 facilitates the preservation of the interconnected systems' dependability, quality, and safety. Given how widely microgeneration is connected to distribution networks, this is very relevant. The technical requirements and testing for the interconnection itself are the main topics of the 1547 standard. It offers specifications about the interconnection's functionality, operation, testing, safety, and upkeep. In addition to the criteria for design, manufacturing, installation evaluation, commissioning, and periodic testing, it also contains general requirements, power quality, islanding, reactivity to abnormal conditions, and test specifications. For the interconnection of distributed resources (DR), including synchronous machines, induction machines, and power inverters/converters, the defined specifications are universally necessary and will be sufficient for the majority of installations. All DR technologies that have an aggregate capacity of 10 MVA or less at the common coupling point linked to EPSs at standard primary and/or secondary distribution voltages are subject to these standards. The major focus of the 1547 standard is the installation of distributed resistance (DR) on radial primary and secondary distribution systems, although primary and secondary network distribution systems are also taken into consideration (T. S. Basso and DeBlasio, 2004).

3.3. Why choose IEEE 13-buses

This study's electrical power system is one of the test systems created by the IEEE Distribution Systems Analysis Subcommittee to help field engineers and software developers confirm the accuracy of their research. This study examined the impact of connecting a photovoltaic system to an imbalanced three-phase system in the event of failures and increased loads using the IEEE 13 Bus Distribution Feeder technology.

The properties of this small test feeder with heavy loads connected are intriguing. The grid has a voltage level of 4.16 kV and is short yet substantially loaded. The system comprises 13 buses connected by 10 overhead and underground lines, 200 kVar parallel capacitor banks, a generator, a secondary voltage-changing voltage regulator, a Y-configuration 4.16 kV/480 V in-line transformer, distributed loads, an unbalanced spot, and a breaker. The modeled microgrid is integrated via this network (Mohammed, 2022), (Imtiaz et al., 2021).

It is particularly helpful to utilize a swing generator in place of a generator with preset settings and to eliminate voltage regulators when designing distribution grids. The model is made simpler without sacrificing accuracy in this way. The IEEE 13- Bus Distribution Feeder network's voltage regulator was eliminated in this study due to the potential for voltage level changes caused by renewable DG. Recalculating power flow and adjusting generator settings are unnecessary with a swing generator since it will adjust to the new configuration. The generator can also be directly linked to distribution lines and adjusted to 4.16 kV (Stanisavljevic et al., 2018). As a result, the system was scaled down to 9 transmission lines and 12 buses, as shown in Figure 3.4.

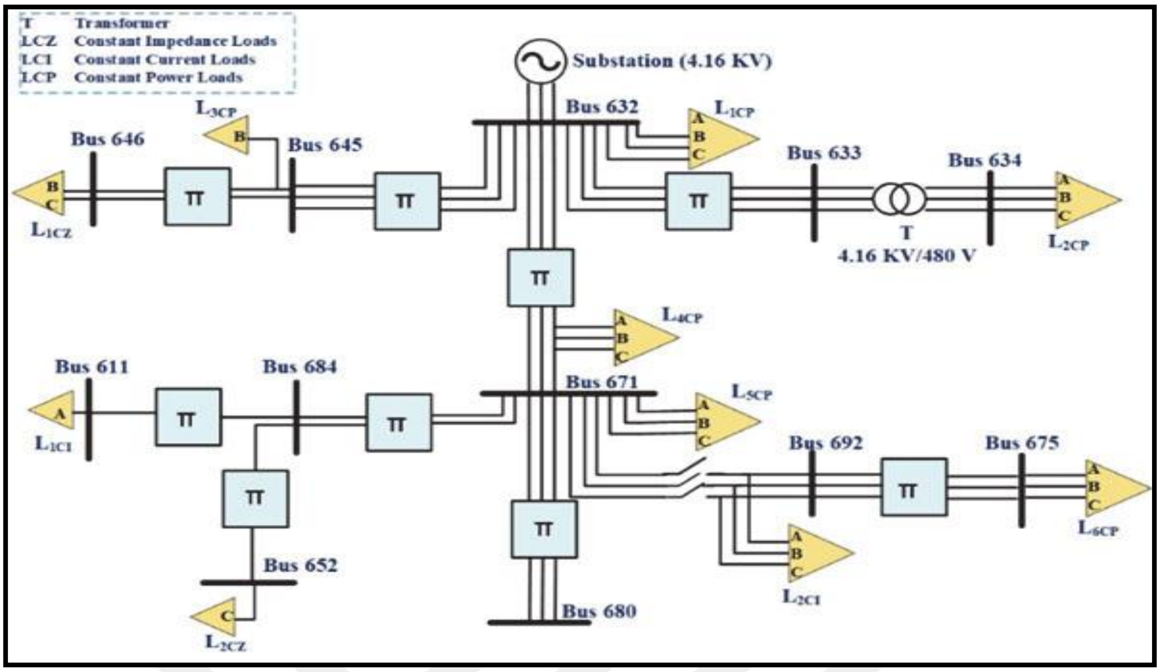

Figure 3.4. Modified IEEE 13-bus distribution feeder

Also, this power system includes unbalanced three-phase loads and single-phase loads. Table 3.1 shows the associated loads in this system. In this study, two PV systems will be added to the standard IEEE Modified Bus13-Feeder Distribution power system to form the system.

Table 3.1. Local load data for the electrical power system Modified IEEE 13-Bus Test System

Bus	Load (Model)	Phase A		Phase B		Phase C		P Total (KW)	Q Total (KVAR)
		P(KW)	Q(KVAR)	P(KW)	Q(KVAR)	P(KW)	Q(KVAR)		
632	Y-PQ	8.5	5	33	19	58.5	34	100	58
634	Y-PQ	160	110	120	90	120	90	400	290
645	Y-PQ	0	0	170	125	0	0	170	125
646	D-Z	0	0	230	132	0	0	230	132
652	Y-Z	128	86	0	0	0	0	128	86
671	D-PQ	385	220	385	220	385	220	1155	660
671	Y-PQ	8.5	5	33	19	58.5	34	100	58
675	Y-PQ	485	190	68	60	290	212	843	462
692	D-I	0	0	0	0	170	151	170	151
611	Y-I	0	0	0	0	170	80	170	80

3.4. Flow chart of the work

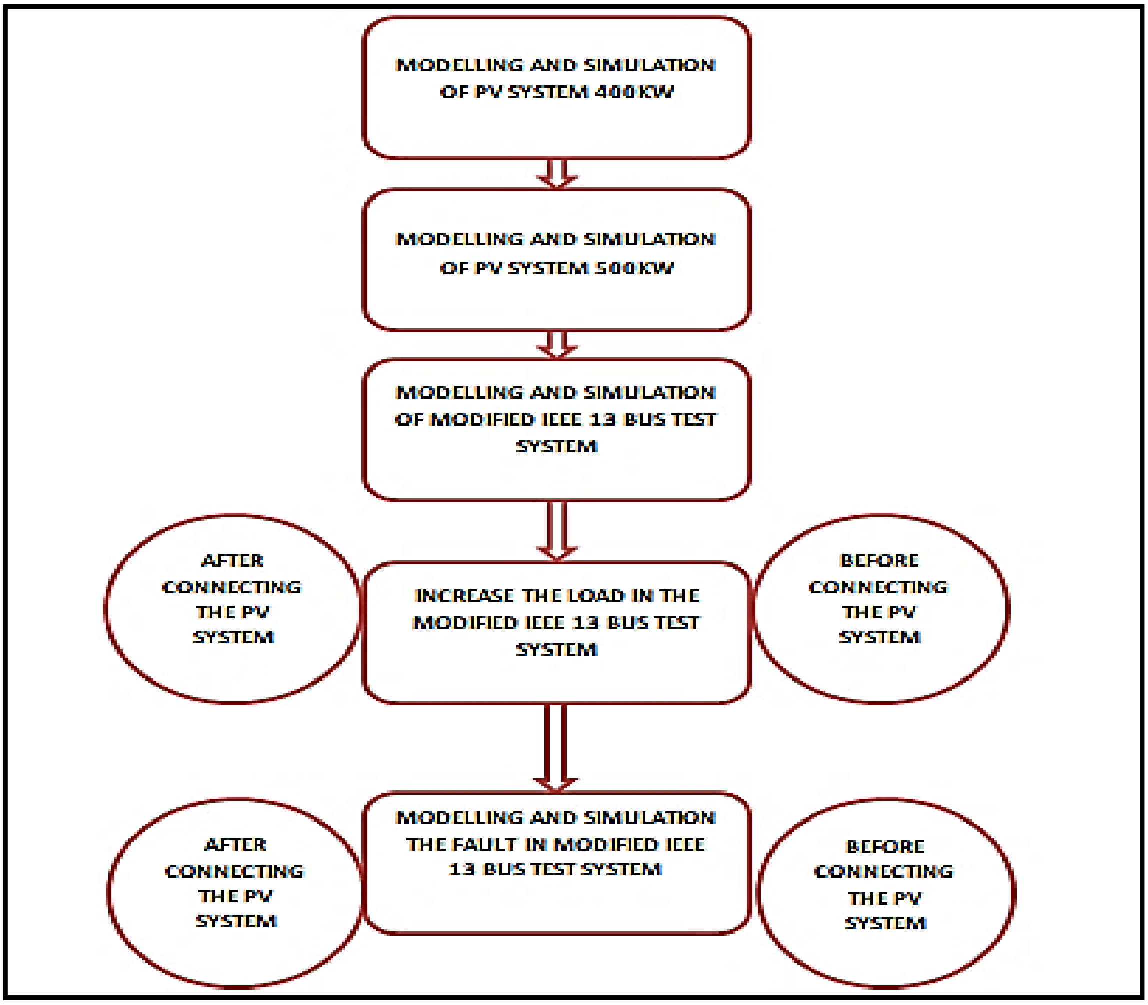

Figure 3.5. Flow chart of the work

This flowchart illustrates the steps that are carried out during this work. Using MATLAB/Simulation at first, a 400 kW PV system is designed, then a 500 kW PV system is designed. After that, a modified IEEE 13 bus system is designed, the load on some buses is increased, and the effect of the increased load on the voltage of those buses is observed, and then the PV system is integrated and its impact is shown to improve the voltage. Finally, a fault is made between one of the phases and the ground in the modified IEEE 13 bus system. How the voltage is affected as a result is observed, then the PV system is integrated to improve the voltage.

3.5. Modeling and Simulation of PV system (400KW & 500KW)

There are two types of grid-connected solar PV systems:

1. Single-stage Power Conversion System.
2. Double-Stage Power Conversion System.

In a single-phase power conversion system, the inverter regulates the MPPT systems as well as the voltage and current delivered to the grid. A transformer is used to increase the voltage, which makes the system heavier and larger. However, low input voltage and poor power quality are problems with the inverter design. Single-phase power conversions can be avoided in these situations.

This study used a two-stage power conversion system, which eliminated the requirement for a transformer during power conversion by using a DC-DC converter to raise the PV array's voltage in the first stage.

Additionally, a MPPT algorithm was used during the DC-DC conversion step to guarantee the PV array's maximum power extraction under all circumstances. An AC/DC inverter, which regulates the power transfer by regulating the grid current by the grid requirements and synchronizing the grid, connects the enhanced DC-DC converter to the electrical system.

This study designed a two-PV system. Four arrays of PV panels connected in parallel make up the first system, which can produce 400 kW of power effectively. The MATLAB program's representation of it is displayed in Figure 3.5.

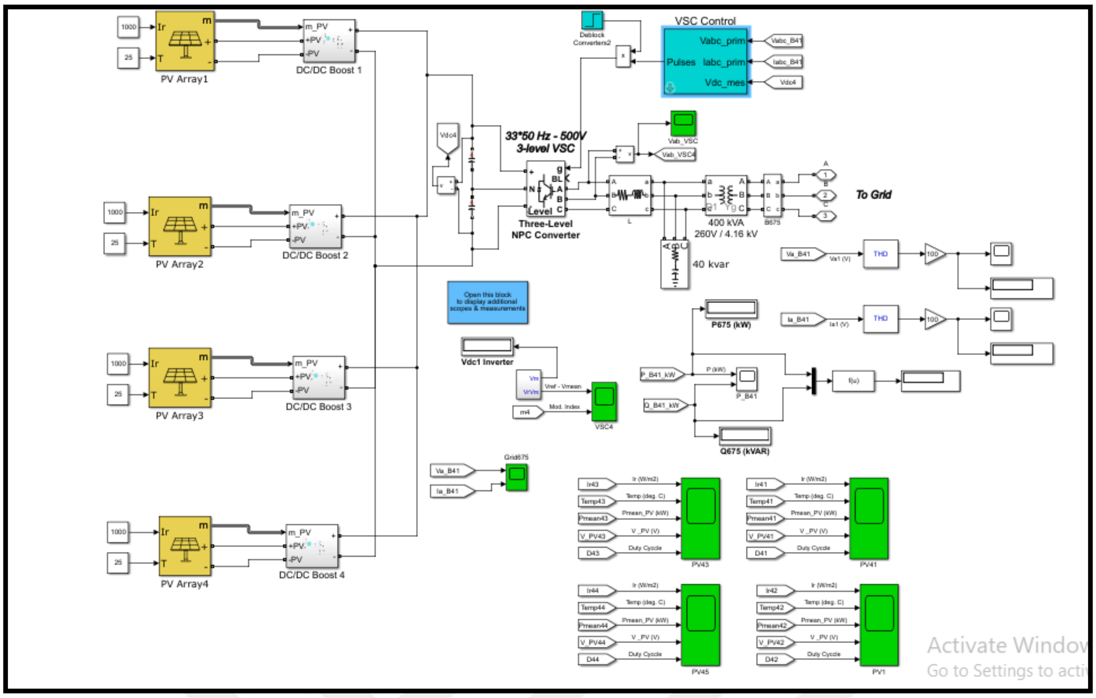

Figure 3.6. 400 kW PV system

Five arrays of PV panels connected in parallel make up the second system, which produces 500 kW of electricity, as the MATLAB software illustrates in Figure 3.7. The Sun Power SPR-305E-WHT-D PV panel array was used to design the two systems. Each array produces 100 kW of electrical power, and all arrays were configured to function under standard test conditions (STC), which include 1000 W/m2 of solar radiation and 25°C.

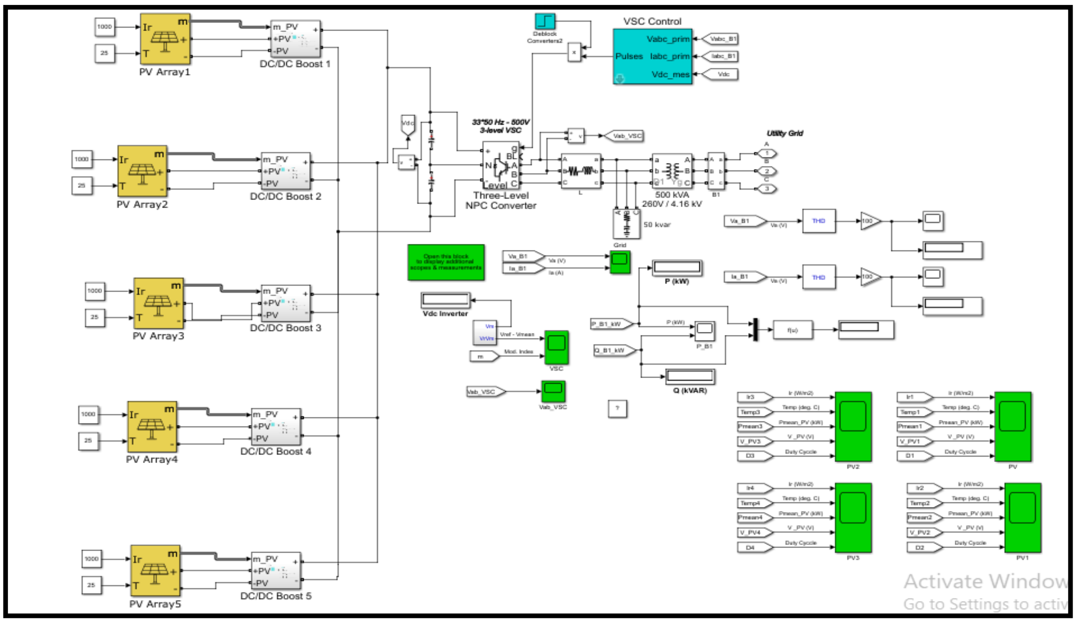

Figure 3.7. 500 kW PV system

The (V-I) and (V-P) characteristics of the suggested PV array model at various light radiation ratios and a temperature of 25°C are displayed in Figure 3.8. Temperature and radiation ratio are key determinants of the (V-I) characteristics, and the impacts of both should be considered while designing the photovoltaic system.

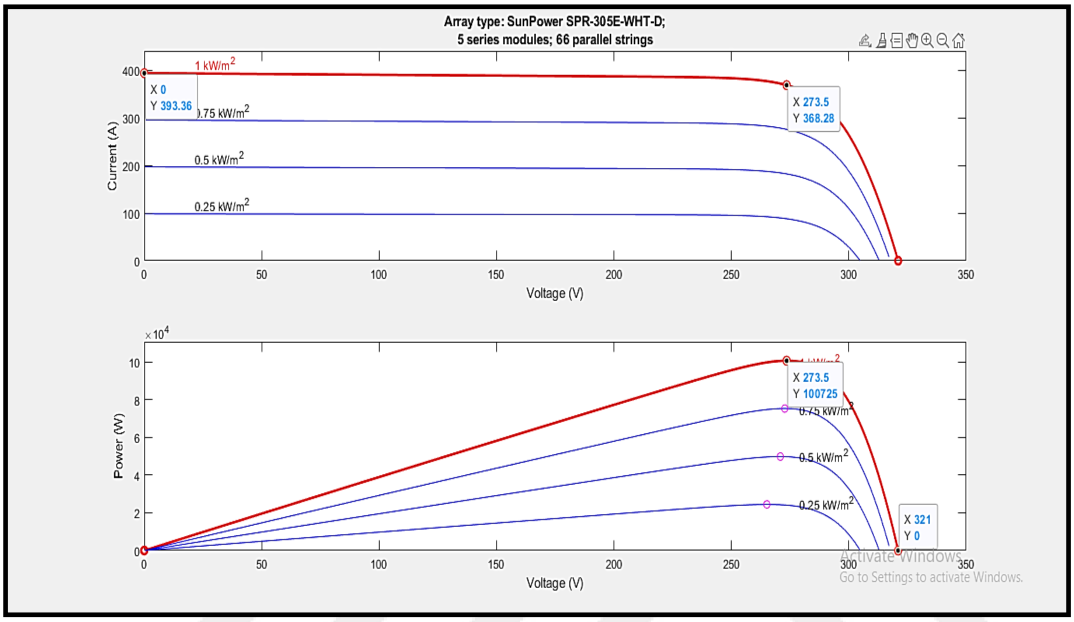

Figure 3.8. The suggested PV array model's V-I and V-P characteristics at various irradiations(25°C)

It is clear from Figure 3.8. that the effects of the variation in solar radiation are mostly on the PV current, as the more solar radiation, the more current increases. At the same time, it is noted that the effect of this on the voltage is much less. It is also stated that with the increase in solar radiation, the generated photovoltaic energy increases due to the rise in current.

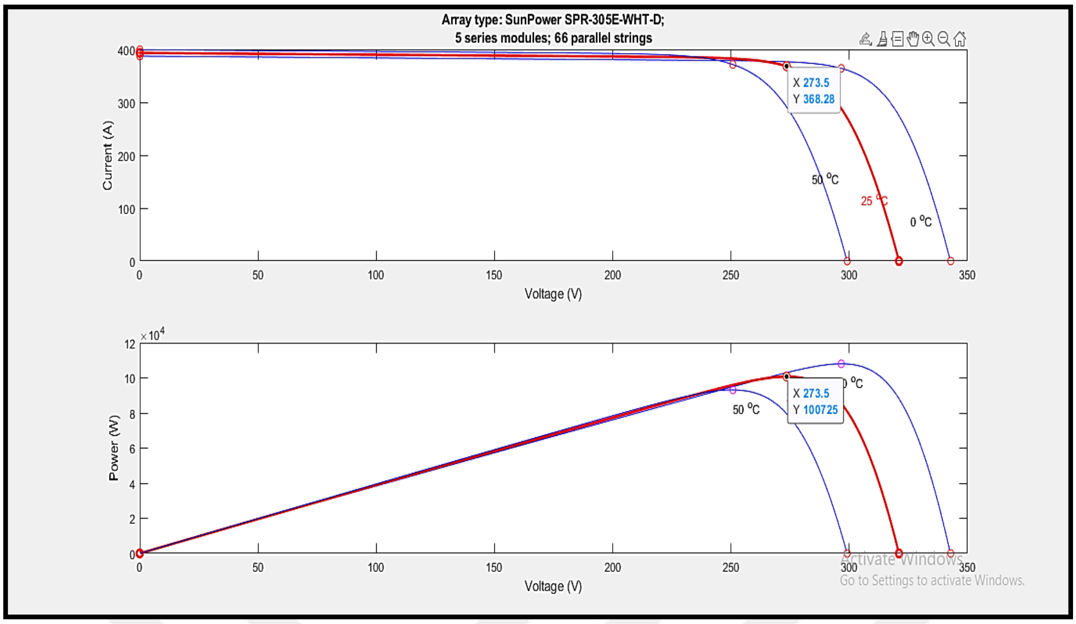

Figure 3.9. The suggested PV array model's V-I and V-P properties at various temperatures.

It is clear from Figure 3.9 that the effects of the temperature variation are mostly on the PV voltage, as the higher the temperature, the more voltage decreases. At the same time, it is noted that the effect of this on the current is much less. It is also stated that with the increase in temperature, the generated photovoltaic energy decreases due to the decline in voltage. The maximum power point obtained for the irradiance level of 100.725 kW is 1000 W/m² of the proposed PV array under standard test conditions (STC) of 1000 W/m² of solar radiation at 25°C. It is shown in Table 3.2.

Table 3.2. PV module specifications (Sunpower SPR-305E-WHT-D) (Othman and Al-Yozbaky, 2023)

(PV Module) Parameter	Value
Maximum Power (P_{MAX})	305.226 W
Voltage at Maximum Power Point (V_{mp})	54.7 V
Current at Maximum Power Point (I_{mp})	5.58 A
Open Circuit Voltage (V_{oc})	64.2 V
Short Circuit Current (I_{sc})	5.96 A
Temperature Coefficient of V_{oc} (K_v)	-0.2727 V/°C
Temperature Coefficient of $I_{sc}(K_i)$	0.061745 A/°C
Diode Saturation Current (I_o)	6.3076*10^{-12} A
Shunt Resistance (R_{sh})	393.2054 Ω
Series Resistance (R_s)	0.37428 Ω
(PV Array) Parameter	Value
Total No. of Modules in Series (N_s)	5
Total No. of Modules in Parallel (N_p)	66
Maximum Power (kW) = N_s * N_p * P_{MAX}	100.724 kW
Voltage at Maximum Power (V_{mp}) = V_{mp} * N_s	273.5 V
Current at Maximum Power (I_{mp}) = I_{mp} * N_p	368.28 A
Open Circuit Voltage (V_{oc}) = V_{oc} * N_s	321 V
Short Circuit Current (I_{sc}) = I_{sc} * N_p	393.36

3.5.1. Maximum power point tracking technology (MPPT)

According to traditional solar panels, only 30 to 40 percent of solar radiation can be converted into electrical energy. The PV operating point may range from zero to the open-circuit voltage, as can be observed from the I-V curve. The operating point fluctuates with load and does not always remain at the maximum power point. As a result, the system does not always give the load all of the available solar energy. To address this issue, a very straightforward solution is to increase the system's PV module count above what is necessary. However, this will result in higher energy losses and system costs. To find the maximum operating point, a novel kind of power electronic device called MPPT is created to address this issue. By connecting to an MPPT controller, a PV system may find the MPP and maximize the performance of the PV array. This ensures that the PV system will always run at the real MPP. Using the MPPT technique increases the efficiency of the solar panel.

With MPPT technology, the PV module has a non-linear feature with a single maximum power point that is dependent on both cell temperature and radiation intensity. The

Maximum Power Transfer Theorem states that when the source impedance and load impedance are equal, a circuit's power output is maximized, and the greatest amount of power is transmitted from the source to the load. On the source side, a boost converter is connected to a solar panel in order to raise the output voltage. By appropriately modifying the boost converter's duty cycle, the source and load impedances are matched. This is accomplished by modifying the boost DC-DC converter's duty cycle. To get the most power out of the PV array, the duty cycle of the boost DC-DC converter must be adjusted to account for changing weather conditions. The duty cycle is also described as the ratio of the on switch time to the entire switching period (Gomathy, 2012), (Kamarzaman and Tan, 2014), (Saidi and Benachaiba, 2016).

With the use of MPPT, PV modules may be operated in a way that modifies their electrical working point, enabling them to generate the most power possible (Banu et al., 2013). Solar panels have a very low efficiency. The output power of the solar array will rise together with the levels of irradiation, as well as the PV current and voltage. Conversely, if the temperature of the cells rises while the intensity of the solar radiation remains constant, the PV array's voltage will sharply drop, causing a significant fall in the array's output power. Thus, the MPPT algorithm is utilized to increase solar panel efficiency in a variety of environmental circumstances (Mohamed and Abd El Sattar, 2019).

A control signal that feeds the IGBT switches in the DC-DC converter is generated by the PV array's output voltage and output current, which are the two inputs to the MPPT controller (Figure 3.9.).

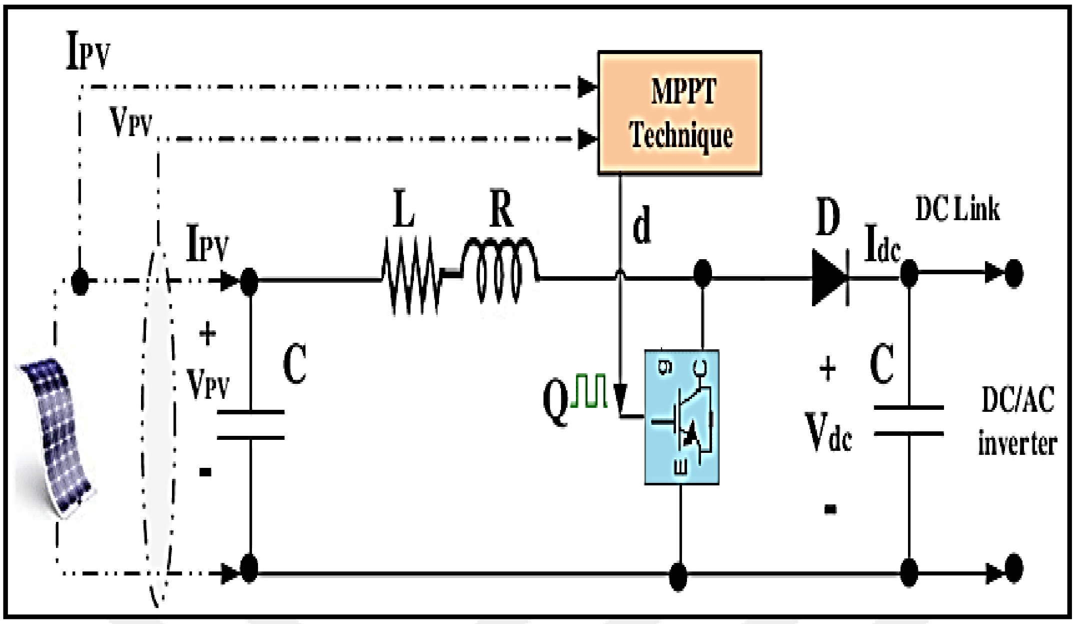

Figure 3.10. An MPPT-controlled DC-DC boost converter circuit diagram (V. Kumar and Singh, 2021)

3.5.2. The perturb and observe (P&O) algorithm

The most popular algorithms used for MPPT modeling are the Incremental Conductance (IC) and Perturb and Observe (P&O) algorithms because of their straightforward architectures. Even while the IC method can monitor changing circumstances faster than the P&O algorithm, it produces less consistent output power because it oscillates around the Maximum Power Point (MPP) and necessitates a more sophisticated and costly MPPT P&O control unit (Hlaili and Mechergui, 2016).

The P&O algorithm's fundamental idea is to disturb the solar PV operating points that correlate to the sign of the most recent PV power increase. With this approach, the algorithm commands the PV module's operating voltage to adjust in response to any perturbation in the voltage ΔV. The P&O will decide whether to raise or lower the operating voltage by ΔV following the output power observation process (Alik et al., 2015).

Since there are no sudden shifts in the climate, the P&O technique, which is depicted in Figure 3.10, is introduced in this study. Apart from being the most widely used MPPT algorithm for PV generator control, it also has a simple design, is inexpensive, is easy to implement, has fewer parameters, and may be improved. It could lead to a high degree of effectiveness (Elgendy et al., 2012).

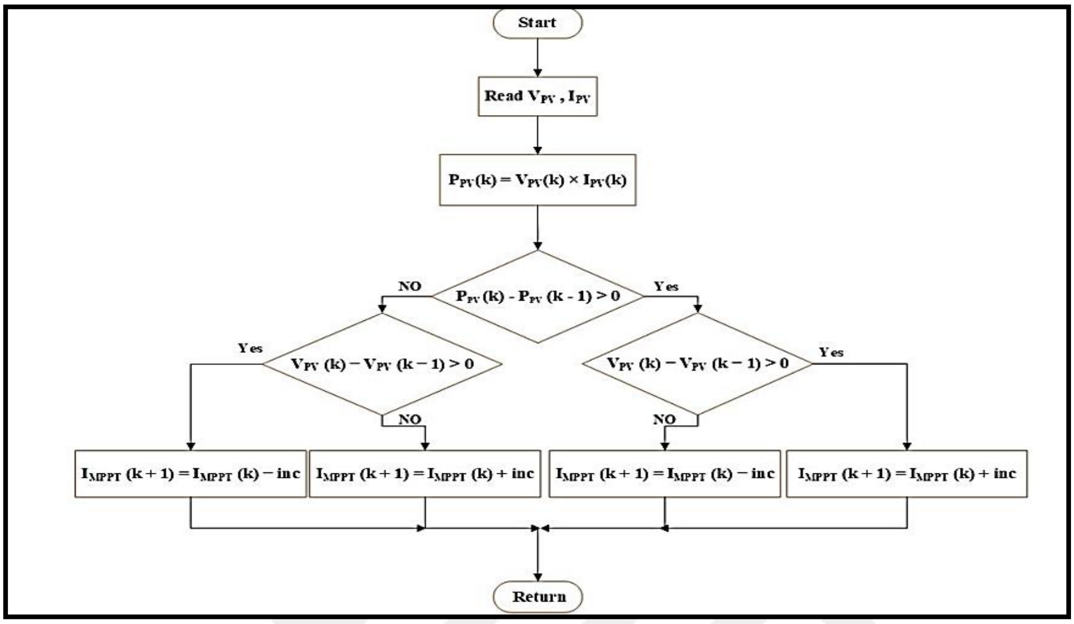

Figure 3.11. MPPT P&O technology flow chart

This algorithm's foundation is examining the relationship between the voltage and the PV module's output power. Using this method, the PV module's operational voltage is regularly perturbed, and the PV output power is compared to the preceding perturbation cycle (Sahnoun et al., 2013).

If the change in power P that results from a slight increase in the PV module's operating voltage is positive, we go in the direction of the MPP and keep perturbing in that direction. We stray from the MPP's direction and need to alter the perturbation's sign if P is negative. However, this algorithm only uses one sensor—the voltage sensor—to detect the PV array's voltage, making it easier to construct and lowering implementation costs. Although this algorithm has a significantly lower time complexity, it continues to perturb as it approaches the MPP without stopping. This algorithm has a significantly lower temporal complexity, but it continues to perturb in both directions after approaching the MPP without stopping. When this occurs, the algorithm is extremely close to the MPP, and we may either utilize a waiting function, which increases the algorithm's time complexity, or choose an appropriate error threshold.

The P&O algorithm measures the solar array's output voltage and current to determine the actual power produced by it, as seen in Figure 3.11. Following that, it will determine whether or not ΔP = 0. The present operating point will be the maximum power point (MPP) if this requirement is satisfied. A second criterion, ΔP > 0, will be checked if this one is not satisfied. If this is true, it will verify that ΔV > 0. It shows that the operational point is on the left side of the MPP if this criterion is satisfied. In the event that this requirement is not satisfied, the operating point is on the right side of the MPP (ΔV > 0). This procedure is continually carried out. The MPP is reached by repeating this method repeatedly. The P&O algorithm, thus, always strikes a balance between the sampling rate and the increments (Patel, 2016).

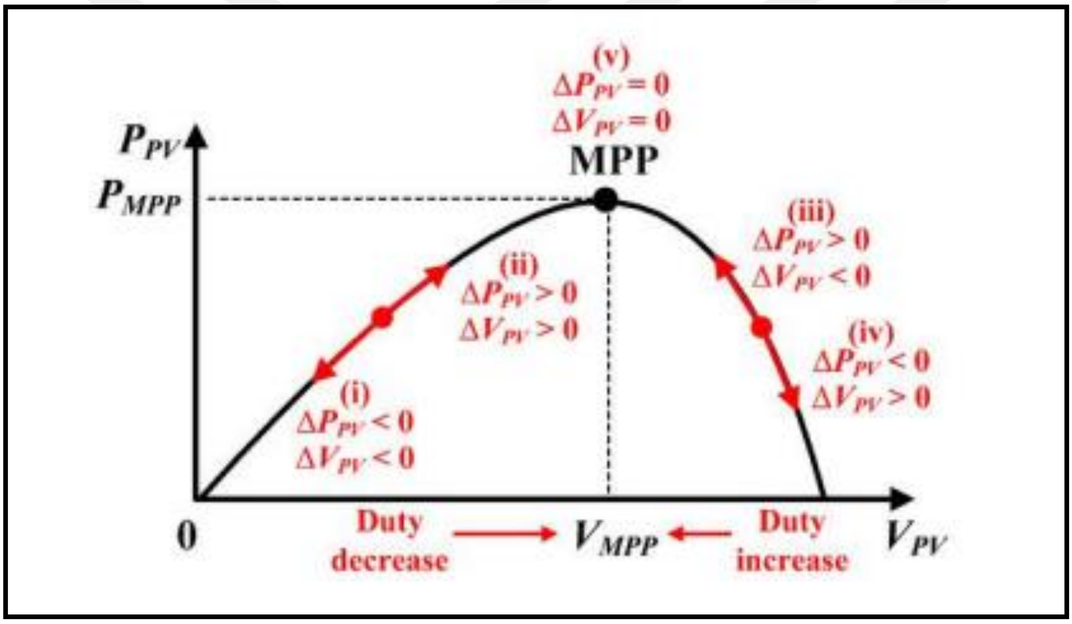

Figure 3.12. Principle of operation for the hill-climbing and P&O algorithms (Lee and Yun, 2019)

3.5.3. DC-DC boost converter

Among nonisolated step-up converters, the boost converter has significant importance. An output DC voltage higher than the input DC voltage of a power converter is called a boost converter. A diode and a transistor are the two semiconductor switches that make up this type of switching-mode power supply (SMPS), together with at least one energy storage component. Adding filters to a converter's output to enhance performance often involves combining inductors and capacitors. An increase in DC voltage from a fixed low level to a desired high level is accomplished using a boost converter, which is a DC-TO-DC converter (Ismail et al., 2010).

A lot of regulated switch mode DC power sources employ DC/DC converters. Since the PV array provides the unregulated DC voltage that these converters use as input, variations in temperature and radiation will cause the voltage to vary. Even when the input voltage of these converters is fluctuating, the average DC output voltage needs to be adjusted to equal the required value. From an energy perspective, the DC/DC converter's output voltage regulation is accomplished by continuously varying the energy injected into the load and absorbed from the source. This is controlled by the relative lengths of the injection and absorption periods.

Only four external parts are required for the DC/DC boost converter: an output capacitor, an electronic switch, an inductor, and a diode. As a result, the converter can operate in two different modes based on its energy storage capacity and switching time. These two working modes—the continuous conduction mode, or CCM, and the discontinuous conduction mode, or DCM—relate to the scenarios with and without an idle interval, respectively.

The Discontinuous Conduction Mode (DCM) is used for low-power or standby applications, whereas the Continuous Conduction Mode (CCM) is used for efficient power conversion.

<u>The continuous conduction mode (CCM)</u>

- Mode 1 ($0 < t \leq t_{on}$)

When IGBT is turned on at $t = 0$, Mode 1 starts and ends at $t = t_{on}$.

Figure 3.12a. depicts the equivalent circuit for mode 1.

There is a linear ramp up in the inductor current $iL(t)$, which is larger than zero.

Vi is the inductor voltage.

- Mode 2 ($t_{on} < t \leq Ts$)

When the IGBT is turned off at $t = t_{on}$, mode 2 starts, and it ends at $t = T_s$. Figure 3.12b. depicts the equivalent circuit for the mode 2. Until the IGBTs are turned on once more during the subsequent cycle, the inductor current decreases. During this time, the voltage across the inductor is $Vi - Vo$.

Since the inductor voltage's time integral over a single period of time must be zero in a stable state.

$$V_i t_{on} + (V_i - V_o)t_{off} = 0 \tag{3.1}$$

Where;

- V_i : The input voltage, V.
- V_o : The average output voltage, V.
- t_{on} : The switching on of the IGBT's, s
- t_{off} : The switching off of the IGBT's, s

Dividing both sides by Ts and rearranging items yield

$$\frac{V_o}{V_i} = \frac{T_s}{t_{off}} = \frac{1}{1-D} \tag{3.2}$$

Where;

- T_s : The switching period, s.
- D : The duty cycle.

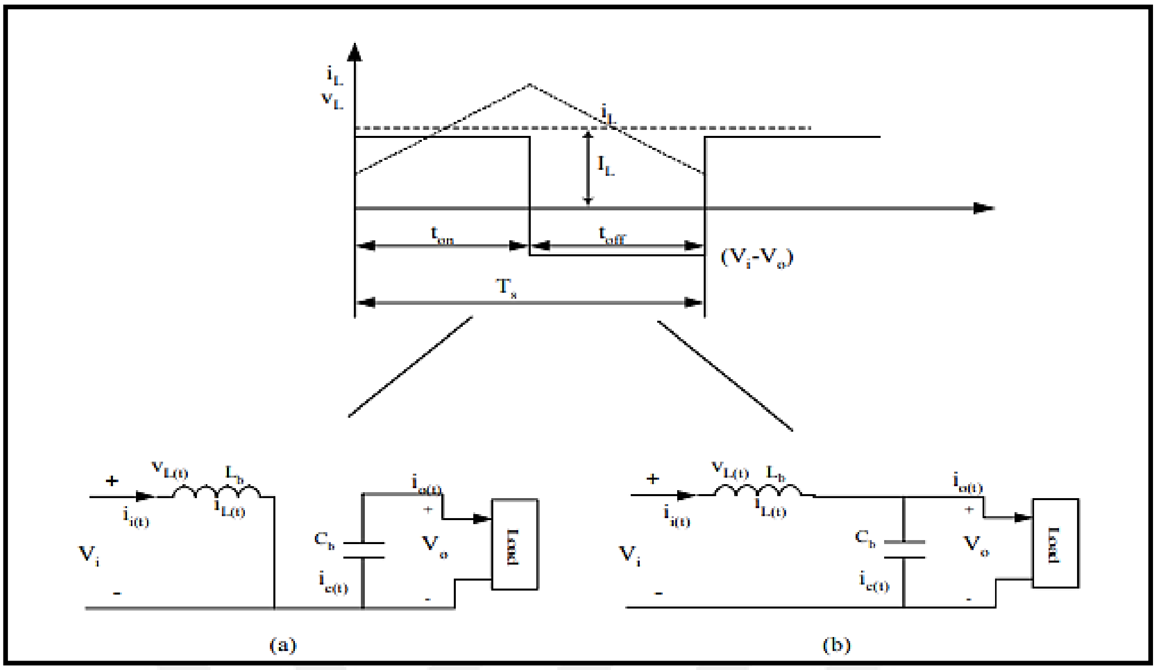

Figure 3.13. Equivalent Circuit for boost Converter in CCM (Hasaneen and Elbaset Mohammed, 2008).

a) Mode 1 $(0 < t \leq t_{on})$

b) Mode 2 $(t_{on} < t \leq Ts)$

V_o is therefore inversely related to $(1 - D)$. It is evident that energy cannot be transferred to the output if the duty cycle, D, is equal to 1. Considering a lossless circuit with $Pi = Po$,

$$I_i V_i = I_o V_o \qquad (3.3)$$

and,

$$\frac{I_o}{I_i} = 1 - D \qquad (3.4)$$

Where;

- I_o : The average output current, Amp.
- I_i : The average input current, Amp.

Discontinuons conduction mode (DCM)

If the current flowing through the inductor becomes zero before the switching IGBTs turn back on, the boost converter is said to be in the discontinuous conduction mode. As seen in figure 3.13., if we set the integral of the inductor voltage over a single time period to zero,

$$V_i D T_s + (V_i - V_o) D_1 T_s = 0 \tag{3.5}$$

Then;

$$\frac{V_o}{V_i} = \frac{D_1 + D}{D_1} \tag{3.6}$$

And

$$\frac{I_o}{I_i} = \frac{D_1}{D_1 + D} \quad \text{since}(P_i = P_o) \tag{3.7}$$

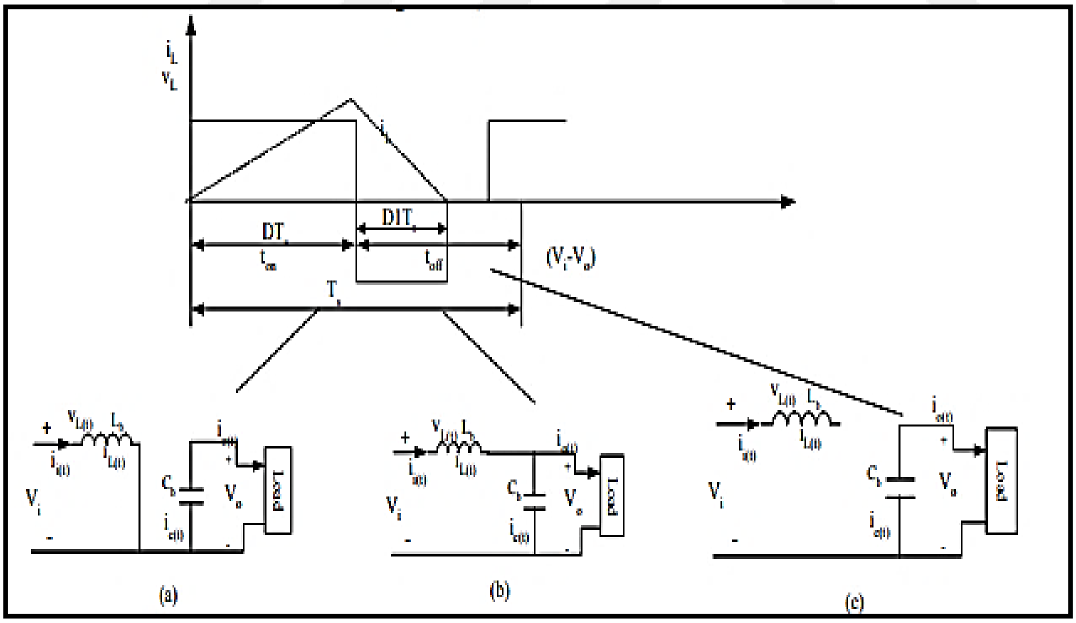

Figure 3.14. Equivalent Circuit for boost Converter in DCM (Hasaneen and Elbaset Mohammed, 2008).

a) Mode 1 $(0 < t \leq t_{on})$
b) Mode 2 $(t_{on} < t \leq (D + D1)T_s)$
c) Mode 3$(D + D1)T_s < t \leq T_s)$

From Figure 3.13c., the average input current, which is equal to the inductor current, is

$$I_i = \frac{V_i}{2L_b} DT_s(D + D_1) \tag{3.8}$$

Using equation (3-8) in the foregoing equation yields

$$I_o = \left(\frac{V_i T_s}{2L_b}\right) DD_1 \tag{3.9}$$

In actuality, it is more helpful to determine the necessary duty cycle, D, as a function of load current for a range of Vo/Vi values since Vo is kept constant while D changes in response to variations in Vi. Equations (3-6) and (3-9) allow us to ascertain that:

$$D = \left[\frac{4}{27} \frac{V_o}{V_i} \left(\frac{V_o}{V_i} - 1\right) \frac{I_o}{I_{o,aver,max}}\right]^{0.5} \tag{3.10}$$

Where;

$I_{o,aver,max}$:The maximum average output current at the edge of continuous conduction and can be found by the following Equation.

$$I_{o,aver} = \frac{T_s V_o}{2L_b} D(1 - D)^2 \tag{3.11}$$

The average output current has its maximum at D=1/3.

$$I_{o,aver,max} = \frac{2}{27} \frac{T_s V_o}{L_b} \tag{3.12}$$

The inductance at the boundary between continuous and discontinuous modes is known as the critical inductance, or L_{bc}. It is defined as follows:

$$L_{bc} = \frac{R\, D(1-D)^2}{2F_s} \tag{3.13}$$

where;

- R : The equivalent load, Ω.
- Fs : The switching frequency, Hz

The switching frequency was selected at random in order to reduce the boost inductor's size and the semiconductor device's loss. The IGBTs' switching losses rise at increasing frequencies, which lowers the circuit's overall efficiency. Lower frequencies result in a decrease in the volumetric efficiency of the supply and an increase in the needed output capacitance and boost inductor size (Hasaneen and Elbaset Mohammed, 2008).

In this study, a DC-DC booster circuit was designed according to the values shown in Table 3.3 and in Figure 3.14. DC-DC booster circuit representation.

Table 3.3. The DC-DC boost converter parameters

Parameters	Value
Duty Cycle	0.453
Switching Frequency	5 kHz
DC- Link Voltage	500 V
Boost Inductor	5 mH
Input Capacitor	100 µF
DC-Link Capacitor	12000 µF

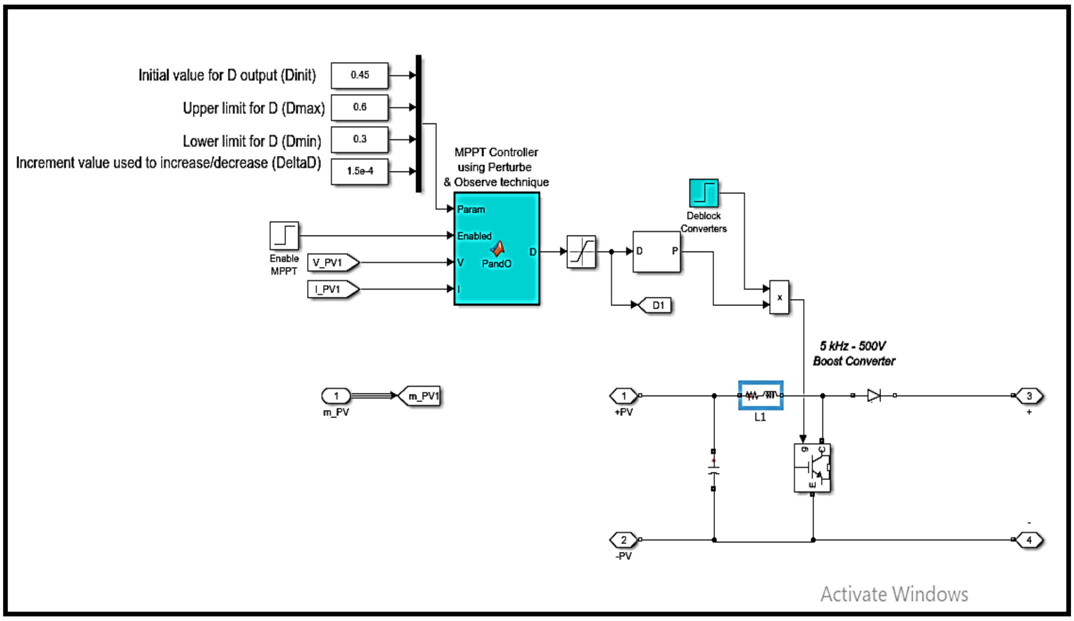

Figure 3.15. DC-DC boost converter representation in Matlab/Simulink

3.5.4. Voltage source converter (VSC)

Three-phase voltage source converters (VSCs) convert 500 V DC to 260 V AC while maintaining a unity power factor. The converter is connected to the grid via a three-phase coupling transformer with a voltage of 260V/4.16kV. The AC voltage averaged during a single switching frequency cycle is produced by equivalent voltage sources that represent the boost and VSC converters in the average model. Although harmonics are not represented by such a model, the dynamics that arise from the interplay between the power and control systems are maintained. This model makes it possible to use much longer time increments (50 us), which speeds up the simulation significantly.

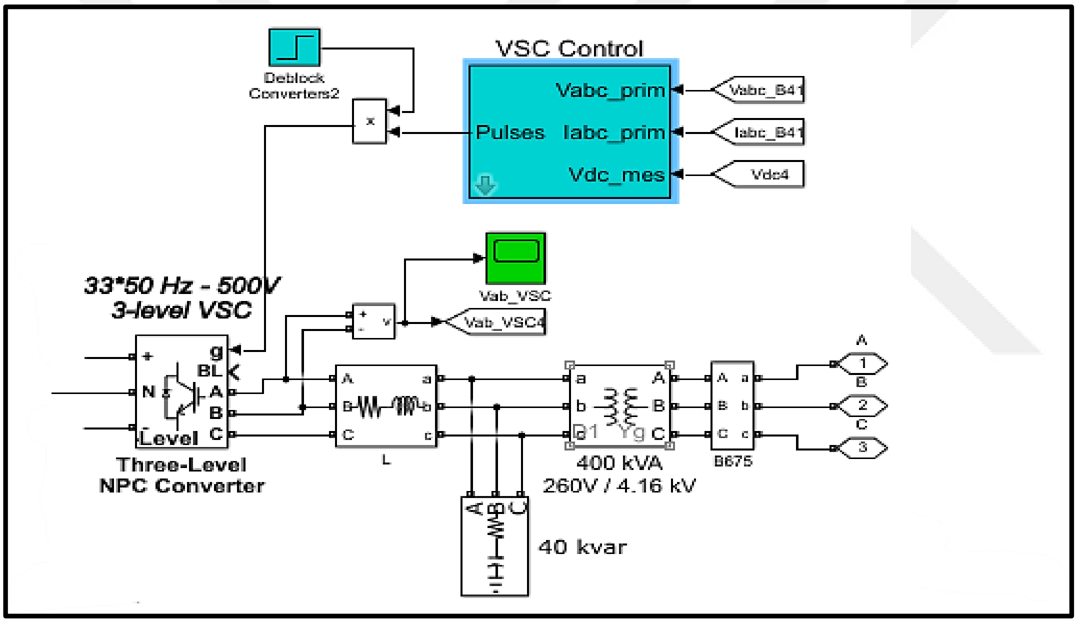

Figure 3.16. VSC Control circuit representation in Matlab/Simulink

3.6. Modelling and Simulation of Modified IEEE 13-bus system

The test grid for IEEE 13-bus will be utilized. The distribution grid in North America is represented by this sample, which consists of three-phase lines with two-phase and single-phase lines near feeder lateral (load side) ends. There is a 4.16 kV distribution voltage. The Modified IEEE-13 Bus model is the power systems network that Matlab/Simulink will be used to simulate. In an IEEE 13-bus system, one swing source is located at bus 632 (4.16 kV/50 Hz).

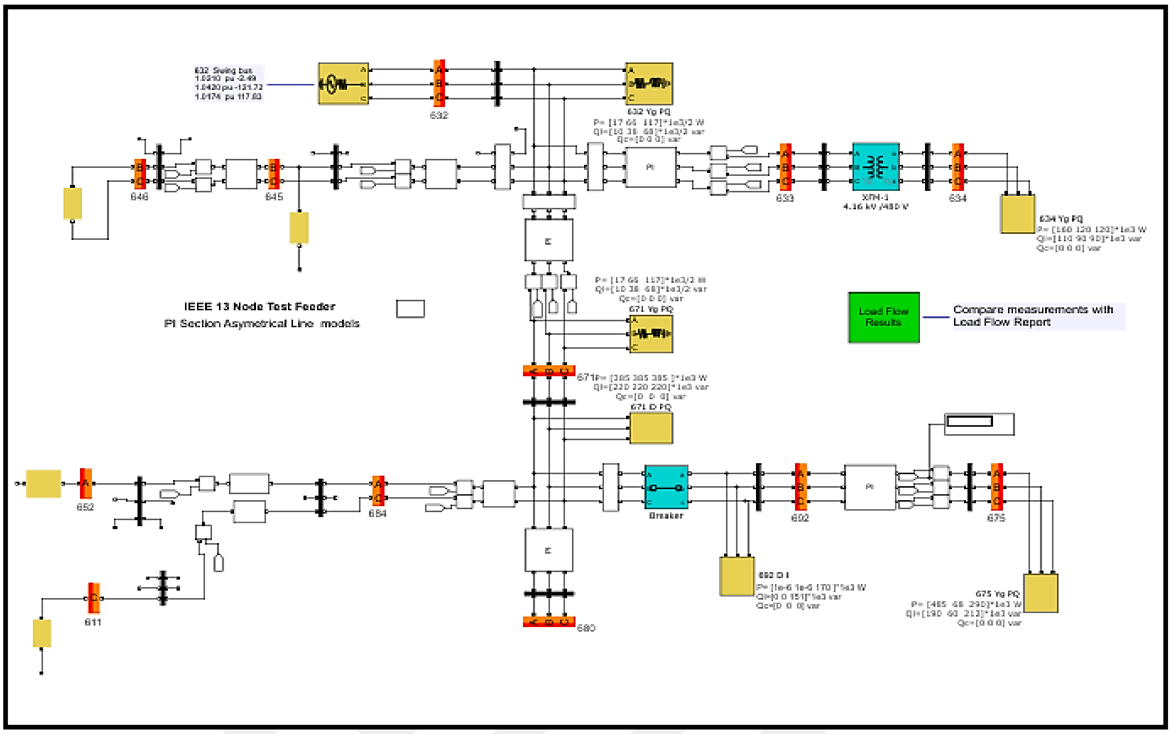

Figure 3.17. Modified IEEE 13-bus test circuit representation in Matlab/Simulink

3.7. Modelling and Simulation of Modified IEEE 13-bus system with single fault

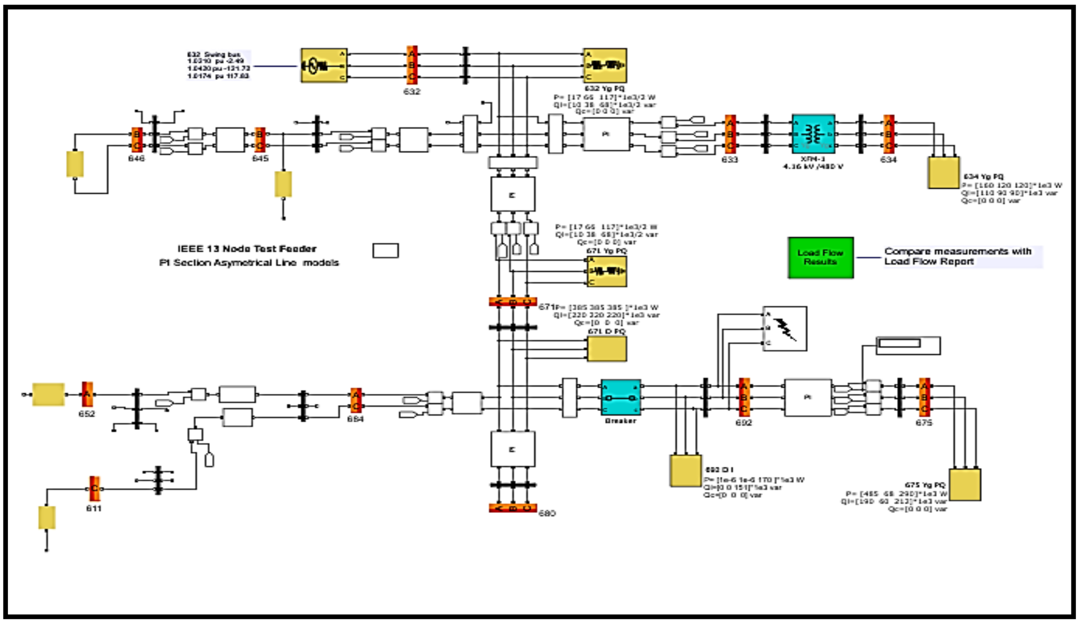

Figure 3.18. Modified IEEE 13-bus test circuit with fault representation in Matlab/Simulink

4. RESULTS AND DISCUSSION

To demonstrate the impact of integrating PV cells on the voltage stability in electrical systems in cases of overloads and faults, this chapter deals with the results of the computer representation that was conducted during this study using the program (MATLAB/Simulink/R-2022a). This computer representation was made using the photovoltaic system, which is a renewable energy source, connected to the electrical power system (Modified IEEE13-Bus Test System). The impact of this effect on the buses that were locally linked to the renewable energy systems displayed in this chapter—which were obtained for various operating cases and conditions—and the results on the coupling point of these systems with the electrical power system were examined.

4.1. Voltage measurement in the modified IEEE 13-Bus Test system

To illustrate how the integration of the photovoltaic system affects the electrical power system (Modified IEEE 13-Bus Test System) shown in Figure 4.1, the voltage measurement on all buses must first be performed to ensure the stable operation of the proposed electrical system.

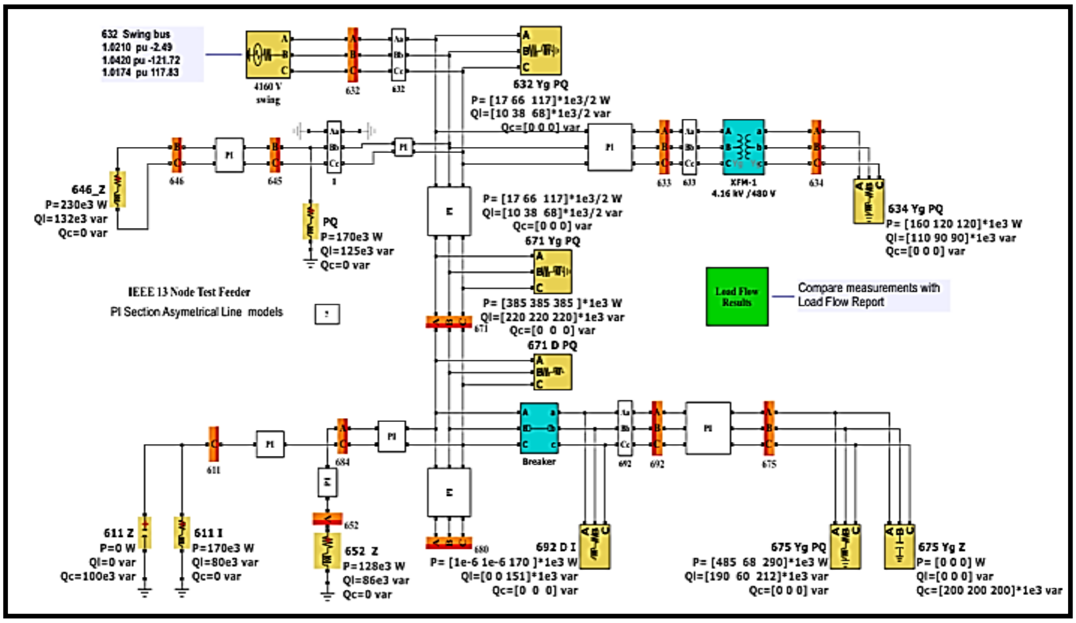

Figure 4.1. The electrical power system (Modified IEEE 13-Bus Test System)

The table 4.1. displays the voltage measurement results for the buses in the suggested system while it is not connected to a solar system, a renewable energy source.

Table 4.1. Voltage measurement for the buses in the Modified IEEE 13-Bus System without renewable energy sources

Table 4.1. Voltage measurement for the buses

V-BUSES	R	S	T
Vabc-632	1.021	1.042	1.017
Vabc-633	1.018	1.04	1.015
Vabc-692	0.9871	1.045	0.971
Vabc-645	0	1.033	1.015
Vabc-646	0	1.032	1.014
Vabc-671	0.9871	1.045	0.971
Vabc-675	0.9798	1.046	0.9676
Vabc-652	0.9799	0	0
Vabc-634	0.9941	1.022	0.9961
Vabc-611	0	0	0.9648
Vabc-680	0.9871	1.045	0.971
Vabc-684	0.9853	0	0.9679

According to the voltage measurements findings for the proposed unbalanced multiphase electrical power system displayed in table 4.1. Bus (611) has the lowest voltage of (R_{611}=0, S_{611}=0, T_{611}=0.9648 Pu), followed by bus (675) with (R_{675}=0.9798, S_{675}=1.046, T_{675}=0.9676 Pu), bus (652) with (R_{652}=0.9799, S_{652}=0, T_{652}=0 Pu), bus (684) with (R_{684}=0.9853, S_{684}=0, T_{684}=0.9679), and buses (692, 671, and 680) with (R_{671}=0.9871, S_{671}=1.045, T_{671}=0.971).

The following figures show the voltage, current, and power in the buses 671 and 675.

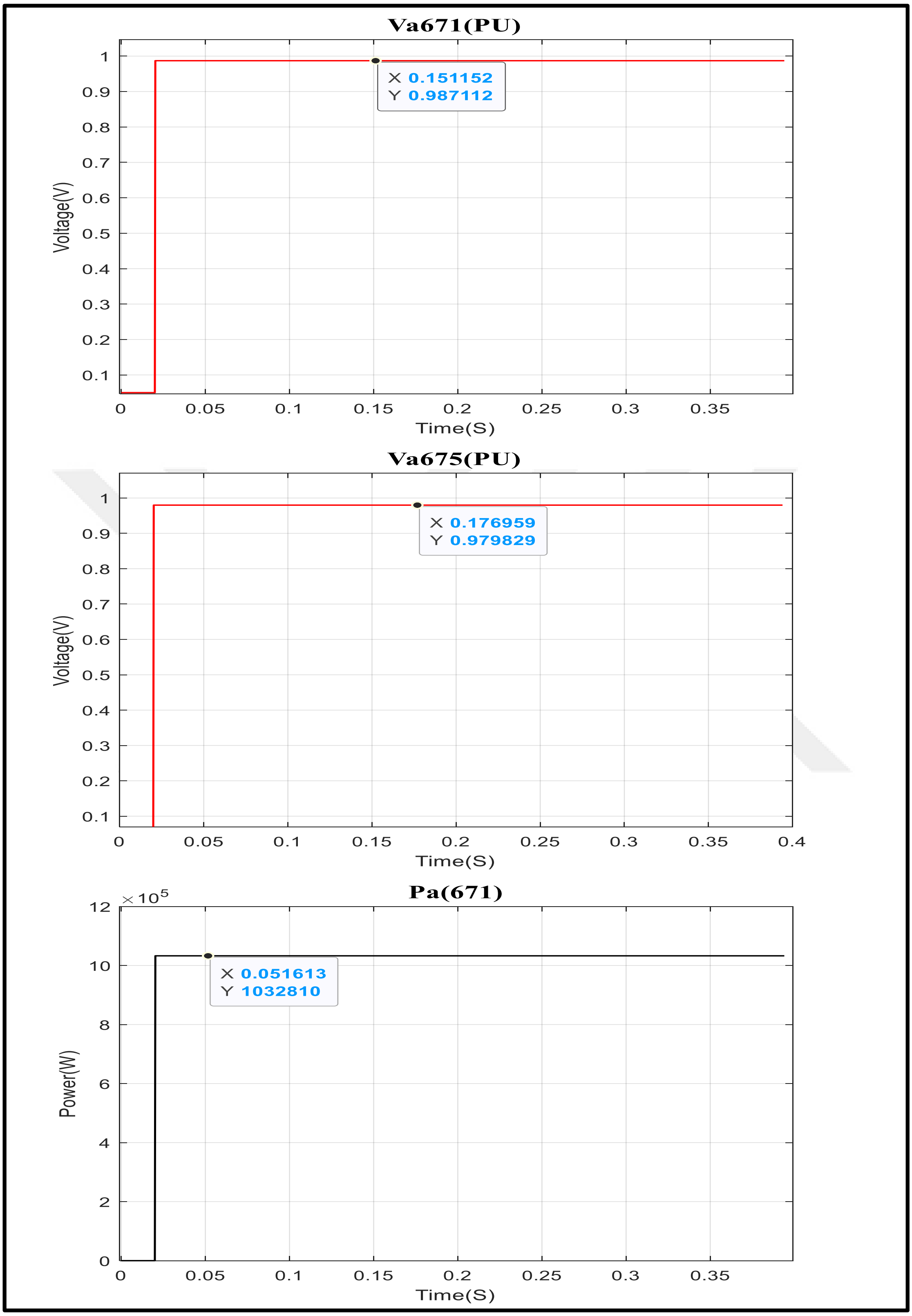

Figure 4.2. The voltage, current, and power in the buses 671 and 675 (phase R).

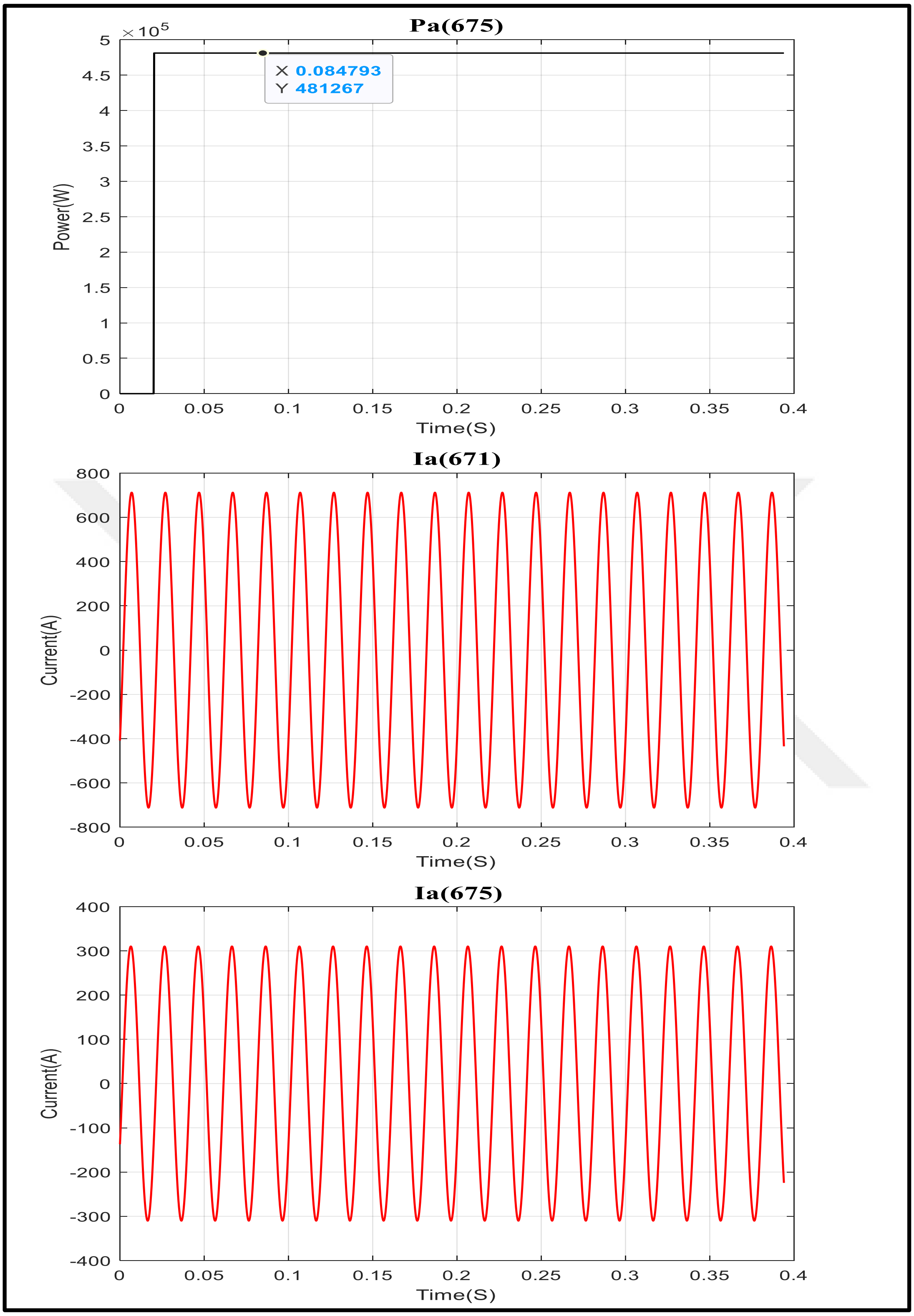

Figure 4.2. (continue) The voltage, current, and power in the buses 671 and 675 (phase R).

To study the impact of renewable energy sources (photovoltaic systems) on the modified IEEE bus 13 electrical system in terms of voltage and stability. The following photovoltaic system will be connected, and the results will be discussed for different operating cases:

- Increase the load by 25% on bus 671 and measure the voltages on all buses.
- Connecting a 500 kW PV system to the bus 671 in modes (Iq =0, Iq = -0.5, and Iq = -1) while measuring the voltage of the buses in all modes.
- Increase the load by 50% on the bus 671 and measure the voltages on all buses.
- Connecting a 500 kW PV system to the bus 671 in modes (Iq =0, Iq = -0.5, and Iq = -1) while measuring the voltage of the buses in all modes.
- Increase the load by 75% on the bus 671 and measure the voltages on all buses.
- Connecting a 500 kW PV system to the bus 671 in modes (Iq =0, Iq = -0.5, and Iq = -1) while measuring the voltage of the buses in all modes.
- Increase the load by 100% on bus 671 and measure the voltages on all buses.
- Connecting a 500 kW PV system to the bus 671 in modes (Iq =0, Iq = -0.5, and Iq = -1) while measuring the voltage of the buses in all modes.
- Increase the load by 25% on the bus 675 and measure the voltages on all buses.
- Connecting a 400 kW PV system to the bus 675 in modes (Iq =0, Iq = -0.5, and Iq = -1) while measuring the voltage of the buses in all modes.
- Increasing the load by 50% on the bus 675 and measuring the voltages on all buses.
- Connecting a 400 kW PV system to the bus 671 in modes (Iq =0, Iq = -0.5, and Iq = -1) while measuring the voltage of the buses in all modes.
- Increase the load by 75% on the bus 675 and measure the voltages on all buses.
- Connecting a 400 kW PV system to a bus 675 in modes (Iq =0, Iq =- 0.5, and Iq = -1) while measuring the voltage of the buses in all modes.
- Increase the load by 100% on the bus 675 and measure the voltages on all buses.
- Connecting a 400 kW PV system to the bus 675 in modes (Iq =0, Iq = -0.5, and Iq = -1) while measuring the voltage of the buses in all modes.
- Increase the load by 25% on the bus 675 and the bus 671 and measure the voltages on all buses.
- Connecting a 500 kW PV system to the bus 671 + 400 kW to the bus 675 in modes (Iq =0, Iq = -0.5 and Iq = -1) while measuring the voltage of the buses in all modes.
- Increase the load by 50% on the bus 675 and the bus 671 and measure the voltages on all buses.
- Connect the (PV) system with a capacity of 500 kW to the bus 671 + 400 kW to the bus 675 in modes (Iq =0, Iq = -0.5 and Iq = -1) with measuring the voltage of the buses in all modes.

- Increase the load by 75% on the bus 675 and the bus 671 and measure the voltages on all buses.
- Connect the (PV) system with a capacity of 500 kW to the bus 671 + 400 kW to the bus 675 in modes (Iq =0, Iq = -0.5 and Iq = -1) with measuring the voltage of the buses in all modes.
- Increase the load by 100% on the bus 675 and the bus 671 and measure the voltages on all buses.
- Connect the (PV) system with a capacity of 500 kW to the bus 671 + 400 kW to the bus 675 in the modes (Iq =0, Iq = -0.5 and Iq = -1) by measuring the voltage of the buses in all modes.

4.1.1. First case: Increase the load on bus 671

Increase the load on bus 671 by 25%

The active and reactive power load on bus 671 was raised by 25% in the modified IEEE 13 bus test system circuit. The balanced loads on bus 671 were Q(R = 220kVar, S = 220kVar, and T = 220kVar), and P(R = 385kW, S = 385kW, and T = 385kW). The voltage of each bus was measured when the loads were increased to P(R = 481.25kW, S = 481.25kW, and T = 481.25kW), and Q(R = 275kVar, S = 275kVar, and T = 275kVar). Below is Table 4.2. that displays the voltage measurements along with the percentage decrease that occurred in all buses.

Table 4.2. The voltage on the buses before increasing the load and after increasing the load on the bus 671 by 25%

V-Buses	Normal Case			After Increase the Load 25% (bus671)			Drop Rate%		
	R	S	T	R	S	T	R	S	T
Vabc-632	1.021	1.042	1.017	1.021	1.042	1.017	0	0	0
Vabc-633	1.018	1.04	1.015	1.018	1.04	1.015	0	0	0
Vabc-692	0.9871	1.045	0.971	0.984	1.043	0.9679	-0.32%	-0.19%	-0.32%
Vabc-645	0	1.033	1.015	0	1.033	1.015	0	0	0
Vabc-646	0	1.032	1.014	0	1.032	1.014	0	0	0
Vabc-671	0.9871	1.045	0.971	0.984	1.043	0.9679	-0.32%	-0.19%	-0.32%
Vabc-675	0.9798	1.046	0.9676	0.9767	1.044	0.9646	-0.32%	-0.19%	-0.31%
Vabc-652	0.9799	0	0	0.9768	0	0	-0.32%	0	0
Vabc-634	0.9941	1.022	0.9961	0.9941	1.022	0.9961	0	0	0
Vabc-611	0	0	0.9648	0	0	0.9618	0	0	-0.31%
Vabc-680	0.9871	1.045	0.971	0.984	1.043	0.9679	-0.32%	-0.19%	-0.32%
Vabc-684	0.9853	0	0.9679	0.9822	0	0.9648	-0.32%	0	-0.32%

Table 4.2. shows that when the load on bus 671 increased the buses nearest it were impacted because the voltage dropped at varying rates, but the system did not totally collapse.

Connecting a 500 kW (PV system) to the Bus 671 with Iq=0

Five sets of SunPower PV panels (SPR-305E-WHT-D) were linked in parallel to provide a 500 kW renewable energy system. In this case, at standard conditions (STC) of 25 °C and 1000 W/m² of solar radiation, each set of PV panels produces 100 kW of power. The total power of all five groups is 500 kW. A modified IEEE 13 bus system was connected to the PV system through a bus 671 to compensate for the voltage drop. Only active power (pure P) was injected when Iq = 0 was entered. Before increasing the load, before and after connecting the 500 kW photovoltaic system, the buses' voltage is displayed in Table 4.3.

Table 4.3. The voltage of the buses before the load is increased and both before and after the 500 kW photovoltaic system is connected.

V-Buses	Normal Case			After Increase the Load 25% (bus671) & Before connecting the500kW PV system			After Increase the Load 25% (bus671) & After connecting the500kW PV system		
	R	S	T	R	S	T	R	S	T
Vabc-632	1.021	1.042	1.017	1.021	1.042	1.017	1.021	1.042	1.017
Vabc-633	1.018	1.04	1.015	1.018	1.04	1.015	1.018	1.04	1.015
Vabc-692	0.9871	1.045	0.971	0.984	1.043	0.9679	0.989	1.039	0.975
Vabc-645	0	1.033	1.015	0	1.033	1.015	0	1.033	1.015
Vabc-646	0	1.032	1.014	0	1.032	1.014	0	1.032	1.014
Vabc-671	0.9871	1.045	0.971	0.984	1.043	0.9679	0.989	1.036	0.975
Vabc-675	0.9798	1.046	0.9676	0.9767	1.044	0.9646	0.9817	1.037	0.9716
Vabc-652	0.9799	0	0	0.9768	0	0	0.9818	0	0
Vabc-634	0.9941	1.022	0.9961	0.9941	1.022	0.9961	0.9941	1.022	0.9961
Vabc-611	0	0	0.9648	0	0	0.9618	0	0	0.9688
Vabc-680	0.9871	1.045	0.971	0.984	1.043	0.9679	0.989	1.036	0.975
Vabc-684	0.9853	0	0.9679	0.9822	0	0.9648	0.9872	0	0.9719

According to the above table, the voltage considerably improved following the installation of the photovoltaic system, allowing for the treatment of the drop brought on by the increasing load. The voltage of bus 671, for instance, was R_{671}=0.9871, S_{671}=1.045, and T_{671}=0.971. When the load was increased, the voltage dropped to R_{671}=0.984, S_{671}=1.043, and T_{671}=0.9679. The PV system was next added, and the voltage improved to R_{671}=0.989, S_{671}=1.036, and T_{671}=0.975.

Connecting a 500 kW (PV system) to the Bus 671 with Iq= -0.5

Five sets of SunPower PV panels (SPR-305E-WHT-D) were linked in parallel to provide a 500 kW renewable energy system. In this case, at standard conditions (STC) of 25 °C and 1000 W/m² of solar radiation, each set of PV panels produces 100 kW of power. The total power of all five groups is 500 kW. A modified IEEE 13 bus system was connected to the PV system through a bus 671 to compensate for the voltage drop. Active power (P), and 50% reactive power(Q) ware injected when Iq = -0.5 was entered. Before increasing the load, before and after connecting the 400 kW photovoltaic system, the buses' voltage is displayed in Table 4.4.

Table 4.4. The voltage of the buses before the load is increased and both before and after the 500 kW photovoltaic system is connected.

V-Buses	Normal Case			After Increase the Load 25% (bus671) & Before connecting the500kW PV system			After Increase the Load 25% (bus671) & After connecting the500kW PV system		
	R	S	T	R	S	T	R	S	T
Vabc-632	1.021	1.042	1.017	1.021	1.042	1.017	1.021	1.042	1.017
Vabc-633	1.018	1.04	1.015	1.018	1.04	1.015	1.018	1.04	1.015
Vabc-692	0.9871	1.045	0.971	0.984	1.043	0.9679	0.9914	1.039	0.9777
Vabc-645	0	1.033	1.015	0	1.033	1.015	0	1.033	1.015
Vabc-646	0	1.032	1.014	0	1.032	1.014	0	1.032	1.014
Vabc-671	0.9871	1.045	0.971	0.984	1.043	0.9679	0.9914	1.039	0.9777
Vabc-675	0.9798	1.046	0.9676	0.9767	1.044	0.9646	0.9841	1.04	0.9744
Vabc-652	0.9799	0	0	0.9768	0	0	0.9842	0	0
Vabc-634	0.9941	1.022	0.9961	0.9941	1.022	0.9961	0.9941	1.022	0.9961
Vabc-611	0	0	0.9648	0	0	0.9618	0	0	0.9716
Vabc-680	0.9871	1.045	0.971	0.984	1.043	0.9679	0.9914	1.039	0.9777
Vabc-684	0.9853	0	0.9679	0.9822	0	0.9648	0.9896	0	0.9747

According to the above table, the voltage considerably improved following the installation of the photovoltaic system, allowing for the treatment of the drop brought on by the increasing load. Example: The voltage on bus 671 was in normal condition (R_{671}=0.9871, S_{671}=1.045, T_{671}=0.971); after increasing the load by 25% on bus 671, the voltage dropped, and the readings were (R_{671}=0.984, S_{671}=1.043, T_{671}=0.9679), and then after connecting PV, the voltage improved significantly, and the readings became (R_{671}=0.9914, S_{671}=1.039, T_{671}=0.9777).

Connecting a 500 kW (PV system) to the Bus 671 with Iq= -1

Five sets of SunPower PV panels (SPR-305E-WHT-D) were linked in parallel to provide a 500 kW renewable energy system. In this case, at standard conditions (STC) of 25 °C and

1000 W/m² of solar radiation, each set of PV panels produces 100 kW of power. The total power of all five groups is 500 kW. A modified IEEE 13 bus system was connected to the PV system through a bus 671 to compensate for the voltage drop. Active power (P), and 100% reactive power(Q) ware injected when Iq = -1 was entered. Before increasing the load, before and after connecting the 400 kW photovoltaic system, the buses' voltage is displayed in Table 4.5.

Table 4.5. The voltage of the buses before the load is increased and both before and after the 500 kW photovoltaic system is connected.

V-BUSES	Normal Case			After Increase the Load 25% (bus671) & Before connecting the500kW PV system			After Increase the Load 25% (bus671) & After connecting the500kW PV system		
	R	S	T	R	S	T	R	S	T
Vabc-632	1.021	1.042	1.017	1.021	1.042	1.017	1.021	1.042	1.017
Vabc-633	1.018	1.04	1.015	1.018	1.04	1.015	1.018	1.04	1.015
Vabc-692	0.9871	1.045	0.971	0.984	1.043	0.9679	0.9935	1.042	0.9805
Vabc-645	0	1.033	1.015	0	1.033	1.015	0	1.033	1.015
Vabc-646	0	1.032	1.014	0	1.032	1.014	0	1.032	1.014
Vabc-671	0.9871	1.045	0.971	0.984	1.043	0.9679	0.9935	1.042	0.9805
Vabc-675	0.9798	1.046	0.9676	0.9767	1.044	0.9646	0.9862	1.043	0.9771
Vabc-652	0.9799	0	0	0.9768	0	0	0.9863	0	0
Vabc-634	0.9941	1.022	0.9961	0.9941	1.022	0.9961	0.9941	1.022	0.9961
Vabc-611	0	0	0.9648	0	0	0.9618	0	0	0.9743
Vabc-680	0.9871	1.045	0.971	0.984	1.043	0.9679	0.9935	1.042	0.9805
Vabc-684	0.9853	0	0.9679	0.9822	0	0.9648	0.9917	0	0.9774

The voltage significantly improved after the photovoltaic system was installed, enabling the treatment of the drop caused by the rising load, as seen in the above table. Nevertheless, the voltage rose above usual, which can be harmful. For instance, bus 671's voltage was in normal condition (R_{671}=0.9871, S_{671}=1.045, and T_{671}=0.971). However, when the load was increased by 25%, the voltage decreased and the readings were (R_{671}=0.984, S_{671}=1.043, and T_{671}=0.9679). The voltage then improved significantly after connecting PV, and the readings became (R_{671}=0.9935, S_{671}=1.042, and T_{671}=0.9805).

Increase the load on bus 671 by 50%

The active and reactive power load on bus 671 was raised by 50% in the modified IEEE 13 bus test system circuit. The balanced loads on bus 671 were Q(R = 220kVar, S = 220kVar, and T = 220kVar), and P(R = 385kW, S = 385kW, and T = 385kW). The voltage of each bus was measured when the loads were increased to P(R = 577.5kW, S = 577.5kW, and T = 577.5kW), and Q(R = 330kVar, S = 330kVar, and T = 330kVar). Below is Table 4.6.

that displays the voltage measurements along with the percentage decrease that occurred in all buses.

Table 4.6. The voltage on the buses both before and after the bus 671's load was increased by 50%.

V-Buses	Normal Case			After Increase the Load 50% (bus671)			Drop Rate%		
	R	S	T	R	S	T	R	S	T
Vabc-632	1.021	1.042	1.017	1.021	1.042	1.017	0	0	0
Vabc-633	1.018	1.04	1.015	1.018	1.04	1.015	0	0	0
Vabc-692	0.9871	1.045	0.971	0.9809	1.04	0.9648	-0.63%	-0.48%	-0.64%
Vabc-645	0	1.033	1.015	0	1.033	1.015	0	0	0
Vabc-646	0	1.032	1.014	0	1.032	1.014	0	0	0
Vabc-671	0.9871	1.045	0.971	0.9809	1.04	0.9648	-0.63%	-0.48%	-0.64%
Vabc-675	0.9798	1.046	0.9676	0.9737	1.041	0.9615	-0.63%	-0.48%	-0.63%
Vabc-652	0.9799	0	0	0.9737	0	0	-0.64%	0	0
Vabc-634	0.9941	1.022	0.9961	0.9941	1.022	0.9961	0	0	0
Vabc-611	0	0	0.9648	0	0	0.9587	0	0	-0.64%
Vabc-680	0.9871	1.045	0.971	0.9809	1.04	0.9648	-0.63%	-0.48%	-0.64%
Vabc-684	0.9853	0	0.9679	0.9791	0	0.9618	-0.63%	0	-0.63%

Although the system did not completely fail, Table 4.6 demonstrates that the buses closest to bus 671 were affected when its load increased because the voltage dropped at different rates.

Figure 4.3. shows the voltage, current, and power on bus 671(phase R) after increasing the load by 50% on bus 671.

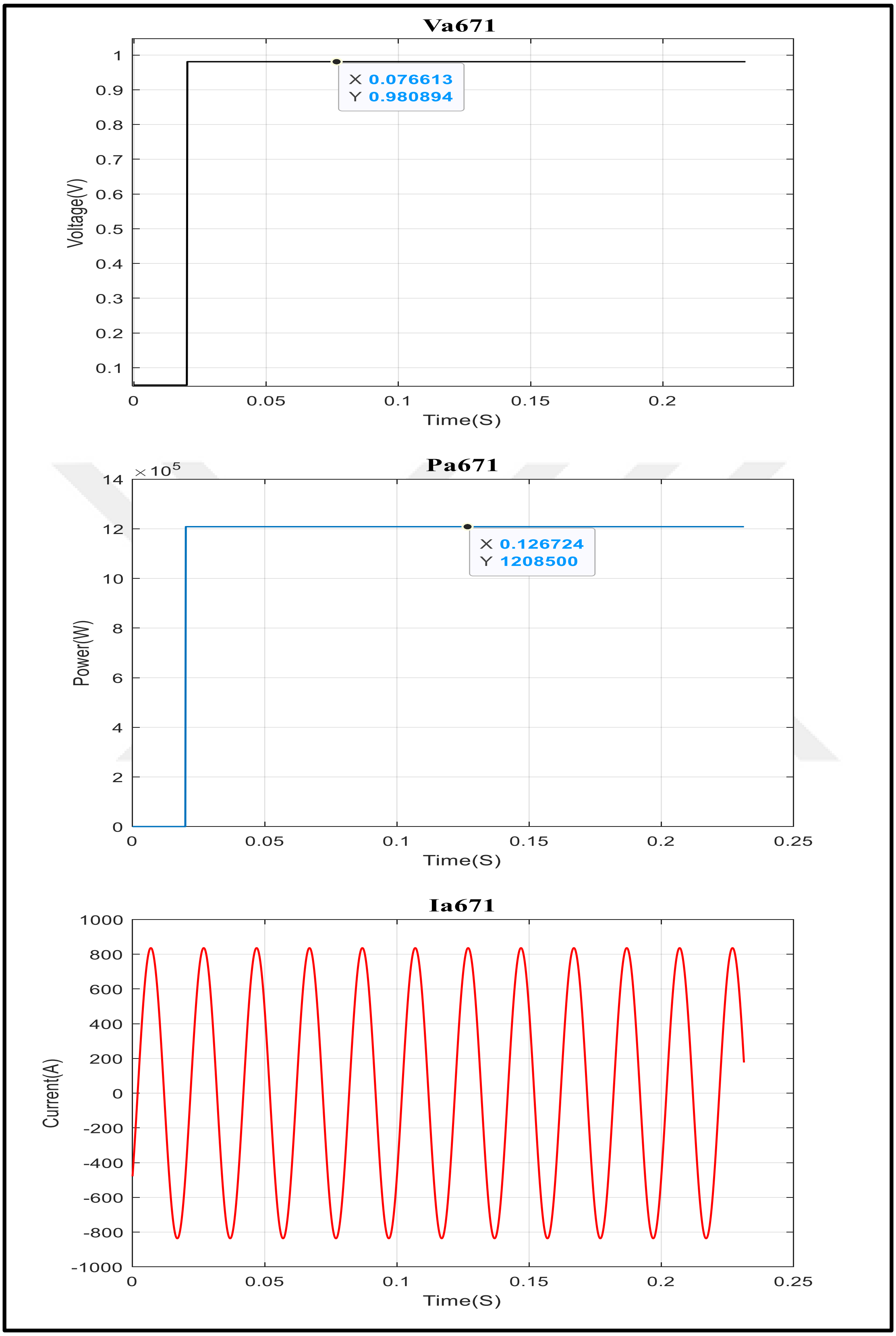

Figure 4.3. The voltage, current, and power on bus 671(phase R) after increasing the load by 50% on bus 671.

Connecting a 500 kW (PV system) to the Bus 671 with Iq=0

Five sets of SunPower PV panels (SPR-305E-WHT-D) were linked in parallel to provide a 500 kW renewable energy system. In this case, at standard conditions (STC) of 25 °C and 1000 W/m² of solar radiation, each set of PV panels produces 100 kW of power. The total power of all five groups is 500 kW. A modified IEEE 13 bus system was connected to the PV system through a bus 671 to compensate for the voltage drop. Only active power (pure P) was injected when Iq = 0 was entered. Before increasing the load, before and after connecting the 500 kW photovoltaic system, the buses' voltage is displayed in Table 4.7.

Table 4.7. The voltage of the buses before increasing load, before and after connecting the 500 kW photovoltaic system.

V-Buses	Normal Case			After Increase the Load 50% (bus671) & Before connecting the500kW PV system			After Increase the Load 50% (bus671) & After connecting the500kW PV system		
	R	S	T	R	S	T	R	S	T
Vabc-632	1.021	1.042	1.017	1.021	1.042	1.017	1.021	1.042	1.017
Vabc-633	1.018	1.04	1.015	1.018	1.04	1.015	1.018	1.04	1.015
Vabc-692	0.9871	1.045	0.971	0.9809	1.04	0.9648	0.986	1.034	0.9718
Vabc-645	0	1.033	1.015	0	1.033	1.015	0	1.033	1.015
Vabc-646	0	1.032	1.014	0	1.032	1.014	0	1.032	1.014
Vabc-671	0.9871	1.045	0.971	0.9809	1.04	0.9648	0.986	1.034	0.9719
Vabc-675	0.9798	1.046	0.9676	0.9737	1.041	0.9615	0.9787	1.035	0.9685
Vabc-652	0.9799	0	0	0.9737	0	0	0.9788	0	0
Vabc-634	0.9941	1.022	0.9961	0.9941	1.022	0.9961	0.9941	1.022	0.9961
Vabc-611	0	0	0.9648	0	0	0.9587	0	0	0.9657
Vabc-680	0.9871	1.045	0.971	0.9809	1.04	0.9648	0.986	1.034	0.9719
Vabc-684	0.9853	0	0.9679	0.9791	0	0.9618	0.9842	0	0.9688

According to the above table, the voltage considerably improved following the installation of the photovoltaic system, allowing for the treatment of the drop brought on by the increasing load. The voltage of bus 671, for instance, was R_{671}=0.9871, S_{671}=1.045, and T_{671}=0.971. When the load was increased, the voltage dropped to R_{671}=0.9809, S_{671}=1.04, and T_{671}=0.9648. The PV system was next added, and the voltage improved to R_{671}=0.986, S_{671}=1.034, and T_{671}=0.9719.

Figure 4.4. shows the voltage, current, and power on bus 671(phase R) after increasing the load by 50% on bus 671 with a PV system (Iq=0).

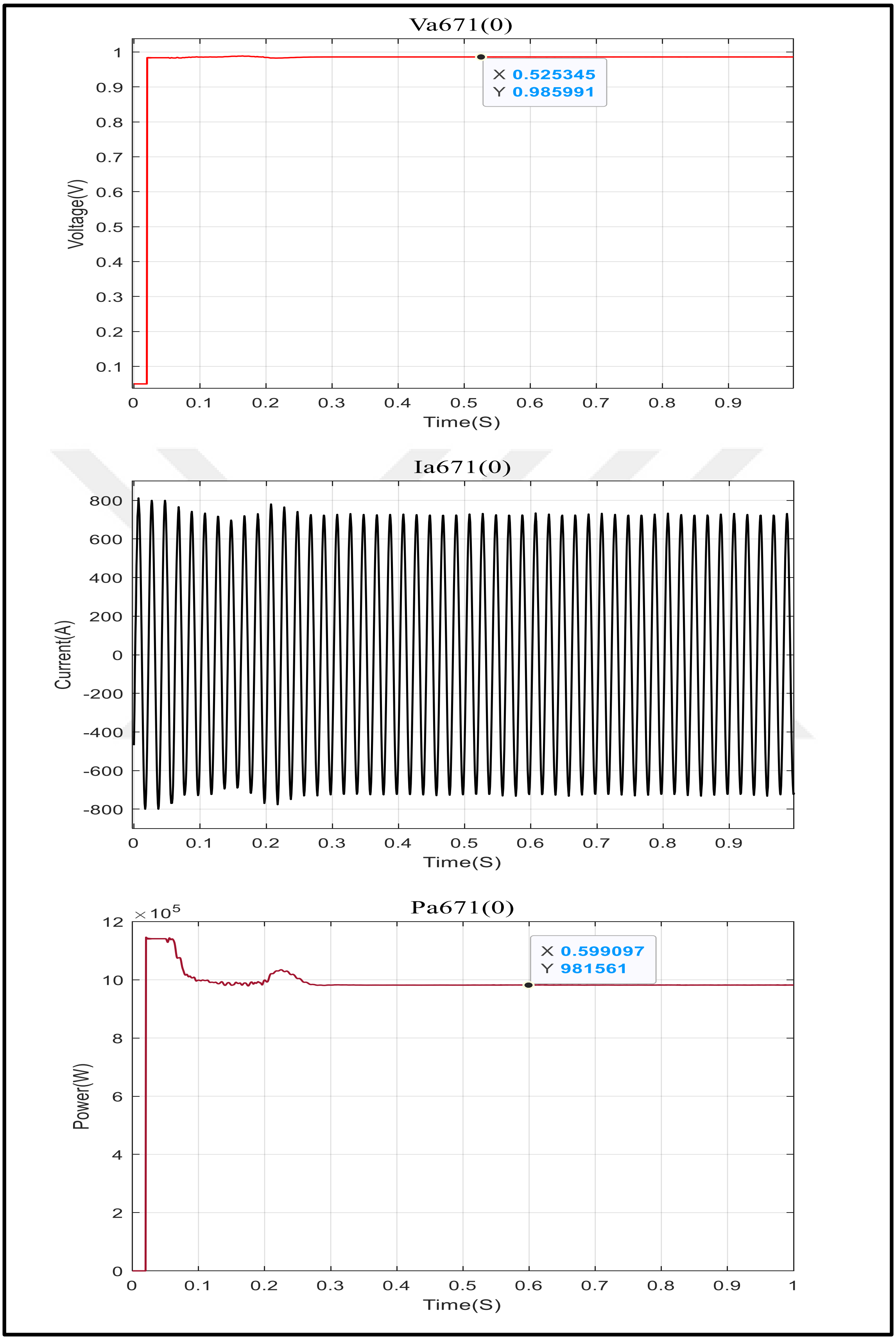

Figure 4.4. The voltage, current, and power on bus 671(phase R) after increasing the load by 50% on bus 671 with a PV system (Iq=0).

Connecting a 500 kW (PV system) to the Bus 671 with Iq= -0.5

Five sets of SunPower PV panels (SPR-305E-WHT-D) were linked in parallel to provide a 500 kW renewable energy system. In this case, at standard conditions (STC) of 25 °C and 1000 W/m² of solar radiation, each set of PV panels produces 100 kW of power. The total power of all five groups is 500 kW. A modified IEEE 13 bus system was connected to the PV system through a bus 671 to compensate for the voltage drop. Active power (P), and 50% reactive power(Q) ware injected when Iq = -0.5 was entered. Before increasing the load, before and after connecting the 400 kW photovoltaic system, the buses' voltage is displayed in Table 4.8.

Table 4.8. The voltage of the buses before the load is increased and both before and after the 500 kW photovoltaic system is connected.

V-Buses	Normal Case			After Increase the Load 50% (bus671) & Before connecting the500kW PV system			After Increase the Load 50% (bus671) & After connecting the500kW PV system		
	R	S	T	R	S	T	R	S	T
Vabc-632	1.021	1.042	1.017	1.021	1.042	1.017	1.021	1.042	1.017
Vabc-633	1.018	1.04	1.015	1.018	1.04	1.015	1.018	1.04	1.015
Vabc-692	0.9871	1.045	0.971	0.9809	1.04	0.9648	0.9883	1.037	0.9747
Vabc-645	0	1.033	1.015	0	1.033	1.015	0	1.033	1.015
Vabc-646	0	1.032	1.014	0	1.032	1.014	0	1.032	1.014
Vabc-671	0.9871	1.045	0.971	0.9809	1.04	0.9648	0.9884	1.037	0.9747
Vabc-675	0.9798	1.046	0.9676	0.9737	1.041	0.9615	0.981	1.038	0.9714
Vabc-652	0.9799	0	0	0.9737	0	0	0.9811	0	0
Vabc-634	0.9941	1.022	0.9961	0.9941	1.022	0.9961	0.9941	1.022	0.9961
Vabc-611	0	0	0.9648	0	0	0.9587	0	0	0.9688
Vabc-680	0.9871	1.045	0.971	0.9809	1.04	0.9648	0.9884	1.037	0.9747
Vabc-684	0.9853	0	0.9679	0.9791	0	0.9618	0.9865	0	0.9717

According to the above table, the voltage considerably improved following the installation of the photovoltaic system, allowing for the treatment of the drop brought on by the increasing load. Example: Output: The voltage on bus 671 was in normal condition (R_{671}=0.9871, S_{671}=1.045, and T_{671}=0.971); after increasing the load by 50% on bus 671, the voltage dropped, and the readings were (R_{671}=0.9809, S_{671}=1.04, and T_{671}=0.9648), and then after connecting PV, the voltage improved significantly, and the readings became (R_{671}=0.9884, S_{671}=1.037, and T_{671}=0.9747).

Figure 4.5. shows the voltage, current, and power on bus 671(phase R) after increasing the load by 50% on bus 671 with a PV system (Iq=-0.5).

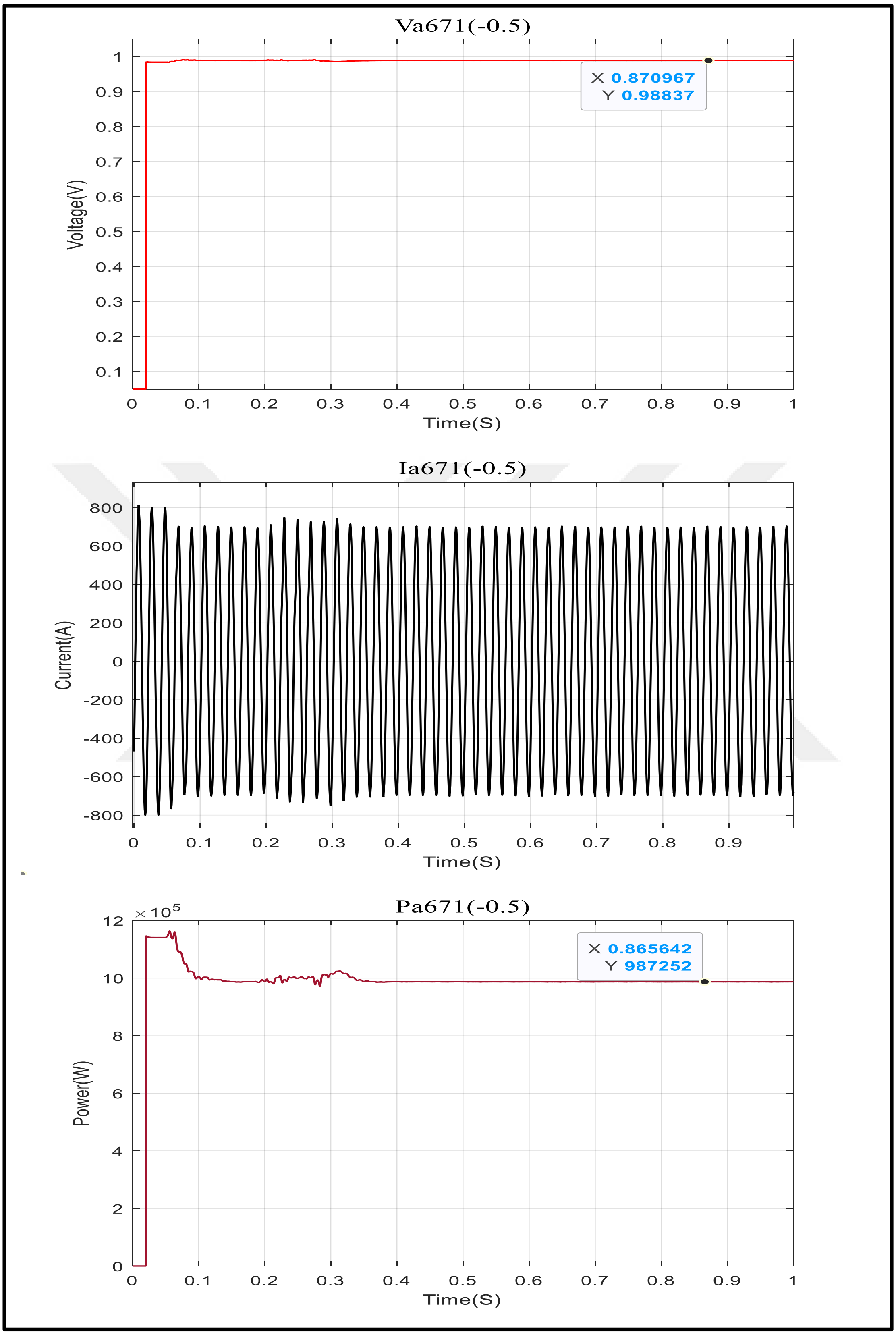

Figure 4.5. The voltage, current, and power on bus 671(phase R) after increasing the load by 50% on bus 671 with a PV system (Iq=-0.5).

Connecting a 500 kW (PV system) to the Bus 671 with Iq= -1

Five sets of SunPower PV panels (SPR-305E-WHT-D) were linked in parallel to provide a 500 kW renewable energy system. In this case, at standard conditions (STC) of 25 °C and 1000 W/m² of solar radiation, each set of PV panels produces 100 kW of power. The total power of all five groups is 500 kW. A modified IEEE 13 bus system was connected to the PV system through a bus 671 to compensate for the voltage drop. Active power (P), and 100% reactive power(Q) ware injected when Iq = -1 was entered. Before increasing the load, before and after connecting the 400 kW photovoltaic system, the buses' voltage is displayed in Table 4.9.

Table 4.9. The voltage of the buses before the load is increased and both before and after the 500 kW photovoltaic system is connected.

V-Buses	Normal Case			After Increase the Load 50% (bus671) & Before connecting the500kW PV system			After Increase the Load 50% (bus671) & After connecting the500kW PV system		
	R	S	T	R	S	T	R	S	T
Vabc-632	1.021	1.042	1.017	1.021	1.042	1.017	1.021	1.042	1.017
Vabc-633	1.018	1.04	1.015	1.018	1.04	1.015	1.018	1.04	1.015
Vabc-692	0.9871	1.045	0.971	0.9809	1.04	0.9648	0.9904	1.039	0.9773
Vabc-645	0	1.033	1.015	0	1.033	1.015	0	1.033	1.015
Vabc-646	0	1.032	1.014	0	1.032	1.014	0	1.032	1.014
Vabc-671	0.9871	1.045	0.971	0.9809	1.04	0.9648	0.9905	1.039	0.9773
Vabc-675	0.9798	1.046	0.9676	0.9737	1.041	0.9615	0.9831	1.04	0.974
Vabc-652	0.9799	0	0	0.9737	0	0	0.9832	0	0
Vabc-634	0.9941	1.022	0.9961	0.9941	1.022	0.9961	0.9941	1.022	0.9961
Vabc-611	0	0	0.9648	0	0	0.9587	0	0	0.9712
Vabc-680	0.9871	1.045	0.971	0.9809	1.04	0.9648	0.9905	1.039	0.9773
Vabc-684	0.9853	0	0.9679	0.9791	0	0.9618	0.9886	0	0.9743

The voltage significantly improved after the photovoltaic system was installed, enabling the treatment of the drop caused by the rising load, as seen in the above table. For instance, bus 671's voltage was in normal condition (R_{671}=0.9871, S_{671}=1.045, and T_{671}=0.971). However, when the load was increased by 50%, the voltage decreased and the readings were (R_{671}=0.9809, S_{671}=1.04, and T_{671}=0.9648). The voltage then improved significantly after connecting PV, and the readings became (R_{671}=0.9905, S_{671}=1.039, and T_{671}=0.9773).

Figure 4.6. shows the voltage, current, and power on bus 671(phase R) after increasing the load by 50% on bus 671 with a PV system (Iq=-1).

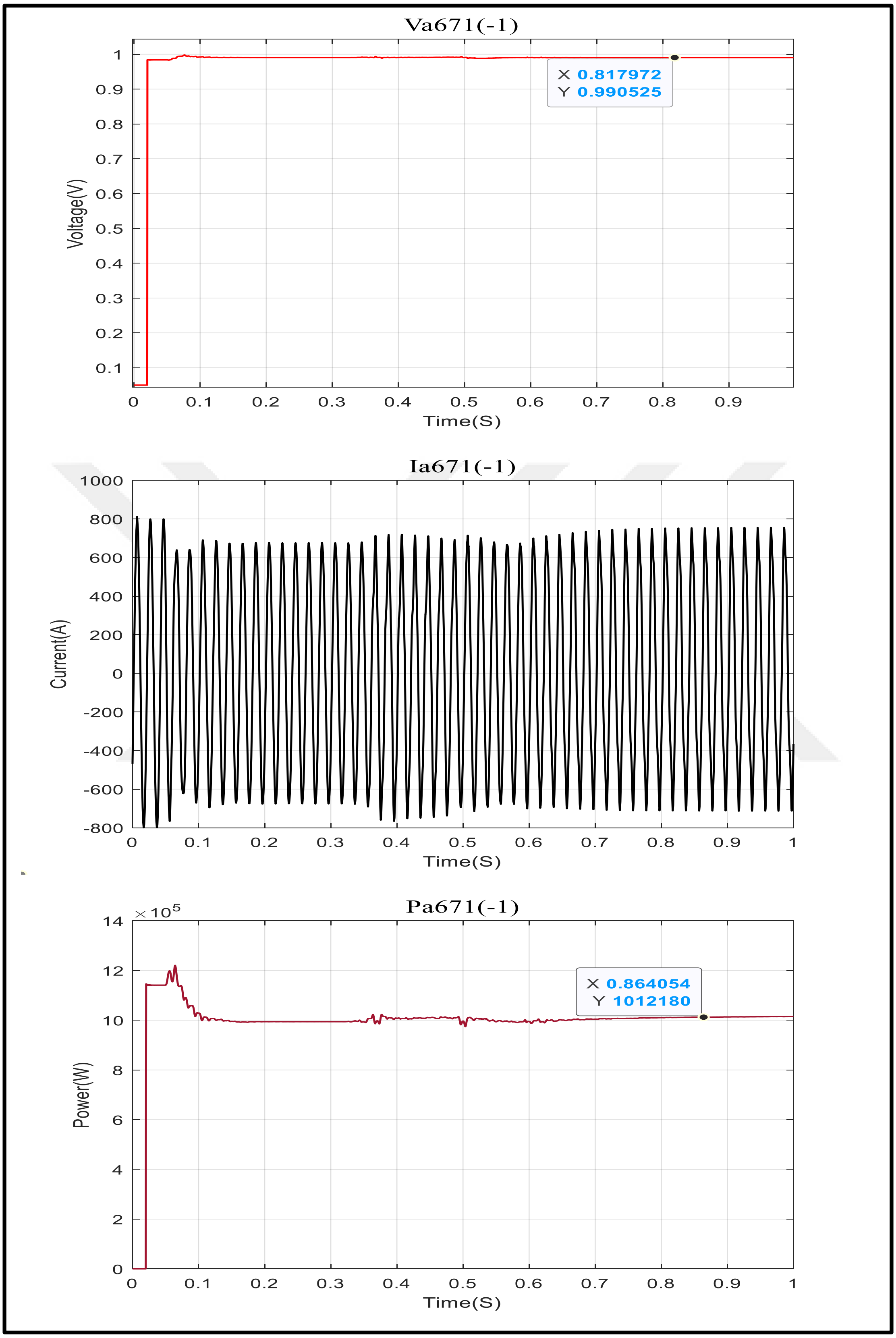

Figure 4.6. The voltage, current, and power on bus 671(phase R) after increasing the load by 50% on bus 671 with a PV system (Iq=-1).

Increase the load on bus 671 by 75%

The active and reactive power load on bus 671 was raised by 75% in the modified IEEE 13 bus test system circuit. The balanced loads on bus 671 were Q(R = 220kVar, S = 220kVar, and T = 220kVar), and P(R = 385kW, S = 385kW, and T = 385kW). The voltage of each bus was measured when the loads were increased to P(R = 673.75kW, S = 673.75kW, and T = 673.75kW), and Q(R = 385kVar, S = 385kVar, and T = 385kVar). Below is Table 4.10. that displays the voltage measurements along with the percentage decrease that occurred in all buses.

Table 4.10. The voltage on the buses both before and after the bus 671's load was increased by 75%.

V-Buses	Normal Case			After Increase the Load 75% (bus671)			Drop Rate%		
	R	S	T	R	S	T	R	S	T
Vabc-632	1.021	1.042	1.017	1.021	1.042	1.017	0	0	0
Vabc-633	1.018	1.04	1.015	1.018	1.04	1.015	0	0	0
Vabc-692	0.9871	1.045	0.971	0.9778	1.038	0.9617	-0.95%	-0.67%	-0.97%
Vabc-645	0	1.033	1.015	0	1.033	1.015	0	0	0
Vabc-646	0	1.032	1.014	0	1.032	1.014	0	0	0
Vabc-671	0.9871	1.045	0.971	0.9778	1.038	0.9618	-0.95%	-0.67%	-0.96%
Vabc-675	0.9798	1.046	0.9676	0.9706	1.039	0.9585	-0.95%	-0.67%	-0.95%
Vabc-652	0.9799	0	0	0.9707	0	0	-0.95%	0	0
Vabc-634	0.9941	1.022	0.9961	0.9941	1.022	0.9961	0	0	0
Vabc-611	0	0	0.9648	0	0	0.9557	0	0	-0.95%
Vabc-680	0.9871	1.045	0.971	0.9778	1.038	0.9618	-0.95%	-0.67%	-0.96%
Vabc-684	0.9853	0	0.9679	0.976	0	0.9587	-0.95%	0	-0.96%

Table 4.10 shows that when bus 671's load grew, the buses nearest to it were impacted because the voltage dropped at different rates, even though the system did not fail entirely.

Connecting a 500 kW (PV system) to the Bus 671 with Iq=0

Five sets of SunPower PV panels (SPR-305E-WHT-D) were linked in parallel to provide a 500 kW renewable energy system. In this case, at standard conditions (STC) of 25 °C and 1000 W/m² of solar radiation, each set of PV panels produces 100 kW of power. The total power of all five groups is 500 kW. A modified IEEE 13 bus system was connected to the PV system through a bus 671 to compensate for the voltage drop. Only active power (pure P) was injected when Iq = 0 was entered. Before increasing the load, before and after connecting the 500 kW photovoltaic system, the buses' voltage is displayed in Table 4.11.

Table 4.11. The voltage of the buses before increasing load, before and after connecting the 500 kW photovoltaic system.

V-Buses	Normal Case			After Increase the Load 75% (bus671) & Before connecting the500kW PV system			After Increase the Load 75% (bus671) & After connecting the500kW PV system		
	R	S	T	R	S	T	R	S	T
Vabc-632	1.021	1.042	1.017	1.021	1.042	1.017	1.021	1.042	1.017
Vabc-633	1.018	1.04	1.015	1.018	1.04	1.015	1.018	1.04	1.015
Vabc-692	0.9871	1.045	0.971	0.9778	1.038	0.9617	0.9829	1.031	0.9688
Vabc-645	0	1.033	1.015	0	1.033	1.015	0	1.033	1.015
Vabc-646	0	1.032	1.014	0	1.032	1.014	0	1.032	1.014
Vabc-671	0.9871	1.045	0.971	0.9778	1.038	0.9618	0.9829	1.031	0.9688
Vabc-675	0.9798	1.046	0.9676	0.9706	1.039	0.9585	0.9757	1.032	0.9654
Vabc-652	0.9799	0	0	0.9707	0	0	0.9758	0	0
Vabc-634	0.9941	1.022	0.9961	0.9941	1.022	0.9961	0.9941	1.022	0.9961
Vabc-611	0	0	0.9648	0	0	0.9557	0	0	0.9626
Vabc-680	0.9871	1.045	0.971	0.9778	1.038	0.9618	0.9829	1.031	0.9688
Vabc-684	0.9853	0	0.9679	0.976	0	0.9587	0.9811	0	0.9657

According to the above table, the voltage considerably improved following the installation of the photovoltaic system, allowing for the treatment of the drop brought on by the increasing load. The voltage of bus 671, for instance, was R_{671}=0.9871, S_{671}=1.045, and T_{671}=0.971. When the load was increased, the voltage dropped to R_{671}=0.9778, S_{671}=1.038, and T_{671}=0.9618. The PV system was next added, and the voltage improved to R_{671}=0.9829, S_{671}=1.031, and T_{671}=0.9688.

Connecting a 500 kW (PV system) to the Bus 671 with Iq = -0.5

Five sets of SunPower PV panels (SPR-305E-WHT-D) were linked in parallel to provide a 500 kW renewable energy system. In this case, at standard conditions (STC) of 25 °C and 1000 W/m² of solar radiation, each set of PV panels produces 100 kW of power. The total power of all five groups is 500 kW. A modified IEEE 13 bus system was connected to the PV system through a bus 671 to compensate for the voltage drop. Active power (P), and 50% reactive power(Q) ware injected when Iq = -0.5 was entered. Before increasing the load, before and after connecting the 400 kW photovoltaic system, the buses' voltage is displayed in Table 4.12.

Table 4.12. The voltage of the buses before the load is increased and both before and after the 500 kW photovoltaic system is connected.

V-Buses	Normal Case			After Increase the Load 75% (bus671) & Before connecting the500kW PV system			After Increase the Load 75% (bus671) & After connecting the500kW PV system		
	R	S	T	R	S	T	R	S	T
Vabc-632	1.021	1.042	1.017	1.021	1.042	1.017	1.021	1.042	1.017
Vabc-633	1.018	1.04	1.015	1.018	1.04	1.015	1.018	1.04	1.015
Vabc-692	0.9871	1.045	0.971	0.9778	1.038	0.9617	0.9853	1.034	0.9716
Vabc-645	0	1.033	1.015	0	1.033	1.015	0	1.033	1.015
Vabc-646	0	1.032	1.014	0	1.032	1.014	0	1.032	1.014
Vabc-671	0.9871	1.045	0.971	0.9778	1.038	0.9618	0.9853	1.034	0.9716
Vabc-675	0.9798	1.046	0.9676	0.9706	1.039	0.9585	0.978	1.035	0.9682
Vabc-652	0.9799	0	0	0.9707	0	0	0.9781	0	0
Vabc-634	0.9941	1.022	0.9961	0.9941	1.022	0.9961	0.9941	1.022	0.9961
Vabc-611	0	0	0.9648	0	0	0.9557	0	0	0.9654
Vabc-680	0.9871	1.045	0.971	0.9778	1.038	0.9618	0.9853	1.034	0.9716
Vabc-684	0.9853	0	0.9679	0.976	0	0.9587	0.9835	0	0.9685

According to the above table, the voltage considerably improved following the installation of the photovoltaic system, allowing for the treatment of the drop brought on by the increasing load. Example: The voltage on bus 671 was in normal condition (R_{671}=0.9871, S_{671}=1.045, and T_{671}=0.971); after increasing the load by 75% on bus 671, the voltage dropped, and the readings were (R_{671}=0.9778, S_{671}=1.038, and T_{671}=0.9618), and then after connecting PV, the voltage improved significantly, and the readings became (R_{671}=0.9853, S_{671}=1.034, and T_{671}=0.9716).

Connecting a 500 kW (PV system) to the Bus 671 with Iq= -1

Five sets of SunPower PV panels (SPR-305E-WHT-D) were linked in parallel to provide a 500 kW renewable energy system. In this case, at standard conditions (STC) of 25 °C and 1000 W/m² of solar radiation, each set of PV panels produces 100 kW of power. The total power of all five groups is 500 kW. A modified IEEE 13 bus system was connected to the PV system through a bus 671 to compensate for the voltage drop. Active power (P), and 100% reactive power(Q) ware injected when Iq = -1 was entered. Before increasing the load, before and after connecting the 400 kW photovoltaic system, the buses' voltage is displayed in Table 4.13.

Table 4.13. The voltage of the buses before the load is increased and both before and after the 500 kW photovoltaic system is connected.

V-Buses	Normal Case			After Increase the Load 75% (bus671) & Before connecting the500kW PV system			After Increase the Load 75% (bus671) & After connecting the500kW PV system		
	R	S	T	R	S	T	R	S	T
Vabc-632	1.021	1.042	1.017	1.021	1.042	1.017	1.021	1.042	1.017
Vabc-633	1.018	1.04	1.015	1.018	1.04	1.015	1.018	1.04	1.015
Vabc-692	0.9871	1.045	0.971	0.9778	1.038	0.9617	0.9874	1.037	0.9742
Vabc-645	0	1.033	1.015	0	1.033	1.015	0	1.033	1.015
Vabc-646	0	1.032	1.014	0	1.032	1.014	0	1.032	1.014
Vabc-671	0.9871	1.045	0.971	0.9778	1.038	0.9618	0.9874	1.037	0.9742
Vabc-675	0.9798	1.046	0.9676	0.9706	1.039	0.9585	0.9801	1.038	0.9709
Vabc-652	0.9799	0	0	0.9707	0	0	0.9802	0	0
Vabc-634	0.9941	1.022	0.9961	0.9941	1.022	0.9961	0.9941	1.022	0.9961
Vabc-611	0	0	0.9648	0	0	0.9557	0	0	0.9681
Vabc-680	0.9871	1.045	0.971	0.9778	1.038	0.9618	0.9874	1.037	0.9742
Vabc-684	0.9853	0	0.9679	0.976	0	0.9587	0.9856	0	0.9712

The voltage significantly improved after the photovoltaic system was installed, enabling the treatment of the drop caused by the rising load, as seen in the above table. For instance, bus 671's voltage was in normal condition (R_{671}=0.9871, S_{671}=1.045, and T_{671}=0.971). However, when the load was increased by 75%, the voltage decreased and the readings were (R_{671}=0.9778, S_{671}=1.038, and T_{671}=0.9618). The voltage then improved significantly after connecting PV, and the readings became (R_{671}=0.9874, S_{671}=1.037, and T_{671}=0.9742).

Increase the load on bus 671 by 100%)

The active and reactive power load on bus 671 was raised by 100% in the modified IEEE 13 bus test system circuit. The balanced loads on bus 671 were Q(R = 220kVar, S = 220kVar, and T = 220kVar), and P(R = 385kW, S = 385kW, and T = 385kW). The voltage of each bus was measured when the loads were increased to P(R = 770kW, S = 770kW, and T = 770kW), and Q(R = 440kVar, S = 440kVar, and T = 440kVar). Below is Table 4.14. that displays the voltage measurements along with the percentage decrease that occurred in all buses.

Table 4.14. The voltage on the buses both before and after the bus 671's load was increased by 100%.

V-Buses	Normal Case			After Increase the Load 100% (bus671)			Drop Rate%		
	R	S	T	R	S	T	R	S	T
Vabc-632	1.021	1.042	1.017	1.021	1.042	1.017	0	0	0
Vabc-633	1.018	1.04	1.015	1.018	1.04	1.015	0	0	0
Vabc-692	0.9871	1.045	0.971	0.9747	1.035	0.9587	-1.27%	0.67%	-1.45%
Vabc-645	0	1.033	1.015	0	1.033	1.015	0	0	0%
Vabc-646	0	1.032	1.014	0	1.032	1.014	0	0	0
Vabc-671	0.9871	1.045	0.971	0.9747	1.035	0.9587	-1.27%	0.67%	-1.44%
Vabc-675	0.9798	1.046	0.9676	0.9675	1.036	0.9554	-1.27%	0.76%	-1.69%
Vabc-652	0.9799	0	0	0.9676	0	0	-1.27%	0	0
Vabc-634	0.9941	1.022	0.9961	0.9941	1.022	0.9961	0	0	0
Vabc-611	0	0	0.9648	0	0	0.9527	0	0	-1.44%
Vabc-680	0.9871	1.045	0.971	0.9747	1.035	0.9587	-1.27%	0.67%	-1.44%
Vabc-684	0.9853	0	0.9679	0.9729	0	0.9557	-1.27%	0	-1.44%

Table 4.14 shows that when bus 671's load grew, the buses nearest to it were impacted because the voltage dropped at different rates, even though the system did not fail entirely.

Figure 4.7. shows the voltage, current, and power on bus 671 after increasing the load by 100% on bus 671.

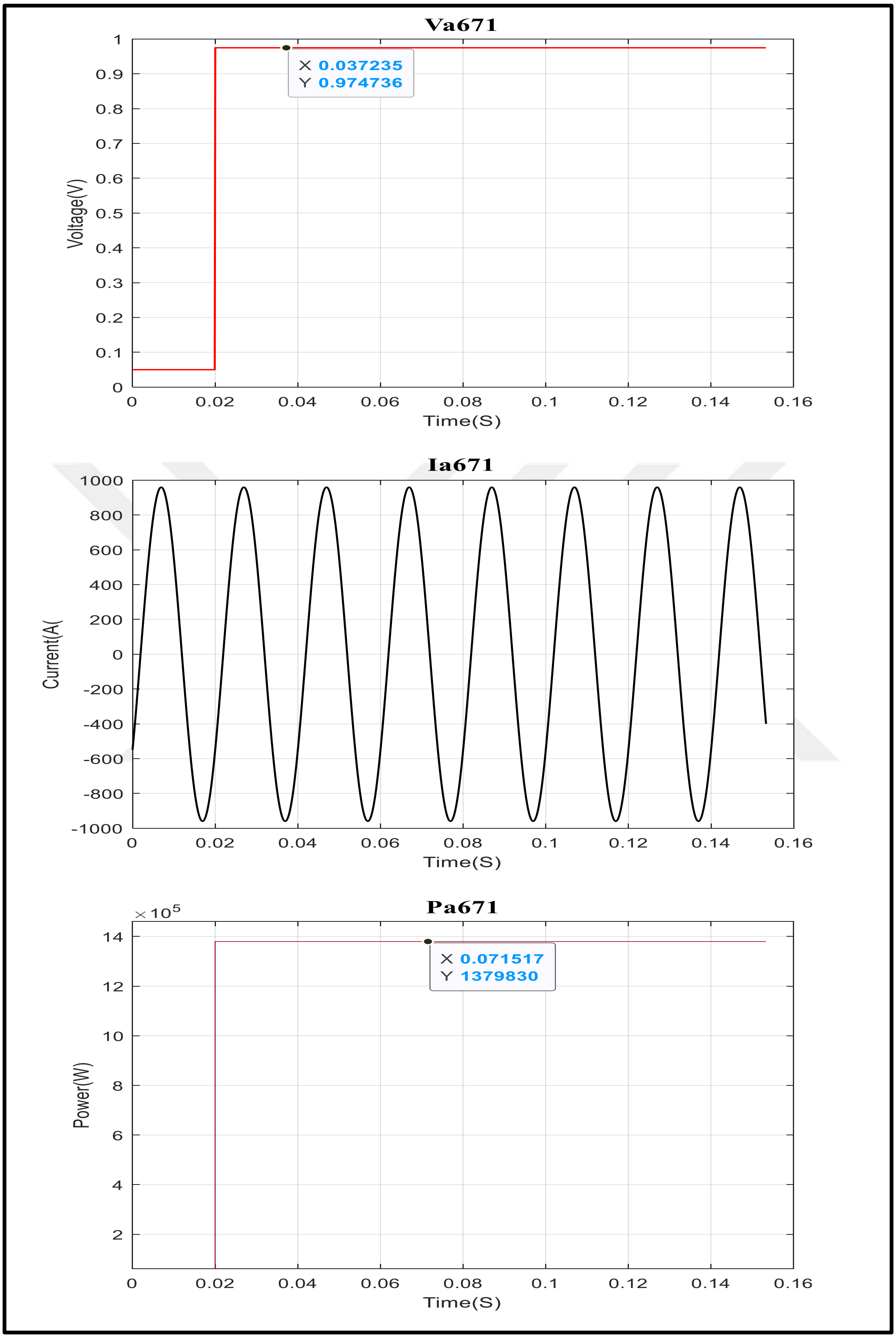

Figure 4.7. The voltage, current, and power on bus 671 after increasing the load by 100% on bus 671.

Connecting a 500 kW (PV system) to the Bus 671 with Iq=0

Five sets of SunPower PV panels (SPR-305E-WHT-D) were linked in parallel to provide a 500 kW renewable energy system. In this case, at standard conditions (STC) of 25 °C and 1000 W/m² of solar radiation, each set of PV panels produces 100 kW of power. The total power of all five groups is 500 kW. A modified IEEE 13 bus system was connected to the PV system through a bus 671 to compensate for the voltage drop. Only active power (pure P) was injected when Iq = 0 was entered. Before increasing the load, before and after connecting the 500 kW photovoltaic system, the buses' voltage is displayed in Table 4.15.

Table 4.15. The voltage of the buses before increasing load, before and after connecting the 500 kW photovoltaic system.

V-Buses	Normal Case			After Increase the Load 100% (bus671) & Before connecting the500kW PV system			After Increase the Load 100% (bus671) & After connecting the500kW PV system		
	R	S	T	R	S	T	R	S	T
Vabc-632	1.021	1.042	1.017	1.021	1.042	1.017	1.021	1.042	1.017
Vabc-633	1.018	1.04	1.015	1.018	1.04	1.015	1.018	1.04	1.015
Vabc-692	0.9871	1.045	0.971	0.9747	1.035	0.9587	0.9799	1.029	0.9658
Vabc-645	0	1.033	1.015	0	1.033	1.015	0	1.033	1.015
Vabc-646	0	1.032	1.014	0	1.032	1.014	0	1.032	1.014
Vabc-671	0.9871	1.045	0.971	0.9747	1.035	0.9587	0.9799	1.029	0.9658
Vabc-675	0.9798	1.046	0.9676	0.9675	1.036	0.9554	0.9727	1.03	0.9625
Vabc-652	0.9799	0	0	0.9676	0	0	0.9728	0	0
Vabc-634	0.9941	1.022	0.9961	0.9941	1.022	0.9961	0.9941	1.022	0.9961
Vabc-611	0	0	0.9648	0	0	0.9527	0	0	0.9597
Vabc-680	0.9871	1.045	0.971	0.9747	1.035	0.9587	0.9799	1.029	0.9658
Vabc-684	0.9853	0	0.9679	0.9729	0	0.9557	0.9781	0	0.9627

According to the above table, the voltage considerably improved following the installation of the photovoltaic system, allowing for the treatment of the drop brought on by the increasing load. The voltage of bus 671, for instance, was R_{671}=0.9871, S_{671}=1.045, and T_{671}=0.971. When the load was increased, the voltage dropped to R_{671}=0.9747, S_{671}=1.035, and T_{671}=0.9587. The PV system was next added, and the voltage improved to R_{671}=0.9799, S_{671}=1.029, and T_{671}=0.9658.

Figure 4.8. shows the voltage, current, and power on bus 671(phase R) after increasing the load by 100% on bus 671 with a PV system (Iq=0).

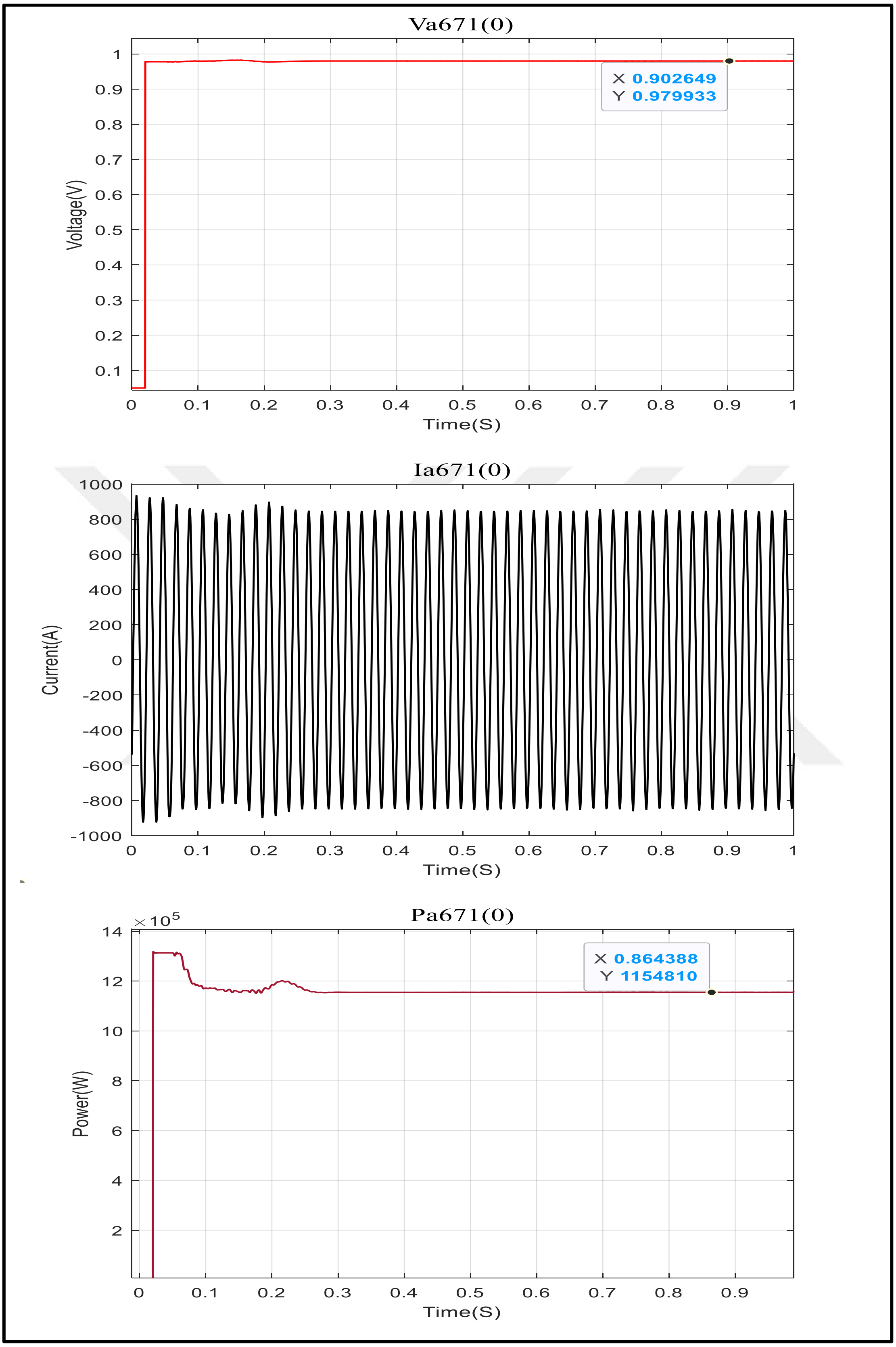

Figure 4.8. The voltage, current, and power on bus 671(phase R) after increasing the load by 100% on bus 671 with a PV system (Iq=0).

Connecting a 500 kW (PV system) to the Bus 671 with Iq= -0.5

Five sets of SunPower PV panels (SPR-305E-WHT-D) were linked in parallel to provide a 500 kW renewable energy system. In this case, at standard conditions (STC) of 25 °C and 1000 W/m² of solar radiation, each set of PV panels produces 100 kW of power. The total power of all five groups is 500 kW. A modified IEEE 13 bus system was connected to the PV system through a bus 671 to compensate for the voltage drop. Active power (P), and 50% reactive power(Q) ware injected when Iq = -0.5 was entered. Before increasing the load, before and after connecting the 400 kW photovoltaic system, the buses' voltage is displayed in Table 4.16.

Table 4.16. The voltage of the buses before the load is increased and both before and after the 500 kW photovoltaic system is connected.

V-Buses	Normal Case			After Increase the Load 100% (bus671) & Before connecting the500kW PV system			After Increase the Load 100% (bus671) & After connecting the500kW PV system		
	R	S	T	R	S	T	R	S	T
Vabc-632	1.021	1.042	1.017	1.021	1.042	1.017	1.021	1.042	1.017
Vabc-633	1.018	1.04	1.015	1.018	1.04	1.015	1.018	1.04	1.015
Vabc-692	0.9871	1.045	0.971	0.9747	1.035	0.9587	0.9823	1.031	0.9685
Vabc-645	0	1.033	1.015	0	1.033	1.015	0	1.033	1.015
Vabc-646	0	1.032	1.014	0	1.032	1.014	0	1.032	1.014
Vabc-671	0.9871	1.045	0.971	0.9747	1.035	0.9587	0.9823	1.031	0.9685
Vabc-675	0.9798	1.046	0.9676	0.9675	1.036	0.9554	0.975	1.033	0.9652
Vabc-652	0.9799	0	0	0.9676	0	0	0.9751	0	0
Vabc-634	0.9941	1.022	0.9961	0.9941	1.022	0.9961	0.9941	1.022	0.9961
Vabc-611	0	0	0.9648	0	0	0.9527	0	0	0.9624
Vabc-680	0.9871	1.045	0.971	0.9747	1.035	0.9587	0.9823	1.031	0.9685
Vabc-684	0.9853	0	0.9679	0.9729	0	0.9557	0.9804	0	0.9655

According to the above table, the voltage considerably improved following the installation of the photovoltaic system, allowing for the treatment of the drop brought on by the increasing load. Example: The voltage on bus 671 was in normal condition (R_{671}=0.9871, S_{671}=1.045, and T_{671}=0.971); after increasing the load by 100% on bus 671, the voltage dropped, and the readings were (R_{671}=0.9747, S_{671}=1.035, and T_{671}=0.9587), and then after connecting PV, the voltage improved significantly, and the readings became (R_{671}=0.9823, S_{671}=1.031, and T_{671}=0.9685).

Figure 4.9. shows the voltage, current, and power on bus 671(phase R) after increasing the load by 100% on bus 671 with a PV system (Iq=-0.5).

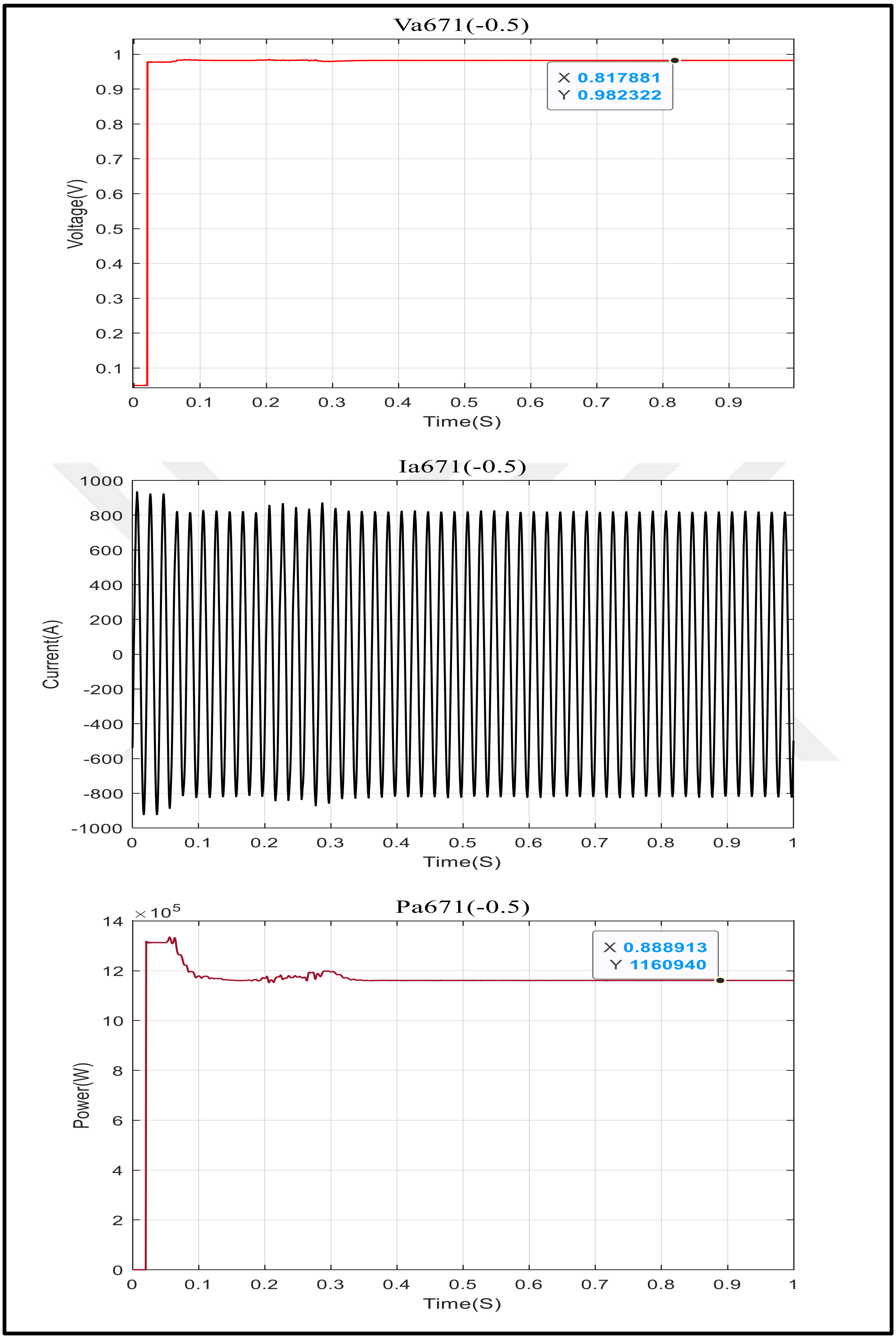

Figure 4.9. The voltage, current, and power on bus 671(phase R) after increasing the load by 100% on bus 671 with a PV system (Iq=-0.5).

Connecting a 500 kW (PV system) to the Bus 671 with Iq= -1

Five sets of SunPower PV panels (SPR-305E-WHT-D) were linked in parallel to provide a 500 kW renewable energy system. In this case, at standard conditions (STC) of 25 °C and 1000 W/m² of solar radiation, each set of PV panels produces 100 kW of power. The total power of all five groups is 500 kW. A modified IEEE 13 bus system was connected to the PV system through a bus 671 to compensate for the voltage drop. Active power (P), and 100% reactive power(Q) ware injected when Iq = -1 was entered. Before increasing the load, before and after connecting the 400 kW photovoltaic system, the buses' voltage is displayed in Table 4.17.

Table 4.17. The voltage of the buses before the load is increased and both before and after the 500 kW photovoltaic system is connected.

V-Buses	Normal Case			After Increase the Load 100% (bus671) & Before connecting the500kW PV system			After Increase the Load 100% (bus671) & After connecting the500kW PV system		
	R	S	T	R	S	T	R	S	T
Vabc-632	1.021	1.042	1.017	1.021	1.042	1.017	1.021	1.042	1.017
Vabc-633	1.018	1.04	1.015	1.018	1.04	1.015	1.018	1.04	1.015
Vabc-692	0.9871	1.045	0.971	0.9747	1.035	0.9587	0.9844	1.034	0.9711
Vabc-645	0	1.033	1.015	0	1.033	1.015	0	1.033	1.015
Vabc-646	0	1.032	1.014	0	1.032	1.014	0	1.032	1.014
Vabc-671	0.9871	1.045	0.971	0.9747	1.035	0.9587	0.9844	1.034	0.9711
Vabc-675	0.9798	1.046	0.9676	0.9675	1.036	0.9554	0.9771	1.035	0.9678
Vabc-652	0.9799	0	0	0.9676	0	0	0.9772	0	0
Vabc-634	0.9941	1.022	0.9961	0.9941	1.022	0.9961	0.9941	1.022	0.9961
Vabc-611	0	0	0.9648	0	0	0.9527	0	0	0.965
Vabc-680	0.9871	1.045	0.971	0.9747	1.035	0.9587	0.9844	1.034	0.9711
Vabc-684	0.9853	0	0.9679	0.9729	0	0.9557	0.9826	0	0.9681

The voltage significantly improved after the photovoltaic system was installed, enabling the treatment of the drop caused by the rising load, as seen in the above table. For instance, bus 671's voltage was in normal condition (R_{671}=0.9871, S_{671}=1.045, and T_{671}=0.971). However, when the load was increased by 100%, the voltage decreased and the readings were (R_{671}=0.9747, S_{671}=1.035, and T_{671}=0.9587). The voltage then improved significantly after connecting PV, and the readings became (R_{671}=0.9844, S_{671}=1.034, and T_{671}=0.9711).

Figure 4.10. shows the voltage, current, and power on bus 671(phase R) after increasing the load by 100% on bus 671 with a PV system (Iq=-1).

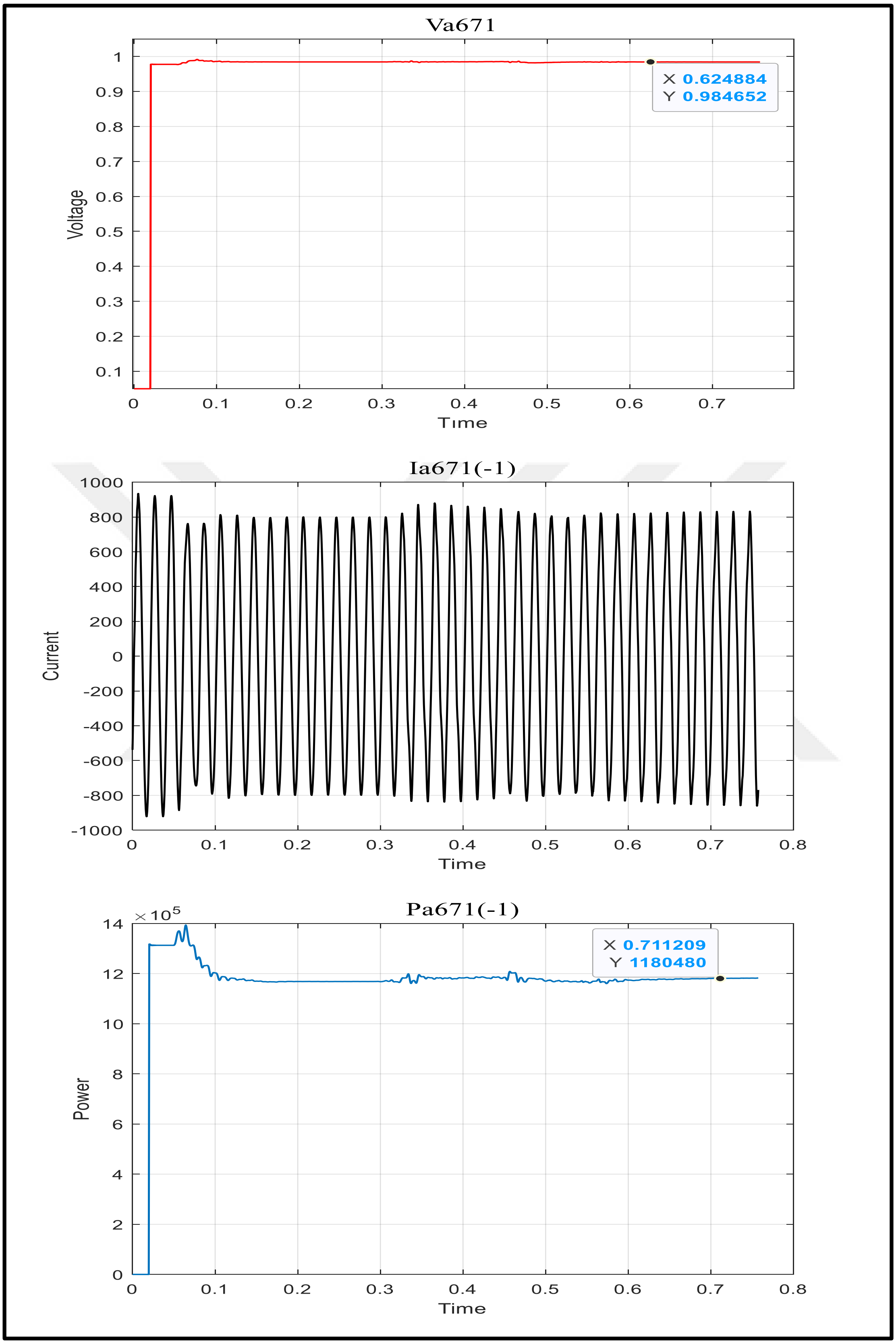

Figure 4.10. The voltage, current, and power on bus 671(phase R) after increasing the load by 100% on bus 671 with a PV system (Iq=-1).

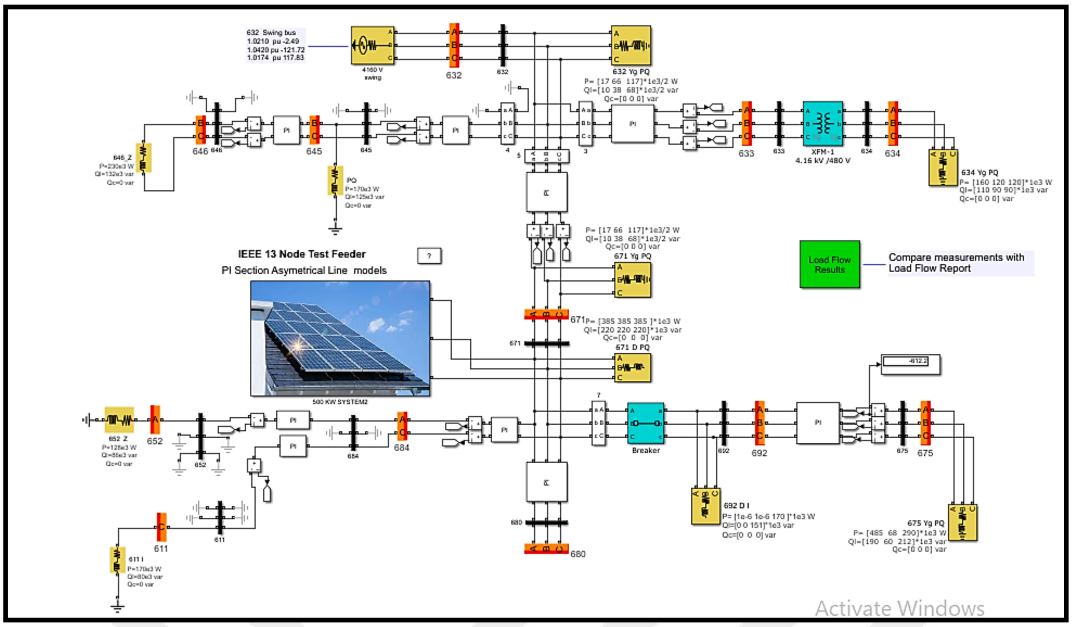

Figure 4.11. The electrical power system (Modified IEEE 13-Bus Test System) with 500KW PV system in bus 671

The modified IEEE 13 bus test system circuit model is displayed in Figure 4.11. after the connection of the PV system to bus 671. Through bus 671, the PV system was integrated with the modified IEEE 13 bus test system, and four scenarios were examined.

Scenario 1: The load connected to bus 671 was increased by 25%. Then the voltage on the buses was recorded to see the voltage drop that occurred. Then, the PV system (500 kW) was integrated via bus 671. Then the voltage on the buses was measured under the following conditions: injection of pure active power only (Iq = 0), injection of 50% reactive power and 100% active power (Iq = -0.5), and injection of 100% reactive power and 100% active power (Iq = -1). It was found that the PV system compensated for the voltage drop caused by the 25% increase in load. According to the measurements, we also found that the voltage on the buses was larger than its actual value before the load increase, which may have a negative impact. For example, The voltage of the bus 671 is (R_{671}=0.9871, S_{671}=1.045, and T_{671}=0.971). The voltage on the bus 671 after increasing the load. (R_{671}=0.984, S_{671}=1.043, and T_{671}=0.9679), and after adding the PV system, we noticed that the bus voltage was at

- when Iq=0 (R_{671}=0.989, S_{671}=1.036, and T_{671}=0.975),
- when Iq = -0.5 (R_{671} = 0.9914, S_{671} = 1.039, and T_{671} = 0.9777),

- and when Iq = -1 (R = 0.9935, S_{671} = 1.042, and T_{671} = 0.9805).

Scenario 2: The load connected to bus 671 was increased by 50%. Then the voltage on the buses was recorded to see the voltage drop that occurred. Then, the PV system (500 kW) was integrated via bus 671. Then the voltage on the buses was measured under the following conditions: injection of pure active power only (Iq = 0), injection of 50% reactive power and 100% active power (Iq = -0.5), and injection of 100% reactive power and 100% active power (Iq = -1). We saw that the PV system compensated for the voltage drop caused by the 50% increase in load. For example, The voltage of the bus 671 is (R_{671}=0.9871, S_{671}=1.045, and T_{671}=0.971). After increasing the load (R_{671} = 0.9809, S_{671} = 1.04, and T_{671} = 0.9648) and after adding the PV system, we noticed that the overall voltage was at

- When Iq = 0 (R_{671} = 0.986, S_{671} = 1.034, and T_{671} = 0.9719),
- when Iq = -0.5 (R_{671} = 0.9884, S_{671} = 1.037, and T_{671} = 0.9747),
- and when Iq = -1 (R_{671} = 0.9905, S_{671} = 1.039, and T_{671} = 0.9773).

We notice that in the case of Iq = -0.5, the voltage was raised to its state before increasing the load.

Scenario 3: The load connected to bus 671 was increased by 75%. Then the voltage on the buses was recorded to see the voltage drop that occurred. Then, the PV system (500 kW) was integrated via bus 671. Then the voltage on the buses was measured under the following conditions: injection of pure active power only (Iq = 0), injection of 50% reactive power and 100% active power (Iq = -0.5), and injection of 100% reactive power and 100% active power (Iq = -1). We saw that the PV system compensated for the voltage drop caused by the 75% increase in load. For example, the bus voltage is 671 (R_{671}=0.9871, S_{671}=1.045, and T_{671}=0.971). After increasing the load (R_{671} = 0.9778, S_{671}= 1.038, and T_{671} = 0.9618) and after adding the PV system, we noticed that the overall voltage was at

- When Iq = 0 (R_{671} = 0.9829, S_{671} = 1.031, and T_{671} = 0.9688),
- when Iq = -0.5 (R_{671} = 0.9853, S_{671} = 1.034, and T_{671} = 0.9716).
- When Iq = -1 (R_{671} = 0.9874, S_{671}= 1.037, and T_{671} = 0.9742),

We notice that in the case of Iq = -1, the voltage was raised to its state before increasing the load.

Scenario 4: The load connected to bus 671 was increased by 100%. Then the voltage on the buses was recorded to see the voltage drop that occurred. Then, the PV system (500 kW) was integrated via bus 671. Then the voltage on the buses was measured under the following conditions: injection of pure active power only (Iq = 0), injection of 50% reactive power and 100% active power (Iq = -0.5), and injection of 100% reactive power and 100% active power (Iq = -1). We saw that the PV system compensated for the voltage drop caused by the 100% increase in load. For example, the bus voltage is 671 (R_{671}=0.9871, S_{671}=1.045, and T_{671}=0.971). After increasing the load (R_{671} = 0.9747, S_{671} = 1.035, and T_{671} = 0.9587) and after adding the PV system, we noticed that the overall voltage was at

- When Iq = 0 (R_{671} = 0.9799, S_{671} = 1.029, and T_{671}= 0.9658),
- when Iq = -0.5 (R_{671} = 0.9823, S_{671} = 1.031, and T_{671} = 0.9685),
- when Iq = -1 (R_{671}= 0.9844, S_{671} = 1.034, and T_{671} = 0.9711),

We notice that in the case of Iq = -1, the voltage did not return to its previous state, which indicates that the increase in the load was not compensated for by the power injected through the photovoltaic system.

4.1.2. Second case: Increase the load on bus 675

Increase the load on bus 675 by 25%

The active and reactive power load on bus 675 was raised by 25% in the modified IEEE 13 bus test system circuit. The imbalanced loads on bus 675 were Q(R = 190kVar, S = 60kVar, and T = 212kVar), and P(R = 485kW, S = 68kW, and T = 290kW). The voltage of each bus was measured when the loads were increased to P(R = 606.25kW, S = 85kW, and T = 362.5kW), and Q(R = 237.5kVar, S = 75kVar, and T = 265kVar). Below is Table 4.18 that displays the voltage measurements along with the percentage decrease that occurred in all buses.

Table 4.18. The voltage on the buses both before and after the bus 675's load was increased by 25%.

V-Buses	Normal Case			After Increase the Load 25% (bus675)			Drop Rate%		
	R	S	T	R	S	T	R	S	T
Vabc-632	1.021	1.042	1.017	1.021	1.042	1.017	0	0	0
Vabc-633	1.018	1.04	1.015	1.018	1.04	1.015	0	0	0
Vabc-692	0.9871	1.045	0.971	0.9836	1.048	0.9663	-0.36%	0.29%	-0.49%
Vabc-645	0	1.033	1.015	0	1.033	1.015	0	0	0
Vabc-646	0	1.032	1.014	0	1.032	1.014	0	0	0
Vabc-671	0.9871	1.045	0.971	0.9836	1.048	0.9663	-0.36%	0.29%	-0.49%
Vabc-675	0.9798	1.046	0.9676	0.9745	1.049	0.9621	-0.54%	0.29%	-0.57%
Vabc-652	0.9799	0	0	0.9764	0	0	-0.36%	0	0
Vabc-634	0.9941	1.022	0.9961	0.9941	1.022	0.9961	0	0	0
Vabc-611	0	0	0.9648	0	0	0.9602	0	0	-0.48%
Vabc-680	0.9871	1.045	0.971	0.9836	1.048	0.9663	-0.36%	0.29%	-0.49%
Vabc-684	0.9853	0	0.9679	0.9818	0	0.9632	-0.36%	0	-0.49%

Table 4.18. shows that when bus 675's load grew, the buses nearest to it were impacted because the voltage dropped at different rates, even though the system did not fail entirely.

Connecting a 400 kW (PV system) to the Bus 675 with Iq=0

Four sets of SunPower PV panels (SPR-305E-WHT-D) were linked in parallel to provide a 400 kW renewable energy system. In this case, at standard conditions (STC) of 25 °C and 1000 W/m² of solar radiation, each set of PV panels produces 100 kW of power. The total power of all four groups is 400 kW. A modified IEEE 13 bus system was connected to the PV system through a bus 675 to compensate for the voltage drop. Only active power (pure P) was injected when Iq = 0 was entered. Before increasing the load, before and after connecting the 400 kW photovoltaic system, the buses' voltage is displayed in Table 4.19.

Table 4.19. The voltage of the buses before increasing load, before and after connecting the 400 kW photovoltaic system.

V-Buses	Normal Case			After Increase the Load 25% (bus675) & Before connecting the400kW PV system			After Increase the Load 25% (bus675) & After connecting the400kW PV system		
	R	S	T	R	S	T	R	S	T
Vabc-632	1.021	1.042	1.017	1.021	1.042	1.017	1.021	1.042	1.017
Vabc-633	1.018	1.04	1.015	1.018	1.04	1.015	1.018	1.04	1.015
Vabc-692	0.9871	1.045	0.971	0.9836	1.048	0.9663	0.9886	1.041	0.9723
Vabc-645	0	1.033	1.015	0	1.033	1.015	0	1.033	1.015
Vabc-646	0	1.032	1.014	0	1.032	1.014	0	1.032	1.014
Vabc-671	0.9871	1.045	0.971	0.9836	1.048	0.9663	0.9886	1.041	0.9723
Vabc-675	0.9798	1.046	0.9676	0.9745	1.049	0.9621	0.9822	1.042	0.9688
Vabc-652	0.9799	0	0	0.9764	0	0	0.9814	0	0
Vabc-634	0.9941	1.022	0.9961	0.9941	1.022	0.9961	0.9941	1.022	0.9961
Vabc-611	0	0	0.9648	0	0	0.9602	0	0	0.9662
Vabc-680	0.9871	1.045	0.971	0.9836	1.048	0.9663	0.9886	1.041	0.9723
Vabc-684	0.9853	0	0.9679	0.9818	0	0.9632	0.9868	0	0.9693

According to the above table, the voltage considerably improved following the installation of the photovoltaic system, allowing for the treatment of the drop brought on by the increasing load. The voltage of bus 675, for instance, was R_{675}=0.9798, S_{675}=1.046, and T_{675}=0.9676. When the load was increased, the voltage dropped to R_{675}=0.9745, S_{675}=1.049, and T_{675}=0.9621. The PV system was next added, and the voltage improved to R_{675}=0.9822, S_{675}=1.042, and T_{675}=0.9688.

Connecting a 400 kW (PV system) to the Bus 675 with Iq= -0.5

Four sets of SunPower PV panels (SPR-305E-WHT-D) were linked in parallel to provide a 400 kW renewable energy system. In this case, at standard conditions (STC) of 25 °C and 1000 W/m² of solar radiation, each set of PV panels produces 100 kW of power. The total power of all four groups is 400 kW. A modified IEEE 13 bus system was connected to the PV system through a bus 675 to compensate for the voltage drop. Active power (P), and 50% reactive power(Q) ware injected when Iq = -0.5 was entered. Before increasing the load, before and after connecting the 400 kW photovoltaic system, the buses' voltage is displayed in Table 4.20.

Table 4.20. The voltage of the buses before increasing load, before and after connecting the 400 kW photovoltaic system.

V-Buses	Normal Case			After Increase the Load 25% (bus675) & Before connecting the400kW PV system			After Increase the Load 25% (bus675) & After connecting the400kW PV system		
	R	S	T	R	S	T	R	S	T
Vabc-632	1.021	1.042	1.017	1.021	1.042	1.017	1.021	1.042	1.017
Vabc-633	1.018	1.04	1.015	1.018	1.04	1.015	1.018	1.04	1.015
Vabc-692	0.9871	1.045	0.971	0.9836	1.048	0.9663	0.9905	1.043	0.9745
Vabc-645	0	1.033	1.015	0	1.033	1.015	0	1.033	1.015
Vabc-646	0	1.032	1.014	0	1.032	1.014	0	1.032	1.014
Vabc-671	0.9871	1.045	0.971	0.9836	1.048	0.9663	0.9906	1.043	0.9745
Vabc-675	0.9798	1.046	0.9676	0.9745	1.049	0.9621	0.9845	1.045	0.9714
Vabc-652	0.9799	0	0	0.9764	0	0	0.9833	0	0
Vabc-634	0.9941	1.022	0.9961	0.9941	1.022	0.9961	0.9941	1.022	0.9961
Vabc-611	0	0	0.9648	0	0	0.9602	0	0	0.9684
Vabc-680	0.9871	1.045	0.971	0.9836	1.048	0.9663	0.9906	1.043	0.9745
Vabc-684	0.9853	0	0.9679	0.9818	0	0.9632	0.9887	0	0.9715

According to the above table, the voltage considerably improved following the installation of the photovoltaic system, allowing for the treatment of the drop brought on by the increasing load. Example: The voltage on bus 675 was in normal condition (R_{675}=0.9798, S_{675}=1.046, and T_{675}=0.9676); after increasing the load by 25% on bus 675, the voltage dropped, and the readings were (R_{675}=0.9745, S_{675}=1.049, and T_{675}=0.9621), and then after connecting PV, the voltage improved significantly, and the readings became (R_{675}=0.9845, S_{675}=1.045, and T_{675}=0.9714).

Connecting a 400 kW (PV system) to the Bus 675 with Iq= -1

Four sets of SunPower PV panels (SPR-305E-WHT-D) were linked in parallel to provide a 400 kW renewable energy system. In this case, at standard conditions (STC) of 25 °C and 1000 W/m² of solar radiation, each set of PV panels produces 100 kW of power. The total power of all four groups is 400 kW. A modified IEEE 13 bus system was connected to the PV system through a bus 675 to compensate for the voltage drop. Active power (P), and 100% reactive power(Q) ware injected when Iq = -1 was entered. Before increasing the load, before and after connecting the 400 kW photovoltaic system, the buses' voltage is displayed in Table 4.21.

Table 4.21. The voltage of the buses before the load is increased and both before and after the 400 kW photovoltaic system is connected.

V-Buses	Normal Case			After Increase the Load 25% (bus675) & Before connecting the400kW PV system			After Increase the Load 25% (bus675) & After connecting the400kW PV system		
	R	S	T	R	S	T	R	S	T
Vabc-632	1.021	1.042	1.017	1.021	1.042	1.017	1.021	1.042	1.017
Vabc-633	1.018	1.04	1.015	1.018	1.04	1.015	1.018	1.04	1.015
Vabc-692	0.9871	1.045	0.971	0.9836	1.048	0.9663	0.9924	1.045	0.9767
Vabc-645	0	1.033	1.015	0	1.033	1.015	0	1.033	1.015
Vabc-646	0	1.032	1.014	0	1.032	1.014	0	1.032	1.014
Vabc-671	0.9871	1.045	0.971	0.9836	1.048	0.9663	0.9924	1.045	0.9767
Vabc-675	0.9798	1.046	0.9676	0.9745	1.049	0.9621	0.9866	1.047	0.974
Vabc-652	0.9799	0	0	0.9764	0	0	0.9851	0	0
Vabc-634	0.9941	1.022	0.9961	0.9941	1.022	0.9961	0.9941	1.022	0.9961
Vabc-611	0	0	0.9648	0	0	0.9602	0	0	0.9706
Vabc-680	0.9871	1.045	0.971	0.9836	1.048	0.9663	0.9924	1.045	0.9767
Vabc-684	0.9853	0	0.9679	0.9818	0	0.9632	0.9905	0	0.9737

According to the above table, the voltage considerably improved following the installation of the photovoltaic system, allowing for the treatment of the drop brought on by the increasing load. Example: The voltage on bus 675 was in normal condition (R_{675}=0.9798, S_{675}=1.046, and T_{675}=0.9676). After increasing the load by 25% on bus 675, the voltage dropped, and the readings were (R_{675}=0.9745, S_{675}=1.049, and T_{675}=0.9621), and then after connecting PV, the voltage improved significantly, and the readings became (R_{675}=0.9866, S_{675}=1.047, and T_{675}=0.974).

Increase the load on bus 675 by 50%

The active and reactive power load on bus 675 was raised by 50% in the modified IEEE 13 bus test system circuit. The imbalanced loads on bus 675 were Q(R = 190kVar, S = 60kVar, and T = 212kVar), and P(R = 485kW, S = 68kW, and T = 290kW). The voltage of each bus was measured when the loads were increased to P(R = 727.5kW, S = 102kW, and T = 435kW), and Q(R = 285kVar, S = 90kVar, and T = 318kVar). Below is Table 4.22. that displays the voltage measurements along with the percentage decrease that occurred in all buses.

Table 4.22. The voltage on the buses both before and after the bus 675’s load was increased by 50%.

V-Buses	Normal Case			After Increase the Load 50% (bus675)			Drop Rate%		
	R	S	T	R	S	T	R	S	T
Vabc-632	1.021	1.042	1.017	1.021	1.042	1.017	0	0	0
Vabc-633	1.018	1.04	1.015	1.018	1.04	1.015	0	0	0
Vabc-692	0.9871	1.045	0.971	0.98	1.05	0.9617	-0.72%	0.48%	-1.45%
Vabc-645	0	1.033	1.015	0	1.033	1.015	0	0	0
Vabc-646	0	1.032	1.014	0	1.032	1.014	0	0	0
Vabc-671	0.9871	1.045	0.971	0.9801	1.05	0.9617	-0.71%	0.48%	-1.44%
Vabc-675	0.9798	1.046	0.9676	0.9693	1.052	0.9568	-1.08%	0.57%	-1.69%
Vabc-652	0.9799	0	0	0.9729	0	0	-0.72%	0	0
Vabc-634	0.9941	1.022	0.9961	0.9941	1.022	0.9961	0	0	0
Vabc-611	0	0	0.9648	0	0	0.9556	0	0	-1.44%
Vabc-680	0.9871	1.045	0.971	0.9801	1.05	0.9617	-0.71%	0.48%	-1.44%
Vabc-684	0.9853	0	0.9679	0.9782	0	0.9587	-0.73%	0	-1.44%

Table 4.22. shows that when bus 675’s load grew, the buses nearest to it were impacted because the voltage dropped at different rates, even though the system did not fail entirely.

Figure 4.12. shows the voltage, current, and power on bus 675 after increasing the load by 50% on bus 675.

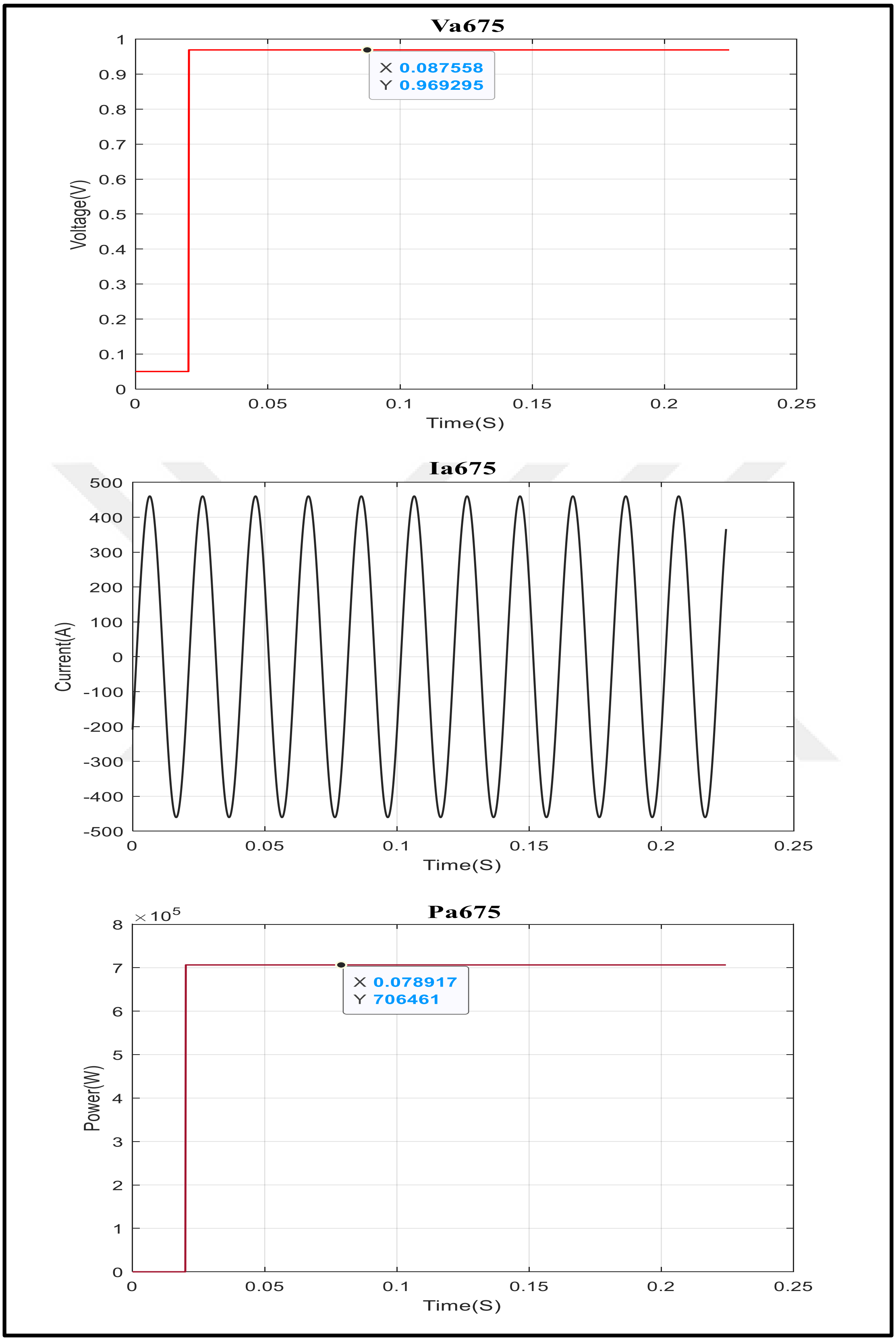

Figure 4.12. The voltage, current, and power on bus 675 after increasing the load by 50% on bus 675.

Connecting a 400 kW (PV system) to the Bus 675 with Iq=0

Four sets of SunPower PV panels (SPR-305E-WHT-D) were linked in parallel to provide a 400 kW renewable energy system. In this case, at standard conditions (STC) of 25 °C and 1000 W/m² of solar radiation, each set of PV panels produces 100 kW of power. The total power of all four groups is 400 kW. A modified IEEE 13 bus system was connected to the PV system through a bus 675 to compensate for the voltage drop. Only active power (pure P) was injected when Iq = 0 was entered. Before increasing the load, before and after connecting the 400 kW photovoltaic system, the buses' voltage is displayed in Table 4.23.

Table 4.23. The voltage of the buses before increasing load, before and after connecting the 400 KW photovoltaic system.

V-Buses	Normal Case			After Increase the Load 50% (bus675) & Before connecting the400kW PV system			After Increase the Load 50% (bus675) & After connecting the400kW PV system		
	R	S	T	R	S	T	R	S	T
Vabc-632	1.021	1.042	1.017	1.021	1.042	1.017	1.021	1.042	1.017
Vabc-633	1.018	1.04	1.015	1.018	1.04	1.015	1.018	1.04	1.015
Vabc-692	0.9871	1.045	0.971	0.98	1.05	0.9617	0.9856	1.043	0.968
Vabc-645	0	1.033	1.015	0	1.033	1.015	0	1.033	1.015
Vabc-646	0	1.032	1.014	0	1.032	1.014	0	1.032	1.014
Vabc-671	0.9871	1.045	0.971	0.9801	1.05	0.9617	0.9856	1.043	0.968
Vabc-675	0.9798	1.046	0.9676	0.9693	1.052	0.9568	0.9776	1.044	0.9636
Vabc-652	0.9799	0	0	0.9729	0	0	0.9784	0	0
Vabc-634	0.9941	1.022	0.9961	0.9941	1.022	0.9961	0.9941	1.022	0.9961
Vabc-611	0	0	0.9648	0	0	0.9556	0	0	0.9619
Vabc-680	0.9871	1.045	0.971	0.9801	1.05	0.9617	0.9856	1.043	0.968
Vabc-684	0.9853	0	0.9679	0.9782	0	0.9587	0.9838	0	0.965

According to the above table, the voltage considerably improved following the installation of the photovoltaic system, allowing for the treatment of the drop brought on by the increasing load. The voltage of bus 675, for instance, was R_{675}=0.9798, S_{675}=1.046, and T_{675}=0.9676. When the load was increased, the voltage dropped to R_{675}=0.9693, S_{675}=1.052, and T_{675}=0.9568. The PV system was next added, and the voltage improved to R_{675}=0.9776, S_{675}=1.044, and T_{675}=0.9636.

Figure 4.13. shows the voltage, current, and power on bus 675 after increasing the load by 50% on bus 675 with a PV system (Iq=0).

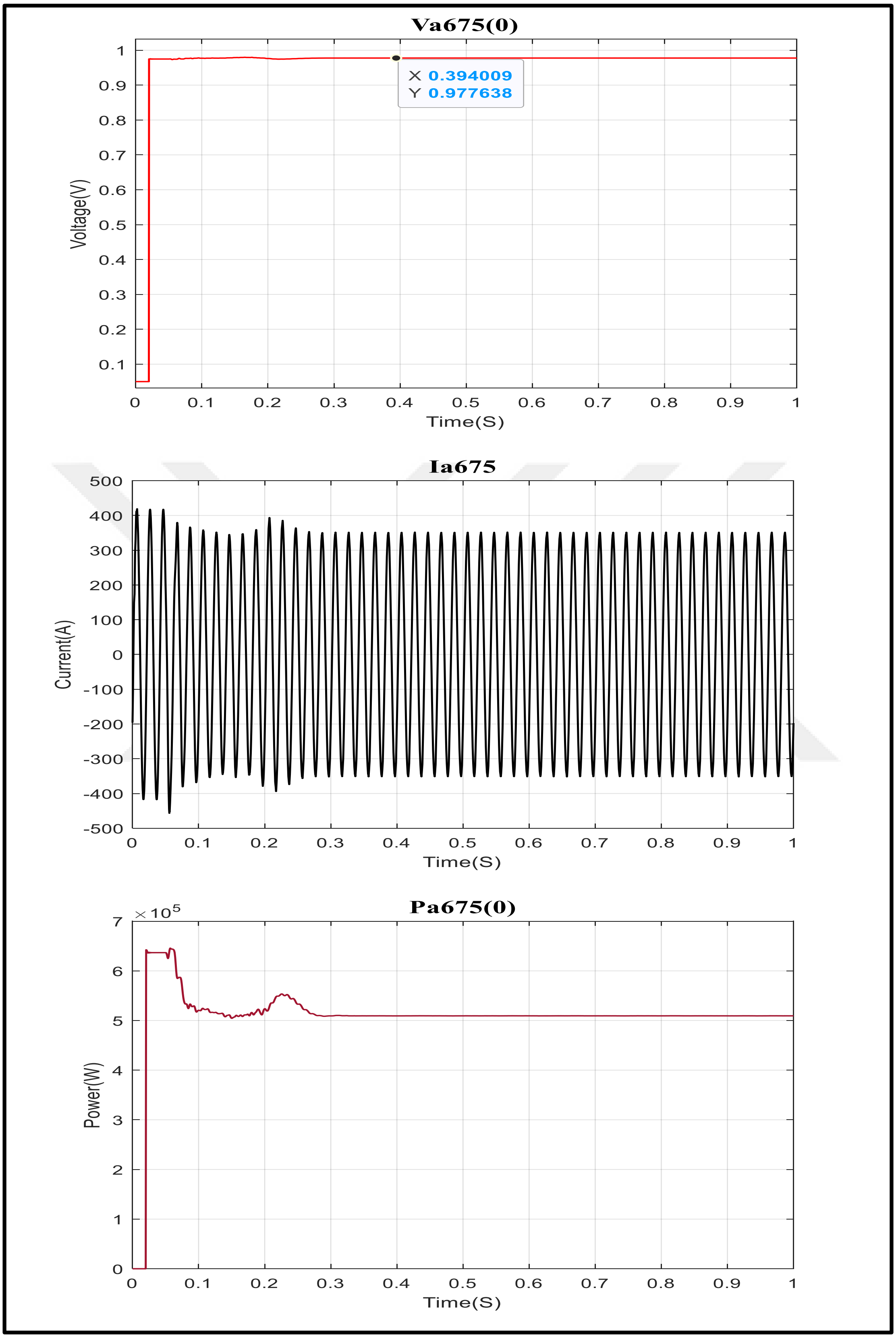

Figure 4.13. The voltage, current, and power on bus 675 after increasing the load by 50% on bus 675 with a PV system (Iq=0).

Connecting a 400 kW (PV system) to the Bus 675 with Iq= -0.5

Four sets of SunPower PV panels (SPR-305E-WHT-D) were linked in parallel to provide a 400 kW renewable energy system. In this case, at standard conditions (STC) of 25 °C and 1000 W/m² of solar radiation, each set of PV panels produces 100 kW of power. The total power of all four groups is 400 kW. A modified IEEE 13 bus system was connected to the PV system through a bus 675 to compensate for the voltage drop. Active power (P), and 50% reactive power(Q) ware injected when Iq = -0.5 was entered. Before increasing the load, before and after connecting the 400 kW photovoltaic system, the buses' voltage is displayed in Table 4.24.

Table 4.24. The voltage of the buses before increasing load, before and after connecting the 400 kW photovoltaic system.

V-Buses	Normal Case			After Increase the Load 50% (bus675) & Before connecting the400kW PV system			After Increase the Load 50% (bus675) & After connecting the400kW PV system		
	R	S	T	R	S	T	R	S	T
Vabc-632	1.021	1.042	1.017	1.021	1.042	1.017	1.021	1.042	1.017
Vabc-633	1.018	1.04	1.015	1.018	1.04	1.015	1.018	1.04	1.015
Vabc-692	0.9871	1.045	0.971	0.98	1.05	0.9617	0.9875	1.045	0.9702
Vabc-645	0	1.033	1.015	0	1.033	1.015	0	1.033	1.015
Vabc-646	0	1.032	1.014	0	1.032	1.014	0	1.032	1.014
Vabc-671	0.9871	1.045	0.971	0.9801	1.05	0.9617	0.9875	1.045	0.9702
Vabc-675	0.9798	1.046	0.9676	0.9693	1.052	0.9568	0.9799	1.046	0.9662
Vabc-652	0.9799	0	0	0.9729	0	0	0.9803	0	0
Vabc-634	0.9941	1.022	0.9961	0.9941	1.022	0.9961	0.9941	1.022	0.9961
Vabc-611	0	0	0.9648	0	0	0.9556	0	0	0.964
Vabc-680	0.9871	1.045	0.971	0.9801	1.05	0.9617	0.9875	1.045	0.9702
Vabc-684	0.9853	0	0.9679	0.9782	0	0.9587	0.9857	0	0.9671

According to the above table, the voltage considerably improved following the installation of the photovoltaic system, allowing for the treatment of the drop brought on by the increasing load. Example: The voltage on bus 675 was in normal condition (R_{675}=0.9798, S_{675}=1.046, and T_{675}=0.9676); after increasing the load by 50% on bus 675, the voltage dropped, and the readings were (R_{675}=0.9693, S_{675}=1.052, and T_{675}=0.9568), and then after connecting PV, the voltage improved significantly, and the readings became (R_{675}=0.9799, S_{675}=1.046, and T_{675}=0.9662).

Figure 4.14. shows the voltage, current, and power on bus 675 after increasing the load by 50% on bus 675 with a PV system (Iq=-0.5).

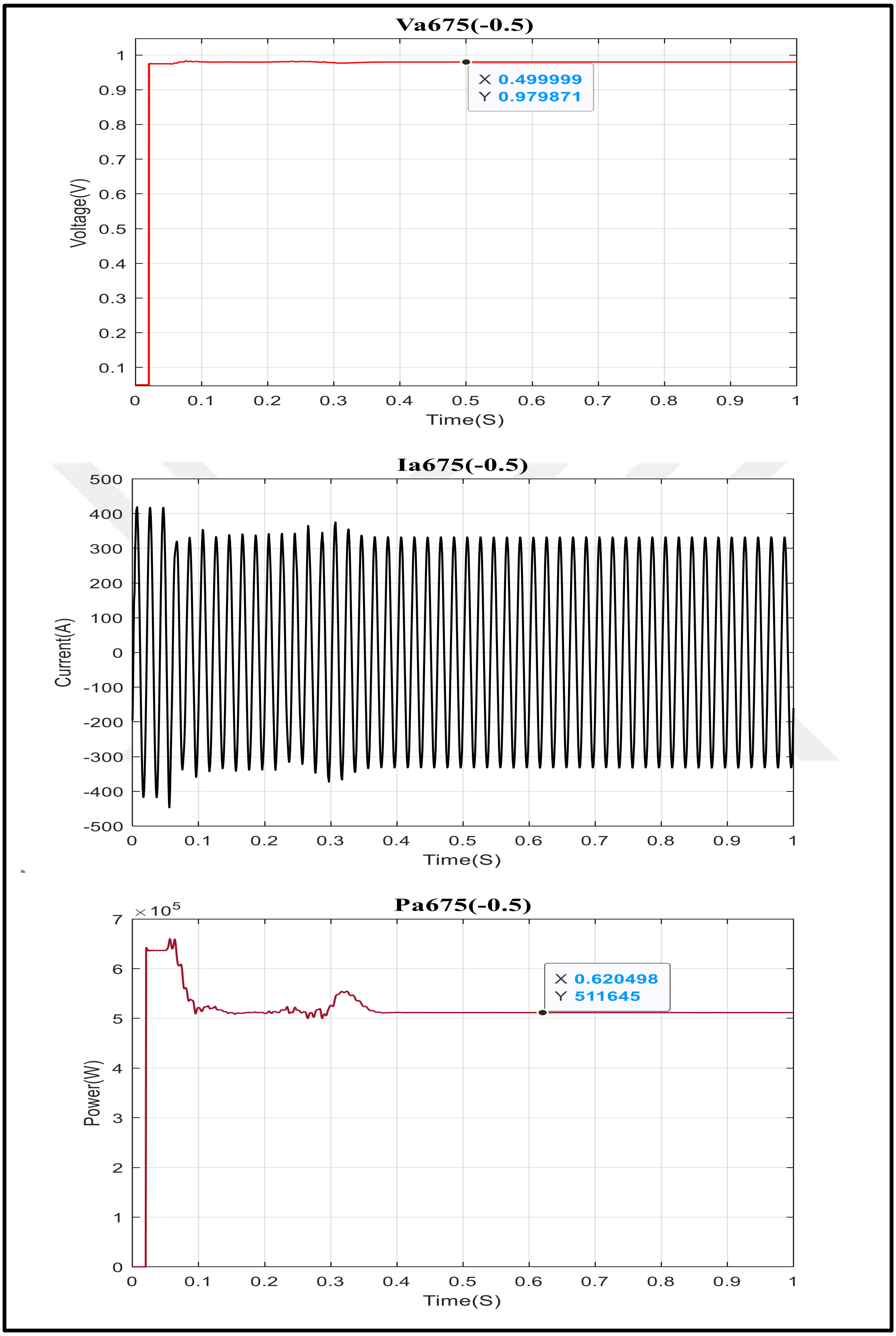

Figure 4.14. The voltage, current, and power on bus 675 after increasing the load by 50% on bus 675 with a PV system (Iq=-0.5).

Connecting a 400 kW (PV system) to the Bus 675 with Iq= -1

Four sets of SunPower PV panels (SPR-305E-WHT-D) were linked in parallel to provide a 400 kW renewable energy system. In this case, at standard conditions (STC) of 25 °C and 1000 W/m² of solar radiation, each set of PV panels produces 100 kW of power. The total power of all four groups is 400 kW. A modified IEEE 13 bus system was connected to the PV system through a bus 675 to compensate for the voltage drop. Active power (P), and 100% reactive power(Q) ware injected when Iq = -1 was entered. Before increasing the load, before and after connecting the 400 kW photovoltaic system, the buses' voltage is displayed in Table 4.25.

Table 4.25. The voltage of the buses before the load is increased, and both before and after the 400 kW photovoltaic system is connected.

V-Buses	Normal Case			After Increase the Load 50% (bus675) & Before connecting the400kW PV system			After Increase the Load 50% (bus675) & After connecting the400kW PV system		
	R	S	T	R	S	T	R	S	T
Vabc-632	1.021	1.042	1.017	1.021	1.042	1.017	1.021	1.042	1.017
Vabc-633	1.018	1.04	1.015	1.018	1.04	1.015	1.018	1.04	1.015
Vabc-692	0.9871	1.045	0.971	0.98	1.05	0.9617	0.9893	1.047	0.9724
Vabc-645	0	1.033	1.015	0	1.033	1.015	0	1.033	1.015
Vabc-646	0	1.032	1.014	0	1.032	1.014	0	1.032	1.014
Vabc-671	0.9871	1.045	0.971	0.9801	1.05	0.9617	0.9893	1.047	0.9724
Vabc-675	0.9798	1.046	0.9676	0.9693	1.052	0.9568	0.982	1.049	0.9688
Vabc-652	0.9799	0	0	0.9729	0	0	0.9821	0	0
Vabc-634	0.9941	1.022	0.9961	0.9941	1.022	0.9961	0.9941	1.022	0.9961
Vabc-611	0	0	0.9648	0	0	0.9556	0	0	0.9663
Vabc-680	0.9871	1.045	0.971	0.9801	1.05	0.9617	0.9893	1.047	0.9724
Vabc-684	0.9853	0	0.9679	0.9782	0	0.9587	0.9875	0	0.9693

According to the above table, the voltage considerably improved following the installation of the photovoltaic system, allowing for the treatment of the drop brought on by the increasing load. Example: The voltage on bus 675 was in normal condition (R_{675}=0.9798, S_{675}=1.046, and T_{675}=0.9676); after increasing the load by 50% on bus 675, the voltage dropped, and the readings were (R_{675}=0.9693, S_{675}=1.052, and T_{675}=0.9568), and then after connecting PV, the voltage improved significantly, and the readings became (R_{675}=0.982, S_{675}=1.049, and T_{675}=0.9688).

Figure 4.15. shows the voltage, current, and power on bus 675 after increasing the load by 50% on bus 675 with a PV system (Iq=-1).

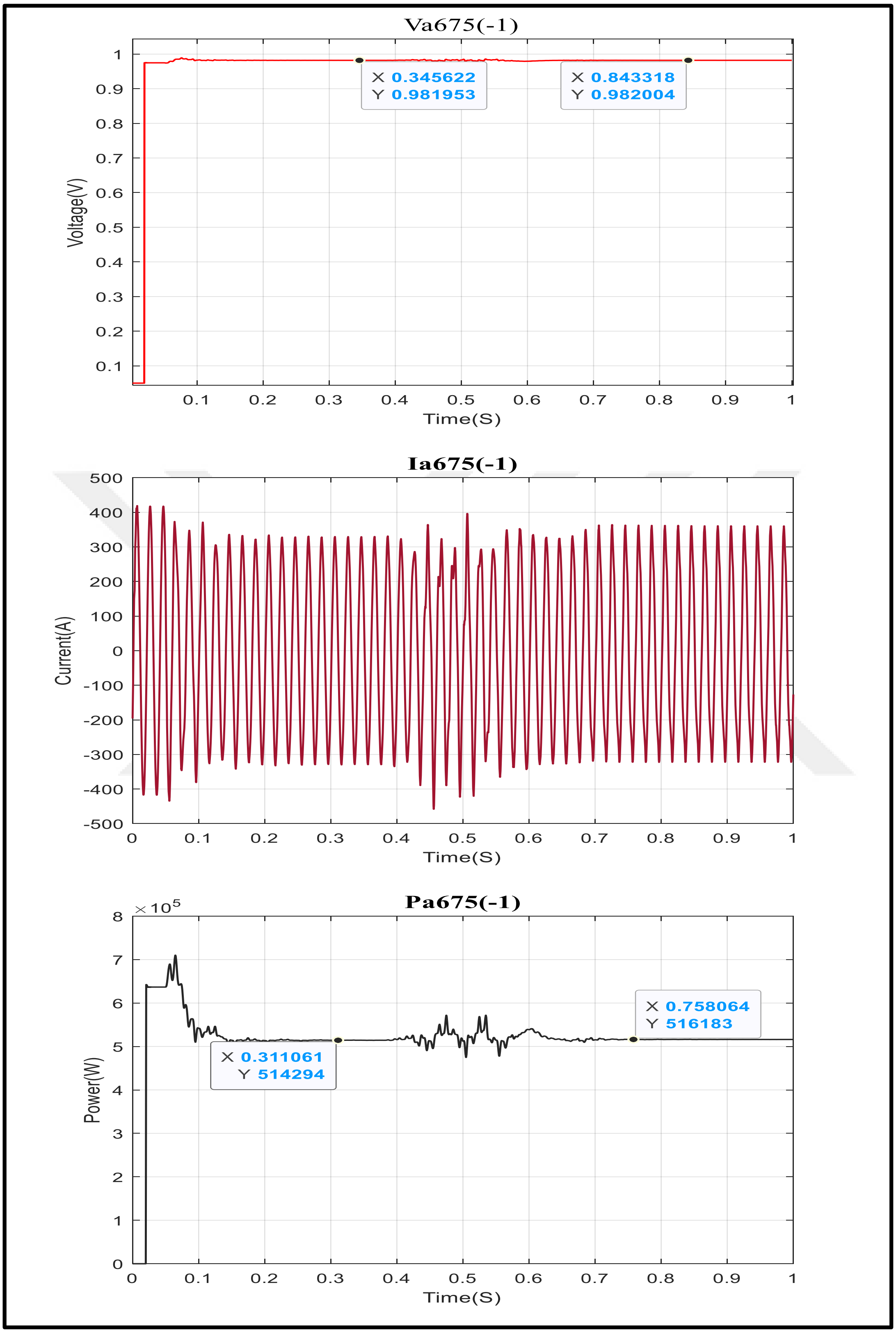

Figure 4.15. The voltage, current, and power on bus 675 after increasing the load by 50% on bus 675 with a PV system (Iq=-1).

Increase the load on bus 675 by 75%

The active and reactive power load on bus 675 was raised by 75% in the modified IEEE 13 bus test system circuit. The imbalanced loads on bus 675 were Q(R = 190kVar, S = 60kVar, and T = 212kVar), and P(R = 485kW, S = 68kW, and T = 290kW). The voltage of each bus was measured when the loads were increased to P(R = 848.75kW, S = 119kW, and T = 507.5kW), and Q(R = 332.5kVar, S = 105kVar, and T = 371kVar). Below is Table 4.26. that displays the voltage measurements along with the percentage decrease that occurred in all buses.

Table 4.26. The voltage on the buses both before and after the bus 675's load was increased by 75%.

V-Buses	Normal Case			After Increase the Load 75% (bus675)			Drop Rate%		
	R	S	T	R	S	T	R	S	T
Vabc-632	1.021	1.042	1.017	1.021	1.042	1.017	0	0	0
Vabc-633	1.018	1.04	1.015	1.018	1.04	1.015	0	0	0
Vabc-692	0.9871	1.045	0.971	0.9765	1.052	0.9571	-1.09%	0.67%	-1.45%
Vabc-645	0	1.033	1.015	0	1.033	1.015	0	0	0
Vabc-646	0	1.032	1.014	0	1.032	1.014	0	0	0
Vabc-671	0.9871	1.045	0.971	0.9765	1.052	0.9572	-1.09%	0.67%	-1.44%
Vabc-675	0.9798	1.046	0.9676	0.9641	1.054	0.9515	-1.63%	0.76%	-1.69%
Vabc-652	0.9799	0	0	0.9694	0	0	-1.08%	0	0
Vabc-634	0.9941	1.022	0.9961	0.9941	1.022	0.9961	0	0	0
Vabc-611	0	0	0.9648	0	0	0.9511	0	0	-1.44%
Vabc-680	0.9871	1.045	0.971	0.9765	1.052	0.9572	-1.09%	0.67%	-1.44%
Vabc-684	0.9853	0	0.9679	0.9747	0	0.9542	-1.09%	0	-1.44%

Table 4.26. shows that when bus 675's load grew, the buses nearest to it were impacted because the voltage dropped at different rates, even though the system did not fail entirely.

Connecting a 400 kW (PV system) to the Bus 675 with Iq=0

Four sets of SunPower PV panels (SPR-305E-WHT-D) were linked in parallel to provide a 400 kW renewable energy system. In this case, at standard conditions (STC) of 25 °C and 1000 W/m² of solar radiation, each set of PV panels produces 100 kW of power. The total power of all four groups is 400 kW. A modified IEEE 13 bus system was connected to the PV system through a bus 675 to compensate for the voltage drop. Only active power (pure P) was injected when Iq = 0 was entered. Before increasing the load, before and after connecting the 400 kW photovoltaic system, the buses' voltage is displayed in Table 4.27.

Table 4.27. The voltage of the buses before increasing load, before and after connecting the 400 kW photovoltaic system.

V-Buses	Normal Case			After Increase the Load 75% (bus675) & Before connecting the400kW PV system			After Increase the Load 75% (bus675) & After connecting the400kW PV system		
	R	S	T	R	S	T	R	S	T
Vabc-632	1.021	1.042	1.017	1.021	1.042	1.017	1.021	1.042	1.017
Vabc-633	1.018	1.04	1.015	1.018	1.04	1.015	1.018	1.04	1.015
Vabc-692	0.9871	1.045	0.971	0.9765	1.052	0.9571	0.9826	1.044	0.9637
Vabc-645	0	1.033	1.015	0	1.033	1.015	0	1.033	1.015
Vabc-646	0	1.032	1.014	0	1.032	1.014	0	1.032	1.014
Vabc-671	0.9871	1.045	0.971	0.9765	1.052	0.9572	0.9826	1.044	0.9638
Vabc-675	0.9798	1.046	0.9676	0.9641	1.054	0.9515	0.9731	1.046	0.9585
Vabc-652	0.9799	0	0	0.9694	0	0	0.9754	0	0
Vabc-634	0.9941	1.022	0.9961	0.9941	1.022	0.9961	0.9941	1.022	0.9961
Vabc-611	0	0	0.9648	0	0	0.9511	0	0	0.9577
Vabc-680	0.9871	1.045	0.971	0.9765	1.052	0.9572	0.9826	1.044	0.9638
Vabc-684	0.9853	0	0.9679	0.9747	0	0.9542	0.9807	0	0.9607

According to the above table, the voltage considerably improved following the installation of the photovoltaic system, allowing for the treatment of the drop brought on by the increasing load. The voltage of bus 675, for instance, was R_{675}=0.9798, S_{675}=1.046, and T_{675}=0.9676. When the load was increased, the voltage dropped to R_{675}=0.9641, S_{675}=1.054, and T_{675}=0.9515. The PV system was next added, and the voltage improved to R_{675}=0.9731, S_{675}=1.046, and T_{675}=0.9585.

Connecting a 400 kW (PV system) to the Bus 675 with Iq= -0.5

Four sets of SunPower PV panels (SPR-305E-WHT-D) were linked in parallel to provide a 400 kW renewable energy system. In this case, at standard conditions (STC) of 25 °C and 1000 W/m² of solar radiation, each set of PV panels produces 100 kW of power. The total power of all four groups is 400 kW. A modified IEEE 13 bus system was connected to the PV system through a bus 675 to compensate for the voltage drop. Active power (P), and 50% reactive power(Q) ware injected when Iq = -0.5 was entered. Before increasing the load, before and after connecting the 400 kW photovoltaic system, the buses' voltage is displayed in Table 4.28.

Table 4.28. The voltage of the buses before increasing load, before and after connecting the 400 kW photovoltaic system.

V-Buses	Normal Case			After Increase the Load 75% (bus675) & Before connecting the400kW PV system			After Increase the Load 75% (bus675) & After connecting the400kW PV system		
	R	S	T	R	S	T	R	S	T
Vabc-632	1.021	1.042	1.017	1.021	1.042	1.017	1.021	1.042	1.017
Vabc-633	1.018	1.04	1.015	1.018	1.04	1.015	1.018	1.04	1.015
Vabc-692	0.9871	1.045	0.971	0.9765	1.052	0.9571	0.9844	1.046	0.9659
Vabc-645	0	1.033	1.015	0	1.033	1.015	0	1.033	1.015
Vabc-646	0	1.032	1.014	0	1.032	1.014	0	1.032	1.014
Vabc-671	0.9871	1.045	0.971	0.9765	1.052	0.9572	0.9845	1.048	0.9659
Vabc-675	0.9798	1.046	0.9676	0.9641	1.054	0.9515	0.9753	1.048	0.9611
Vabc-652	0.9799	0	0	0.9694	0	0	0.9773	0	0
Vabc-634	0.9941	1.022	0.9961	0.9941	1.022	0.9961	0.9941	1.022	0.9961
Vabc-611	0	0	0.9648	0	0	0.9511	0	0	0.9598
Vabc-680	0.9871	1.045	0.971	0.9765	1.052	0.9572	0.9845	1.046	0.9659
Vabc-684	0.9853	0	0.9679	0.9747	0	0.9542	0.9828	0	0.9629

According to the above table, the voltage considerably improved following the installation of the photovoltaic system, allowing for the treatment of the drop brought on by the increasing load. Example: The voltage on bus 675 was in normal condition (R_{675}=0.9798, S_{675}=1.046, and T_{675}=0.9676); after increasing the load by 75% on bus 675, the voltage dropped, and the readings were (R_{675}=0.9641, S_{675}=1.054, and T_{675}=0.9515), and then after connecting PV, the voltage improved significantly, and the readings became (R_{675}=0.9753, S_{675}=1.048, and T_{675}=0.9611).

Connecting a 400 kW (PV system) to the Bus 675 with Iq= -1

Four sets of SunPower PV panels (SPR-305E-WHT-D) were linked in parallel to provide a 400 kW renewable energy system. In this case, at standard conditions (STC) of 25 °C and 1000 W/m² of solar radiation, each set of PV panels produces 100 kW of power. The total power of all four groups is 400 kW. A modified IEEE 13 bus system was connected to the PV system through a bus 675 to compensate for the voltage drop. Active power (P), and 100% reactive power(Q) ware injected when Iq = -1 was entered. Before increasing the load, before and after connecting the 400 kW photovoltaic system, the buses' voltage is displayed in Table 4.29.

Table 4.29. The voltage of the buses before the load is increased and both before and after the 400 kW photovoltaic system is connected.

V-Buses	Normal Case			After Increase the Load 75% (bus675) & Before connecting the400kW PV system			After Increase the Load 75% (bus675) & After connecting the400kW PV system		
	R	S	T	R	S	T	R	S	T
Vabc-632	1.021	1.042	1.017	1.021	1.042	1.017	1.021	1.042	1.017
Vabc-633	1.018	1.04	1.015	1.018	1.04	1.015	1.018	1.04	1.015
Vabc-692	0.9871	1.045	0.971	0.9765	1.052	0.9571	0.9862	1.049	0.9681
Vabc-645	0	1.033	1.015	0	1.033	1.015	0	1.033	1.015
Vabc-646	0	1.032	1.014	0	1.032	1.014	0	1.032	1.014
Vabc-671	0.9871	1.045	0.971	0.9765	1.052	0.9572	0.9863	1.049	0.9681
Vabc-675	0.9798	1.046	0.9676	0.9641	1.054	0.9515	0.9774	1.051	0.9637
Vabc-652	0.9799	0	0	0.9694	0	0	0.9791	0	0
Vabc-634	0.9941	1.022	0.9961	0.9941	1.022	0.9961	0.9941	1.022	0.9961
Vabc-611	0	0	0.9648	0	0	0.9511	0	0	0.962
Vabc-680	0.9871	1.045	0.971	0.9765	1.052	0.9572	0.9863	1.049	0.9681
Vabc-684	0.9853	0	0.9679	0.9747	0	0.9542	0.9844	0	0.9651

According to the above table, the voltage considerably improved following the installation of the photovoltaic system, allowing for the treatment of the drop brought on by the increasing load. Example: The voltage on bus 675 was in normal condition (R_{675}=0.9798, S_{675}=1.046, and T_{675}=0.9676); after increasing the load by 75% on bus 675, the voltage dropped, and the readings were (R_{675}=0.9641, S_{675}=1.054, and T_{675}=0.9515), and then after connecting PV, the voltage improved significantly, and the readings became (R_{675}=0.9774, S_{675}=1.051, and T_{675}=0.9637).

Increase the load on bus 675 by 100%

The active and reactive power load on bus 675 was raised by 100% in the modified IEEE 13 bus test system circuit. The imbalanced loads on bus 675 were Q(R = 190kVar, S = 60kVar, and T = 212kVar), and P(R = 485kW, S = 68kW, and T = 290kW). The voltage of each bus was measured when the loads were increased to P(R = 970kW, S = 136kW, and T = 580kW), and Q(R = 380kVar, S = 120kVar, and T = 424kVar). Below is Table 4.30. that displays the voltage measurements along with the percentage decrease that occurred in all buses.

Table 4.30. The voltage on the buses both before and after the bus 675's load was increased by 100%.

V-Buses	Normal Case			After Increase the Load 100% (bus675)			Drop Rate%		
	R	S	T	R	S	T	R	S	T
Vabc-632	1.021	1.042	1.017	1.021	1.042	1.017	0	0	0
Vabc-633	1.018	1.04	1.015	1.018	1.04	1.015	0	0	0
Vabc-692	0.9871	1.045	0.971	0.973	1.055	0.9527	-1.45%	0.95%	-1.92%
Vabc-645	0	1.033	1.015	0	1.033	1.015	0	0	0
Vabc-646	0	1.032	1.014	0	1.032	1.014	0	0	0
Vabc-671	0.9871	1.045	0.971	0.973	1.055	0.9527	-1.45%	0.95%	-1.92%
Vabc-675	0.9798	1.046	0.9676	0.9589	1.057	0.9463	-2.18%	1.04%	-2.25%
Vabc-652	0.9799	0	0	0.9659	0	0	-1.45%	0	0
Vabc-634	0.9941	1.022	0.9961	0.9941	1.022	0.9961	0	00	0
Vabc-611	0	0	0.9648	0	0	0.9467	0	0	-1.91%
Vabc-680	0.9871	1.045	0.971	0.973	1.055	0.9527	-1.45%	0.95%	-1.92%
Vabc-684	0.9853	0	0.9679	0.9712	0	0.9498	-1.45%	0	-1.91%

Table 4.30. shows that when bus 675's load grew, the buses nearest to it were impacted because the voltage dropped at different rates. In some buses, the voltage value drops below 0.95 pu, and breakdown occurs.

Figure 4.16. shows the voltage, current, and power on bus 675 after increasing the load by 100% on bus 675.

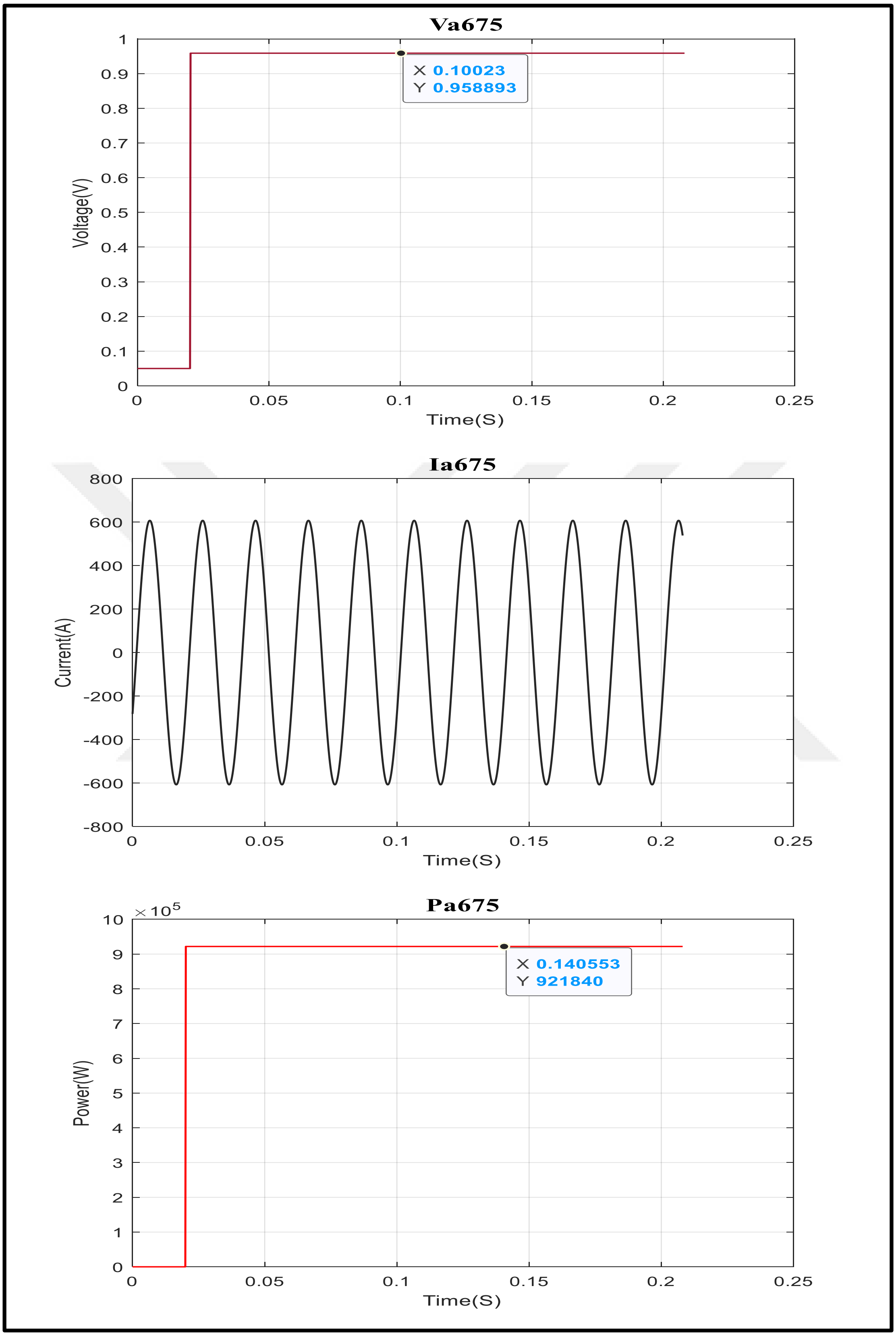

Figure 4.16. The voltage, current, and power on bus 675 after increasing the load by 100% on bus 675.

Connecting a 400 kW (PV system) to the Bus 675 with Iq=0

Four sets of SunPower PV panels (SPR-305E-WHT-D) were linked in parallel to provide a 400 kW renewable energy system. In this case, at standard conditions (STC) of 25 °C and 1000 W/m² of solar radiation, each set of PV panels produces 100 kW of power. The total power of all four groups is 400 kW. A modified IEEE 13 bus system was connected to the PV system through a bus 675 to compensate for the voltage drop. Only active power (pure P) was injected when Iq = 0 was entered. Before increasing the load, before and after connecting the 400 kW photovoltaic system, the buses' voltage is displayed in Table 4.31.

Table 4.31. The voltage of the buses before increasing load, before and after connecting the 400 kW photovoltaic system.

V-Buses	Normal Case			After Increase the Load 100% (bus675) & Before connecting the400kW PV system			After Increase the Load 100% (bus675) & After connecting the400kW PV system		
	R	S	T	R	S	T	R	S	T
Vabc-632	1.021	1.042	1.017	1.021	1.042	1.017	1.021	1.042	1.017
Vabc-633	1.018	1.04	1.015	1.018	1.04	1.015	1.018	1.04	1.015
Vabc-692	0.9871	1.045	0.971	0.973	1.055	0.9527	0.9795	1.046	0.9596
Vabc-645	0	1.033	1.015	0	1.033	1.015	0	1.033	1.015
Vabc-646	0	1.032	1.014	0	1.032	1.014	0	1.032	1.014
Vabc-671	0.9871	1.045	0.971	0.973	1.055	0.9527	0.9795	1.046	0.9596
Vabc-675	0.9798	1.046	0.9676	0.9589	1.057	0.9463	0.9685	1.047	0.9535
Vabc-652	0.9799	0	0	0.9659	0	0	0.9724	0	0
Vabc-634	0.9941	1.022	0.9961	0.9941	1.022	0.9961	0.9941	1.022	0.9961
Vabc-611	0	0	0.9648	0	0	0.9467	0	0	0.9535
Vabc-680	0.9871	1.045	0.971	0.973	1.055	0.9527	0.9795	1.046	0.9596
Vabc-684	0.9853	0	0.9679	0.9712	0	0.9498	0.9777	0	0.9566

According to the above table, the voltage considerably improved following the installation of the photovoltaic system, allowing for the treatment of the drop brought on by the increasing load. The voltage of bus 675, for instance, was R_{675}=0.9798, S_{675}=1.046, and T_{675}=0.9676. When the load was increased, the voltage dropped to R_{675}=0.9589, S_{675}=1.057, and T_{675}=0.9463. The PV system was next added, and the voltage improved to R_{675}=0.9685, S_{675}=1.047, and T_{675}=0.9535.

Figure 4. 17. shows the voltage, current, and power on bus 675 after increasing the load by 100% on bus 675 with a PV system (Iq=0).

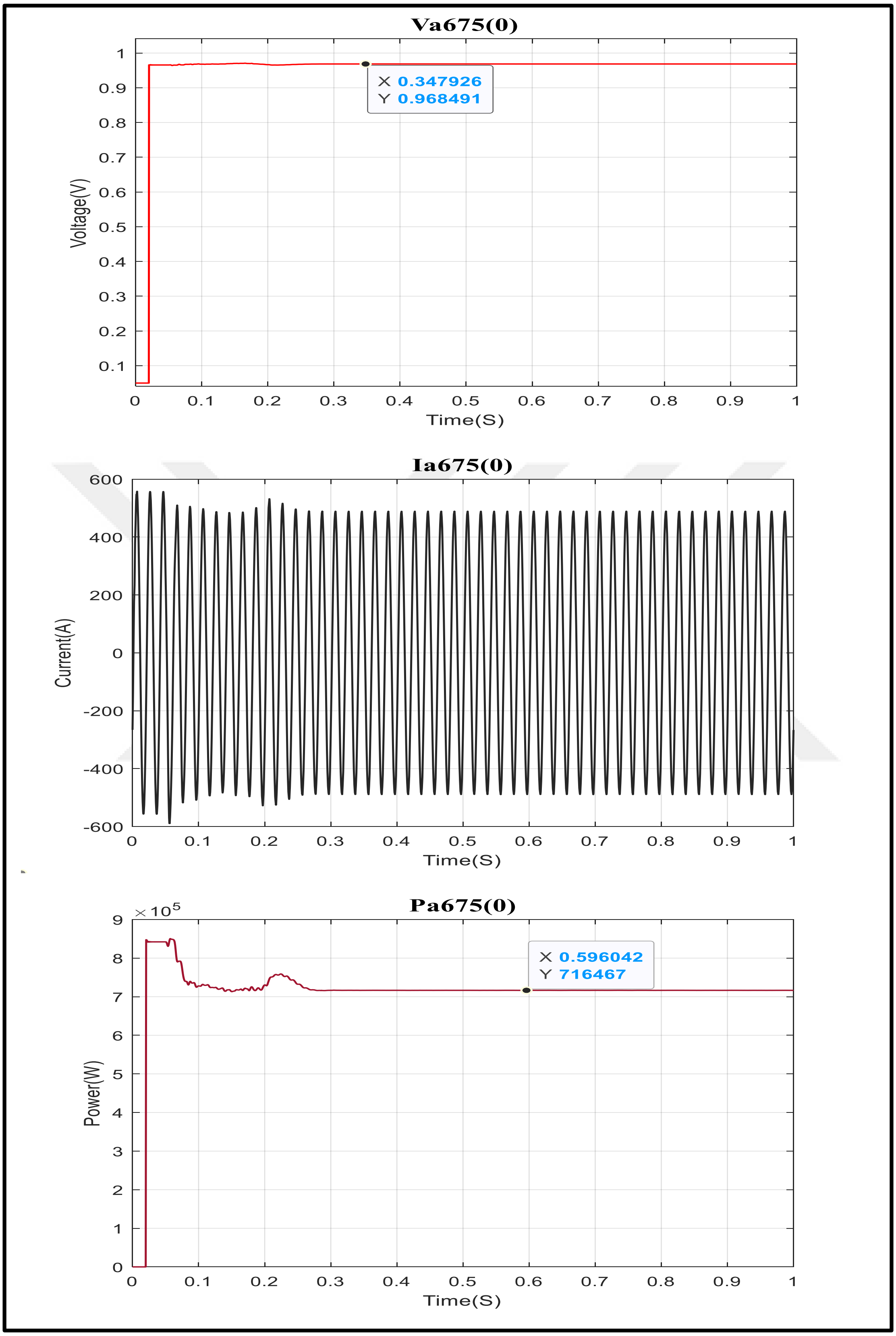

Figure 4.17. The voltage, current, and power on bus 675 after increasing the load by 100% on bus 675 with a PV system (Iq=0).

Connecting a 400 kW (PV system) to the Bus 675 with Iq= -0.5

Four sets of SunPower PV panels (SPR-305E-WHT-D) were linked in parallel to provide a 400 kW renewable energy system. In this case, at standard conditions (STC) of 25 °C and 1000 W/m² of solar radiation, each set of PV panels produces 100 kW of power. The total power of all four groups is 400 kW. A modified IEEE 13 bus system was connected to the PV system through a bus 675 to compensate for the voltage drop. Active power (P), and 50% reactive power(Q) ware injected when Iq = -0.5 was entered. Before increasing the load, before and after connecting the 400 kW photovoltaic system, the buses' voltage is displayed in Table 4.32.

Table 4.32. The voltage of the buses before increasing load, before and after connecting the 400 kW photovoltaic system.

V-Buses	Normal Case			After Increase the Load 100% (bus675) & Before connecting the400kW PV system			After Increase the Load 100% (bus675) & After connecting the400kW PV system		
	R	S	T	R	S	T	R	S	T
Vabc-632	1.021	1.042	1.017	1.021	1.042	1.017	1.021	1.042	1.017
Vabc-633	1.018	1.04	1.015	1.018	1.04	1.015	1.018	1.04	1.015
Vabc-692	0.9871	1.045	0.971	0.973	1.055	0.9527	0.9814	1.048	0.9617
Vabc-645	0	1.033	1.015	0	1.033	1.015	0	1.033	1.015
Vabc-646	0	1.032	1.014	0	1.032	1.014	0	1.032	1.014
Vabc-671	0.9871	1.045	0.971	0.973	1.055	0.9527	0.9814	1.048	0.9617
Vabc-675	0.9798	1.046	0.9676	0.9589	1.057	0.9463	0.9707	1.05	0.9561
Vabc-652	0.9799	0	0	0.9659	0	0	0.9742	0	0
Vabc-634	0.9941	1.022	0.9961	0.9941	1.022	0.9961	0.9941	1.022	0.9961
Vabc-611	0	0	0.9648	0	0	0.9467	0	0	0.9557
Vabc-680	0.9871	1.045	0.971	0.973	1.055	0.9527	0.9814	1.048	0.9617
Vabc-684	0.9853	0	0.9679	0.9712	0	0.9498	0.9796	0	0.9587

According to the above table, the voltage considerably improved following the installation of the photovoltaic system, allowing for the treatment of the drop brought on by the increasing load. Example: The voltage on bus 675 was in normal condition (R_{675}=0.9798, S_{675}=1.046, and T_{675}=0.9676); after increasing the load by 100% on bus 675, the voltage dropped, and the readings were (R_{675}=0.9589, S_{675}=1.057, and T_{675}=0.9463), and then after connecting PV, the voltage improved significantly, and the readings became (R_{675}=0.9707, S_{675}=1.05, and T_{675}=0.9561).

Figure 4.18. shows the voltage, current, and power on bus 675 after increasing the load by 100% on bus 675 with a PV system (Iq=-0.5).

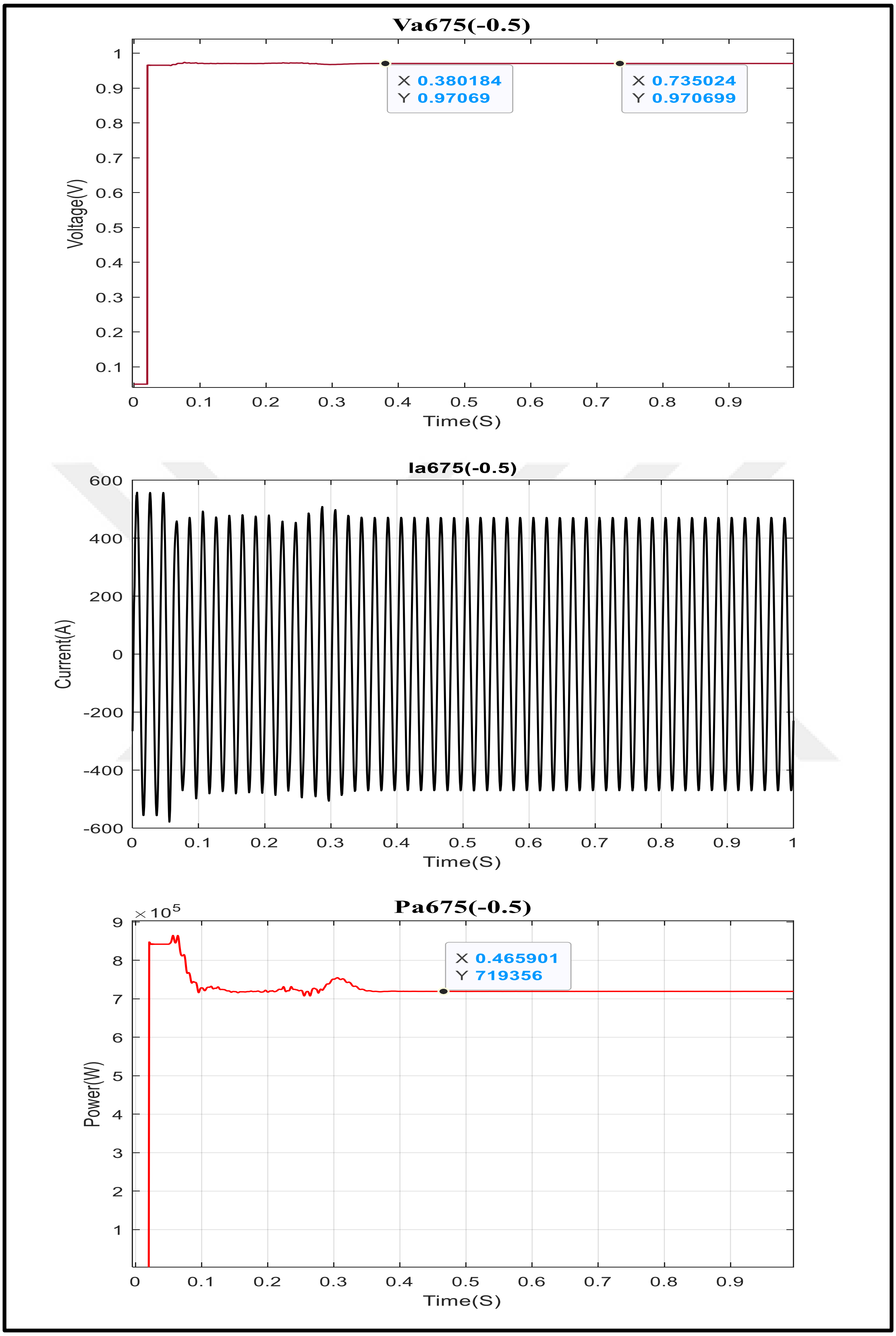

Figure 4.18. The voltage, current, and power on bus 675 after increasing the load by 100% on bus 675 with a PV system (Iq=-0.5).

Connecting a 400 kW (PV system) to the Bus 675 with Iq= -1

Four sets of SunPower PV panels (SPR-305E-WHT-D) were linked in parallel to provide a 400 kW renewable energy system. In this case, at standard conditions (STC) of 25 °C and 1000 W/m² of solar radiation, each set of PV panels produces 100 kW of power. The total power of all four groups is 400 kW. A modified IEEE 13 bus system was connected to the PV system through a bus 675 to compensate for the voltage drop. Active power (P), and 100% reactive power(Q) ware injected when Iq = -1 was entered. Before increasing the load, before and after connecting the 400 kW photovoltaic system, the buses' voltage is displayed in Table 4.33.

Table 4.33. The voltage of the buses before the load is increased and both before and after the 400 kW photovoltaic system is connected.

V-Buses	Normal Case			After Increase the Load 100% (bus675) & Before connecting the400kW PV system			After Increase the Load 100% (bus675) & After connecting the400kW PV system		
	R	S	T	R	S	T	R	S	T
Vabc-632	1.021	1.042	1.017	1.021	1.042	1.017	1.021	1.042	1.017
Vabc-633	1.018	1.04	1.015	1.018	1.04	1.015	1.018	1.04	1.015
Vabc-692	0.9871	1.045	0.971	0.973	1.055	0.9527	0.9832	1.05	0.9639
Vabc-645	0	1.033	1.015	0	1.033	1.015	0	1.033	1.015
Vabc-646	0	1.032	1.014	0	1.032	1.014	0	1.032	1.014
Vabc-671	0.9871	1.045	0.971	0.973	1.055	0.9527	0.9832	1.05	0.9639
Vabc-675	0.9798	1.046	0.9676	0.9589	1.057	0.9463	0.9728	1.05	0.9586
Vabc-652	0.9799	0	0	0.9659	0	0	0.976	0	0
Vabc-634	0.9941	1.022	0.9961	0.9941	1.022	0.9961	0.9941	1.022	0.9961
Vabc-611	0	0	0.9648	0	0	0.9467	0	0	0.9578
Vabc-680	0.9871	1.045	0.971	0.973	1.055	0.9527	0.9832	1.05	0.9639
Vabc-684	0.9853	0	0.9679	0.9712	0	0.9498	0.9814	0	0.9609

According to the above table, the voltage considerably improved following the installation of the photovoltaic system, allowing for the treatment of the drop brought on by the increasing load. Example: The voltage on bus 675 was in normal condition (R_{675}=0.9798, S_{675}=1.046, and T_{675}=0.9676); after increasing the load by 100% on bus 675, the voltage dropped, and the readings were (R_{675}=0.9589, S_{675}=1.057, and T_{675}=0.9463), and then after connecting PV, the voltage improved significantly, and the readings became (R_{675}=0.9728, S_{675}=1.05, and T_{675}=0.9586).

Figure 4.19. shows the voltage, current, and power on bus 675 after increasing the load by 100% on bus 675 with a PV system (Iq=-1).

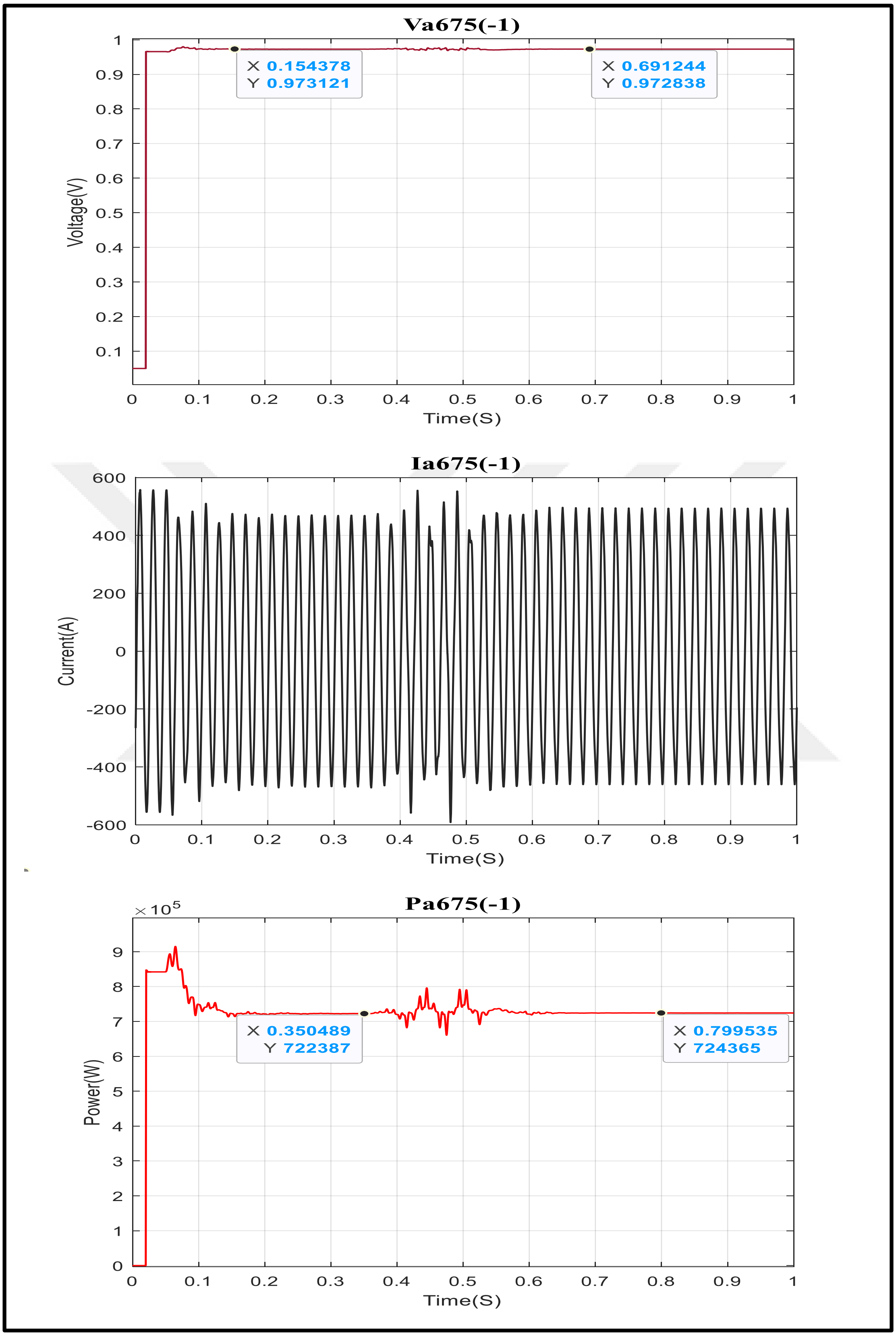

Figure 4.19. The voltage, current, and power on bus 675 after increasing the load by 100% on bus 675 with a PV system (Iq=-1).

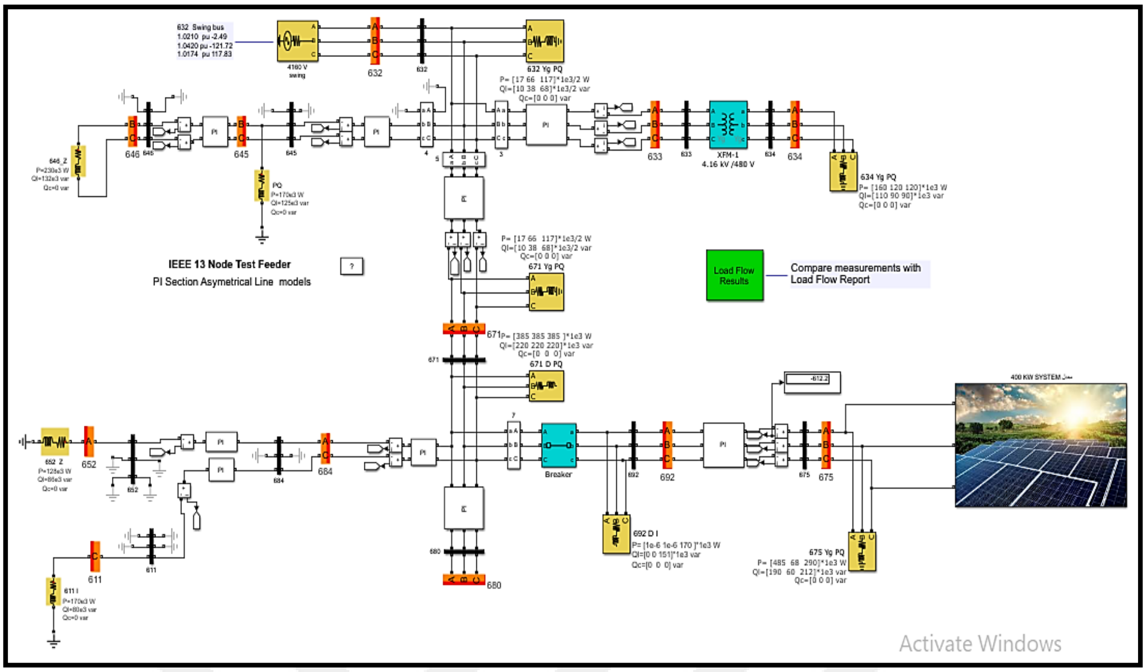

Figure 4.20. The electrical power system (Modified IEEE 13-Bus Test System) with 400KW PV system in bus 675

The modified IEEE 13 bus test system circuit model is displayed in Figure 4.20. after the connection of the PV system to bus 675. Through bus 675, the PV system was integrated with the modified IEEE 13 bus test system, and four scenarios were examined.

Scenario 1: The load connected to bus 675 was increased by 25%. Then the voltage on the buses was recorded to see the voltage drop that occurred. Then, the PV system (400 kW) was integrated via bus 675. Then the voltage on the buses was measured under the following conditions: injection of pure active power only (Iq = 0), injection of 50% reactive power and 100% active power (Iq = -0.5), and injection of 100% reactive power and 100% active power (Iq = -1). It was found that the PV system compensated for the voltage drop caused by the 25% increase in load. According to the measurements, we also found that the voltage on the buses was larger than its actual value before the load increase, which may have a negative impact. For example, The voltage of the bus 675 is (R=0.9798, S=1.046, and T=0.9676). The voltage of the bus 675 after increasing the load. (R=0.9745, S=1.049, and T=0.9621), and after adding the PV system, we noticed that the public voltage was at

- when Iq=0 (R = 0.9822, S = 1.042, and T = 0.9688),
- when Iq = -0.5 (R = 0.9845, S = 1.045, and T = 0.9714),

- and when Iq = -1 (R = 0.9924, S = 1.047, T = 0.974).

Scenario 2: The load connected to bus 675 was increased by 50%. Then the voltage on the buses was recorded to see the voltage drop that occurred. Then, the PV system (400 kW) was integrated via bus 675. Then the voltage on the buses was measured under the following conditions: injection of pure active power only (Iq = 0), injection of 50% reactive power and 100% active power (Iq = -0.5), and injection of 100% reactive power and 100% active power (Iq = -1). We saw that the PV system compensated for the voltage drop caused by the 50% increase in load. For example, the voltage of the bus 675 is (R = 0.9798, S = 1.046, and T = 0.9676). After increasing the load (R = 0.9693, S = 1.052, and T = 0.9568) and after adding the PV system, we noticed that the overall voltage was at

- When Iq = 0 (R = 0.9776, S = 1.044, and T = 0.9636),
- when Iq = -0.5 (R = 0.9799, S = 1.046, and T = 0.9662),
- and when Iq = -1 (R = 0.982, S = 1.049, and T = 0.9688).

We notice that in the case of Iq = -0.5, the voltage was raised to its state before increasing the load.

Scenario 3: The load connected to bus 675 was increased by 75%. Then the voltage on the buses was recorded to see the voltage drop that occurred. Then, the PV system (400 kW) was integrated via bus 675. Then the voltage on the buses was measured under the following conditions: injection of pure active power only (Iq = 0), injection of 75% reactive power and 100% active power (Iq = -0.5), and injection of 100% reactive power and 100% active power (Iq = -1). We saw that the PV system compensated for the voltage drop caused by the 75% increase in load. For example, the bus voltage is 675 (R = 0.9798, S = 1.046, and T = 0.9676). After increasing the load (R = 0.9641, S = 1.054, and T = 0.9515) and after adding the PV system, we noticed that the overall voltage was at

- When Iq = 0 (R = 0.9731, S = 1.046, and T = 0.9585),
- when Iq = -0.5 (R = 0.9753, S = 1.048, and T = 0.9611).
- When Iq = -1 (R = 0.9774, S = 1.051, and T = 0.9637),

We notice that in the case of Iq = -1, the voltage was raised to its state before increasing the load.

Scenario 4: The load connected to bus 675 was increased by 100%. Then the voltage on the buses was recorded to see the voltage drop that occurred. Then, the PV system (400 kW) was integrated via bus 675. Then the voltage on the buses was measured under the following conditions: injection of pure active power only (Iq = 0), injection of 50% reactive power and 100% active power (Iq = -0.5), and injection of 100% reactive power and 100% active power (Iq = -1). We saw that the PV system compensated for the voltage drop caused by the 100% increase in load. For example, the bus voltage is 675 (R = 0.9798, S = 1.046, and T = 0.9676). After increasing the load (R = 0.9589, S = 1.057, and T = 0.9463) and after adding the PV system, we noticed that the overall voltage was at

- When Iq = 0 (R = 0.9685, S = 1.047, and T = 0.9535),
- when Iq = -0.5 (R = 0.9707, S = 1.05, and T = 0.9561),
- when Iq = -1 (R = 0.9728, S = 1.05, and T = 0.9586),

We notice that in the case of Iq = -1, the voltage did not return to its previous state, which indicates that the increase in the load was not compensated for by the power injected through the photovoltaic system.

4.1.3. Third case: Increase the load on bus 675+671

A 25% increase in the load on buses 675 and 671

The active and reactive power load on buses 675 & 671 were raised by 25% in the modified IEEE 13 bus test system circuit. The imbalanced loads on bus 675 were Q (R = 190 kVar, S = 60 kVar, and T = 212 kVar) and P (R = 485 kW, S = 68 kW, and T = 290 kW), whereas the balanced loads on bus 671 were Q (R = 220 kVar, S = 220 kVar, and T = 220 kVar) and P (R = 385 kW, S = 385 kW, and T = 385 kW). The voltage of each bus was measured when the loads were increased. The balanced loads on bus 671 after increasing load Q (R = 275 kVar, S = 275 kVar, and T = 275 kVar) and P (R = 481.25 kW, S = 481.25 kW, and T = 481.25 kW), whereas the imbalanced loads on bus 675 Q (R = 237.5 kVar, S = 75 kVar, and T = 265 kVar) and P (R = 606.25 kW, S = 85 kW, and T =

362.5 kW). Below is Table 4.34, which displays the voltage measurements and the percentage decrease that occurred in all buses.

Table 4.34. The voltage on the buses both before and after increasing the load on the bus 675 and 671 by 25%.

V-Buses	Normal Case			After Increase the Load by 25% (bus 671+bus675)			Drop Rate%		
	R	S	T	R	S	T	R	S	T
Vabc-632	1.021	1.042	1.017	1.021	1.042	1.017	0	0	0
Vabc-633	1.018	1.04	1.015	1.018	1.04	1.015	0	0	0
Vabc-692	0.9871	1.045	0.971	0.9805	1.045	0.9632	-0.67%	0.00%	-0.81%
Vabc-645	0	1.033	1.015	0	1.033	1.015	0	0	0
Vabc-646	0	1.032	1.014	0	1.032	1.014	0	0	0
Vabc-671	0.9871	1.045	0.971	0.9805	1.045	0.9632	-0.67%	0.00%	-0.81%
Vabc-675	0.9798	1.046	0.9676	0.9715	1.046	0.9591	-0.85%	0.00%	-0.89%
Vabc-652	0.9799	0	0	0.9733	0	0	-0.68%	0	0
Vabc-634	0.9941	1.022	0.9961	0.9941	1.022	0.9961	0	0	0
Vabc-611	0	0	0.9648	0	0	0.9571	0	0	-0.80%
Vabc-680	0.9871	1.045	0.971	0.9805	1.045	0.9632	-0.67%	0.00%	-0.81%
Vabc-684	0.9853	0	0.9679	0.9787	0	0.9602	-0.67%	0	-0.80%

Table 4.34 shows that when the load grew on buses 675 and 671, the buses nearest to it were impacted because the voltage dropped at different rates. In some buses.

<u>Connecting a 500 kW and a 400 kW PV system to Bus 671 and Bus 675, respectively, with Iq = 0</u>

Five sets of SunPower SPR-305E-WHT-D PV panels are connected in parallel to make a 500 kW renewable energy system, and four sets are connected in parallel to create a 400 kW renewable energy system. Every set of PV panels produces 100 kW of power under standard conditions (STC), which include 1000 W/m² of solar energy and a temperature of 25 °C. The voltage on buses is displayed in Table 4.35. below when the modified IEEE 13 bus system is connected to the PV system by connecting the 400 kW system to bus 675 and the 500 kW system to bus 671 with Iq = 0, where only pure active power is injected.

Table 4.35. The voltage of the buses before increasing load, before and after connecting the 500 kW +400 kW photovoltaic system.

V-Buses	Normal Case			After increasing load & Before connecting the400 kW+500 kW PV system			After increasing load & After connecting the 400 kW+500 kW PV system		
	R	S	T	R	S	T	R	S	T
Vabc-632	1.021	1.042	1.017	1.021	1.042	1.017	1.021	1.042	1.017
Vabc-633	1.018	1.04	1.015	1.018	1.04	1.015	1.018	1.04	1.015
Vabc-692	0.9871	1.045	0.971	0.9805	1.045	0.9632	0.9895	1.034	0.9764
Vabc-645	0	1.033	1.015	0	1.033	1.015	0	1.033	1.015
Vabc-646	0	1.032	1.014	0	1.032	1.014	0	1.032	1.014
Vabc-671	0.9871	1.045	0.971	0.9805	1.045	0.9632	0.9895	1.034	0.9764
Vabc-675	0.9798	1.046	0.9676	0.9715	1.046	0.9591	0.9828	1.036	0.9732
Vabc-652	0.9799	0	0	0.9733	0	0	0.9823	0	0
Vabc-634	0.9941	1.022	0.9961	0.9941	1.022	0.9961	0.9941	1.022	0.9961
Vabc-611	0	0	0.9648	0	0	0.9571	0	0	0.9703
Vabc-680	0.9871	1.045	0.971	0.9805	1.045	0.9632	0.9895	1.034	0.9764
Vabc-684	0.9853	0	0.9679	0.9787	0	0.9602	0.9877	0	0.9734

According to the above table, the voltage considerably improved following the installation of the photovoltaic system, allowing for the treatment of the drop brought on by the increasing load. The voltage of bus 671, for instance, was R_{671}=0.9871, S_{671}=1.045, T_{671}=0.971. When the load was increased, the voltage dropped to R_{671}=0.9805, S_{671}=1.045, and T_{671}=0.9632. The PV system was next added, and the voltage improved to R_{671}=0.9895, S_{671}=1.034, and T_{671}=0.9764, and the voltage of bus 675 was R_{675}=0.9798, S_{675}=1.046, and T_{675}=0.9676. When the load was increased, the voltage dropped to R_{675} = 0.9715, S_{675} = 1.046, and T_{675} = 0.9591. The PV system was next added, and the voltage improved to R_{675}=0.9828, S_{675}=1.036, and T_{675}=0.9732.

Connecting a 500 kW and a 400 kW PV system to Bus 671 and Bus 675, respectively, with Iq = -0.5

Five sets of SunPower SPR-305E-WHT-D PV panels are connected in parallel to make a 500 kW renewable energy system, and four sets are connected in parallel to create a 400 kW renewable energy system. Every set of PV panels produces 100 kW of power under standard conditions (STC), which include 1000 W/m² of solar energy and a temperature of 25 °C. The voltage on buses is displayed in Table 4.36. below when the modified IEEE 13 bus system is connected to the PV system by connecting the 400 kW system to bus 675 and the 500 kW system to bus 671 with Iq = -0.5, where active power and 50% of the reactive power are injected.

Table 4.36. The voltage of the buses before increasing load, before and after connecting the 500 kW +400 kW photovoltaic system.

V-Buses	Normal Case			After increasing load & Before connecting the 400 kW+500 kW PV system			After increasing load & After connecting the 400 kW+500 kW PV system		
	R	S	T	R	S	T	R	S	T
Vabc-632	1.021	1.042	1.017	1.021	1.042	1.017	1.021	1.042	1.017
Vabc-633	1.018	1.04	1.015	1.018	1.04	1.015	1.018	1.04	1.015
Vabc-692	0.9871	1.045	0.971	0.9805	1.045	0.9632	0.9937	1.039	0.9809
Vabc-645	0	1.033	1.015	0	1.033	1.015	0	1.033	1.015
Vabc-646	0	1.032	1.014	0	1.032	1.014	0	1.032	1.014
Vabc-671	0.9871	1.045	0.971	0.9805	1.045	0.9632	0.9937	1.039	0.9809
Vabc-675	0.9798	1.046	0.9676	0.9715	1.046	0.9591	0.9873	1.041	0.978
Vabc-652	0.9799	0	0	0.9733	0	0	0.9864	0	0
Vabc-634	0.9941	1.022	0.9961	0.9941	1.022	0.9961	0.9941	1.022	0.9961
Vabc-611	0	0	0.9648	0	0	0.9571	0	0	0.9747
Vabc-680	0.9871	1.045	0.971	0.9805	1.045	0.9632	0.9937	1.039	0.9809
Vabc-684	0.9853	0	0.9679	0.9787	0	0.9602	0.9918	0	0.9779

According to the above table, the voltage considerably improved following the installation of the photovoltaic system, allowing for the treatment of the drop brought on by the increasing load. The voltage of bus 671, for instance, was R_{671}=0.9871, S_{671}=1.045, and T_{671}=0.971. When the load was increased, the voltage dropped to R_{671}=0.9805, S_{671}=1.045, and T_{671}=0.9632. The PV system was next added, and the voltage improved to R_{671}=0.9937, S_{671}=1.039, and T_{671}=0.9809, and the voltage of bus 675 was R_{675}=0.9798, S_{675}=1.046, and T_{675}=0.9676. When the load was increased, the voltage dropped to R_{675} = 0.9715, S_{675} = 1.046, and T_{675} = 0.9591. The PV system was next added, and the voltage improved to R_{675}=0.9873, S_{675}=1.041, and T_{675}=0.978.

Connecting a 500 kW and a 400 kW PV system to Bus 671 and Bus 675, respectively, with Iq = -1

Five sets of SunPower SPR-305E-WHT-D PV panels are connected in parallel to make a 500 kW renewable energy system, and four sets are connected in parallel to create a 400 kW renewable energy system. Every set of PV panels produces 100 kW of power under standard conditions (STC), which include 1000 W/m² of solar energy and a temperature of 25 °C. The voltage on buses is displayed in Table 4.37. below when the modified IEEE 13 bus system is connected to the PV system by connecting the 400 kW system to bus 675 and the 500 kW system to bus 671 with Iq = -1, where active power and 100% of the reactive power are injected.

Table 4.37. The voltage of the buses before increasing load, before and after connecting the 500 kW +400 kW photovoltaic system.

V-Buses	Normal Case			After increasing load & Before connecting the400 kW+500 kW PV system			After increasing load & After connecting the400 kW+500 kW PV system		
	R	S	T	R	S	T	R	S	T
Vabc-632	1.021	1.042	1.017	1.021	1.042	1.017	1.021	1.042	1.017
Vabc-633	1.018	1.04	1.015	1.018	1.04	1.015	1.018	1.04	1.015
Vabc-692	0.9871	1.045	0.971	0.9805	1.045	0.9632	0.9974	1.044	0.9854
Vabc-645	0	1.033	1.015	0	1.033	1.015	0	1.033	1.015
Vabc-646	0	1.032	1.014	0	1.032	1.014	0	1.032	1.014
Vabc-671	0.9871	1.045	0.971	0.9805	1.045	0.9632	0.9974	1.044	0.9855
Vabc-675	0.9798	1.046	0.9676	0.9715	1.046	0.9591	0.9913	1.046	0.9828
Vabc-652	0.9799	0	0	0.9733	0	0	0.9901	0	0
Vabc-634	0.9941	1.022	0.9961	0.9941	1.022	0.9961	0.9941	1.022	0.9961
Vabc-611	0	0	0.9648	0	0	0.9571	0	0	0.9792
Vabc-680	0.9871	1.045	0.971	0.9805	1.045	0.9632	0.9974	1.044	0.9855
Vabc-684	0.9853	0	0.9679	0.9787	0	0.9602	0.9956	0	0.9824

According to the above table, the voltage considerably improved following the installation of the photovoltaic system, allowing for the treatment of the drop brought on by the increasing load. The voltage of bus 671, for instance, was R_{671}=0.9871, S_{671}=1.045, and T_{671}=0.971. When the load was increased, the voltage dropped to R_{671}=0.9805, S_{671}=1.045, and T_{671}=0.9632. The PV system was next added, and the voltage improved to R_{671}=0.9974, S_{671}=1.044, and T_{671}=0.9855, and the voltage of bus 675 was R_{675}=0.9798, S_{675}=1.046, and T_{675}=0.9676. When the load was increased, the voltage dropped to R_{675}=0.9715, S_{675}=1.046, and T_{675}=0.9591. The PV system was next added, and the voltage improved to R_{675}=0.9913, S_{675}=1.046, ans T_{675}=0.9828.

A 50% increase in the load on busses 675 and 671

The active and reactive power load on buses 675 & 671 were raised by 50% in the modified IEEE 13 bus test system circuit. The imbalanced loads on bus 675 were Q (R = 190 kVar, S = 60 kVar, and T = 212 kVar) and P (R = 485 kW, S = 68 kW, and T = 290 kW), whereas the balanced loads on bus 671 were Q (R = 220 kVar, S = 220 kVar, and T = 220 kVar) and P (R = 385 kW, S = 385 kW, and T = 385 kW). The voltage of each bus was measured when the loads were increased. The balanced loads on bus 671 after increasing load Q (R = 330 kVar, S = 330 kVar, and T = 330 kVar) and P (R = 577.5 kW, S = 577.5 kW, and T = 577.5 kW), whereas the imbalanced loads on bus 675 Q (R = 285 kVar, S = 90 kVar, and T = 318 kVar) and P (R = 727.5 kW, S = 102 kW, and T = 435 kW). Below is Table 4.38, which displays the voltage measurements and the percentage decrease that occurred in all buses.

Table 4.38. The voltage on the buses both before and after increasing the load on the bus 675 and 671 by 50%.

V-Buses	Normal Case			After Increase the Load by 50% (bus 671+bus675)			Drop Rate%		
	R	S	T	R	S	T	R	S	T
Vabc-632	1.021	1.042	1.017	1.021	1.042	1.017	0	0	0
Vabc-633	1.018	1.04	1.015	1.018	1.04	1.015	0	0	0
Vabc-692	0.9871	1.045	0.971	0.9739	1.045	0.9555	-1.36%	0.00%	-1.62%
Vabc-645	0	1.033	1.015	0	1.033	1.015	0	0	0
Vabc-646	0	1.032	1.014	0	1.032	1.014	0	0	0
Vabc-671	0.9871	1.045	0.971	0.9739	1.045	0.9556	-1.36%	0.00%	-1.61%
Vabc-675	0.9798	1.046	0.9676	0.9632	1.047	0.9507	-1.72%	0.10%	-1.78%
Vabc-652	0.9799	0	0	0.9668	0	0	-1.35%	0	0
Vabc-634	0.9941	1.022	0.9961	0.9941	1.022	0.9961	0	0	0
Vabc-611	0	0	0.9648	0	0	0.9495	0	0	-1.61%
Vabc-680	0.9871	1.045	0.971	0.9739	1.045	0.9556	-1.36%	0.00%	-1.61%
Vabc-684	0.9853	0	0.9679	0.9721	0	0.9526	-1.36%	0	-1.61%

Table 4.38. shows that when the load grew on buses 675 and 671, the buses nearest to it were impacted because the voltage dropped at different rates. The above table shows that voltage drops occur in some buses at varying rates after the load increases. In some buses, the voltage value drops below 0.95 pu, and breakdown occurs. Where the voltage on bus 611 dropped below 0.95.

Figure 4.21. shows the voltage, current, and power on buses 671 and 675 after increasing the load by 50% on bus 671 and bus 675.

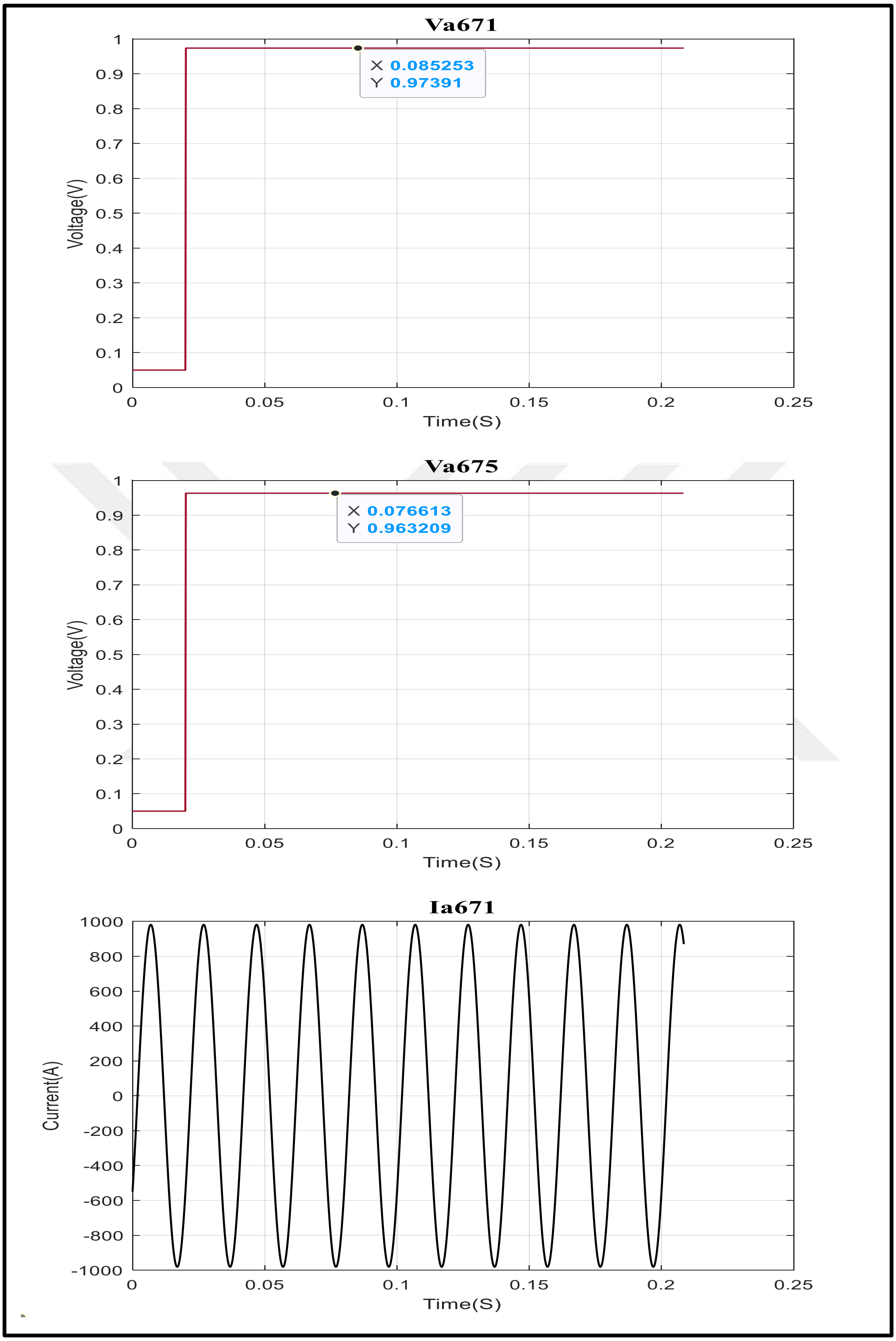

Figure 4.21. The voltage, current, and power on buses 671 and 675 after increasing the load by 50% on bus 671 and bus 675.

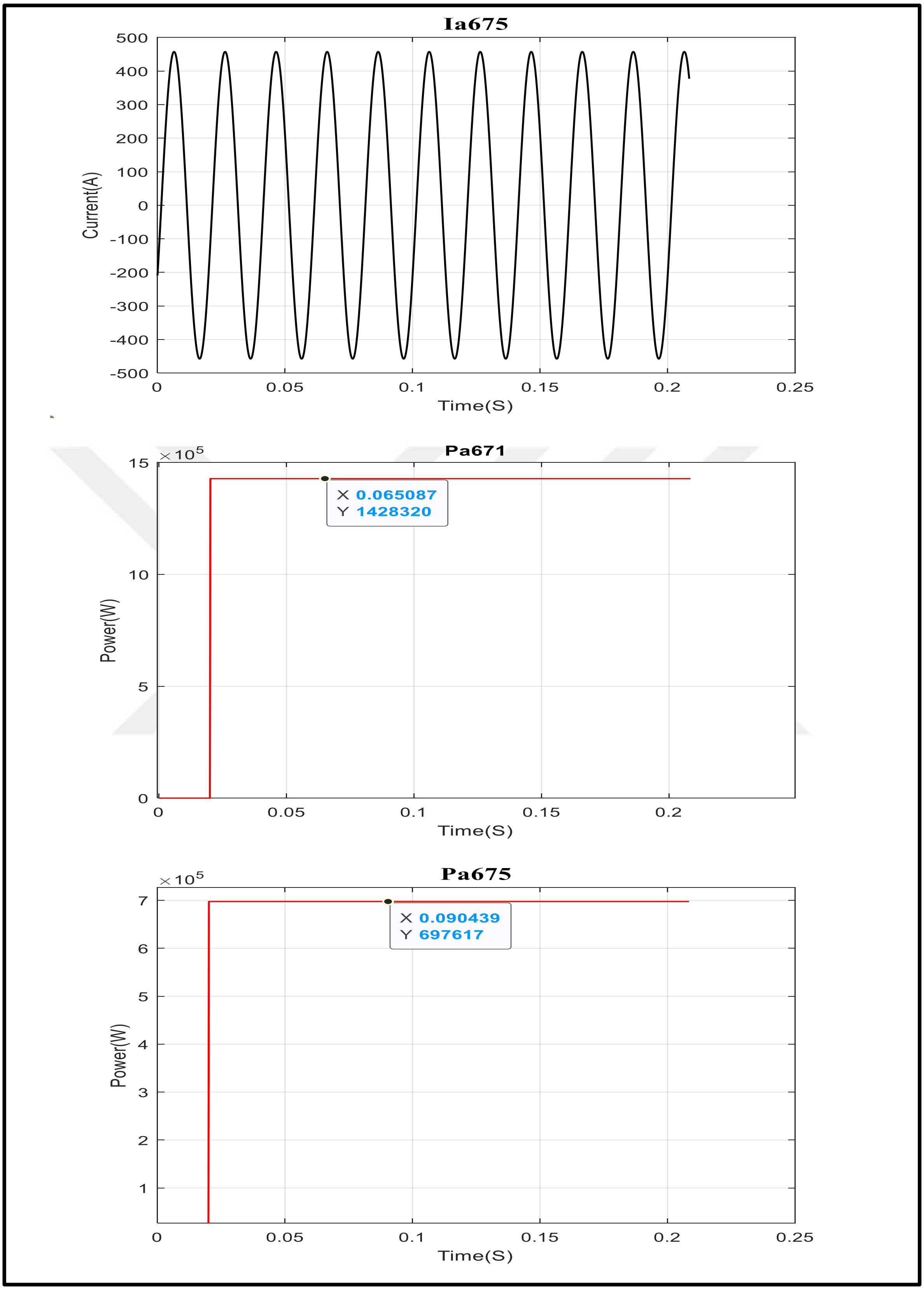

Figure 4.21. (continue) The voltage, current, and power on buses 671 and 675 after increasing the load by 50% on bus 671 and bus 675.

Connecting a 500 kW and 400 kW PV to Bus 671 and Bus 675, respectively, with Iq = 0

Five sets of SunPower SPR-305E-WHT-D PV panels are connected in parallel to make a 500 kW renewable energy system, and four sets are connected in parallel to create a 400 kW renewable energy system. Every set of PV panels produces 100 kW of power under standard conditions (STC), which include 1000 W/m² of solar energy and a temperature of 25 °C. The voltage on buses is displayed in Table 4.39. below when the modified IEEE 13 bus system is connected to the PV system by connecting the 400 kW system to bus 675 and the 500 kW system to bus 671 with Iq = 0, where only pure active power is injected.

Table 4.39. The voltage of the buses before increasing load, before and after connecting the 500 kW +400 kW photovoltaic system.

V-Buses	Normal Case			After increasing load & Before connecting the400 kW+500 kW PV system			After increasing load & After connecting the400 kW+500 kW PV system		
	R	S	T	R	S	T	R	S	T
Vabc-632	1.021	1.042	1.017	1.021	1.042	1.017	1.021	1.042	1.017
Vabc-633	1.018	1.04	1.015	1.018	1.04	1.015	1.018	1.04	1.015
Vabc-692	0.9871	1.045	0.971	0.9739	1.045	0.9555	0.9837	1.033	0.9693
Vabc-645	0	1.033	1.015	0	1.033	1.015	0	1.033	1.015
Vabc-646	0	1.032	1.014	0	1.032	1.014	0	1.032	1.014
Vabc-671	0.9871	1.045	0.971	0.9739	1.045	0.9556	0.9837	1.033	0.9693
Vabc-675	0.9798	1.046	0.9676	0.9632	1.047	0.9507	0.9754	1.034	0.9652
Vabc-652	0.9799	0	0	0.9668	0	0	0.9765	0	0
Vabc-634	0.9941	1.022	0.9961	0.9941	1.022	0.9961	0.9941	1.022	0.9961
Vabc-611	0	0	0.9648	0	0	0.9495	0	0	0.9632
Vabc-680	0.9871	1.045	0.971	0.9739	1.045	0.9556	0.9837	1.033	0.9693
Vabc-684	0.9853	0	0.9679	0.9721	0	0.9526	0.9818	0	0.9663

According to the above table, the voltage considerably improved following the installation of the photovoltaic system, allowing for the treatment of the drop brought on by the increasing load. The voltage of bus 671, for instance, was R_{671}=0.9871, S_{671}=1.045, and T_{671}=0.971. When the load was increased, the voltage dropped to R_{671}=0.9739, S_{671}=1.045, and T_{671}=0.9556. The PV system was next added, and the voltage improved to R_{671}=0.9837, S_{671}=1.033, and T_{671}=0.9693, and the voltage of bus 675 was R_{675}=0.9798, S_{675}=1.046, and T_{675}=0.9676. When the load was increased, the voltage dropped to R_{675}=0.9632, S_{675}=1.047, and T_{675}=0.9507. The PV system was next added, and the voltage improved to R_{675}=0.9754, S_{675}=1.034, and T_{671}=0.9652.

Figure 4.22. shows the voltage, current, and power on buses 671 and 675 after increasing the load by 50% with a PV system (Iq=0).

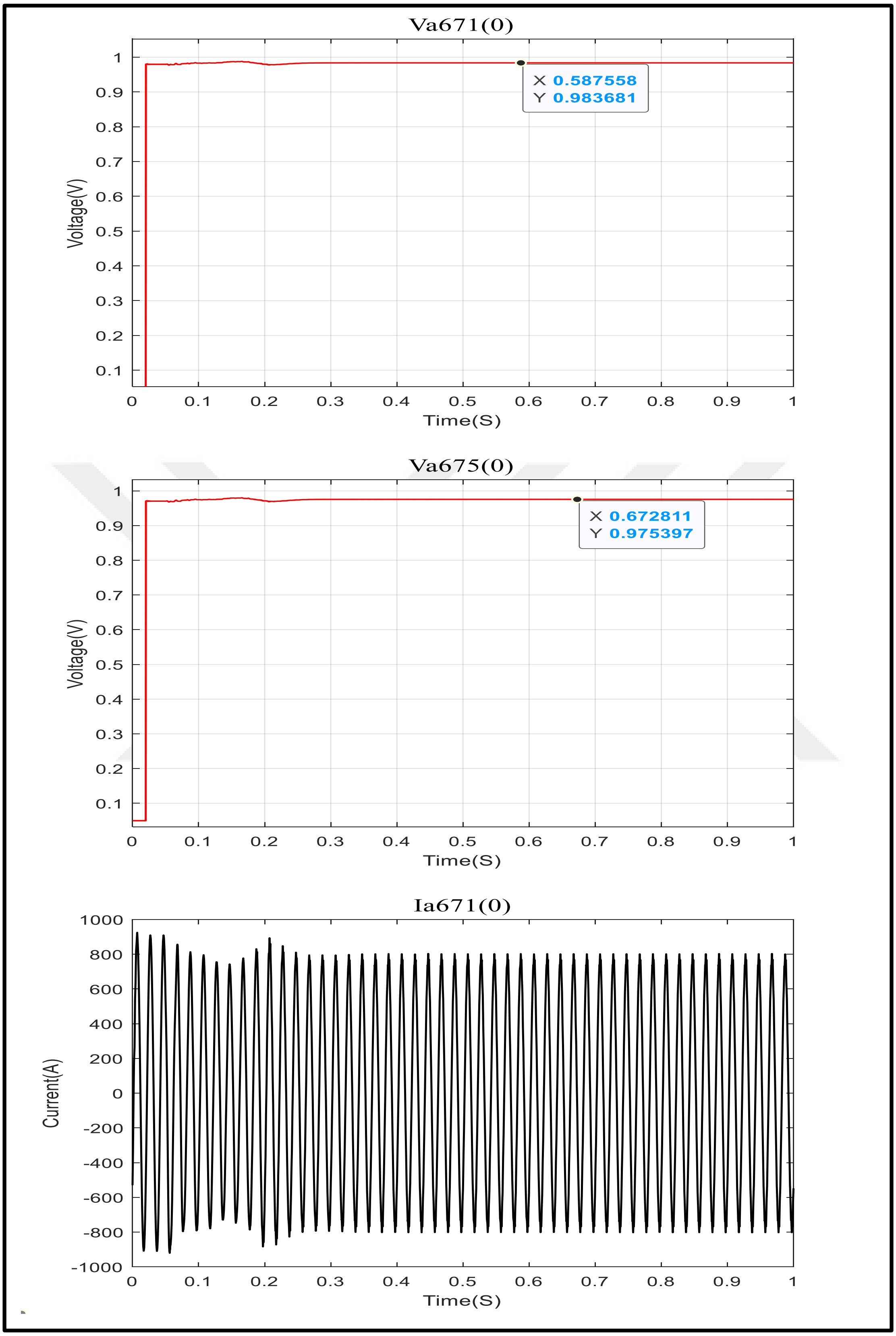

Figure 4.22. The voltage, current, and power on buses 671 and 675 after increasing the load by 50% on bus 671 and bus 675 with a PV system (Iq=0).

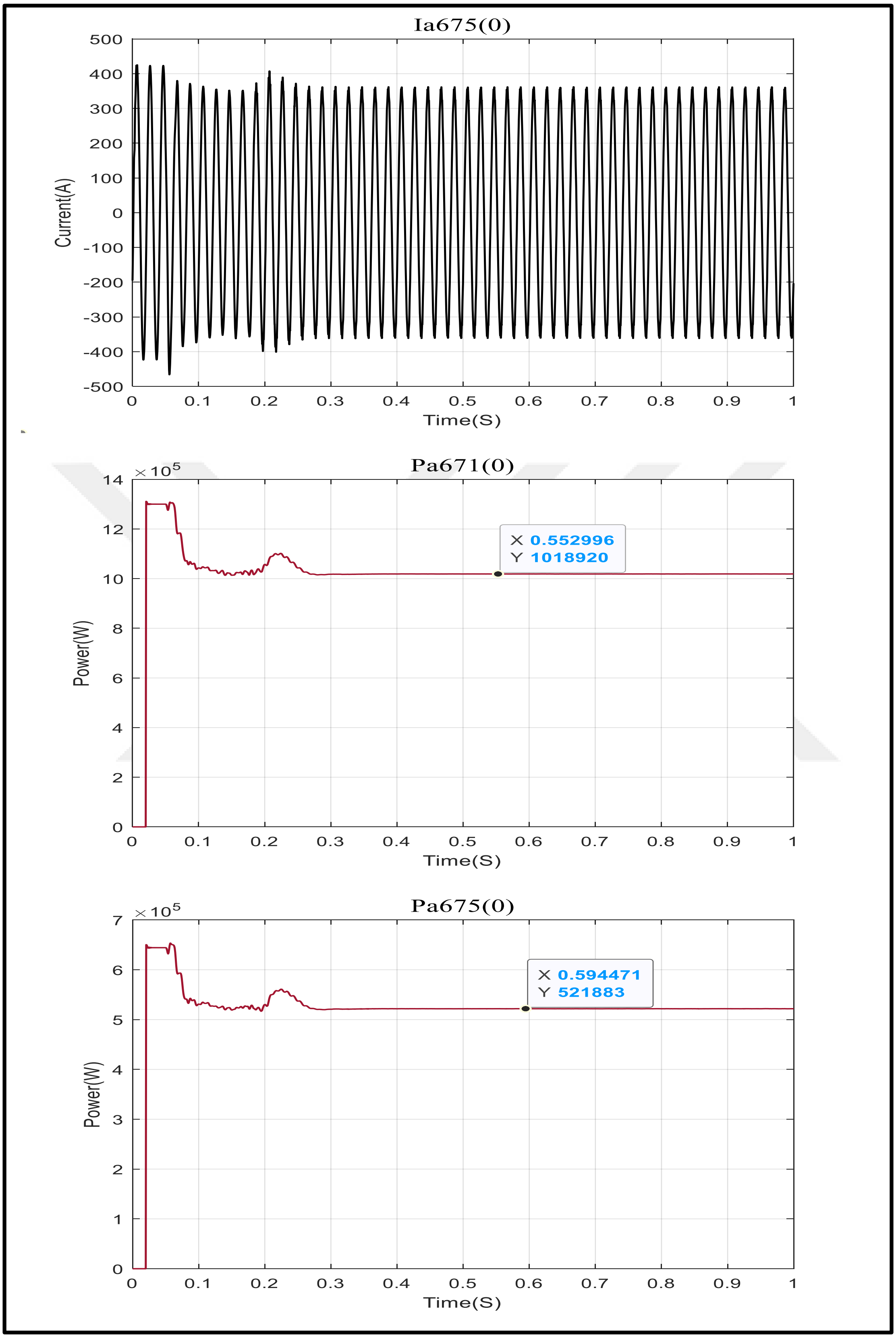

Figure 4.22. (continue) The voltage, current, and power on buses 671 and 675 after increasing the load by 50% on bus 671 and bus 675 with a PV system (Iq=0).

Connecting a 500 kW and 400 kW PV to Bus 671 and Bus 675, respectively, with Iq = -0.5

Five sets of SunPower SPR-305E-WHT-D PV panels are connected in parallel to make a 500 kW renewable energy system, and four sets are connected in parallel to create a 400 kW renewable energy system. Every set of PV panels produces 100 kW of power under standard conditions (STC), which include 1000 W/m² of solar energy and a temperature of 25 °C. The voltage on buses is displayed in Table 4.40. below when the modified IEEE 13 bus system is connected to the PV system by connecting the 400 kW system to bus 675 and the 500 kW system to bus 671 with Iq = -0.5, where active power and 50% of the reactive power are injected.

Table 4.40. The voltage of the buses before increasing load, before and after connecting the 500 kW +400 kW photovoltaic system.

V-Buses	Normal Case			After increasing load & Before connecting the400 kW+500 kW PV system			After increasing load & After connecting the 400 kW+500 kW PV system		
	R	S	T	R	S	T	R	S	T
Vabc-632	1.021	1.042	1.017	1.021	1.042	1.017	1.021	1.042	1.017
Vabc-633	1.018	1.04	1.015	1.018	1.04	1.015	1.018	1.04	1.015
Vabc-692	0.9871	1.045	0.971	0.9739	1.045	0.9555	0.9878	1.038	0.974
Vabc-645	0	1.033	1.015	0	1.033	1.015	0	1.033	1.015
Vabc-646	0	1.032	1.014	0	1.032	1.014	0	1.032	1.014
Vabc-671	0.9871	1.045	0.971	0.9739	1.045	0.9556	0.9878	1.038	0.974
Vabc-675	0.9798	1.046	0.9676	0.9632	1.047	0.9507	0.9798	1.04	0.9702
Vabc-652	0.9799	0	0	0.9668	0	0	0.9806	0	0
Vabc-634	0.9941	1.022	0.9961	0.9941	1.022	0.9961	0.9941	1.022	0.9961
Vabc-611	0	0	0.9648	0	0	0.9495	0	0	0.9679
Vabc-680	0.9871	1.045	0.971	0.9739	1.045	0.9556	0.9878	1.038	0.974
Vabc-684	0.9853	0	0.9679	0.9721	0	0.9526	0.986	0	0.971

According to the above table, the voltage considerably improved following the installation of the photovoltaic system, allowing for the treatment of the drop brought on by the increasing load. The voltage of bus 671, for instance, was R_{671}=0.9871, S_{671}=1.045, and T_{671}=0.971. When the load was increased, the voltage dropped to R_{671}=0.9739, S_{671}=1.045, and T_{671}=0.9556. The PV system was next added, and the voltage improved to R_{671}=0.9878, S_{671}=1.038, and T_{671}=0.974, and the voltage of bus 675 was R_{675}=0.9798, S_{675}=1.046, and T_{675}=0.9676. When the load was increased, the voltage dropped to R_{675}=0.9632, S_{675}=1.047, and T_{675}=0.9507. The PV system was next added, and the voltage improved to R_{675}=0.9798, S_{675}=1.04, and T_{675}=0.9702.

Figure 4. 23. shows the voltage, current, and power on buses 671 and 675 after increasing the load by 50% with a PV system (Iq=-0.5).

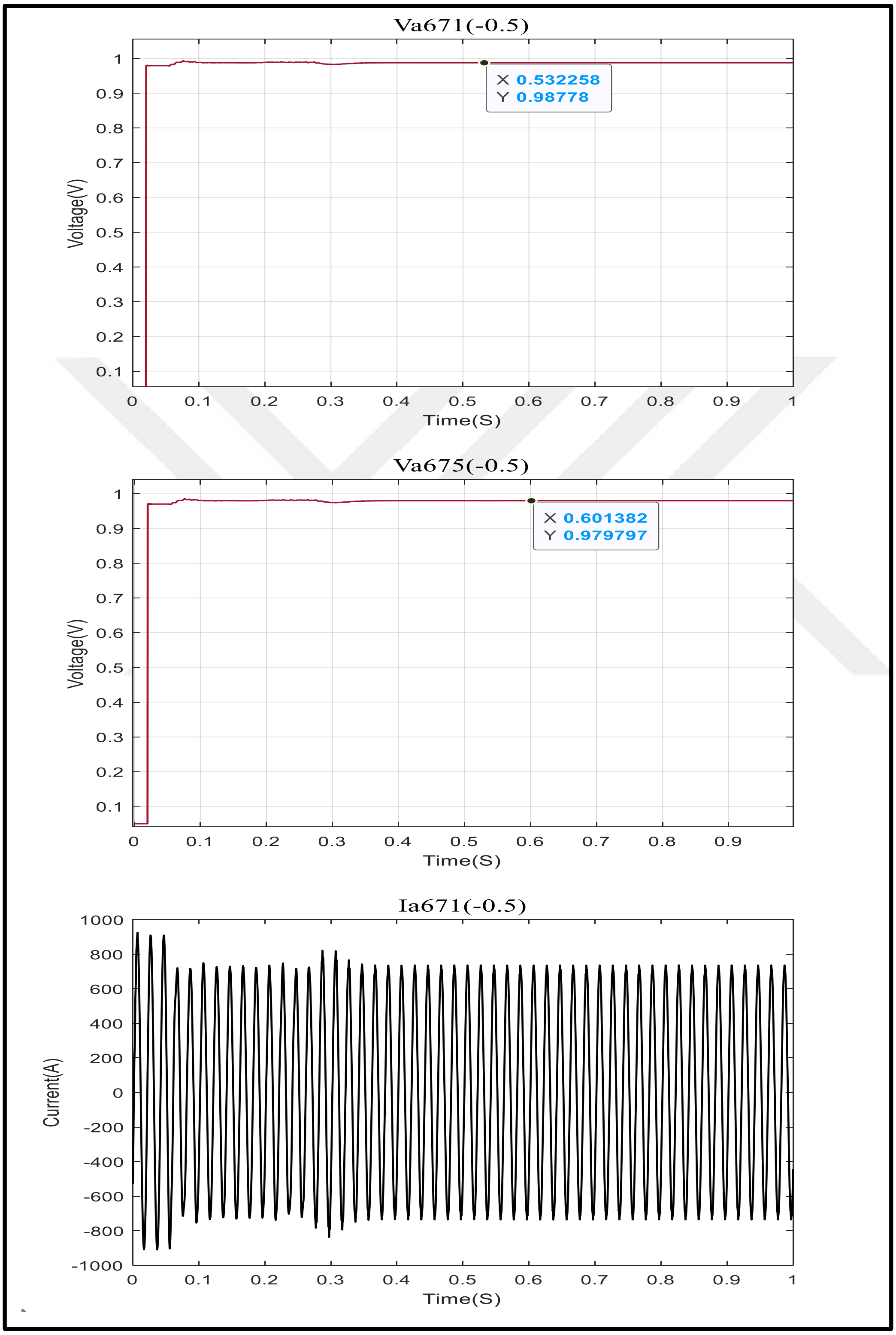

Figure 4.23. The voltage, current, and power on buses 671 and 675 after increasing the load by 50% on bus 671 and bus 675 with a PV system (Iq=-0.5).

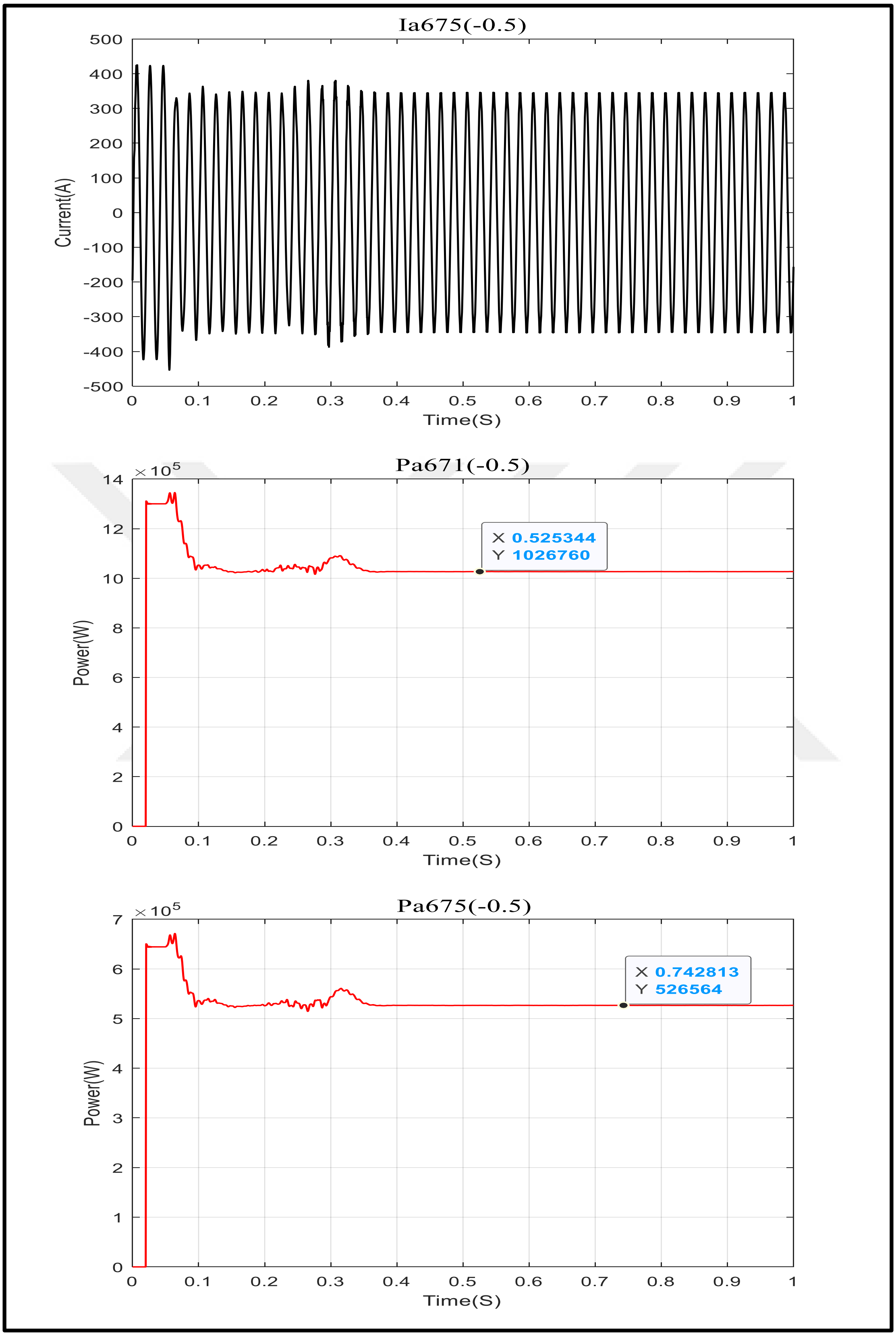

Figure 4.23. (continue) The voltage, current, and power on buses 671 and 675 after increasing the load by 50% on bus 671 and bus 675 with a PV system (Iq=-0.5).

Connecting a 500 kW and 400 kW PV to Bus 671 and Bus 675, respectively, with Iq = -1

Five sets of SunPower SPR-305E-WHT-D PV panels are connected in parallel to make a 500 kW renewable energy system, and four sets are connected in parallel to create a 400 kW renewable energy system. Every set of PV panels produces 100 kW of power under standard conditions (STC), which include 1000 W/m² of solar energy and a temperature of 25 °C. The voltage on buses is displayed in Table 4.41. below when the modified IEEE 13 bus system is connected to the PV system by connecting the 400 kW system to bus 675 and the 500 kW system to bus 671 with Iq = -1, where active power and 100% of the reactive power are injected.

Table 4.41. The voltage of the buses before increasing load, before and after connecting the 500 kW +400 kW photovoltaic system.

V-Buses	Normal Case			After increasing load & Before connecting the400 kW+500 kW PV system			After increasing load & After connecting the400 kW+500 kW PV system		
	R	S	T	R	S	T	R	S	T
Vabc-632	1.021	1.042	1.017	1.021	1.042	1.017	1.021	1.042	1.017
Vabc-633	1.018	1.04	1.015	1.018	1.04	1.015	1.018	1.04	1.015
Vabc-692	0.9871	1.045	0.971	0.9739	1.045	0.9555	0.9915	1.042	0.9783
Vabc-645	0	1.033	1.015	0	1.033	1.015	0	1.033	1.015
Vabc-646	0	1.032	1.014	0	1.032	1.014	0	1.032	1.014
Vabc-671	0.9871	1.045	0.971	0.9739	1.045	0.9556	0.9916	1.042	0.9784
Vabc-675	0.9798	1.046	0.9676	0.9632	1.047	0.9507	0.9838	1.044	0.9748
Vabc-652	0.9799	0	0	0.9668	0	0	0.9843	0	0
Vabc-634	0.9941	1.022	0.9961	0.9941	1.022	0.9961	0.9941	1.022	0.9961
Vabc-611	0	0	0.9648	0	0	0.9495	0	0	0.9722
Vabc-680	0.9871	1.045	0.971	0.9739	1.045	0.9556	0.9916	1.042	0.9784
Vabc-684	0.9853	0	0.9679	0.9721	0	0.9526	0.9897	0	0.9753

According to the above table, the voltage considerably improved following the installation of the photovoltaic system, allowing for the treatment of the drop brought on by the increasing load. The voltage of bus 671, for instance, was R_{671}=0.9871, S_{671}=1.045, and T_{671}=0.971. When the load was increased, the voltage dropped to R_{671}=0.9739, S_{671}=1.045, and T_{671}=0.9556. The PV system was next added, and the voltage improved to R_{671}=0.9916, S_{671}=1.042, and T_{671}=0.9784, and the voltage of bus 675 was R_{675}=0.9798, S_{675}=1.046, and T_{675}=0.9676. When the load was increased, the voltage dropped to R_{675}=0.9632, S_{675}=1.047, and T_{675}=0.9507. The PV system was next added, and the voltage improved to R_{675}=0.9838, S_{675}=1.044, and T_{675}=0.9748.

Figure 4. 24. shows the voltage, current, and power on buses 671 and 675 after increasing the load by 50% with a PV system (Iq=-1).

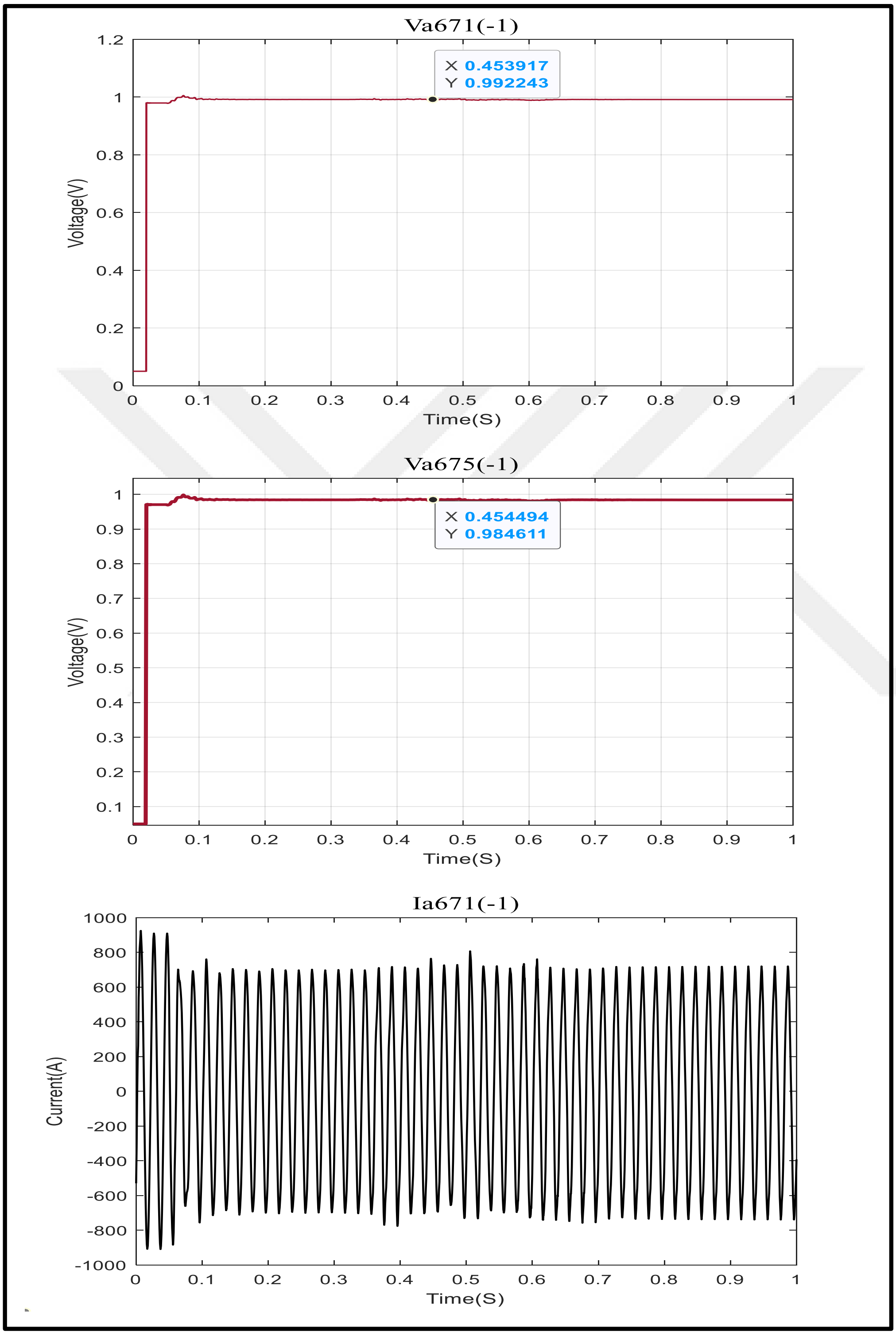

Figure 4.24. The voltage, current, and power on buses 671 and 675 after increasing the load by 50% on bus 671 and bus 675 with a PV system (Iq=-1).

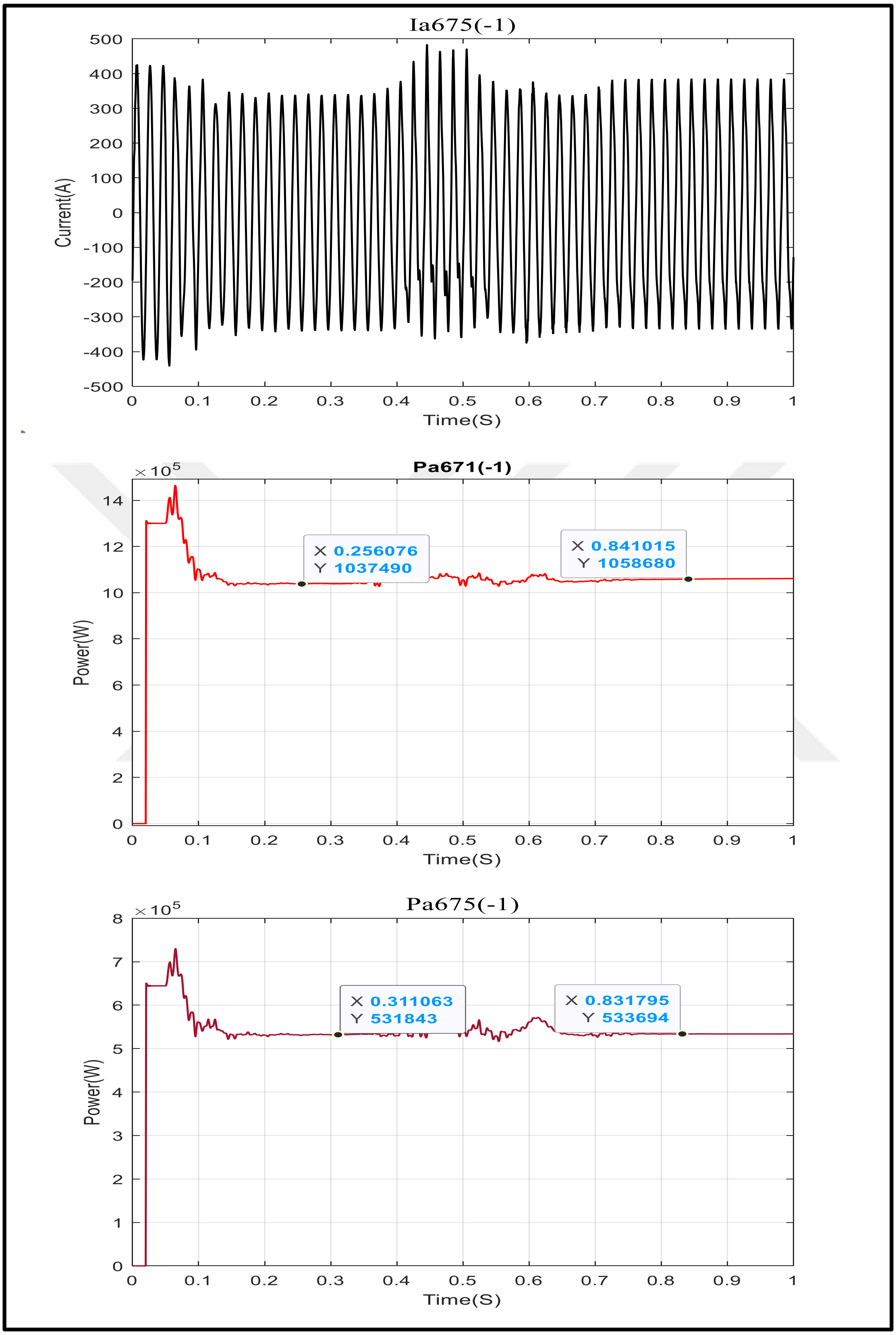

Figure 4.24. (continue) The voltage, current, and power on buses 671 and 675 after increasing the load by 50% on bus 671 and bus 675 with a PV system (Iq=-1).

A 75% increase in the load on busses 675 and 671

The active and reactive power load on buses 675 & 671 were raised by 75% in the modified IEEE 13 bus test system circuit. The imbalanced loads on bus 675 were Q (R = 190 kVar, S = 60 kVar, and T = 212 kVar) and P (R = 485 kW, S = 68 kW, and T = 290 kW), whereas the balanced loads on bus 671 were Q (R = 220 kVar, S = 220 kVar, and T = 220 kVar) and P (R = 385 kW, S = 385 kW, and T = 385 kW). The voltage of each bus was measured when the loads were increased. The balanced loads on bus 671 after increasing load Q (R = 385 kVar, S = 385 kVar, and T = 385 kVar) and P (R = 673.75 kW, S = 637.75 kW, and T = 673.75 kW), whereas the imbalanced loads on bus 675 Q (R = 332.5 kVar, S = 105 kVar, and T = 371 kVar) and P (R = 848.75 kW, S = 119 kW, and T = 507.5 kW). Below is Table 4.42, which displays the voltage measurements and the percentage decrease that occurred in all buses.

Table 4.42. The voltage on the buses both before and after increasing the load on the bus 675 and 671by 75%.

V-Buses	Before Increase the Load			After Increase the Load by 75% (bus 671+bus675)			Drop Rate%		
	R	S	T	R	S	T	R	S	T
Vabc-632	1.021	1.042	1.017	1.021	1.042	1.017	0	0	0
Vabc-633	1.018	1.04	1.015	1.018	1.04	1.015	0	0	0
Vabc-692	0.9871	1.045	0.971	0.9674	1.045	0.948	-2.04%	0.00%	-2.43%
Vabc-645	0	1.033	1.015	0	1.033	1.015	0	0	0
Vabc-646	0	1.032	1.014	0	1.032	1.014	0	0	0
Vabc-671	0.9871	1.045	0.971	0.9674	1.045	0.9481	-2.04%	0.00%	-2.42%
Vabc-675	0.9798	1.046	0.9676	0.955	1.047	0.9424	-2.60%	0.10%	-2.67%
Vabc-652	0.9799	0	0	0.9603	0	0	-2.04%	0	0
Vabc-634	0.9941	1.022	0.9961	0.9941	1.022	0.9961	0	0	0
Vabc-611	0	0	0.9648	0	0	0.9421	0	0	-2.41%
Vabc-680	0.9871	1.045	0.971	0.9674	1.045	0.9481	-2.04%	0.00%	-2.42%
Vabc-684	0.9853	0	0.9679	0.9656	0	0.9451	-2.04%	0	-2.41%

As the load on buses 675 and 671 increased, the buses closest to them experienced voltage drops at varying rates, as shown in Table 4.42. Some buses experienced voltage drops below 0.95 pu, causing a breakdown. In this case, buses 692, 671, 675, 611, 680, and 684 experienced voltage drops below 0.95 pu.

Connecting a 500 kW and 400 kW PV to Bus 671 and Bus 675, respectively, with Iq = 0

Five sets of SunPower SPR-305E-WHT-D PV panels are connected in parallel to make a 500 kW renewable energy system, and four sets are connected in parallel to create a 400 kW renewable energy system. Every set of PV panels produces 100 kW of power under standard conditions (STC), which include 1000 W/m² of solar energy and a temperature of 25 °C. The voltage on buses is displayed in Table 4. 43. below when the modified IEEE 13 bus system is connected to the PV system by connecting the 400 kW system to bus 675 and the 500 kW system to bus 671 with Iq = 0, where only pure active power is injected.

Table 4.43. The voltage of the buses before increasing load, before and after connecting the 500 kW +400 kW photovoltaic system.

V-Buses	Normal Case			After increasing load & Before connecting the 400 kW+500 kW PV system			After increasing load & After connecting the 400 kW+500 kW PV system		
	R	S	T	R	S	T	R	S	T
Vabc-632	1.021	1.042	1.017	1.021	1.042	1.017	1.021	1.042	1.017
Vabc-633	1.018	1.04	1.015	1.018	1.04	1.015	1.018	1.04	1.015
Vabc-692	0.9871	1.045	0.971	0.9674	1.045	0.948	0.9778	1.032	0.9623
Vabc-645	0	1.033	1.015	0	1.033	1.015	0	1.033	1.015
Vabc-646	0	1.032	1.014	0	1.032	1.014	0	1.032	1.014
Vabc-671	0.9871	1.045	0.971	0.9674	1.045	0.9481	0.9778	1.032	0.9623
Vabc-675	0.9798	1.046	0.9676	0.955	1.047	0.9424	0.968	1.033	0.9573
Vabc-652	0.9799	0	0	0.9603	0	0	0.9707	0	0
Vabc-634	0.9941	1.022	0.9961	0.9941	1.022	0.9961	0.9941	1.022	0.9961
Vabc-611	0	0	0.9648	0	0	0.9421	0	0	0.9563
Vabc-680	0.9871	1.045	0.971	0.9674	1.045	0.9481	0.9778	1.032	0.9623
Vabc-684	0.9853	0	0.9679	0.9656	0	0.9451	0.976	0	0.9593

According to the above table, the voltage considerably improved following the installation of the photovoltaic system, allowing for the treatment of the drop brought on by the increasing load. The voltage of bus 671, for instance, was R_{671}=0.9871, S_{671}=1.045, and T_{671}=0.971. When the load was increased, the voltage dropped to R_{671}=0.9674, S_{671}=1.045, and T_{671}=0.9481. The PV system was next added, and the voltage improved to R_{671}=0.9778, S_{671}=1.032, and T_{671}=0.9623, and the voltage of bus 675 was R_{675}=0.9798, S_{675}=1.046, and T_{675}=0.9676. When the load was increased, the voltage dropped to R_{675}=0.955, S_{675}=1.047, and T_{675}=0.9424. The PV system was next added, and the voltage improved to R_{675}=0.968, S_{675}=1.033, and T_{675}=0.9573.

<u>Connecting a 500 kW and 400 kW PV to Bus 671 and Bus 675, respectively, with Iq = -0.5</u>

Five sets of SunPower SPR-305E-WHT-D PV panels are connected in parallel to make a 500 kW renewable energy system, and four sets are connected in parallel to create a 400 kW renewable energy system. Every set of PV panels produces 100 kW of power under standard conditions (STC), which include 1000 W/m² of solar energy and a temperature of

25 °C. The voltage on buses is displayed in Table 4.44. below when the modified IEEE 13 bus system is connected to the PV system by connecting the 400 kW system to bus 675 and the 500 kW system to bus 671 with Iq = -0.5, where active power and 50% of the reactive power are injected.

Table 4.44. The voltage of the buses before increasing load, before and after connecting the 500 kW + 400 kW photovoltaic system.

V-Buses	Normal Case			After increasing load & Before connecting the400 kW+500 kW PV system			After increasing load & After connecting the400 kW+500 kW PV system		
	R	S	T	R	S	T	R	S	T
Vabc-632	1.021	1.042	1.017	1.021	1.042	1.017	1.021	1.042	1.017
Vabc-633	1.018	1.04	1.015	1.018	1.04	1.015	1.018	1.04	1.015
Vabc-692	0.9871	1.045	0.971	0.9674	1.045	0.948	0.982	1.036	0.967
Vabc-645	0	1.033	1.015	0	1.033	1.015	0	1.033	1.015
Vabc-646	0	1.032	1.014	0	1.032	1.014	0	1.032	1.014
Vabc-671	0.9871	1.045	0.971	0.9674	1.045	0.9481	0.982	1.036	0.967
Vabc-675	0.9798	1.046	0.9676	0.955	1.047	0.9424	0.9725	1.038	0.9624
Vabc-652	0.9799	0	0	0.9603	0	0	0.9748	0	0
Vabc-634	0.9941	1.022	0.9961	0.9941	1.022	0.9961	0.9941	1.022	0.9961
Vabc-611	0	0	0.9648	0	0	0.9421	0	0	0.9609
Vabc-680	0.9871	1.045	0.971	0.9674	1.045	0.9481	0.982	1.036	0.967
Vabc-684	0.9853	0	0.9679	0.9656	0	0.9451	0.9802	0	0.964

According to the above table, the voltage considerably improved following the installation of the photovoltaic system, allowing for the treatment of the drop brought on by the increasing load. The voltage of bus 671, for instance, was R_{671}=0.9871, S_{671}=1.045, and T_{671}=0.971. When the load was increased, the voltage dropped to R_{671}=0.9674, S_{671}=1.045, and T_{671}=0.9481. The PV system was next added, and the voltage improved to R_{671}=0.982, S_{671}=1.036, and T_{671}=0.967, and the voltage of bus 675 was R_{675}=0.9798, S_{675}=1.046, and T_{675}=0.9676. When the load was increased, the voltage dropped to R_{675}=0.955, S_{675}=1.047, and T_{675}=0.9424. The PV system was next added, and the voltage improved to R_{675}=0.9725, S_{675}=1.038, and T_{675}=0.9624.

<u>Connecting a 500 kW and 400 kW PV to Bus 671 and Bus 675, respectively, with Iq = -1</u>

Five sets of SunPower SPR-305E-WHT-D PV panels are connected in parallel to make a 500 kW renewable energy system, and four sets are connected in parallel to create a 400 kW renewable energy system. Every set of PV panels produces 100 kW of power under standard conditions (STC), which include 1000 W/m² of solar energy and a temperature of 25 °C. The voltage on buses is displayed in Table 4.45. below when the modified IEEE 13 bus system is connected to the PV system by connecting the 400 kW system to bus 675 and the 500 kW system to bus 671 with Iq = -1, where active power and 100% of the reactive power are injected.

Table 4.45. The voltage of the buses before increasing load, before and after connecting the 500 kW +400 kW photovoltaic system.

V-Buses	Normal Case			After increasing load & Before connecting the400 kW+500 kW PV system			After increasing load & After connecting the400 kW+500 kW PV system		
	R	S	T	R	S	T	R	S	T
Vabc-632	1.021	1.042	1.017	1.021	1.042	1.017	1.021	1.042	1.017
Vabc-633	1.018	1.04	1.015	1.018	1.04	1.015	1.018	1.04	1.015
Vabc-692	0.9871	1.045	0.971	0.9674	1.045	0.948	0.9857	1.04	0.9713
Vabc-645	0	1.033	1.015	0	1.033	1.015	0	1.033	1.015
Vabc-646	0	1.032	1.014	0	1.032	1.014	0	1.032	1.014
Vabc-671	0.9871	1.045	0.971	0.9674	1.045	0.9481	0.9858	1.04	0.9713
Vabc-675	0.9798	1.046	0.9676	0.955	1.047	0.9424	0.9765	1.043	0.967
Vabc-652	0.9799	0	0	0.9603	0	0	0.9786	0	0
Vabc-634	0.9941	1.022	0.9961	0.9941	1.022	0.9961	0.9941	1.022	0.9961
Vabc-611	0	0	0.9648	0	0	0.9421	0	0	0.9652
Vabc-680	0.9871	1.045	0.971	0.9674	1.045	0.9481	0.9858	1.04	0.9713
Vabc-684	0.9853	0	0.9679	0.9656	0	0.9451	0.9839	0	0.9683

According to the above table, the voltage considerably improved following the installation of the photovoltaic system, allowing for the treatment of the drop brought on by the increasing load. The voltage of bus 671, for instance, was R_{671}=0.9871, S_{671}=1.045, and T_{671}=0.971. When the load was increased, the voltage dropped to R_{671}=0.9674, S_{671}=1.045, and T_{671}=0.9481. The PV system was next added, and the voltage improved to R_{671}=0.9858, S_{671}=1.04, and T_{671}=0.9713, and the voltage of bus 675 was R_{675}=0.9798, S_{675}=1.046, and T_{675}=0.9676. When the load was increased, the voltage dropped to R_{675}=0.955, S_{675}=1.047, and T_{675}=0.9424. The PV system was next added, and the voltage improved to R_{675}=0.9765, S_{675}=1.043, and T_{675}=0.967.

A 100% increase in the load on busses 675 and 671

The active and reactive power load on buses 675 & 671 were raised by 100% in the modified IEEE 13 bus test system circuit. The imbalanced loads on bus 675 were Q (R = 190 kVar, S = 60 kVar, and T = 212 kVar) and P (R = 485 kW, S = 68 kW, and T = 290 kW), whereas the balanced loads on bus 671 were Q (R = 220 kVar, S = 220 kVar, and T = 220 kVar) and P (R = 385 kW, S = 385 kW, and T = 385 kW). The voltage of each bus was measured when the loads were increased. The balanced loads on bus 671 after increasing load Q (R = 440 kVar, S = 440 kVar, and T = 440 kVar) and P (R = 770 kW, S = 770 kW, and T = 770 kW), whereas the imbalanced loads on bus 675 Q (R = 380 kVar, S = 120 kVar, and T = 424 kVar) and P (R = 970 kW, S = 136 kW, and T = 580 kW). Below is Table 4.46, which displays the voltage measurements and the percentage decrease that occurred in all buses.

Table 4.46. The voltage on the buses both before and after increasing the load on the bus 675 and 671by 75%.

V-Buses	Normal Case			After Increase the Load by 100% (bus 671+bus675)			Drop Rate%		
	R	S	T	R	S	T	R	S	T
Vabc-632	1.021	1.042	1.017	1.021	1.042	1.017	0	0	0
Vabc-633	1.018	1.04	1.015	1.018	1.04	1.015	0	0	0
Vabc-692	0.9871	1.045	0.971	0.9609	1.045	0.9407	-2.73%	0.00%	-3.22%
Vabc-645	0	1.033	1.015	0	1.033	1.015	0	0	0
Vabc-646	0	1.032	1.014	0	1.032	1.014	0	0	0
Vabc-671	0.9871	1.045	0.971	0.9609	1.045	0.9407	-2.73%	0.00%	-3.22%
Vabc-675	0.9798	1.046	0.9676	0.947	1.047	0.9343	-3.46%	0.10%	-3.56%
Vabc-652	0.9799	0	0	0.9539	0	0	-2.73%	0	0
Vabc-634	0.9941	1.022	0.9961	0.9941	1.022	0.9961	0	0	0
Vabc-611	0	0	0.9648	0	0	0.9348	0	0	-3.21%
Vabc-680	0.9871	1.045	0.971	0.9609	1.045	0.9407	-2.73%	0.00%	-3.22%
Vabc-684	0.9853	0	0.9679	0.9591	0	0.9377	-2.73%	0	-3.22%

As the load on buses 675 and 671 increased, the buses closest to them experienced voltage drops at varying rates, as shown in Table 4.46. Some buses experienced voltage drops below 0.95 pu, causing a breakdown. In this case, buses 692, 671, 675, 611, 680, and 684 experienced voltage drops below 0.95 pu.

Figure 4.25. shows the voltage, current, and power on buses 671 and 675 after increasing the load by 100% on bus 671 and bus 675.

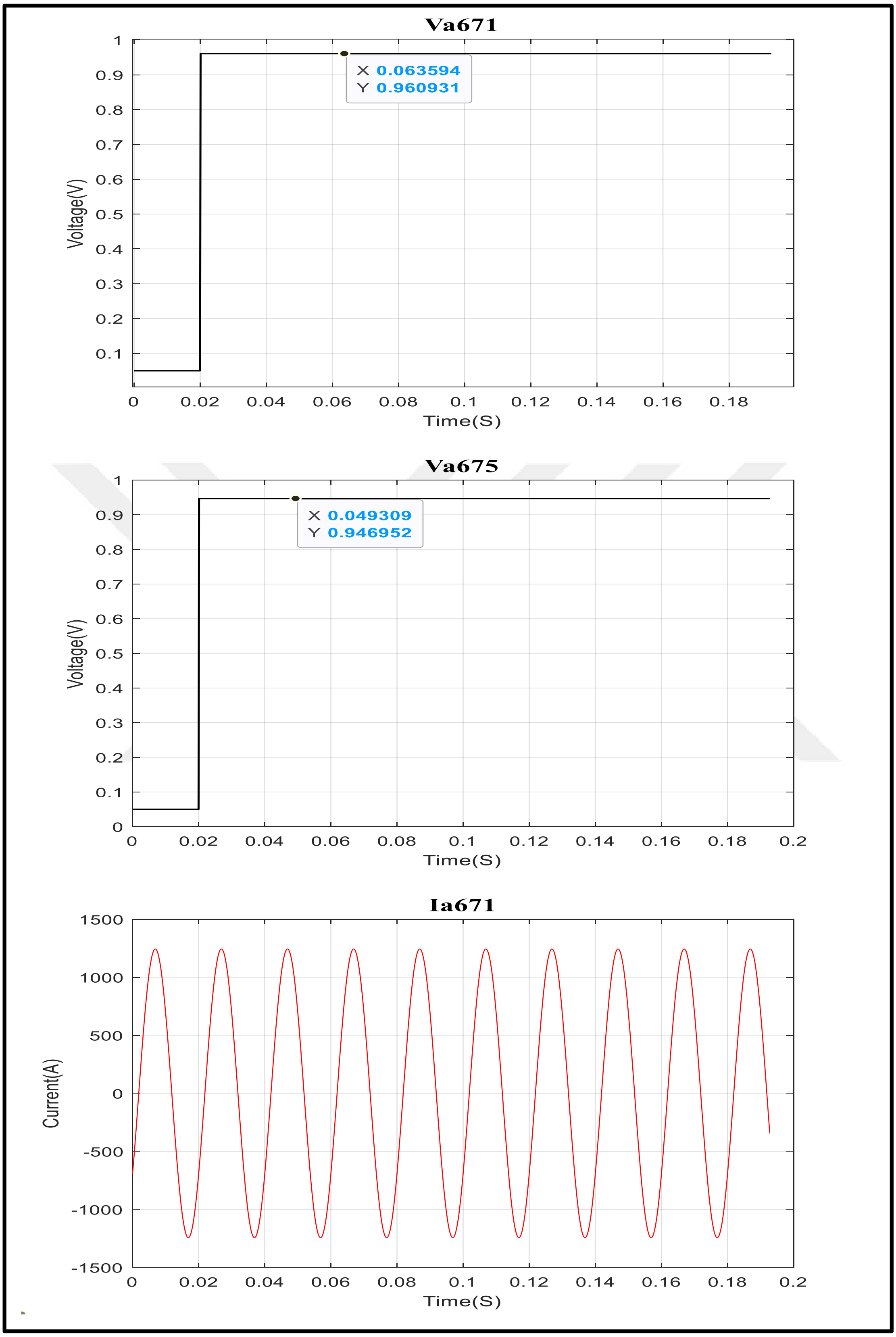

Figure 4.25. The voltage, current, and power on buses 671 and 675 after increasing the load by 100% on bus 671 and bus 675.

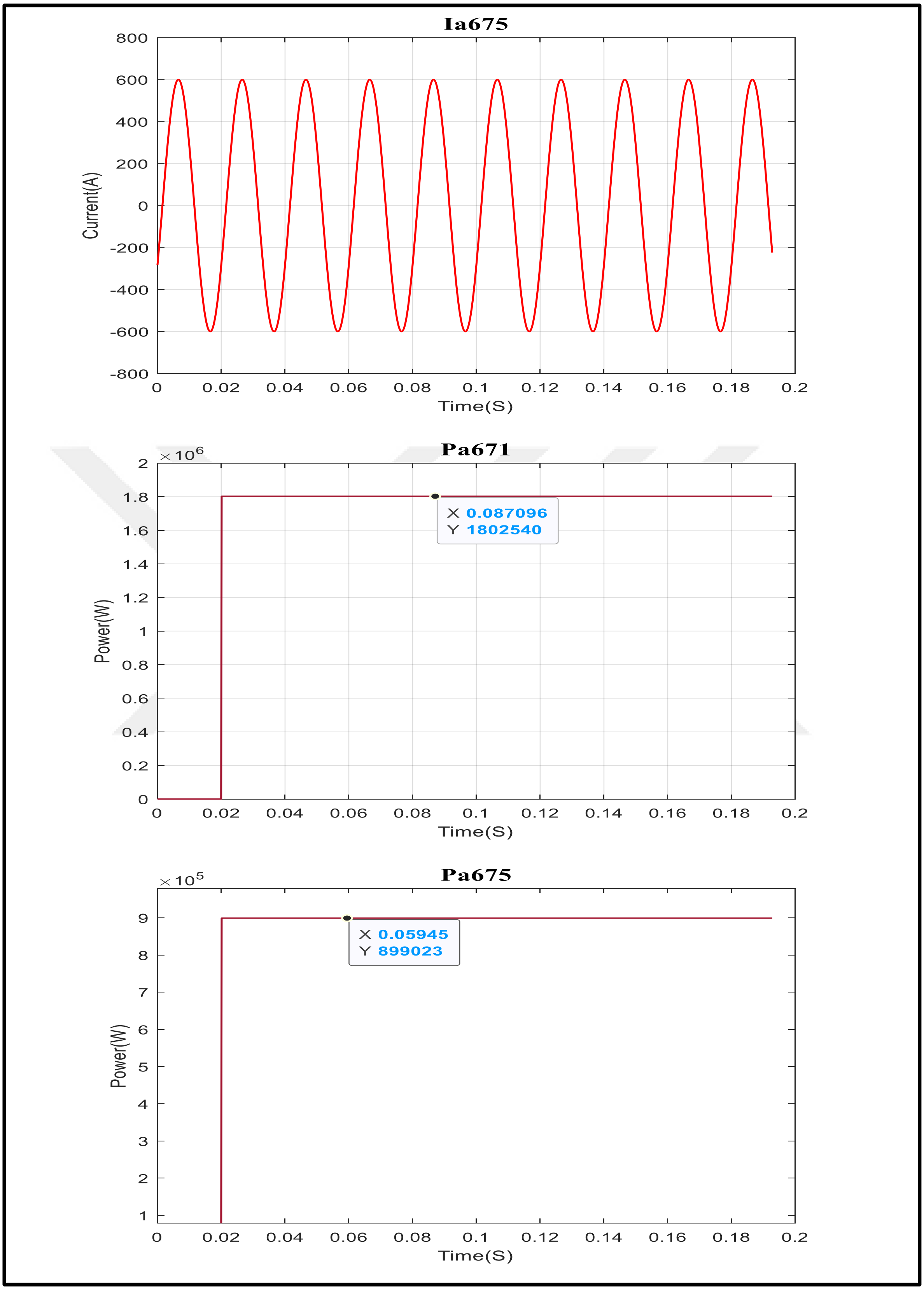

Figure 4.26. (continue) The voltage, current, and power on buses 671 and 675 after increasing the load by 100% on bus 671 and bus 675.

Connecting a 500 kW and 400 kW PV to Bus 671 and Bus 675, respectively, with Iq = 0

Five sets of SunPower SPR-305E-WHT-D PV panels are connected in parallel to make a 500 kW renewable energy system, and four sets are connected in parallel to create a 400 kW renewable energy system. Every set of PV panels produces 100 kW of power under standard conditions (STC), which include 1000 W/m² of solar energy and a temperature of 25 °C. The voltage on buses is displayed in Table 4. 47. below when the modified IEEE 13 bus system is connected to the PV system by connecting the 400 kW system to bus 675 and the 500 kW system to bus 671 with Iq = 0, where only pure active power is injected.

Table 4.47. The voltage of the buses before increasing load, before and after connecting the 500 kW +400 kW photovoltaic system.

V-Buses	Normal Case			After increasing load & Before connecting the 400 kW+500 kW PV system			After increasing load & After connecting the400 kW+500 kW PV system		
	R	S	T	R	S	T	R	S	T
Vabc-632	1.021	1.042	1.017	1.021	1.042	1.017	1.021	1.042	1.017
Vabc-633	1.018	1.04	1.015	1.018	1.04	1.015	1.018	1.04	1.015
Vabc-692	0.9871	1.045	0.971	0.9609	1.045	0.9407	0.9721	1.03	0.9554
Vabc-645	0	1.033	1.015	0	1.033	1.015	0	1.033	1.015
Vabc-646	0	1.032	1.014	0	1.032	1.014	0	1.032	1.014
Vabc-671	0.9871	1.045	0.971	0.9609	1.045	0.9407	0.9721	1.03	0.9554
Vabc-675	0.9798	1.046	0.9676	0.947	1.047	0.9343	0.9608	1.032	0.9496
Vabc-652	0.9799	0	0	0.9539	0	0	0.965	0	0
Vabc-634	0.9941	1.022	0.9961	0.9941	1.022	0.9961	0.9941	1.022	0.9961
Vabc-611	0	0	0.9648	0	0	0.9348	0	0	0.9494
Vabc-680	0.9871	1.045	0.971	0.9609	1.045	0.9407	0.9721	1.03	0.9554
Vabc-684	0.9853	0	0.9679	0.9591	0	0.9377	0.9703	0	0.9524

According to the above table, the voltage considerably improved following the installation of the photovoltaic system, allowing for the treatment of the drop brought on by the increasing load. The voltage of bus 671, for instance, was R_{671}=0.9871, S_{671}=1.045, and T_{671}=0.971. When the load was increased, the voltage dropped to R_{671}=0.9609, S_{671}=1.045, and T_{671}=0.9407. The PV system was next added, and the voltage improved to R_{671}=0.9721, S_{671}=1.03, and T_{671}=0.9554, and the voltage of bus 675 was R_{675}=0.9798, S_{675}=1.046, and T_{675}=0.9676. When the load was increased, the voltage dropped to R_{675}=0.947, S_{675}=1.047, and T_{675}=0.9343. The PV system was next added, and the voltage improved to R_{675}=0.9608, S_{675}=1.032, and T_{675}=0.9496.

Figure 4. 26. shows the voltage, current, and power on buses 671 and 675 after increasing the load by 100% with a PV system (Iq=0).

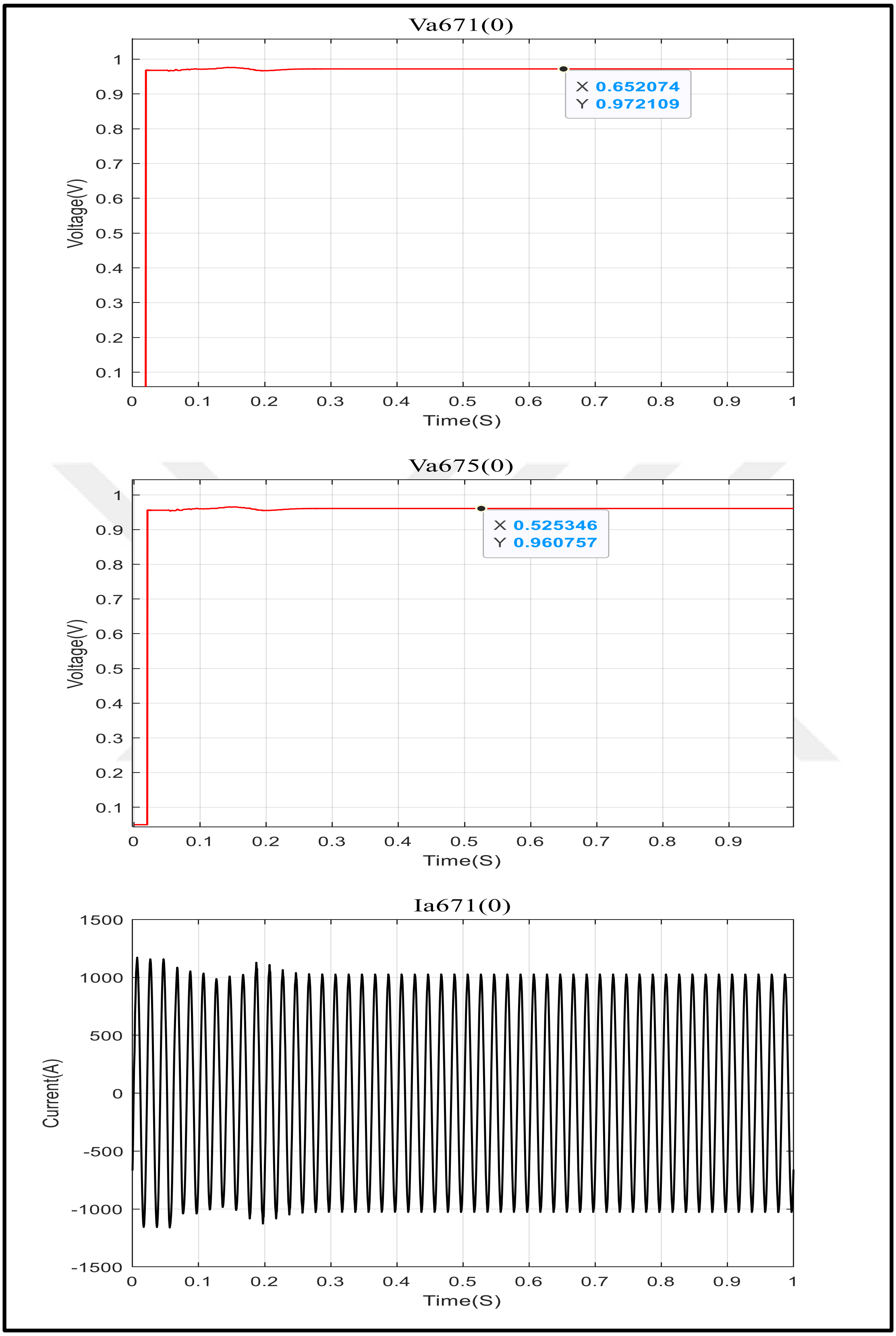

Figure 4.27. The voltage, current, and power on buses 671 and 675 after increasing the load by 100% on bus 671 and bus 675 with a PV system (Iq=0).

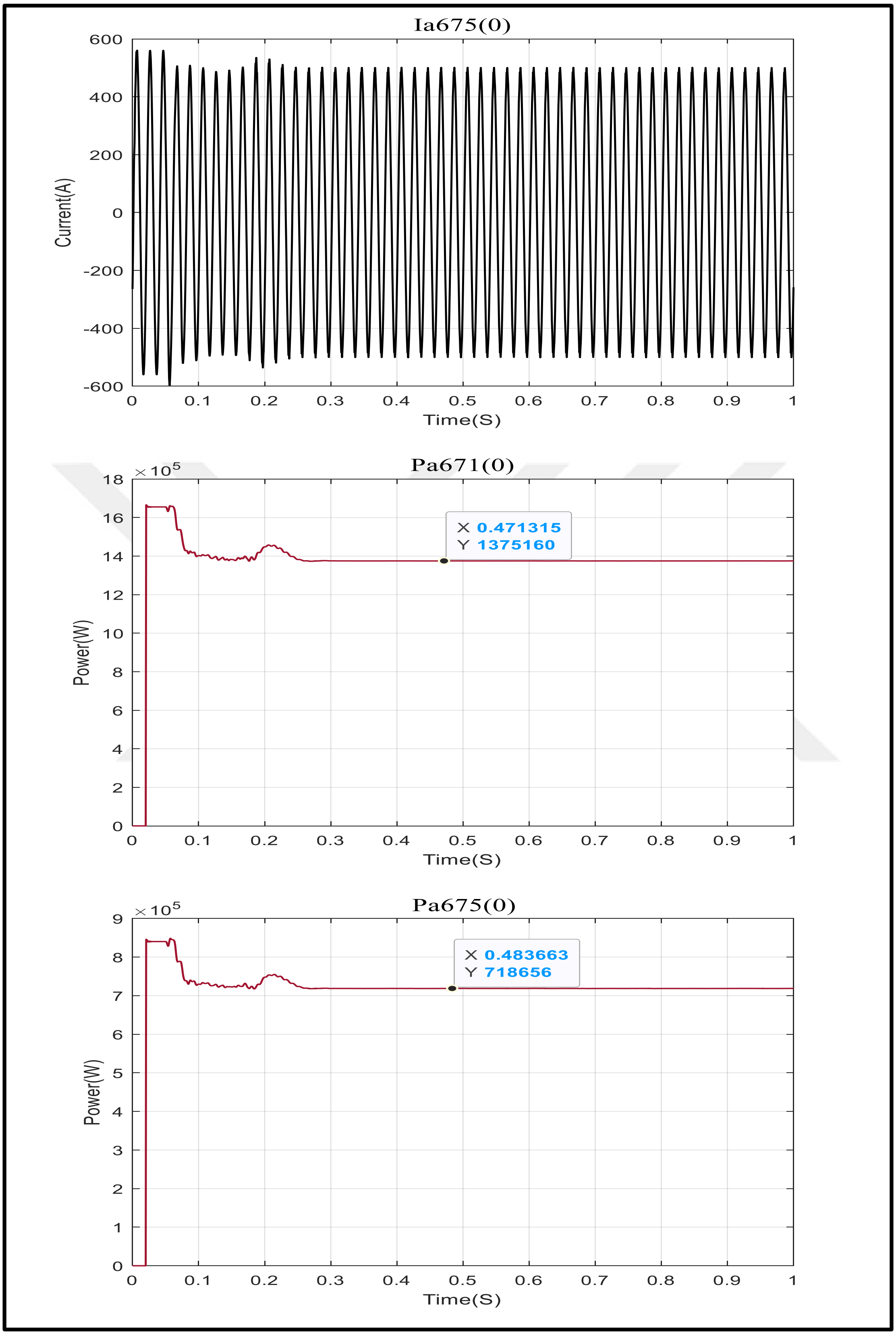

Figure 4.28. (continue) The voltage, current, and power on buses 671 and 675 after increasing the load by 100% on bus 671 and bus 675 with a PV system (Iq=0).

Connecting a 500 kW and 400 kW PV to Bus 671 and Bus 675, respectively, with Iq = -0.5

Five sets of SunPower SPR-305E-WHT-D PV panels are connected in parallel to make a 500 kW renewable energy system, and four sets are connected in parallel to create a 400 kW renewable energy system. Every set of PV panels produces 100 kW of power under standard conditions (STC), which include 1000 W/m² of solar energy and a temperature of 25 °C. The voltage on buses is displayed in Table 4.48. below when the modified IEEE 13 bus system is connected to the PV system by connecting the 400 kW system to bus 675 and the 500 kW system to bus 671 with Iq = -0.5, where active power and 50% of the reactive power are injected.

Table 4.48. The voltage of the buses before increasing load, before and after connecting the 500 kW + 400 kW photovoltaic system.

V-Buses	Normal Case			After increasing load & Before connecting the400KW+500KW PV system			After increasing load & After connecting the400KW+500KW PV system		
	R	S	T	R	S	T	R	S	T
Vabc-632	1.021	1.042	1.017	1.021	1.042	1.017	1.021	1.042	1.017
Vabc-633	1.018	1.04	1.015	1.018	1.04	1.015	1.018	1.04	1.015
Vabc-692	0.9871	1.045	0.971	0.9609	1.045	0.9407	0.9762	1.035	0.9601
Vabc-645	0	1.033	1.015	0	1.033	1.015	0	1.033	1.015
Vabc-646	0	1.032	1.014	0	1.032	1.014	0	1.032	1.014
Vabc-671	0.9871	1.045	0.971	0.9609	1.045	0.9407	0.9763	1.035	0.9601
Vabc-675	0.9798	1.046	0.9676	0.947	1.047	0.9343	0.9652	1.037	0.9546
Vabc-652	0.9799	0	0	0.9539	0	0	0.9691	0	0
Vabc-634	0.9941	1.022	0.9961	0.9941	1.022	0.9961	0.9941	1.022	0.9961
Vabc-611	0	0	0.9648	0	0	0.9348	0	0	0.954
Vabc-680	0.9871	1.045	0.971	0.9609	1.045	0.9407	0.9763	1.035	0.9601
Vabc-684	0.9853	0	0.9679	0.9591	0	0.9377	0.9744	0	0.9571

According to the above table, the voltage considerably improved following the installation of the photovoltaic system, allowing for the treatment of the drop brought on by the increasing load. The voltage of bus 671, for instance, was R_{671}=0.9871, S_{671}=1.045, and T_{671}=0.971. When the load was increased, the voltage dropped to R_{671}=0.9609, S_{671}=1.045, and T_{671}=0.9407. The PV system was next added, and the voltage improved to R_{671}=0.9763, S_{671}=1.035, and T_{671}=0.9601, and the voltage of bus 675 was R_{675}=0.9798, S_{675}=1.046, and T_{675}=0.9676. When the load was increased, the voltage dropped to R_{675}=0.947, S_{675}=1.047, and T_{675}=0.9343. The PV system was next added, and the voltage improved to R_{675}=0.9652, S_{675}=1.037, and T_{675}=0.9546.

Figure 4. 27. shows the voltage, current, and power on buses 671 and 675 after increasing the load by 100% with a PV system (Iq=-0.5).

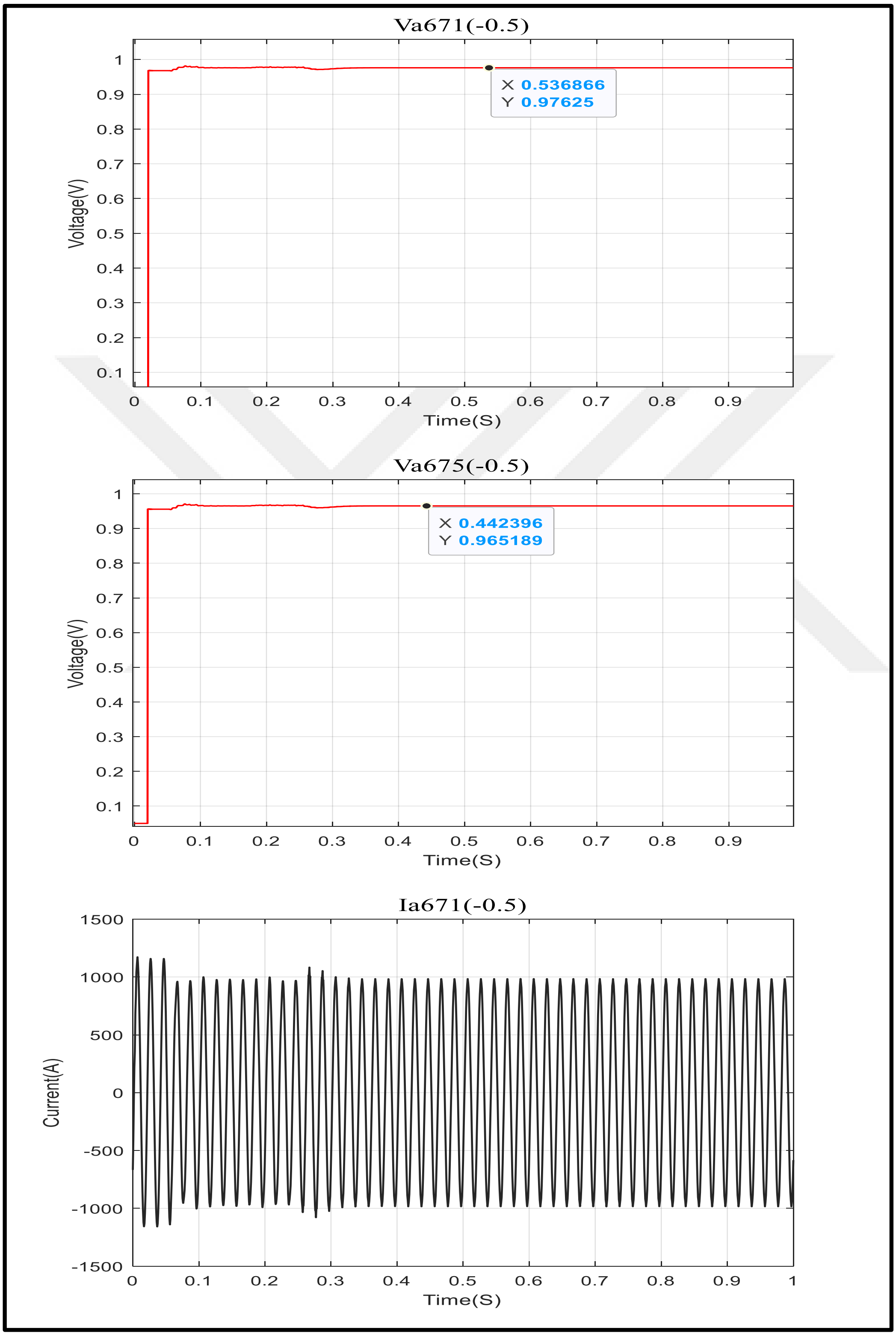

Figure 4.29. The voltage, current, and power on buses 671 and 675 after increasing the load by 100% on bus 671 and bus 675 with a PV system (Iq=-0.5).

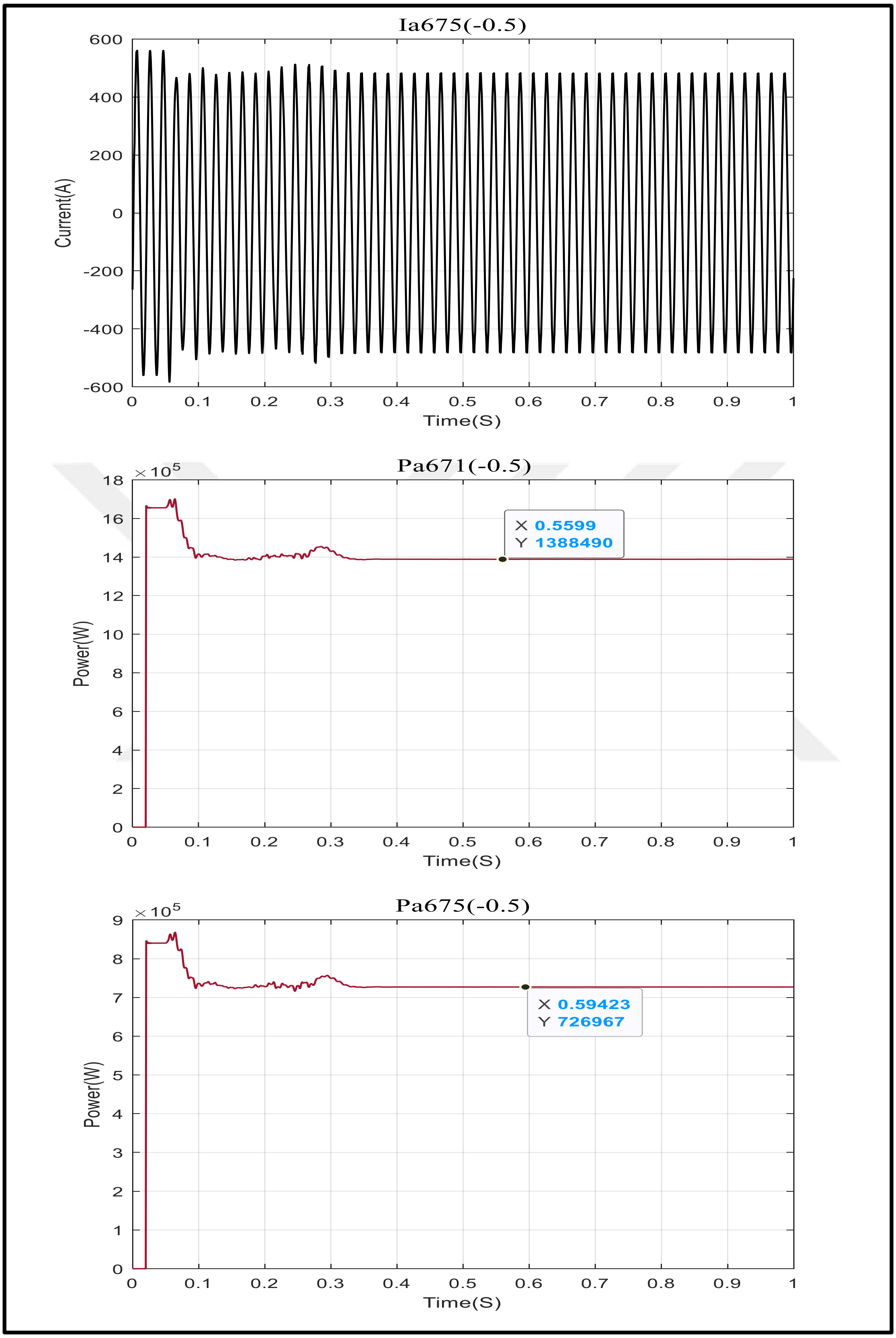

Figure 4.27. (continue) The voltage, current, and power on buses 671 and 675 after increasing the load by 100% on bus 671 and bus 675 with a PV system (Iq=-0.5).

Connecting a 500 kW and 400 kW PV to Bus 671 and Bus 675, respectively, with Iq = -1

Five sets of SunPower SPR-305E-WHT-D PV panels are connected in parallel to make a 500 kW renewable energy system, and four sets are connected in parallel to create a 400 kW renewable energy system. Every set of PV panels produces 100 kW of power under standard conditions (STC), which include 1000 W/m² of solar energy and a temperature of 25 °C. The voltage on buses is displayed in Table 4.49. below when the modified IEEE 13 bus system is connected to the PV system by connecting the 400 kW system to bus 675 and the 500 kW system to bus 671 with Iq = -1, where active power and 100% of the reactive power are injected.

Table 4.49. The voltage of the buses before increasing load, before and after connecting the 500 kW +400 kW photovoltaic system.

V-Buses	Normal Case			After increasing load & Before connecting the400 kW+500 kW PV system			After increasing load & After connecting the400 kW+500 kW PV system		
	R	S	T	R	S	T	R	S	T
Vabc-632	1.021	1.042	1.017	1.021	1.042	1.017	1.021	1.042	1.017
Vabc-633	1.018	1.04	1.015	1.018	1.04	1.015	1.018	1.04	1.015
Vabc-692	0.9871	1.045	0.971	0.9609	1.045	0.9407	0.98	1.039	0.9644
Vabc-645	0	1.033	1.015	0	1.033	1.015	0	1.033	1.015
Vabc-646	0	1.032	1.014	0	1.032	1.014	0	1.032	1.014
Vabc-671	0.9871	1.045	0.971	0.9609	1.045	0.9407	0.98	1.039	0.9644
Vabc-675	0.9798	1.046	0.9676	0.947	1.047	0.9343	0.9692	1.041	0.9592
Vabc-652	0.9799	0	0	0.9539	0	0	0.9729	0	0
Vabc-634	0.9941	1.022	0.9961	0.9941	1.022	0.9961	0.9941	1.022	0.9961
Vabc-611	0	0	0.9648	0	0	0.9348	0	0	0.9583
Vabc-680	0.9871	1.045	0.971	0.9609	1.045	0.9407	0.98	1.039	0.9644
Vabc-684	0.9853	0	0.9679	0.9591	0	0.9377	0.9782	0	0.9614

According to the above table, the voltage considerably improved following the installation of the photovoltaic system, allowing for the treatment of the drop brought on by the increasing load. The voltage of bus 671, for instance, was R_{671}=0.9871, S_{671}=1.045, and T_{671}=0.971. When the load was increased, the voltage dropped to R_{671}=0.9609, S_{671}=1.045, and T_{671}=0.9407. The PV system was next added, and the voltage improved to R_{671}=0.98, S_{671}=1.039, and T_{671}=0.9644, and the voltage of bus 675 was R_{675}=0.9798, S_{675}=1.046, and T_{675}=0.9676. When the load was increased, the voltage dropped to R_{675}=0.947, S_{675}=1.047, and T_{675}=0.9343. The PV system was next added, and the voltage improved to R_{675}=0.9692, S_{675}=1.041, and T_{675}=0.9592.

Figure 4. 28. shows the voltage, current, and power on buses 671 and 675 after increasing the load by 100% with a PV system (Iq=-1).

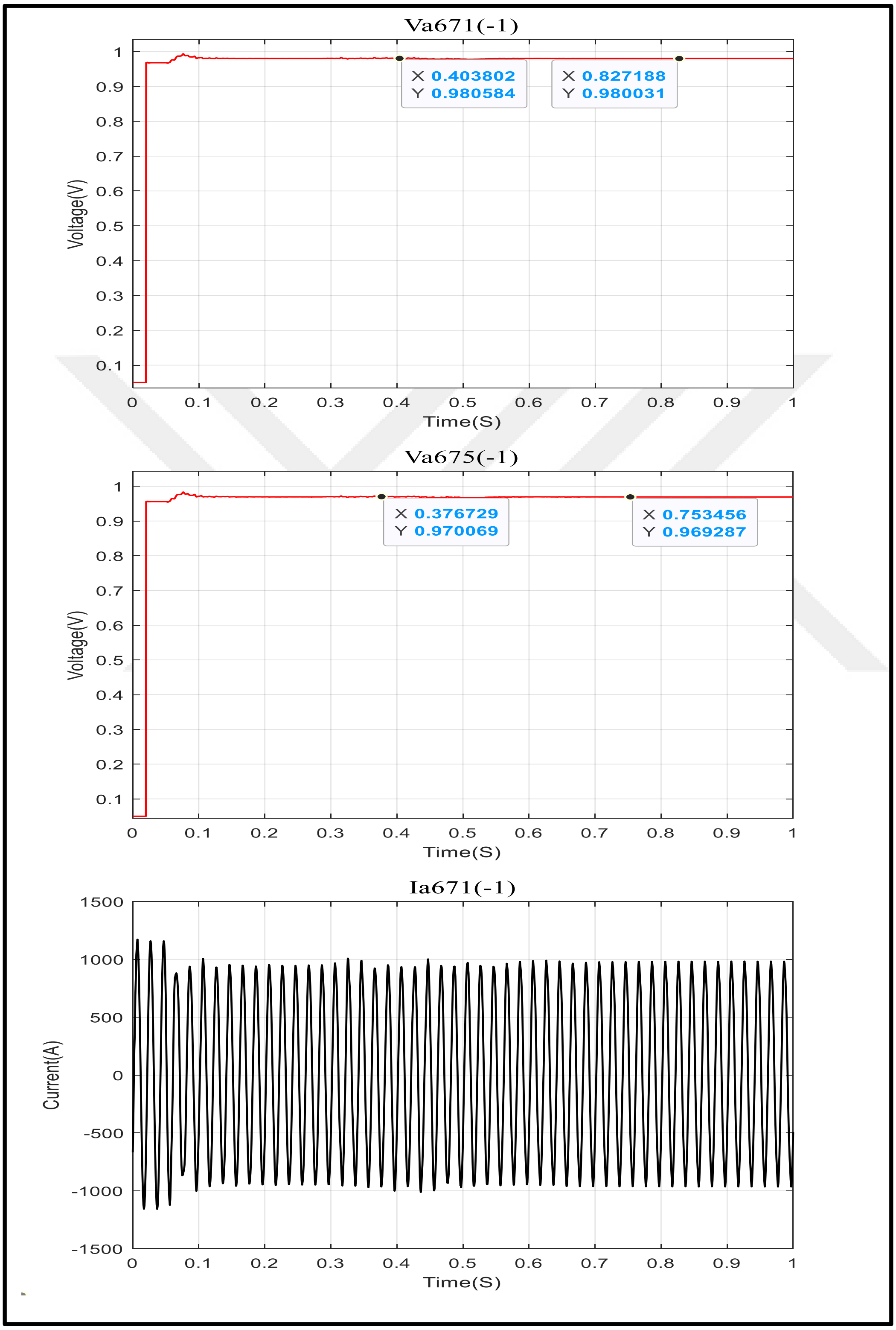

Figure 4.30. The voltage, current, and power on buses 671 and 675 after increasing the load by 100% on bus 671 and bus 675 with a PV system (Iq=-1).

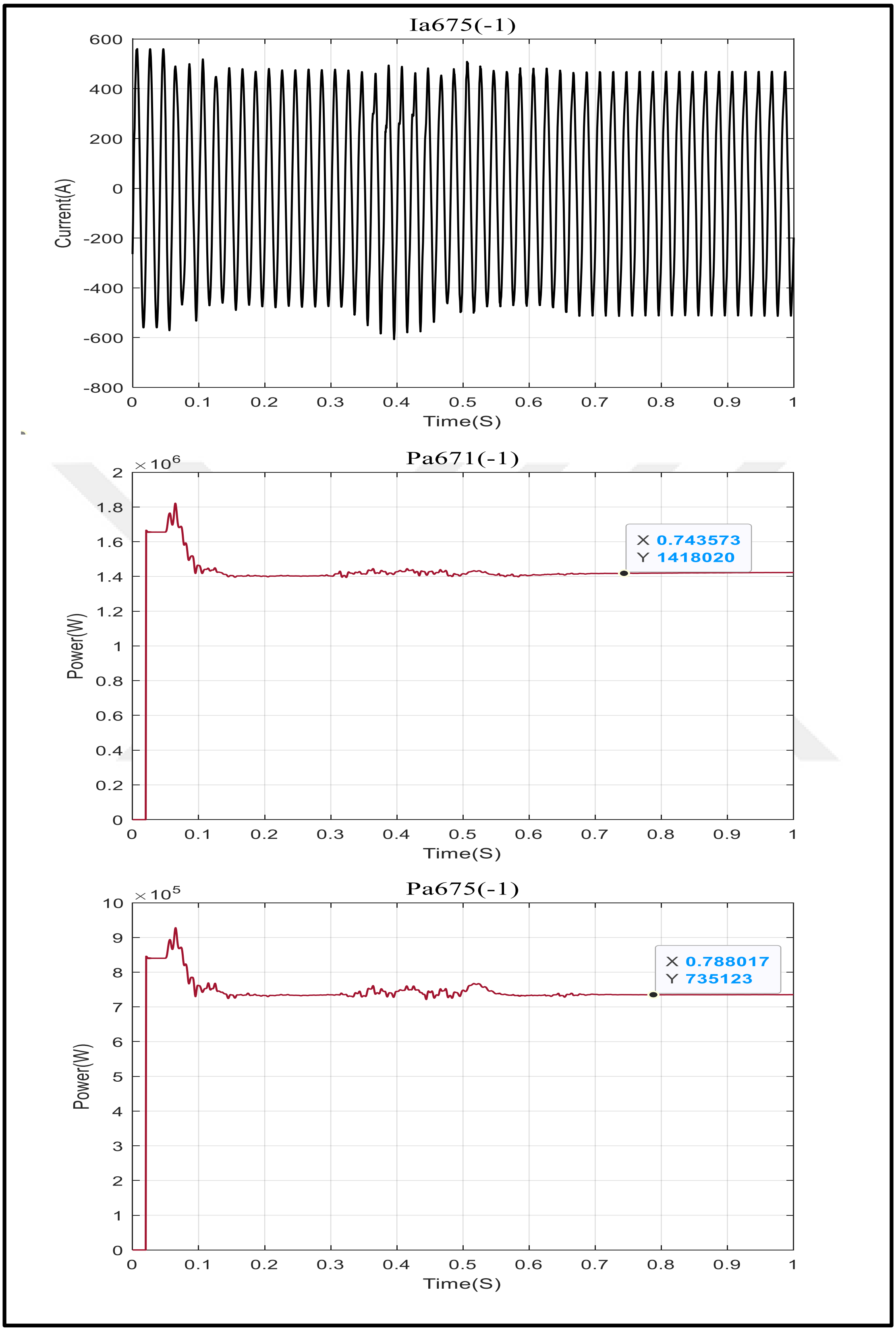

Figure 4.28. (continue) The voltage, current, and power on buses 671 and 675 after increasing the load by 100% on bus 671 and bus 675 with a PV system (Iq=-1).

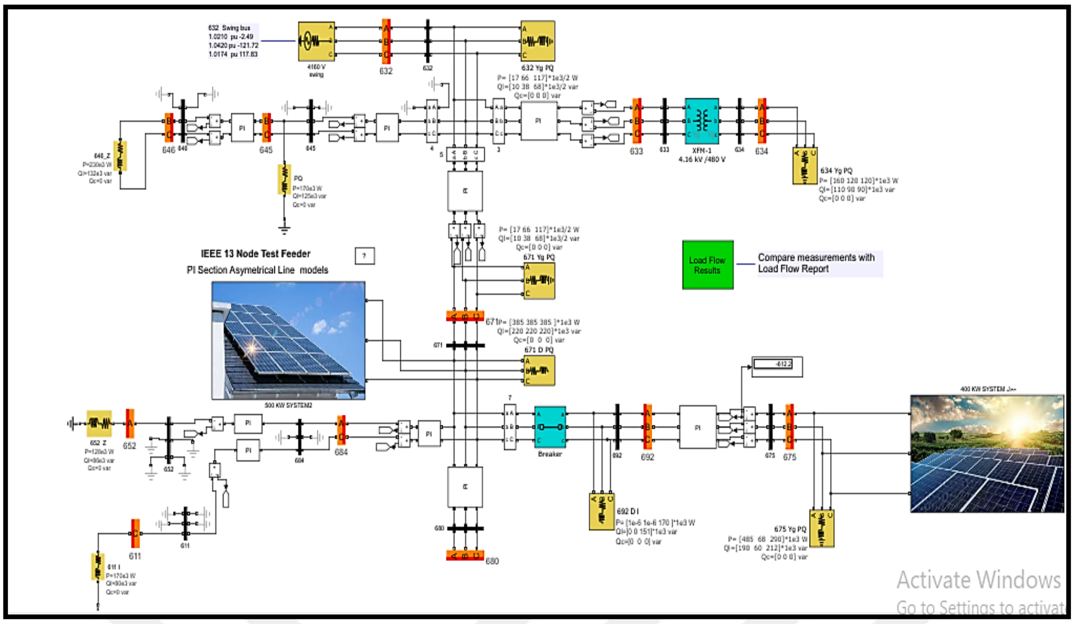

Figure 4.31. The electrical power system (Modified IEEE 13-Bus Test System) with 500KW PV system in bus 671 and 400KW PV system in bus 675

Figure 4.29. displays the modified IEEE 13 bus test system circuit model after the PV system is connected to buses 675 and 671. Through buses 675 and 671, the PV system is integrated with the modified IEEE 13 bus test system, and four scenarios are examined.

Scenario 1: The loads connected to bus 675 and bus 671 increased by 25%. Then the voltage on the buses was recorded to see the voltage drop that occurred. Then, the PV system (400 kW) was integrated via bus 675, and the PV system (500 kW) was integrated via bus 671. Then the voltage on the buses was measured under the following conditions: injection of pure active power only (Iq = 0), injection of 50% reactive power and 100% active power (Iq = -0.5), and injection of 100% reactive power and 100% active power (Iq = -1). It was found that the PV system compensated for the voltage drop caused by the 25% increase in load. According to the measurements, we also found that the voltage on the buses was larger than its actual value before the load increase, which may have a negative impact. For example, the voltage of the bus 675 is (R_{675}=0.9798, S_{675}=1.046, T_{675}=0.9676).

After increasing the load after increasing the load.

(R_{675}=0.9715, S_{675}=1.046, and T_{675}=0.9591), and after adding the PV system, we noticed that the public voltage was at

- when Iq=0 (R_{675}=0.9828, S_{675}=1.036, and T_{675}=0.9732),
- when Iq = -0.5 (R_{675} = 0.9873, S_{675} = 1.041, and T_{675} = 0.978)
- when Iq = -1 (R_{675} = 0.9913, S_{675} = 1.046, and T_{675} = 0.9828)

Scenario 2: The load connected to bus 675 and bus 671 was increased by 50%. Then the voltage on the buses was recorded to see the voltage drop that occurred. Then, the PV system (400 kW) was integrated via bus 675, and the PV system (500 kW) was integrated via bus 671. Then the voltage on the buses was measured under the following conditions: injection of pure active power only (Iq = 0), injection of 50% reactive power and 100% active power (Iq = -0.5), and injection of 100% reactive power and 100% active power (Iq = -1). We saw that the PV system compensated for the voltage drop caused by the 50% increase in load. For example, The voltage of the bus 675 is (R_{675}=0.9798, S_{675}=1.046, and T_{675}=0.9676).

After increasing the load (R_{675} = 0.9632, S_{675} = 1.047, and T_{675} = 0.9507) and after adding the PV system, we noticed that the overall voltage was at

- When Iq=0 (R_{675}=0.9754, S_{675}=1.034, and T_{675}=0.9652),
- When Iq = -0.5 (R_{675} = 0.9798, S_{675} = 1.04, and T_{675} = 0.9702)
- When Iq = -1 (R_{675} = 0.9838, S_{675} = 1.044, and T_{675} = 0.9748)

We notice that in the case of Iq = -0.5, the voltage was raised to its state before increasing the load.

Scenario 3: The load connected to bus 675 and bus 671 was increased by 75%. Then the voltage on the buses was recorded to see the voltage drop that occurred. Then, the PV system (400 kW) was integrated via bus 675, and the PV system (500 kW) was integrated via bus 671. Then the voltage on the buses was measured under the following conditions: injection of pure active power only (Iq = 0), injection of 75% reactive power and 100% active power (Iq = -0.5), and injection of 100% reactive power and 100% active power (Iq = -1). We saw that the PV system compensated for the voltage drop caused by the 75% increase in load. For example. The voltage of the bus 675 is (R_{675}=0.9798, S_{675}=1.046, and T_{675}=0.9676).

After increasing the load (R_{675} = 0.955, S_{675} = 1.047, and T_{675} = 0.9424) and after adding the PV system, we noticed that the overall voltage was at

- When Iq=0 (R_{675}=0.968, S_{675}=1.033, and T_{675}=0.9573),
- When Iq = -0.5 (R_{675} = 0.9725, S_{675} = 1.038, and T_{675} = 0.9624)
- When Iq = -1 (R_{675} = 0.9765, S_{675} = 1.043, and T_{675} = 0.967)

We notice that in the case of Iq = -1, the voltage was raised to its state before increasing the load.

Scenario 4: The load connected to bus 675 and bus 671 was increased by 100%. Then the voltage on the buses was recorded to see the voltage drop that occurred. Then, the PV system (400 kW) was integrated via bus 675, and the PV system (500 kW) was integrated via bus 671. Then the voltage on the buses was measured under the following conditions: injection of pure active power only (Iq = 0), injection of 75% reactive power and 100% active power (Iq = -0.5), and injection of 100% reactive power and 100% active power (Iq = -1). We saw that the PV system compensated for the voltage drop caused by the 100% increase in load. For example, the voltage of the bus 675 is (R_{675}=0.9798, S_{675}=1.046, T_{675}=0.9676).

After increasing the load (R_{675} = 0.947, S_{675} = 1.047, and T_{675} = 0.9343) and after adding the PV system, we noticed that the overall voltage was at

- When Iq=0 (R_{675}=0.9608, S_{675}=1.032, and T_{675}=0.9496),
- When Iq = -0.5 (R_{675} = 0.9652, S_{675} = 1.037, and T_{675} = 0.9546)
- When Iq = -1 (R_{675} = 0.9692, S_{675} = 1.041, and T_{675} = 0.9592)

We notice that in the case of Iq = -1, the voltage did not return to its previous state, which indicates that the increase in the load was not compensated for by the power injected through the photovoltaic system.

4.2. Single fault (A-G fault) between the bus 692 and bus 675

The voltage of the buses is monitored to estimate how much the network is impacted when a fault occurs between the first phase and the ground. The voltage readings on the buses before and after the fault occurs are displayed in the following table, 4.50.

Table 4.50. The voltage of the buses before and after the fault between A & ground

V-Buses	Before Fault(A-G)			After Fault(A-G)			Change Rate%		
	R	S	T	R	S	T	R	S	T
Vabc-632	1.021	1.042	1.017	1.021	1.042	1.017	0	0	0
Vabc-633	1.018	1.04	1.015	1.018	1.04	1.015	0	0	0
Vabc-692	0.9871	1.045	0.971	0.03219	1.35	1.235	1.95%	-0.58%	2.46%
Vabc-645	0	1.033	1.015	0	1.033	1.015	0	0	0
Vabc-646	0	1.032	1.014	0	1.032	1.014	0	0	0
Vabc-671	0.9871	1.045	0.971	0.03249	1.35	0.235	1.95%	-0.58%	2.46%
Vabc-675	0.9798	1.046	0.9676	0.03422	1.35	1.228	2.29%	-0.58%	2.60%
Vabc-652	0.9799	0	0	0.03277	0	0	1.95%	0	0
Vabc-634	0.9941	1.022	0.9961	0.9941	1.022	0.9961	0	0	0
Vabc-611	0	0	0.9648	0	0	1.227	0	0	2.45%
Vabc-680	0.9871	1.045	0.971	0.03249	1.35	1.235	1.95%	-0.58%	2.46%
Vabc-684	0.9853	0	0.9679	0.03295	0	1.231	1.95%	0	2.47%

We noticed this from Table 4.50. that the voltage changed due to the fault and dropped to low values.

To compensate for the voltage drop brought on by the fault, the photovoltaic system was connected to a modified IEEE 13 bus via buses 671 (500 kW) and 675 (400 kW). The results are shown in Table 4.51.

Table 4.51. The the buses' voltage after connecting the PV system when there is a fault between A and ground

V-Buses	Before Fault(A-G)			After Fault(A-G)			After Fault(A-G)& After add PV System		
	R	S	T	R	S	T	R	S	T
Vabc-632	1.021	1.042	1.017	1.021	1.042	1.017	1.021	1.042	1.017
Vabc-633	1.018	1.04	1.015	1.018	1.04	1.015	1.018	1.04	1.015
Vabc-692	0.9871	1.045	0.971	0.03219	1.35	1.235	0.04193	1.294	1.121
Vabc-645	0	1.033	1.015	0	1.033	1.015	0	1.033	1.015
Vabc-646	0	1.032	1.014	0	1.032	1.014	0	1.032	1.014
Vabc-671	0.9871	1.045	0.971	0.03249	1.35	0.235	0.04229	1.294	1.121
Vabc-675	0.9798	1.046	0.9676	0.03422	1.35	1.228	0.07237	1.306	1.091
Vabc-652	0.9799	0	0	0.03277	0	0	0.04245	0	0
Vabc-634	0.9941	1.022	0.9961	0.9941	1.022	0.9961	0.9941	1.022	0.9961
Vabc-611	0	0	0.9648	0	0	1.227	0	0	1.114
Vabc-680	0.9871	1.045	0.971	0.03249	1.35	1.235	0.04229	1.294	1.121
Vabc-684	0.9853	0	0.9679	0.03295	0	1.231	0.04268	0	1.118

We observed a change in the voltage values after connecting the photovoltaic system, demonstrating the beneficial impact of adding the system on enhancing the voltage in the event of breakdowns.

4.3. Limitations of work:

- To avoid reproducing the results, not all faults have been examined (as an example, if we consider the fault between phase A and ground, the results are nearly identical to those if we consider the fault between phase B and ground).
- No discussion was had on the fault's location or the best place to put the PV.

5. CONCLUSIONS AND FUTURE WORK

5.1. Introduction

This chapter includes the conclusions reached in this study, which included modeling and simulation of a renewable energy system (photovoltaic energy system) and integrating with the modified IEEE 13 Bus Test system to create a system with varying generating capacity. to study the effect of the photovoltaic system on voltage stability and improve the quality of power in the electrical grid in cases of overload and faults. The chapter also contains suggestions for further research that would advance the renewable energy system so that the electrical system as a whole may benefit from it.

5.2. Conclusions

- When renewable energy sources are used in multiple areas, the voltage has been shown to be improved more than when they are used in only one.
- Since voltage is related to reactive power, the injection of both active and reactive power will increase the bus voltage.
- In some cases, when reactive power is injected, the voltage increases more than the required limit and only active power injection is required.
- The capacity of the renewable energy system must be within the required capacity of the electrical system; if it is connected to more than that, the system will be negatively affected.
- Renewable energy sources can be used to make up for the necessary electrical power in the case that some of the primary source generation is lost, ensuring that the voltage is stabilized and maintained.
- To increase the system's voltage, a hybrid system that combines several renewable energy sources can be used.
- Buses located far from the major sources are the best places to install renewable energy sources because their voltage is low.
- The voltage improvement increases with the amount of energy injected from renewable sources.
- Increasing renewable energy sources is necessary to ensure voltage stability because larger loads result in lower voltage.

5.3. Future work

- ➢ Examining the electrical system's performance when the renewable energy system is connected in transitory cases.
- ➢ Examining the electrical system's performance when the renewable energy system is connected during faults.
- Afault in the two phases.
- The ground's fault and the two phases' fault.
- A fault in all three phases.
- A fault that connects the earth and the three phases.
- ➢ Evaluate the electrical system's performance when connecting the renewable energy system if a portion of the electrical system's generation is lost.
- ➢ Study how to support the electrical system using multiple forms of renewable energy sources.

REFERENCES

A. Nassar, I. and Weber, H. (2016). Impact of renewable energy sources on the german power system. *Recent Advances in Communications and Networking Technology*, 4(2), 69–77.

Abdullah, B. U. D., Lata, S., Jaiswal, S. P., Bhadoria, V. S., Fotis, G., Santas, A. and Ekonomou, L. (2023). A hybrid artificial ecosystem optimizer and incremental-conductance maximum-power-point-tracking-controlled grid-connected photovoltaic system. *Energies*, 16(14), 5384.

Adefarati, T. and Bansal, R. C. (2016). Integration of renewable distributed generators into the distribution system: A review. *IET Renewable Power Generation*, 10(7), 873–884.

Ahmadi, A., Tavakoli, A., Jamborsalamati, P., Rezaei, N., Miveh, M. R., Gandoman, F. H., Heidari, A. and Nezhad, A. E. (2019). Power quality improvement in smart grids using electric vehicles: A review. *IET Electrical Systems in Transportation*, 9(2), 53–64.

Al-Bashir, A., Al-Dweri, M., Al-Ghandoor, A., Hammad, B. and Al-Kouz, W. (2020). Analysis of effects of solar irradiance, cell temperature and wind speed on photovoltaic systems performance. *International Journal of Energy Economics and Policy*, 10(1), 353–359.

Alik, R., Jusoh, A. and Sutikno, T. (2015). A review on perturb and observe maximum power point tracking in photovoltaic system. *Telecommunication Computing Electronics and Control*, 13(3), 745.

Alnaib, I. I., Alyozbaky, O. S. and Abbawi, A. (2020). A new approach to detecting and classifying multiple faults in IEEE 14-bus system. *Eastern-European Journal of Enterprise Technologies*, 5(8–107), 6–16.

Alshahrani, A., Omer, S., Su, Y., Mohamed, E. and Alotaibi, S. (2019a). The technical challenges facing the integration of small-scale and large-scale PV systems into the grid: A critical review. *Electronics (Switzerland)*, *8*(12), 3-29.

Alshahrani, A., Omer, S., Su, Y., Mohamed, E. and Alotaibi, S. (2019b). The technical challenges facing the integration of small-scale and large-scale PV systems into the grid: A critical review. *Electronics*, 8(12), 1443.

Amin, M. and Stringer, J. (2008). The electric power grid: today and tomorrow. *MRS Bulletin*, 33(4), 399–407.

Arghira, N., Hossu, D., Făgărăşan, I., Iliescu, S. S. and Costianu, D. R. (2011). Modern scada philosophy in power system operation - A survey. *UPB Scientific Bulletin, Series C: Electrical Engineering*, 73(2), 153–166.

Arpadzic, A., Saric, M., Hivziefendic, J. and Avdakovic, S. (2020). Power system efficiency improvement using solar PV systems. *2020 International Symposium on Industrial Electronics and Applications (INDEL)*, 3, 1–6.

Asman, S. H., Ab Aziz, N. F., Ungku Amirulddin, U. A. and Ab Kadir, M. Z. A. (2021). Transient fault detection and location in power distribution network: A review of current practices and challenges in Malaysia. *Energies*, 14(11), 2988.

Ateş, Y., Gökçek, T. and Arabul, A. Y. (2021). Impact of hybrid power generation on voltage, losses, and electricity cost in distribution networks. *Turkish Journal of Electrical Engineering and Computer Sciences*, 29(3), 1720–1735.

Babatunde, A. A., Abbasoglu, S. and Senol, M. (2018). Analysis of the impact of dust, tilt angle and orientation on performance of PV Plants. *Renewable and Sustainable Energy Reviews*, 90(3), 1017–1026.

Banerjee, B. and Islam, S. M. (2011). Reliability based optimum location of distributed generation. *International Journal of Electrical Power & Energy Systems*, 33(8), 1470–1478.

Banu, I. V., Beniugă, R. and Istrate, M. (2013). Comparative analysis of the perturb-and-observe and incremental conductance MPPT methods. *2013 8th International Symposium On Advanced Topics In Electrical Engineering (Atee)*, *1*, 1–4.

Basso, T. (2014). IEEE 1547 and 2030 Standards for Distributed Energy Resources Interconnection and Interoperability with the Electricity Grid IEEE 1547 and 2030 Standards for Distributed Energy Resources Interconnection and Interoperability with the Electricity Grid. *Nrel*, *December*, 22.

Basso, T. S. and DeBlasio, R. (2004). IEEE 1547 series of standards: Interconnection issues. *IEEE Transactions on Power Electronics*, 19(5), 1159–1162.

Ben Youssef, A., Khojet El Khil, S. and Slama Belkhodja, I. (2017). Open-circuit fault diagnosis and voltage sensor fault tolerant control of a single phase pulsed width modulated rectifier. *Mathematics and Computers in Simulation*, 131, 234–252.

Bhatti, B. A., Broadwater, R. and Dilek, M. (2020). Analyzing impact of distributed PV generation on integrated transmission & Distribution system voltage stability—A Graph trace analysis based approach. *Energies*, 13(17), 4526.

Dang, K., Zhao, H., Yu, J. and Dang, T. (2011). Study on interconnection standards of photovoltaic power generation. *2011 International Conference on Electrical and Control Engineering*, 3, 6123–6126.

Dashtdar, M. and Dashtdar, M. (2019). Voltage control in distribution networks in presence of distributed generators based on local and coordinated control structures. *The Scientific Bulletin of Electrical Engineering Faculty*, 19(2), 21–27.

Datta, S., Chattopadhyaya, A., Chattopadhyay, S. and Das, A. (2020). Line to ground and line to line fault analysis in IEEE standard 9 bus system. *Modelling, Measurement and Control A*, 93(1–4), 10–18.

Deng, X. and Lv, T. (2020). Power system planning with increasing variable renewable energy: A review of optimization models. *Journal of Cleaner Production*, 246, 118962.

El-Khattam, W. and Salama, M. M. . (2004). Distributed generation technologies, definitions and benefits. *Electric Power Systems Research*, 71(2), 119–128.

El-Zonkoly, A. M. (2011). Fault Diagnosis in Distribution Networks with Distributed Generation. *Smart Grid and Renewable Energy*, 2(01), 1–11.

Elgallai, T. (2024). Modeling and power quality enhancement of PV interfaced with power grid system. *Brilliance: Research of Artificial Intelligence*, 3(2), 423–433.

Elgendy, M. A., Zahawi, B. and Atkinson, D. J. (2012). Evaluation of perturb and observe MPPT algorithm implementation techniques. *IET Conference Publications*, 12(5), 5-292.

Feilat, E. A., Azzam, S. and Al-Salaymeh, A. (2018). Impact of large PV and wind power plants on voltage and frequency stability of Jordan’s national grid. *Sustainable Cities and Society*, 36, 257–271.

Furse, C. M., Kafal, M., Razzaghi, R. and Shin, Y. J. (2021). Fault diagnosis for electrical systems and power networks: A review. *IEEE Sensors Journal*, 21(2), 888–906.

Gajendra R. and Patel, D. B. P. (2016). Analysis of P&O MPPT Algorithm For PV System. *International Journal of Electrical and Electronics Engineering (IJEEE)*, *5*(6), 1–10.

Gandhi, O., Kumar, D. S., Rodríguez-Gallegos, C. D. and Srinivasan, D. (2020). Review of power system impacts at high PV penetration Part I: Factors limiting PV penetration. *Solar Energy*, 210(7), 181–201.

Gomathy, S. (2012). Design and implementation of maximum power point tracking (MPPT) algorithm for a standalone PV system. *International Journal*, 3(3), 1–7.

Grijalva, S., Khan, A. U., Mbeleg, J. S., Gomez-Peces, C., Reno, M. J. and Blakely, L. (2021, April). *Estimation of PV location in distribution systems based on voltage sensitivities.* 2020 52nd North American Power Symposium, NAPS 2020, April.

Gururajapathy, S. S., Mokhlis, H. and Illias, H. A. (2017). Fault location and detection techniques in power distribution systems with distributed generation: A review. *Renewable and Sustainable Energy Reviews*, 74(1), 949–958.

Mostafa, M., Elshahed, M. and Elmarsfawy, M. (2016). Power flow study and voltage stability analysis for radial system with distributed generation. *International Journal of Computer Applications*, 137(9), 19-26.

Hasaneen, B. M. and Elbaset Mohammed, A. A. (2008). Design and simulation of DC/DC boost converter. *2008 12th International Middle-East Power System Conference*, 335–340.

Hasanuzzaman, M., Zubir, U. S., Ilham, N. I. and Seng Che, H. (2017). Global electricity demand, generation, grid system, and renewable energy polices: a review. *Wiley Interdisciplinary Reviews: Energy and Environment*, *6*(3), 4-21.

Hassani, H., Yeganegi, M. R., Beneki, C., Unger, S. and Moradghaffari, M. (2019). Big data and energy poverty alleviation. *Big Data and Cognitive Computing*, 3(4), 50.

Henderson, M., Novosel, D. and Crow, M. (2017). Electric power grid modernization trends, challenges, and opportunities. *IEEE Technology Trend Paper*, 17(12), 17-18.

Hlaili, M. and Mechergui, H. (2016). Comparison of different MPPT algorithms with a proposed one using a power estimator for grid connected PV systems. *International Journal of Photoenergy*, 16, 4-41.

Hussain, J., Zhou, K., Muhammad, F., Khan, D., Khan, A., Ali, N. and Akhtar, R. (2021). Renewable energy investment and governance in countries along the belt & Road Initiative: Does trade openness matter? *Renewable Energy*, 180(11), 1278–1289.

Ike, C. U. (2013). The effect of temperature on the performance of a photovoltaic solar system in Eastern Nigeria. *Research Inventy: International Journal Of Engineering And Science*, 3(12), 10-14.

Imtiaz, B., Zafar, I. and Yuanhui, C. (2021). Modelling of an optimized microgrid model by integrating DG distributed generation sources to IEEE 13 bus system. *European Journal of Electrical Engineering and Computer Science*, 5(2), 18–25.

Irena, A. (2020). Renewable capacity highlights. *International Renewable Energy Agency (IRENA)*,4, 1-8.

Ismail, N. F. N., Musirin, I., Baharom, R. and Johari, D. (2010). Fuzzy logic controller on DC/DC boost converter. *2010 IEEE International Conference on Power and Energy*, 5, 661–666.

Jamahori, H. F., Abdullah, M. P. and Ali, A. (2023). Impact and evaluation of optimized PV generation in the distribution system with varying load demands. *Jurnal Teknologi*, 85(3), 61–73.

Jena, S., Mishra, D. P. and Salkuti, S. R. (2023). Fault detection, classification, and location in underground cables. *Lecture Notes in Electrical Engineering*, 1039, 195–215.

Kamaruzzaman, Z. A. and Mohamed, A. (2014). Impact of grid-connected photovoltaic generator using P-V curve and improved voltage stability index. *2014 IEEE International Conference on Power and Energy (PECon)*, 196–200.

Kamarzaman, N. A. and Tan, C. W. (2014). A comprehensive review of maximum power point tracking algorithms for photovoltaic systems. *Renewable and Sustainable Energy Reviews*, 37, 585–598.

Kamran, M., Mudassar, M., Fazal, M. R., Asghar, M. U., Bilal, M. and Asghar, R. (2020). Implementation of improved Perturb & Observe MPPT technique with confined search space for standalone photovoltaic system. *Journal of King Saud University - Engineering Sciences*, 32(7), 432–441.

Karimi, M., Mokhlis, H., Naidu, K., Uddin, S. and Bakar, A. H. A. (2016). Photovoltaic penetration issues and impacts in distribution network – A review. *Renewable and Sustainable Energy Reviews*, 53, 594–605.

Kaya, K. and Koç, E. (2015). Enerji kaynaklari-yenilenebilir enerji durumu. *Mühendis ve Makina*, 56(668), 36–47.

Kazem, H. A., Chaichan, M. T., Al-Waeli, A. H. A. and Sopian, K. (2020). Evaluation of aging and performance of grid-connected photovoltaic system northern Oman: Seven years' experimental study. *Solar Energy*, 207(4), 1247–1258.

Kumar, T. P., Ganapathy, S. and Manikandan, M. (2022). Improvement of voltage stability for grid connected solar photovoltaic systems using static synchronous compensator with recurrent neural network. *Electrical Engineering and Electromechanics*, 22(2), 69–77.

Kumar, V. and Singh, M. (2021). Derated mode of power generation in PV system using modified perturb and observe MPPT algorithm. *Journal of Modern Power Systems and Clean Energy*, 9(5), 1183–1192.

Kumarar, T. (2024). Voltage stability analysis for grid connected PV system using optimized control on IOT based anfis. *Przegląd Elektrotechniczny*, 1(2), 261–268.

Kurniawan, R., Daud, M. and Hasibuan, A. (2022). Impact of intermittent renewable energy generations penetration on harmonics in microgrid distribution networks. *Proceeding - ELTICOM 2022: 6th International Conference on Electrical, Telecommunication and Computer Engineering 2022*, *February*, 30–37.

Lee, H.-S. and Yun, J.-J. (2019). Advanced MPPT algorithm for distributed photovoltaic systems. *Energies*, 12(18), 3576.

Li, Y., Tian, X., Liu, C., Su, Y., Li, L., Zhang, L., Sun, Y. and Li, J. (2017). Study on voltage control in distribution network with renewable energy integration. *2017 IEEE Conference on Energy Internet and Energy System Integration (EI2)*, *2018-Janua*, 1–5.

Loji, K., Davidson, I. E. and Tiako, R. (2019). Voltage profile and power losses analysis on a modified IEEE 9-bus system with PV penetration at the distribution ends. *2019 Southern African Universities Power Engineering Conference/Robotics and Mechatronics/Pattern Recognition Association of South Africa (SAUPEC/RobMech/PRASA)*, 703–708.

Masood, B., Saleem, U., Nadeem Anjum, M. and Arshad, U. (2017). Faults detection and diagnosis of transmission lines using wavelet transformed based technique. *2017 IEEE Jordan Conference on Applied Electrical Engineering and Computing Technologies, AEECT 2017*, *2018-Janua*(January 2018), 1–6.

Mohamed, S. A. and Abd El Sattar, M. (2019). A comparative study of P&O and INC maximum power point tracking techniques for grid-connected PV systems. *SN Applied Sciences*, 1(2), 174.

Mohammadi, P., El-Kishyky, H., Abdel-Akher, M. and Abdel-Salam, M. (2014). The impacts of distributed generation on fault detection and voltage profile in power distribution networks. *2014 IEEE International Power Modulator and High Voltage Conference (IPMHVC)*, 191–196.

Mohammed, A. (2022). Multi-domain simulation of IEEE 13 bus system with microgrid. *2022 10th International Conference on Smart Grid (IcSmartGrid),* 314–318.

Molina, M. G. and Mercado, P. E. (2019). Renewable energy technologies for microgrids. In *Microgrids design and implementation,* New York: Springer International Publishing, 27–67.

Moosavi, S. S., Kazemi, A. and Akbari, H. (2019). A comparison of various open-circuit fault detection methods in the IGBT-based DC/AC inverter used in electric vehicle. *Engineering Failure Analysis,* 96(11), 4, 223–235.

Moreno-Munoz, A., De la Rosa, J. J. G., Lopez, M. A. and Gil de Castro, A. R. (2009). Grid interconnection of distributed generation: The Spanish normative. *2009 International Conference on Clean Electrical Power*, 4, 466–470.

Mostafa, A. E. E. A., Bahgaat, N. K., El sayed, M. E. and Othman, E. S. A. (2017). Voltage stability for a photovoltaic system connected to grid by using genetic algorithm technique. *International Journal of Grid and Distributed Computing,* 10(4), 33–42.

Munkhchuluun, E. and Meegahapola, L. (2017). Impact of the solar photovoltaic (PV) generation on long-term voltage stability of a power network. *2017 IEEE Innovative Smart Grid Technologies - Asia (ISGT-Asia),* 1–6. h

N.Sandeep. (2014). *Single phase three level inverter with MPPT for grid connected photovoltaic system project*. *April*.

Niu, S., Zhang, Z., Ke, X., Zhang, G., Huo, C. and Qin, B. (2022). Impact of renewable energy penetration rate on power system transient voltage stability. *Energy Reports*, 8, 487–492.

Othman, R. A. and Al-Yozbaky, O. S. A.-D. Y. (2023). Influence of reactive power compensation from PV systems on electrical grid. *International Journal of Power Electronics and Drive Systems (IJPEDS),* 14(2), 1172.

Poornazaryan, B., Karimyan, P., Gharehpetian, G. B. and Abedi, M. (2016). Optimal allocation and sizing of DG units considering voltage stability, losses and load variations. *International Journal of Electrical Power & Energy Systems,* 79, 42–52.

Rahman, S., Saha, S., Islam, S. N., Arif, M. T., Mosadeghy, M., Haque, M. E. and Oo, A. M. T. (2021a). Analysis of power grid voltage stability with high penetration of solar PV systems. *IEEE Transactions on Industry Applications*, 57(3), 2245–2257.

Rahman, S., Saha, S., Islam, S. N., Arif, M. T., Mosadeghy, M., Haque, M. E. and Oo, A. M. T. (2021b). Analysis of power grid voltage stability with high penetration of solar PV systems. *IEEE Transactions on Industry Applications,* 57(3), 2245–2257.

Ram, J. P., Manghani, H., Pillai, D. S., Babu, T. S., Miyatake, M. and Rajasekar, N. (2018). Analysis on solar PV emulators: A review. *Renewable and Sustainable Energy Reviews,* 81(7), 149–160.

Rasheed, M. A. andVerayiah, R. (2021). Investigation of optimal PV allocation to minimize system losses and improve voltage stability for distribution and transmission networks using MATLAB and Digsilent. *Frontiers in Energy Research*, 9(10), 1–13.

Recioui, A., Benseghier, B. and Khalfallah, H. (2015). Power system fault detection, classification and location using the K-Nearest Neighbors. *2015 4th International Conference on Electrical Engineering (ICEE)*, 1–6.

Rönnberg, S. and Bollen, M. (2016). Power quality issues in the electric power system of the future. *The Electricity Journal*, 29(10), 49–61.

Rudresha, S. J. and Ankaliki, G. S. (2017). Voltage stability improvement with integration of DG into the distribution system. *International Journal of Emerging Trends & Technology in Computer Science (IJETTCS)*, 6(5), 196-200.

Sahnoun, M. A., Ugalde, H. M. R., Carmona, J. C. and Gomand, J. (2013). Maximum power point tracking using P&O control optimized by a neural network approach: A good compromise between accuracy and complexity. *Energy Procedia*, 42, 650–659.

Saidi, A. and Benachaiba, C. (2016). *Comparison of IC and P&O algorithms in MPPT for grid connected PV module.* 2016 8th International Conference on Modelling, Identification and Control (ICMIC), 213–218.

Shang, L., Guo, H. and Zhu, W. (2020). An improved MPPT control strategy based on incremental conductance algorithm. *Protection and Control of Modern Power Systems*, 5(1), 718.

Singh, S. and Vishwakarma, D. N. (2015). *Intelligent techniques for fault diagnosis in transmission lines — An overview.* 2015 International Conference on Recent Developments in Control, Automation and Power Engineering (RDCAPE), 280–285.

Sivakumar, P., Abdul Kader, A., Kaliavaradhan, Y. and Arutchelvi, M. (2015). Analysis and enhancement of PV efficiency with incremental conductance MPPT technique under non-linear loading conditions. *Renewable Energy*, 81, 543–550.

Spooner, E. and Harbidge, G. (2001). Review of international standards for grid connected photovoltaic systems. *Renewable Energy*, 22(1–3), 235–239.

Stanisavljevic, A., Katic, V., Dumnic, B. and Popadic, B. (2018). A brief overview of the distribution test grids with a distributed generation inclusion case study. *Serbian Journal of Electrical Engineering*, 15(1), 115–129.

Suampun, W. (2016). Voltage stability analysis of grid-connected photovoltaic power systems using CPFLOW. *Procedia Computer Science*, 86(3), 301–304.

Subramaniam, T., Abd Rahman, M. S., Ariffin, A. M. and Sahrim, M. (2017). An investigation on the power system stability of photovoltaic grid integrated system. *2017 7th IEEE International Conference on Control System, Computing and Engineering (ICCSCE)*, 17, 356–359.

Subrata, A. C., Sutikno, T., Padmanaban, S. and Purnama, H. S. (2019). Maximum power point tracking in pv arrays with high gain Dc-Dc boost converter. *International Conference on Electrical Engineering, Computer Science and Informatics (EECSI), March 2020*, 358–362.

Sudhakar Babu, T., Prasanth Ram, J., Sangeetha, K., Laudani, A. and Rajasekar, N. (2016). Parameter extraction of two diode solar PV model using Fireworks algorithm. *Solar Energy*, 140, 265–276.

Tamimi, B., Canizares, C. and Bhattacharya, K. (2013). System stability impact of large-scale and distributed solar photovoltaic generation: The case of ontario, Canada. *IEEE Transactions on Sustainable Energy*, 4(3), 680–688.

Villalva, M. G., Gazoli, J. R. and Filho, E. R. (2009). Comprehensive approach to modeling and simulation of photovoltaic arrays. *IEEE Transactions on Power Electronics*, 24(5), 1198–1208.

Vita, V., Alimardan, T. Ekonomou, L. (2016). The impact of distributed generation in the distribution networks' voltage profile and energy losses. *Proceedings - EMS 2015: UKSim-AMSS 9th IEEE European Modelling Symposium on Computer Modelling and Simulation, October 2015*, 260–265.

Wu, Y. K., Lin, J. H. and Lin, H. J. (2017). Standards and guidelines for grid-connected photovoltaic generation systems: A review and comparison. *IEEE Transactions on Industry Applications*, 53(4), 3205–3216.

Yıldırım, B. (2017). Investigation With Modal Analysis Of Effects Of High PV Penetration On Power System Voltage Stability. *International Journal of Energy and Smart Grid*, 2(1), 17–26.

Yunus Khan, T. M., Soudagar, M. E. M., Kanchan, M., Afzal, A., Banapurmath, N. R., Akram, N., Mane, S. D. and Shahapurkar, K. (2020). Optimum location and influence of tilt angle on performance of solar PV panels. *Journal of Thermal Analysis and Calorimetry*, 141(1), 511–532.

Zaraket, J., Aillerie, M., Salame, C. and Losson, E. (2019). Output voltage changes in PV solar modules after electrical and thermal stresses. Experimental analysis. *Energy Procedia*, 157, 1404–1411.

Darwish, Z. A., Kazem, H. A., Sopian, K., Alghoul, M. A. and Chaichan, M. T. (2013). Impact of some environmental variables with dust on solar photovoltaic (PV) performance: review and research status. *International J of Energy and Environment*, 7(4), 152-159.

Zlotecka, D. and Sroka, K. (2018). The characteristics and main causes of power system failures basing on the analysis of previous blackouts in the world. *2018 International Interdisciplinary PhD Workshop (IIPhDW)*, 257–262.

Zubo, R. H. A., Mokryani, G., Rajamani, H. S., Aghaei, J., Niknam, T. and Pillai, P. (2017). Operation and planning of distribution networks with integration of renewable distributed generators considering uncertainties: A review. *Renewable and Sustainable Energy Reviews*, 72(10), 1177–1198.

APPENDICES

APPENDIX 1. Computer Representation of Renewable Energy System Using MATLAB/SIMULATION

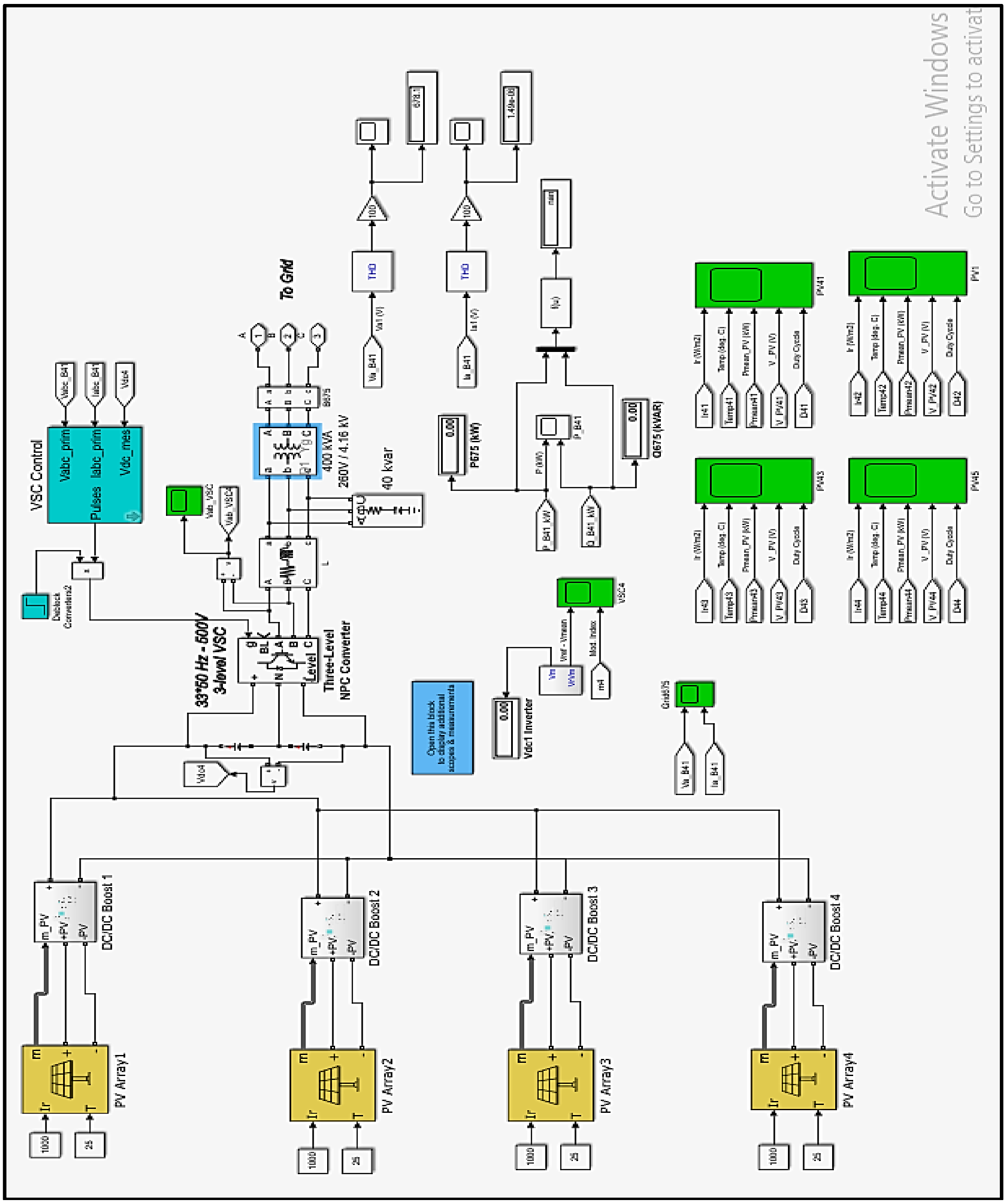

Figure 1.1. 400 kW PV system representation

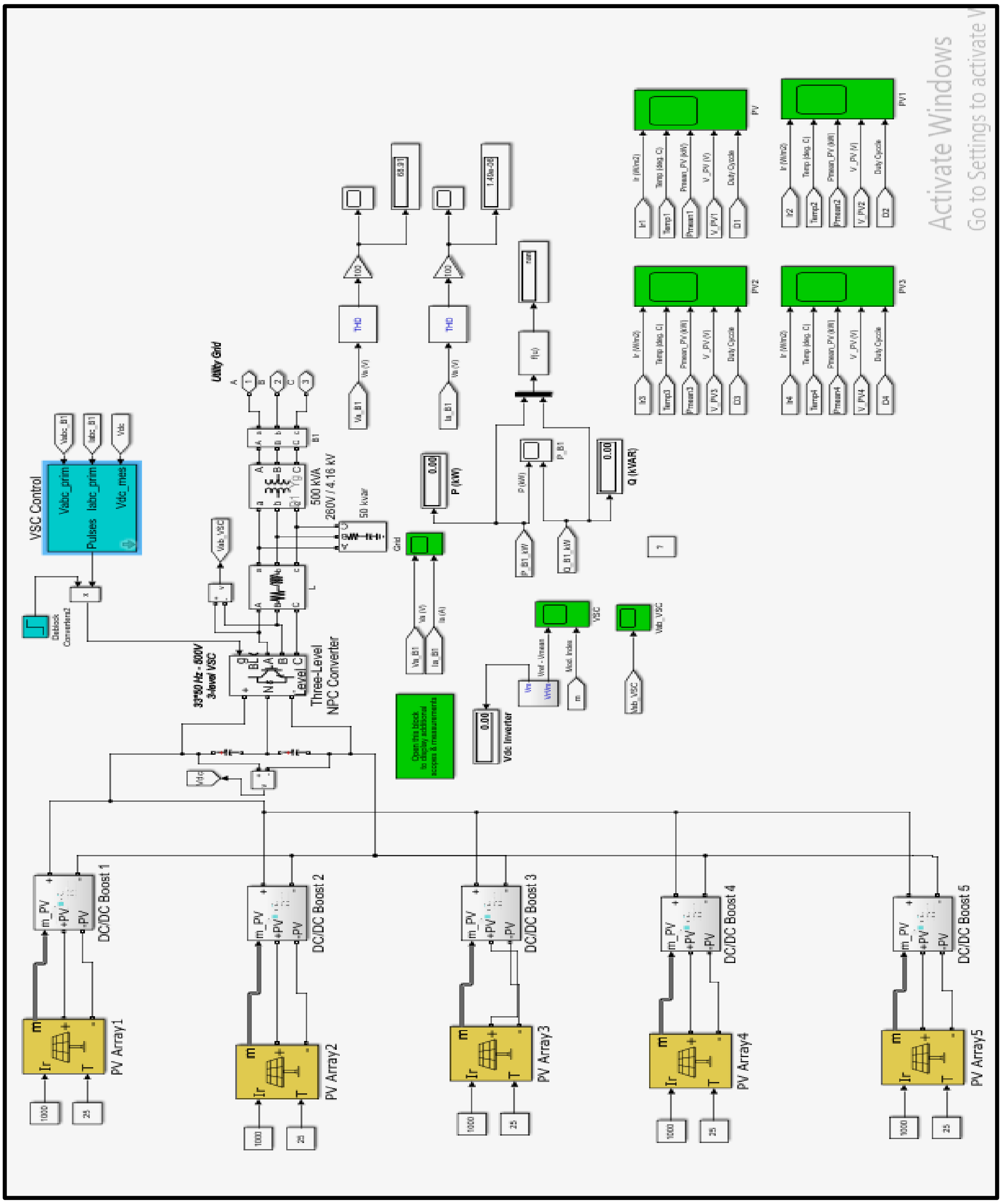

Figure 1.2. 500 kW PV system representation

Gazili olmak ayrıcalıktır